# Physiological Investigation of Causal Genetic Variants in Metabolic Disease

Mahesh M. Umapathysivam

St. Peter's College
University of Oxford

*A thesis submitted for the degree of*
*Doctor of Philosophy*

Hilary 2019

## Abstract

Type 2 diabetes (T2D) is a leading cause of morbidity and mortality. Understanding the molecular pathways that regulate glucose control and weight regulation may help predict disease course and develop novel interventions to improve health outcomes. In this thesis, I use naturally occurring genetic variation in combination with physiological tests to interrogate molecular pathways implicated in metabolic disease. Specifically, I examine impact of T2D risk alleles in *peptidylglycine alpha-amidating monooxygense* (*PAM*) on glucose physiology and the impact of *phosphate and tensing homologue* (*PTEN*) haploinsufficency on brown adipose tissue function (BAT) and insulin sensitivity.

In Chapter 3, I demonstrate that carriers of loss of function alleles (LoF) in *PAM* have altered serum PAM activity and increased glucagon-like peptide-1 (GLP-1) concentrations in the postprandial period. Based on the similar glycaemic profiles despite significantly increased GLP-1 concentration, I speculate that these results may be due to GLP-1 resistance.

In Chapter 4, I perform a prospective study to determine if PAM regulates GLP-1 resistance. I demonstrate that carriers of the LoF allele, S539W, have altered PAM activity, increased post prandial GLP-1 concentration but no difference in the incretin effect, suggesting GLP-1 resistance. I show that carriers of both alleles have a clinically meaningful reduction in response to GLP-1 receptor agonists but no other oral hypoglycaemic agents. I conclude that this may facilitate personalised medication choice in T2D.

In Chapter 5, I explore the role of PTEN in BAT regulation. I recruited individuals with *PTEN* haploinsufficiency which causes Cowden syndrome (CS). I demonstrate that individuals with CS have significantly reduced skin temperature overlying the supraclavicular BAT deposits, reduced maximal cold induced energy expenditure and reduced cold tolerance. I attribute this to reduced BAT function. I conclude that PTEN positively regulates BAT and that reduction in BAT activity contributes to the obesity phenotype seen in individual with CS.

In Chapter 6, I characterised an individual with mosaic CS to assess the importance of tissue specific regulation of the PTEN/PI3K/AKT pathway. I show that the percentage mosaicism in muscle and fat is in keeping with the impact on whole body insulin sensitivity.

In conclusion, I used a combination of physiological and genetic tools to determine how pathways under genetic regulation alter metabolic traits. The results of these studies have added to the understanding of the regulation of GLP-1 and BAT physiology and provide information that may help personalise treatment of T2D in the future and I validate PTEN as a regulator and potential target for activating BAT.

# Physiological Investigation of Causal Genetic Variants in Metabolic Disease


Mahesh M. Umapathysivam

St. Peter's College

University of Oxford

A thesis submitted for the degree of

*Doctor of Philosophy*

Hilary 2019

# Acknowledgements

Completing a DPhil has been one of the biggest challenges and adventures of my life. This journey would not have been possible or as enjoyable (or bearable) without the help and support of my friends, family, colleagues and supervisors.

To my Supervisors, Professor Anna Gloyn and Professor Mark McCarthy, your guidance, encouragement and enthusiasm have made me a better scientist, writer and clinician. I am so grateful that you accepted me as your student. I will look back on PAM Club fondly and remember the day I got the call up to "Molecular PAM club".

To the Gloyn group, you made my time in Oxford so much fun. I appreciated all our interesting scientific discussions over coffee, which were mainly excuses to get coffee. I look forward to seeing you all at conferences as our scientific careers progress. I would particularly like to acknowledge the technical help I received from Dr Amanda Bennett.

My work was largely based in the clinical research unit and would not have been possible with out the assistance of the nursing staff. Particularly, I would like to thank Jane Cheeseman, Rachel Craven-Todd and Michelle Haylock.

My study in Oxford has been supported by a number of institutions. Firstly I would like to thank the Rhodes Trust, who not only supported my studies financially, but made me feel welcome in Oxford. I am gratefully for the experiences, ideas and friendships that have grown through my association with the Rhodes Trust. I would also like to thank the the Radcliffe Department of Medicine for financial support. I would also like to acknowledge the support of Adam Deane and Michael Horowitz at the University of Adelaide who encouraged me to apply for a DPhil and fostered my initial interest in research.

To my friends from St Peter's College, the Rhodes community, the Football club and the Gloyn group; you have made my time at Oxford so much of an adventure. I have enjoyed seeing the world, rowing (poorly), playing football and learning with you.

Especially, I would like to thank Dr Freya Shearer and Dr Michael Mackley for their help with proof reading and formatting suggestions for my thesis.

I am incredibly lucky to have a supportive family. Thank you Mum, Dad, Suri, Priya and Nana for supporting me, calling regularly and travelling half way round the world (and back) to visit me.

Finally, I would like to thank my wife, Catherine. Thank you for taking the chance and travelling to a new country with me. Thank you for putting up with all my PAM and diabetes talk, thank you for listening to me practice oral presentation so many times before conferences you could probably give the talks yourself. Thank you for your love and support, I would not have been able to finish this thesis without you.

# Abstract

Type 2 diabetes (T2D) is a leading cause of morbidity and mortality. Understanding the molecular pathways that regulate glucose control and weight regulation may help predict disease course and develop novel interventions to improve health outcomes. In this thesis, I use naturally occurring genetic variation in combination with physiological tests to interrogate molecular pathways implicated in metabolic disease. Specifically, I examine impact of T2D risk alleles in *peptidylglycine alpha-amidating monooxygense* (*PAM*) on glucose physiology and the impact of *phosphate and tensing homologue* (*PTEN*) haploinsufficency on brown adipose tissue function (BAT) and insulin sensitivity.

In Chapter 3, I demonstrate that carriers of loss of function alleles (LoF) in *PAM* have altered serum PAM activity and increased glucagon-like peptide-1 (GLP-1) concentrations in the postprandial period. Based on the similar glycaemic profiles despite significantly increased GLP-1 concentration, I speculate that these results may be due to GLP-1 resistance.

In Chapter 4, I perform a prospective study to determine if PAM regulates GLP-1 resistance. I demonstrate that carriers of the LoF allele, S539W, have altered PAM activity, increased post prandial GLP-1 concentration but no difference in the incretin effect, suggesting GLP-1 resistance. I show that carriers of both alleles have a clinically meaningful reduction in response to GLP-1 receptor agonists but no other oral hypoglycaemic agents. I conclude that this may facilitate personalised medication choice in T2D.

In Chapter 5, I explore the role of PTEN in BAT regulation. I recruited individuals with *PTEN* haploinsufficiency which causes Cowden syndrome (CS). I demonstrate that individuals with CS have significantly reduced skin temperature overlying the supraclavicular BAT deposits, reduced maximal cold induced energy expenditure and reduced cold tolerance. I attribute this to reduced BAT function. I conclude that PTEN positively regulates BAT and that reduction in BAT activity contributes to the obesity phenotype seen in individual with CS.

In Chapter 6, I characterised an individual with mosaic CS to assess the importance of tissue specific regulation of the PTEN/PI3K/AKT pathway. I show that the percentage mosaicism in muscle and fat is in keeping with the impact on whole body insulin sensitivity.

In conclusion, I used a combination of physiological and genetic tools to determine how pathways under genetic regulation alter metabolic traits. The results of these studies have added to the understanding of the regulation of GLP-1 and BAT physiology and provide information that may help personalise treatment of T2D in the future and I validate PTEN as a regulator and potential target for activating BAT.

# List of publications

## Publication During DPhil

Thomsen SK, Raimondo A1, Hastoy B, Sengupta S,Dai XQ, Bautista A, Censin J,7, Payne AJ, **Umapathysivam MM**, Spigelman AF, Barrett A, Groves CJ, Beer NL, Manning Fox JE, McCarthy MI, Clark A, Mahajan A, Rorsman P, MacDonald PE, Gloyn AL.(2018).**Type 2 diabetes risk alleles in PAM impact insulin release from human pancreatic $\beta$-cells.** *Nature Genetics*.

## Conference Abstracts During DPhil

**Mahesh M Umapathysivam**, Tim McDonald, Sandy Humphries, Matt Neville, Anna L Gloyn, Mark McCarthy, Andrew T Hattersley, Fredrik Karpe, Tim M Frayling. **Strategies for improving statistical power for detailed physiological characterisation of individuals with T2D-associated variants.** *European Association for the Study of Diabetes* September 2016. Munich, Germany. Oral Presentation.

**Mahesh M Umapathysivam**, Shahana Sengupta, Soren Thomsen, Benoit Hastoy, Anna E Jonsson, Niels Grarup, Christian T Have, Kristine Færch, Anette P Gjesing, Jane Cheeseman, Oluf Pedersen, Torben Hansen, Jens J Holst, Fredrik Karpe, Mark I McCarthy, Anna L Gloyn. **Genotype-based recall studies shed light on the impact of type 2 diabetes risk alleles in Peptidylglycine Alpha-amidating Monooxygenase (PAM) on serum PAM enzyme function and determinants of beta-cell function.***Novo Nordisk Fellowship Symposium*. September 2017. Oxford United Kingdom. Poster presentation.

# Statement of contributions

My supervisors, Professor Anna Gloyn and Professor Mark McCarthy provided guidance and technical help throughout the planning, analysis and writing process for each chapter. Additional contributions for each chapter are listed below.

*Chapter 3:* Professor Torben Hansen and Dr Anna Jonsson provided data and analysis from the AdditionPro and Family Study data. Amidation specific GLP-1 assays were perfomed by Professor Jens Holst. Professor Fredrik Karpe provided access to stored samples in the Oxford Biobank. Dr Amanda Bennett supervised genotyping.

*Chapter 4:* Dr Matt Neville and John Miller selected non-carriers to be matched to risk allele carriers based on criteria I provided. This enabled me to remain blinded to the genotype of volunteers. Data collection during isoglycaemic clamp studies required the assistance of nursing staff, this assistance was kindly provided by Rachel Craven-Todd, Jane Cheeseman and Michelle Haylock. Amidation specific hormone assays were performed by Professor Jens Holst and Professor Jens Rehfeld. TSH assays were performed by Dr Tim James. I was assisted in performing the insulin radioimmunnoassays by Marjory Gilbert, I performed approximately 50 percent of all assays independently. All glucose assays were performed by Marjory Gilbert.Professor Ewan Pearson and Dr Adem Dawed provided access to the GoDARTS Study data, Dr Angus Jones provided access to the PRIBA study data.

*Chapter 5:* Michelle Haylock provided assistance with data collection and sample storage. Dr Lisa Walker and Dr Katherine Lachlan referred patients to the study.

*Chapter 6:* Dr Lisa Walker referred the proband to the study. Professor Fredrik Karpe performed the muscle biopsy. Sarah White assisted me with sample collection whilst I performed the Euglycaemic Hyperinsulinaemic Clamp. Jane Cheeseman assisted with sample preparation following fat biopsy. Dr James East provided colonoscopy images.

# Contents

# List of Figures

# List of Tables

# List of Abbreviations

**ACTH** . . . . . Adrenocorticotropic Hormone

**BAT** . . . . . Brown Adipose Tissue

**CCK** . . . . . Cholecystokinin

**CgA** . . . . . Chromogranin A

**CO** . . . . . Carbohydrate Oxidation

**CRU** . . . . . Clinical Research Facility

**CS** . . . . . Cowden Syndrome

**DEXA** . . . . . Dual Energy X-ray Absorptiometry

**DPP-IV** . . . . . Dipeptidyl Peptidase-4

**EE** . . . . . Enegy Expenditure

**EUH** . . . . . Euglycaemic Hyperinsulinaemic

**FO** . . . . . Fatty Acid Oxidation

**GEM** . . . . . Gas Exchange Monitor

**GIP** . . . . . Glucose-dependent Insulinotropic Polypeptide

**GLP-1** . . . . . Glucagon-like Peptide 1

**GoDARTS** . . . . Genetics of Diabetes Audit and Research in Tayside Scotland Study

**GWAS** . . . . . Genome Wide Association Study

**HWE** . . . . . Hardy Weinberg Equilibrium

**IGI** . . . . . Insulinogenic Index

**IMI-DIRECT** . . . Innovative Medicines Initiative: DIabetes REsearCh on patient stratification

**IRT** . . . . . Infrared Thermography

**LD** . . . . . Linkage disequilibrium

**LoF** . . . . . Loss of Function

**MAF** . . . . . Minor Allele Frequency

**OBB** . . . . . Oxford Biobank

**OGTT** . . . . . Oral Glucose Tolerence Test

**OHA** . . . . . Oral Hypoglcaemic Agents

**PAM** . . . . . Peptidyl-glycine Alpha-amidating Monoxygenase

**PHTS** . . . . . PTEN Harmatoma Syndrome

**PI3K** . . . . . Phosphatidylinositol 3 Kinase

**PIP2** . . . . . Phosphatidylinositol 4,5-bisphosphate

**PIP3** . . . . . Phosphatidylinositol (3,4,5)-trisphosphate

**PRIBA** . . . . . The Predicting Response to Incretin Based Agents

**PTEN** . . . . . Phosphate and Tensing Homologue

**RBG** . . . . . Recruit-by-genotype

**RBP** . . . . . Recruit-by-phenotype

**ROI** . . . . . Region of Interest

**RQ** . . . . . Respiratory Quotient

**SCV** . . . . . Supraclavicular

**SGLT2** . . . . . Sodium Glucose Transporter Protein 2

**SNP** . . . . . Single Nucleotide Polymorphism

**SU** . . . . . Sulphonylureas

**T2D** . . . . . Type 2 Diabetes

**TRH** . . . . . Thyroid Releasing Hormone

**TSH** . . . . . Thyroid Stimulating Hormone

**UCP-1** . . . . . Uncoupling Protein 1

# 1

# Thesis introduction and overview

## 1.1 The health economic and mortality burden of type 2 diabetes

The prevalence of Type 2 diabetes T2D is increasing globally, and is set to be one of the major health and economic challenges of the 21st century [1]. Estimates suggest there are currently 415 million people living with diabetes and, by 2040, this number is expected to increase to 642 million [2]. Whilst this increase is largely explained by changes in environmental and lifestyle factors—increased caloric intake and decreased physical activity—there is strong evidence that genetic predisposition plays a pivotal role in determining if individuals will develop T2D [3].

Diabetes is a leading cause of morbidity and mortality globally [1]. Seven percent of all deaths are directly attributable to diabetes [4]. It is the leading cause of adult blindness, non-traumatic lower limb amputation and end-stage kidney disease, as well as increasing the risk of cardiovascular disease [**200**, 5].

It is estimated that in the 2017 calendar year, $727 USD billion was spent on treating T2D and its complications worldwide [2]. This represents approximately 12% of the world's total healthcare expenditure [2]. This is reflected in the United Kingdom, where over 10% of the National Health Service expenditure is spent on the treatment of T2D and its complications [2].

Given the magnitude of financial burden and the morbidity and mortality associated with T2D, there is both an economic and therapeutic imperative to prevent diabetes, develop new treatments and optimise existing treatments to improve patient outcomes.

## 1.2 Type 2 Diabetes definition

Type 2 diabetes is a progressive disease characterised by hyperglycaemia and relative insulin deficiency. This relative insulin deficiency can be driven by a primary beta-cell defect or insulin resistance overwhelming normal beta-cell function. More commonly, it is a combination of these two factors. The current diabetes epidemic is being driven by increased insulin resistance associated with increasing central adiposity [6].

Type 2 diabetes makes up approximately 90% of all cases of diabetes and is diagnosed by elevated blood glucose concentration in the fasting state ( 7.0mmol/L), elevated blood glucose concentration 2 hours after ingestion of 75g of glucose ( 11.1mmol/L) or elevated glycated haemoglobin (HbA1c) (>6.5%) [7].

These criteria are based on the observation that increasing blood glucose exposure as measured by HbA1c or plasma glucose is associated with increased microvascular complications (retinopathy, nephropathy and neuropathy). These diagnostic cutoffs have been defined as being pathological because at these cut points the prevalence of diabetic complications rises rapidly [7].

## 1.3 Management of T2D

The central components of the management of T2D are modification of cardiovascular risk and reduction of overall glucose exposure [8]. There is a robust body of evidence provided by the United Kingdom Prospective Diabetes Study and the Diabetes Control and Complication Trial, that these approaches reduce both macrovascular (e.g. myocardial infarction and stroke) and microvascular (e.g. retinopathy) complications [**189**, 9]. Importantly, early and sustained reduction of glucose exposure has been shown to prevent microvascular complications, providing a rationale for treatment as soon as diabetes is diagnosed, even when asymptomatic [10].

Given the robust body of evidence for the benefit of lowering HbA1c with lifestyle and pharmacological interventions, a focus of T2D research should be identifying novel means, or improvement in the use of current treatments, to improve glycaemic exposure.

## 1.4 Physiology of glucose control

In healthy individuals, blood glucose is tightly regulated. This regulation is the product of multiple endocrine feedback loops. The most important among these are the opposing actions of insulin and glucagon. Insulin is produced by the pancreatic beta-cell in response to elevated plasma glucose [11]. The presence of the insulin independent GLUT1 transporter in the beta-cell membrane allows entry of glucose into the beta-cell [11]. This relatively uncontrolled influx of glucose exposes glucokinase to glucose concentrations reflective of plasma glucose, allowing it to act as a glucose sensor [11]. The phosphorylation of glucose is the rate limiting step in insulin release. In brief, this allows the appropriate generation of ATP, closure of potassium channels, calcium influx and exocytosis of insulin [11].

Insulin is the primary hormone that lowers blood glucose concentrations of plasma. This is mainly achieved by the translocation of GLUT4 (an insulin dependent glucose transporter) into the membrane of peripheral tissues (predominantly in muscle, liver and adipose tissue) allowing the transport of glucose from the blood into the cell [12]. In addition to the facilitation of glucose uptake by cells, insulin also mediates glycogen storage [12]. Beyond these effects, insulin inhibits lipolysis and stimulates lipogenesis and protein synthesis [12].

Glucagon broadly opposes insulin, it increases blood glucose concentration by stimulating hepatic gluconeogenesis and glycogenolysis [13]. The regulation of glucagon secretion by the alpha cell is less well understood than insulin, but on balance, it appears that the alpha cells respond to neural stimuli, direct effects of glucose, and downregulation by insulin [13].

In addition to insulin and glucagon, there are a myriad of homeostatic hormones that work both through stimulation of these insulin and glucagon and other independent pathways. The most well recognised and therapeutically relevant of these are the

incretin hormones: glucagon-like peptide-1 (GLP-1) and glucose-dependent insulinotropic polypeptide (GIP) [14]. Incretin hormones that are released from the gut in response to nutrient ingestion and act to control postprandial glycaemic excursions [15]. Both GLP-1 and GIP are gut-released peptides that increase insulin secretion [16]. Through their insulinogenic effects and regulation of gastric emptying (primarily GLP-1), GLP-1 and GIP potently reduce postprandial glycaemic excursions [**254**, 17]. In the setting of T2D, GLP-1 but not GIP has been shown to increase insulin secretion[18]. For this reason, GLP-1 but not GIP agonists are used to treat T2D [**338**, 16].

The study of glucose regulation in the physiological setting has identified a number of pathways that interact to maintain homeostasis of glucose. Pharmacological augmentation of these molecular pathways has been and continues to be used to treat T2D [19]. Not only have classical pathways like increasing potassium influx to stimulate insulin secretion (sulphonylureas) and increasing insulin sensitivity (thiazolidinediones) been utilized, but more recently the incretin axis (DPP-IV inhibitors - which stop the breakdown of GLP-1 and GLP-1 receptor agonists) and urinary excretion of glucose (sodium glucose transporter protein 2 inhibitors) have been utilized [**255**, **188**, **340**, 20].

By characterising the mechanism underpinning genetic variants that increase risk of T2D there is scope for greater understanding of components of glucose homeostasis, heterogeneity of the T2D phenotype, and development of novel treatments.

## 1.5 Assessing physiological components of glucose homeostasis

The understanding of these discrete contributory pathways for physiological glucose control is important for the identification of specific pathology underpinning the development of diabetes. A mechanistic understanding of these pathways may allow for prevention or therapeutic manipulation with pharmacotherapy. The complexity of glucose regulation in humans poses significant challenges in testing pathways of interest and linking specific genetic or environmental exposure to a discrete mechanism.

One of the many complex relationships that is important to understand when assessing glucose physiology is the hyperbolic relationship between insulin secretion and

insulin resistance [**179**, 21]. Consideration of this relationship is important for interpreting a number of measures of glucose physiology that have been applied to large cohorts [22]. It has been well demonstrated that in healthy individuals, in response to increased insulin resistance, beta-cell function increases and vice versa **(figure 1.1)**. As beta-cell function reduces there is reduced ability to cope with increase requirement associated with resistance. This results in impaired glucose tolerance if the beta-cell defect is mild. In T2D the beta-cell defect is such that there is no or minimal ability to increase beta-cell function to maintain a normal blood glucose concentration. This relationship can be defined by the equation "Insulin secretion = constant/insulin resistance" [23] and creates complexity when interpreting the readily available measure of insulin resistance or beta cell function derived from OGTTs (HOMA-B, HOMA-IR, insulinogenic index, etc.)[**226**, 24]. If a measure of resistance is not considered in combination with beta-cell function, it is often difficult to determine whether the measure of beta-cell function is reduced due to a primary beta-cell defect or due to greater insulin sensitivity and thus lower insulin requirement. These surrogate measures are not as precise or accurate as clamp studies, but they are comparatively less costly and easier to perform. Surrogate measures can therefore be deployed in far greater numbers than clamp studies, making them more appropriate for large cohort studies (e.g.>100 volunteers). As a result, studies that have investigated genetic effects in large numbers tend to use derived measures of beta-cell function from fasting samples or OGTT **(table 1.1)**[**1**, 25]. For example The Meta-analysis of Glucose and Insulin Related Trait Consortium (MAGIC) (comprising over 50 independent cohorts), derived measures from OGTTs (time 0, 30 and sometimes 120 min) to classify T2D risk alleles based on broad mechanistic categories [26].For example, beta-cell functional capacity can be estimated by considering measures of both insulin secretion and insulin sensitivity (e.g. disposition index) and these correlate to the gold standard techniques of the hyper-glycaemic clamp or intravenous glucose tolerance test (IVGTT) [21].

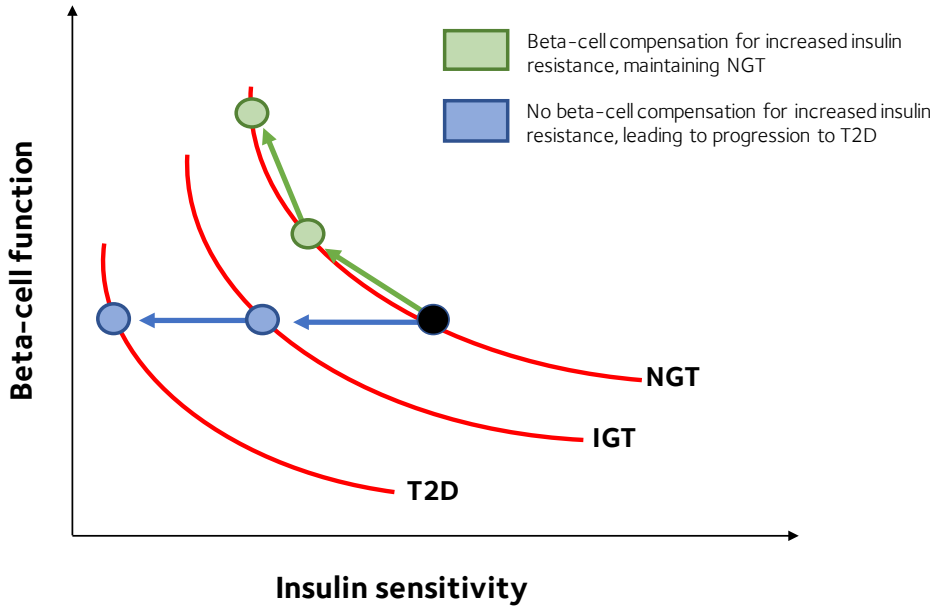


**Figure 1.1: Hyperbolic relationship between beta-cell function and insulin sensitivity**. This figure demonstrates the hyperbolic relationship between insulin secretion and insulin resistance. Three states are depicted: normal glucose tolerance (NGT), impaired glucose tolerance (IGT) and the diabetic state (T2D). The increase in insulin resistance without beta-cell compensation leads to diabetes.

| Derived measure | Physiological trait | Formula |
|---|---|---|
| **HOMA-B** | Beta-cell function | Computer model available via (http://www.dtu.ox.ac.uk/homacalculator/). |
| **Insulinogenic index** | Beta-cell function | (insulin30 – insulin0)/(glucose30 - glucose0) |
| **BIGTT-AIR0-30-120** | Beta-cell function | exp[8.20 + (0.00178 x insulin0) + (0.00168 x insulin30) -(0.000383 x insulin120) - (0.314 x glucose0) - (0.109 x glucose30) + (0.0781 x glucose120) + (0.180 x gender (male=0 and female=1)) - (0.032 x BMI)] |
| **Disposition index** | Beta-cell function | AUCinsulin-OGTT/AUCglucose-OGTT * Matsuda ISI |
| **Corrected insulin response** | Beta-cell function | AUC C-Peptide(0-30)/AUCGlucose(0-30) |
| **Matsuda Index** | Insulin sensitivity | 10 000 / (glucose0 x insulin0 x glucose mean-OGTT x insulin mean-OGTT) |
| **Belfiore index** | Insulin sensitivity | 2/[(0.5 x glucose0 + glucose60 + 0.5 x glucose120)/11.36) x (0.5 x insulin0 + insulin60 + 0.5 x insulin120)/638) + 1] |
| **HOMA-IR** | Insulin resistance | Computer model available via (http://www.dtu.ox.ac.uk/homacalculator/). |
| **Hepatic insulin clearance** | Hepatic insulin clearance | AUC C-Peptide/ AUC Insulin |
| **Fasting insulin clearance** | Fasting insulin clearance | C-peptide(Fasting) / insulin(Fasting) |

**Table 1.1:** OGTT derived measures of beta-cell function and insulin sensitivity
HOMA – B/IR[22], Insulinogenic Index[27], BIGTT [28], Disposition Index [29], Matsuda[29], Belfiore [30], Hepatic fasting insulin clearance corrected insulin response [31]

Clamp studies overcome physiological compensatory mechanisms by isolating the components of various regulatory pathways [**158**, 32]. These studies include (but are not limited to) the isoglycaemic clamp, hyperinsulinaemic-euglycaemic clamp and the hyperglycaemic clamp [32]. Broadly, these tests are all based on the same principle, namely, that if one aspect of glucose physiology is controlled artificially, the opposing/complementary arm of the feedback loop/homeostatic mechanism can be accurately quantified. For example, in the hyperinsulinaemic-euglycaemic clamp (the gold standard measure of insulin sensitivity) endogenous insulin secretion is overwhelmed by exogenous insulin infusion (removing the physiological feedback) and exogenous glucose is infused intravenously to maintain a constant blood glucose level. This allows insulin sensitivity to be measured (by amount of intravenous glucose required to maintain a stable blood glucose concentration) without having to consider the compensatory effects of altered insulin secretion. These studies are costly and difficult to perform, but the comparative increase in sensitivity and accuracy can facilitate identification of important insights in small samples that may be missed by the surrogate markers.

The characteristics described above make clamp studies, with bespoke physiological tests well suited to study of small samples (for example carriers of rare or low frequency genetic variants and their impact on glucose physiology).

## 1.6 Genetics and genomics of T2D

In the last three decades, technological innovation, improvements in data handling and imputation have led to cheaper and more complete assessments of variation in the human genome [33]. These advancements have in part contributed to rapid progress in the field of genetics and genomics, providing a powerful tool for investigating complex genetic disease [**194**, **246**, **8**, 26]. As a result genetic studies have increased in sample size and have improved coverage of the genome. Currently, over 400 regions of the genome have been identified where variations is associated with altered T2D risk [34]. Whilst identification of loci associated with altered to T2D risk has been rapid, translation of these signals into mechanistic insight and clinical impact has been comparatively slow [**94**, 35].

There is hope that investigation of these association signals will provide, a greater molecular understanding of T2D, aiding in the prediction of prognosis and response to current therapeutics, as well as the development of biomarkers.

## 1.7 Genome Wide Association Studies

Genome wide association studies (GWAS) examine the frequency of alleles in individuals with and without the disease in question, and identify regions of the genome where variations is associated with altered disease risk. This approach has been successful in the setting of T2D, with over 400 regions of the genome now associated with altered T2D risk [**8**, **1**, 36]. The advantage of this approach is that it does not require prior biological knowledge to select candidate genes. Instead, each allele (for which genotypic information is available) is tested in a hypothesis free manner. This has led to identification of many genes that were not previously thought to play a role in glucose homeostasis being implicated in T2D pathogenesis (e.g. *PAM*, *RREB1*) [**10**, 37].

Despite success in identifying alleles that contribute to disease risk, when combined, these alleles only account for a small portion of the total risk attributed to genetic predisposition. Estimates suggest that only 18% of the genetic risk for T2D is explained by the alleles identified to date [**90**, 36]. Whilst it has been hypothesised that this so called “missing heritability” could be due to rare variants of large effect that we are currently underpowered to detect, the latest evidence suggests that it is more likely that the missing heritability is in a long tail of common alleles with small effect size [38].

## 1.8 Quantitative Preclinical Trait Analysis

The effect size of most T2D risk alleles is small. This is not surprising as alleles of large effect may experience negative selection. Additionally, the human model is complex, with feedback loops and redundancy enabling compensation for defects in glucose homeostasis. Whilst desirable for human health, this can complicate efforts to delineate mechanisms underpinning risk alleles. One method to minimise the impact of compensation by feedback loops at a cohort level is to examine intermediate or preclinical traits. This method assumes that measurement of an intermediate pathway (that is driving

disease risk) will more readily allow the detection of difference between risk allele carriers and non-carriers than measuring diabetes risk, as the opportunity for compensation is less. Some alleles have profound effects on preclinical traits but a much weaker signal on overall diabetes risk (e.g. the risk allele at rs1260326T>C in *GCKR* locus). When examined in the METSIM cohort (sample size of 8791), the risk allele at rs1260326 in *GCKR* locus was associated with increased fasting glucose (p= 0.0003) however an association with T2D risk was detected with only a p value of 0.01 [**6**, 39]. Additionally, preclinical can traits provide broader mechanistic insight into how alleles alter diabetes risk and can direct further mechanistic investigation. For example, the risk allele in *GCKR* preclinical trait analysis strongly suggests it alters diabetes risk through a hepatic mechanism altering insulin sensitivity [26]. This paved the way for characterization of the gene function in hepatocyte cell lines [40]. However, a limitation of this approach is that only the broad clinical traits (e.g. beta-cell function, insulin resistance, etc) are easily tested on the scale of an entire cohort. One of the major limitations of examining intermediate traits is that it often is not feasible to assess more complex traits across an entire cohort (as the specific testing would be costly and likely only be relevant to a subset of risk alleles).

## 1.9 Challenges in translating GWAS findings into biological insight

Despite the success of GWAS in identifying variants that are associated with disease, progress has been slow in gaining mechanistic insight. There are several challenges in the field which are in part responsible for the difficulty in building on GWAS results. Firstly, it has proven difficult to confidently identify the causal genes mediating the effect of risk alleles (so called “effector transcript”). This in part due to association studies being based on genotyping arrays. These studies sample a portion of the genome and leverage the increased likelihood of coinheritance of nearby single nucleotide polymorphisms (SNPs), to impute the likelihood of whether an individual carries a given SNP. This means that variants identified by a GWAS may reflect the effect of a SNP that is in linkage disequilibrium rather than the named SNP. Determining the SNP driving the effect in cases of high linkage disequilibrium (LD) remains a challenge even with whole genome

sequencing. Additionally, most alleles associated with T2D risk (approx. 90%) are in the non-coding parts of the genome [**90**, 35]. Whilst it is likely that these alleles will act on a nearby gene, this in not always the case. For example, alleles located in *FTO* have been associated with T2D, recent studies suggest that this may be due to regulatory interactions with textitIRX3 over a megabase away [**250**, 41]. Identifying the effector transcript for a risk allele is an ongoing challenge. Approaches to meet this challenge include high throughput screening of effector transcripts and the examination of the interaction of regulatory regions of the genome with the coding regions (e.g. Capture C and Capture Hi-C) [**196**, 35] .

## 1.10 Prioritisation for Post GWAS Follow Up Studies

It is logical to proceed with the physiological characterization of the alleles most likely to yield mechanistic insight and clinical impact. It is therefore important to prioritize which alleles to investigate. There are a number of factors which may predict the ease with which functional insight can be gained. As mentioned in the previous section, it is often not apparent what the causal transcript may be, particularly in the case of regulatory variants. This problem can be somewhat avoided by moving forward with coding variants. However, it should not be assumed that coding variants are always causal. Mahajan and co-authors eloquently showed that whilst coding alleles are often more likely to be causal than any regulatory alleles, they can also be bystanders [36]. Mahajan and co-authors show that coding variants may sit on a long haplotype and as such be correlated with many other variants. Whist the coding variant may be the most likely of these to be causal (on average 10 fold enrichment) the volume of correlated variants may mean that it is more likely that one of the many other non-coding variants may be driving the effect [36].

To maximize utility of follow up experiments it is important that the gene being investigated is credibly linked to the phenotype of interest and that the phenotype is clinically relevant. Multiple sources of corroborating evidence can lend weight to the signal being credible (e.g. directionally consistent effects on preclinical traits like reduced beta-cell function and increased risk of T2D or multiple independent risk alleles in the same gene). Finally, if a hypothesized pathway associated with the risk allele

is drugable or alters response to existing drugs this increases the clinical relevance and utility of the study.

## 1.11 Pipeline to human insight

After a GWAS signal is identified, to facilitate functional characterisation, evidence is sought to determine in which tissue or tissues the variant is exerting its effect. This is important as the expression profile or tissue specific regulation of the gene may lead to the possibility of tissue specific effects, which can provide information as to the mechanism of action [35]. Quantitative trait analysis can also provide important clues as to which tissues are affected (e.g. an effect observed on insulin resistance would suggest that the tissue being affected is likely an insulin sensitive tissue like muscle, liver or fat). This is often coupled with evidence from publically available gene expression resources such as the GTEx Portal. This approach is often only feasible when the effector transcript is known. This is exemplified by the detection and characterization of a truncation risk allele in *TBC1D4* (R363X) that disrupts the full length protein. *TBC1D4* is a mediator of the Rab induced GLUT4 membrane translocation [42]. Examination of expression profiles and preclinical traits revealed the full length isoform is selectively expressed in muscle [42]. This observation paved the way for detailed physiological study of insulin sensitivity with euglycaemic-hyperinsulinaemic clamps which demonstrated that the risk allele increased insulin resistance in skeletal muscle [42].

## 1.12 Extension of the pipeline into human studies

Whilst functional characterisation of T2D risk alleles in cell-lines and animal models can, and has, further delineated molecular pathways [43], it is highly desirable to extend mechanistic studies to humans. The most obvious reason to do this is that the human model is the most relevant to the treatment of disease. Cellular and animal models can have substantial differences to the human model. These are largely the result of differences in physiology between animals and humans. Such have caused confusion in understanding genetic signals in T2D. There is ongoing debate about the role of melatonin and beta-cell function after the legitimacy of investigating Melatonin Receptor 1b in mice

was questioned due to divergent melatonin physiology between species [**136**, 44]. In the case of cell lines, studying immortalised cells that are isolated from physiological regulation can also create difference between experimental *in vitro* behaviour and physiological function. Indeed, even in the best human beta-cell lines developed to date (EndoC-βH1 and EndoC-βH2), there are differences in the magnitude of insulin secretion and gene expression profiles compared to isolated primary human islets [45]. Finally, there are complex intermediate traits that result from the interplay of multiple organ systems and require specific behaviour from volunteers to enable measurement [46]. For example, the measurement of the incretin effect requires tight matching of glucose profiles with oral and intravenous glucose [46]. The premise of the study is that the incretin effect can be determine by reproducing the same glucose profile by administering glucose through two routes (oral and intravenous) and comparing the insulin secretion or glucose disposal between the studies. The test assumes the only difference is the route of glucose administration (and the secretion of incretin hormone associated with the oral route) [46]. Practically this means the subject must consume a standard volume of glucose, have their blood sampled frequently to ensure closely matched glucose profiles, and remain inactive throughout the study. Such experiments cannot be performed in cell models and are difficult to reproduce in animal models. It is for these reasons that human physiological studies are important, and necessary, for assessing the effect of genetic variation on certain intermediate traits.

## 1.13 Recruit-by-genotype and recruit-by-phenotype studies

Recruit-by-genotype (RBG) studies select individuals with genotypes of interest from consented and genotyped populations and recruit them into bespoke physiological studies. Recently, this method when paired with 1-1 matching and sampling from the extremes of genetic risk/protection, has been shown to be statistically efficient compared to cross-sectional hypothesis testing (i.e. selection of a random sample and applying the test on interest and then genotyping volunteers) [**166**, 47]. Biobanks of genotyped individuals now exist that are large enough to allow variant carriers to be closely matched

to non-carriers for confounding factors (such as age, sex, and BMI). The first recruit-by-genotype (RBG) study to utilise a biobank was performed using the Oxford Biobank in 2006 [48]. Since then, a number of RBG studies have elicited mechanistic understanding of T2D risk variants [**137**, **136**, **144**, **142**, **135**, 49].

Before the development of biobanks that allowed the recruitment of less phenotypically pronounced variants, genetic studies relied on identifying genotypes by linking them to striking clinical phenotypes. These recruit-by-phenotype (RBP) studies are a precursor to modern RBG studies. The most obvious and established use of the RBG/RBP design in T2D research has been to study individuals with rare mutations of large effect where diabetes is an overt feature (e.g. maturity-onset diabetes of the young). Additionally, phenotypes other than diabetes have been used to identify and recruit variant carriers where metabolic derangement is a less obvious component of the phenotype [**148**, 50]. An example of this is the use of Cowden Syndrome (CS) to identify and recruit carriers of variants in *PTEN* to study the impact of these variants on insulin sensitivity [50].

## 1.14 Physiological characterization of peptidyl-glycine alpha amidating monoxygenase (PAM)

In 2013, exome array analysis aimed at identifying and assessing low frequency (0.5-5%) and rare (<0.5%) coding variation was performed in 8,229 Finnish males from the METSIM cohort [37]. This study identified a missense allele in *PAM* (rs35658696 (p. Asp563Gly)) associated with reduced beta-cell function as measured by insulinogenic index (IGI) (beta=-0.21+/-0.04, p=0.044) [37]. The initial finding of Huyghe and co-authors was reproduced by an independent GWAS performed by Steinthorsdottir and co-authors in a case-control data-set comprising 4 ethnicities (primarily Icelandic but also Danish, Iranian, and Finnish ethnicities). In addition to reproducing the effect on IGI, Steinthorsdottir and co-authors also identified a second independent missense allele in textitPAM at rs78408340 (p.Ser539Trp), and demonstrated that both alleles increased risk of T2D and reduced beta cell function as measure by IGI **(table 1.2)** [51].

Following the study by Huyghe and co-authors, the candidacy of PAM as the causal transcript was still in question. The risk allele at rs35658696, is in near perfect LD (r2

| Variant | Amino acid change | MAF | Insulinogenic Index | OR Diabetes |
|---|---|---|---|---|
| **rs35658696** | D563G | 5.30% | -1.96 | 1.23 |
| **rs78408340** | S539W | 0.65% | -8.42 | 1.47 |

**Table 1.2:** T2D associated alleles and characteristics in *PAM*. Data are taken from the study by Steinthorsdottir and co-authors [51]

= 0.997) with another nonsynonymous allele in a nearby gene, *PPIP5K2*, rs36046591 (p.Ser1228Gly) [37]. Whilst both SNPs result in protein changes, the reference aspartic acid at rs35658696 is highly conserved across species and the substitution of a glycine is predicted to be deleterious. This contrasts with the SNP at rs36046591, where the reference serine is not well conserved and the substitution of a glycine is predicted to be tolerated [37].

The identification of a second independent coding allele at rs78408340 strengthened the candidacy of PAM as the causal transcript. This allele was not in LD with the risk allele at rs35658696 or any SNPs in *PIPP5K2* [51]. The SNP at rs78408340 was associated with increased risk of T2D (OR 1.47) and the amino acid substitution was also predicted to be deleterious. These initial studies have been supported by large scale fine-mapping studies in individuals of European ancestry [36]. The risk allele at rs35658696 will be referred to as D563G and the risk allele at rs78408340 will be referred to as S539W.

## Peptidyl-glycine alpha amidating monoxygenase function

Peptidyl-glycine alpha-amidating monooxygenase is the only enzyme in the body capable of amidation of glycine extended peptides [52]. Amidation is an important process in producing mature hormones. Fifty percent of all peptide hormones require amidation for complete biological function (including some which have been implicated in glucose homeostasis) [52]. Most notable among the amidated hormones implicated in glucose homeostasis is GLP-1. Glucagon-like peptide 1 is of particular interest as alteration of GLP-1 plasma concentration may alter response to medications that work through the incretin axis.

Peptidyl-glycine alpha-amidating monooxygenase is expressed widely, but expression in the pancreatic islets, L-cells (which secrete GLP-1) [personal communications,

Professor Fiona Gribble (Cambridge University)] and the heart, is particularly high [45]. Peptidyl-glycine alpha-amidating monooxygenase is expressed in most neuroendocrine cells, in keeping with the protein's role in post-translational modification of peptide hormones [53].

Given the wide range of tissues in which PAM is expressed, the diabetes phenotype in *PAM* risk allele carriers could be driven by effects within the pancreatic islet or through systemically released peptides acting on the beta-cell (e.g. GLP-1). Examining the impact of *PAM* risk alleles on the release and amidation of hormones that regulate blood glucose control may identify intermediate phenotypes contributing to disease risk. Chapter 3 4 will test the hypothesis that S539W and D563G reduce PAM enzyme function, alter amidated peptide concentration and action, and assess whether carrying these alleles affects the response to common diabetes medications.

## Biological function of PAM

The PAM protein has two functional catalytic domains. Together these facilitate the amidation of glycine extended peptides. [**11**, **14**, 54]. Peptidyl-glycine alpha-amidating monooxygenase facilitates the final step in a series of posttranslational modifications that produce active proteins [52]. Following translation, inactive pre-proproteins undergo proteolytic cleavage at dibasic consensus sequences by prohormone convertases (e.g. PC1, and PC2) [52]. Carboxyl groups revealed by this process are in turn removed by carboxypeptidases[52]. Finally, if a glycine occupies the terminal position it can interact with PAM and an amide group is added. Peptidyl-glycine alpha-amidating monooxygenase is the only enzyme in the human body that is capable of amidating peptides [**220**, 55]. The effect of amidation is variable, often altering potency, receptor binding, or plasma stability [**15**, 53].

Peptidyl-glycine alpha-amidating monooxygenase requires copper, ascorbate, and molecular oxygen to catalyse the two step amidation process **(figure 1.2)** [56]. The optimal pH for PAM function is 5.5, and at a pH of 7.4 seen in the serum, it is not active [**232**, 57]. This suggests it acts intracellularly, likely in the secretory granule (where the pH is

between 5-6), where it co-locates with glycine extended substrates [**349**, **232**, 57]. Non-tethered forms of PAM are then exocytosed into the blood. Sampling blood may allow assessment of amadation activity in individuals who carry loss of function mutations (when this is tested at an optimal pH) [58]. This may provide a surrogate measure of PAM activity in the secretory vesicle. In addition to its catalytic activity PAM has also been proposed to play important roles in intracellular trafficking [59].

PAM is subject to complex post-translational modification, with multiple cleavage sites [52]. This results in multiple distinct forms, or isoforms, of PAM. The most important distinctions between these isoforms appears to be that some are soluble and free to be secreted, and some are membrane tethered and remain in the cell [52]. If the trans-membrane domain is cleaved the resulting protein can be secreted in to the circulation. Cleavage at the linker site may result in PAM with only one of the two required catalytic domains **(figure 1.3)**. This variation in isoform expression gives rise to the intriguing possibility of tissue specific regulation of PAM function [58]. The cleavage site that results in these three distinct groups of isoforms of PAM are depicted in figure 1.3 [58].

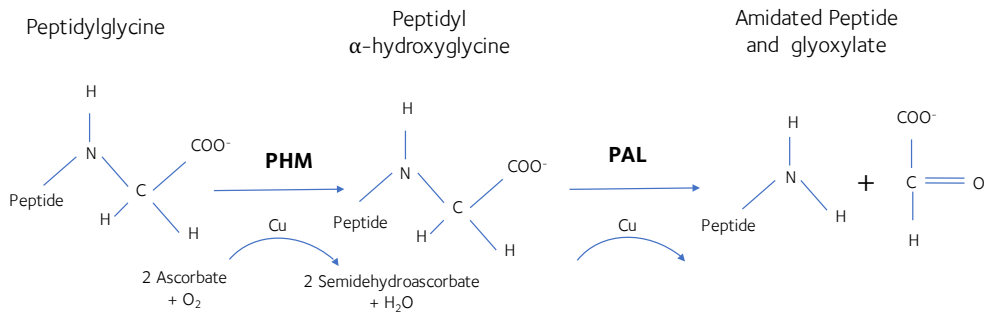


**Figure 1.2: Two step amidation reaction catalysed by PAM**. This figure demonstrates the two step amidation process catalysed by PAM. Glycine extended peptides interact with the PHM domain of the PAM protein which in the presence of ascorbate, copper (Cu) and oxygen (O2) catalyses the conversion to an alpha-hydroxylglycine. This intermediate then interacts with the PAL domain and is converted to the biologically active amidated mature protein.

## Animal models suggest PAM plays a role in glucose homeostasis

Rodent studies suggest that PAM is crucial for many biological functions. The importance of PAM is emphasised by rodent knockout models, where homozygous knockout is embryologically lethal [60]. Heterozygous *Pam* knockout resulted in reduced PAM

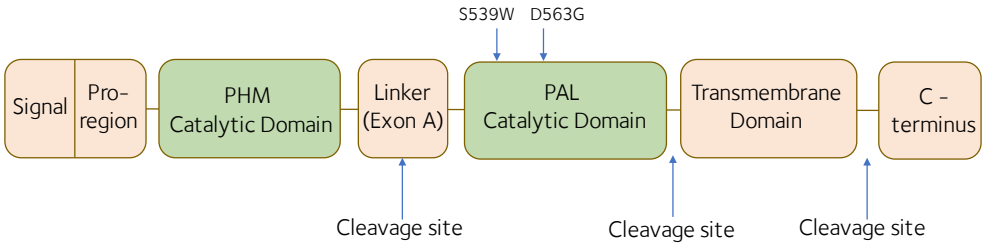


**Figure 1.3: Domain structure and potential cleavage sites of PAM**. This figure depicts the domain structure of the PAM protein. The catalytic domains, which are responsible for amidation are coloured green. Arrows indicate the cleavage sites, and the two T2D risk alleles (S539W and D563G).

tissue activity, increased adiposity, and hyperglycaemia following intraperitoneal glucose tolerance test in rodents. No difference was detected in the plasma concentration of amidated peptides, but few peptides were tested [60]. These results reflect those from the GWAS where the main effect observed in non-diabetic individuals was altered dynamic measures of beta-cell function (IGI) but no difference in the fasting state [37].

## Cellular characterisation of *PAM* reveals alleles associated with T2D result in loss of function and reduced beta-cell function

Peptidyl-glycine alpha-amidating monooxygenase has been studied in EndoC-βH1 cells in the Gloyn laboratory (Univiversity of Oxford) [59]. Using the HEK 293 cell model, Dr Anne Raimondo (research scientist, University of Oxford) demonstrated that the risk allele at S539W has aberrant PAM protein expression [59]. When HEK 293 cells were stably transfected with this variant, no soluble PAM was secreted in the supernatant [59]. Additionally, whilst the D536G variant displayed normal protein expression, the function of the secreted protein was substantially and significantly reduced **(figure 1.4)** [59]. These observations suggest that both the D563G and S539W alleles result in loss of function. However, the mechanism by which loss of function occurs is different. S539W results in decreased expression, and D563G results in reduced catalytic activity. This may result in different characteristics in carriers of the D563G and S539W alleles. Reduced expression from S539W will affect not only the catalytic function of PAM, but also the non-catalytic functions like intra-cellular trafficking, whereas D563G will only affect catalytic function.

In the EndoC-βH1 model (a glucose-responsive human beta-cell line) the role of PAM was investigated by knocking down *PAM* with siRNA and reducing amidation activity by using an amidation inhibitor (4P3BA)[45]. By reducing protein expression, the use of siRNA mimicked the hypothesised effect of the S539W allele, whilst the inhibitor mimicked the effect observed in cells transfected with D563G by reducing amidation activity. The siRNA knockdown resulted in reduced glucose stimulated insulin secretion, reduced insulin content and altered kinetics of exocytosis. In contrast, the amidation inhibitor only reproduced the effect on insulin content, supporting the hypothesis that PAM has both catalytic and non-catalytic roles in beta-cell function.

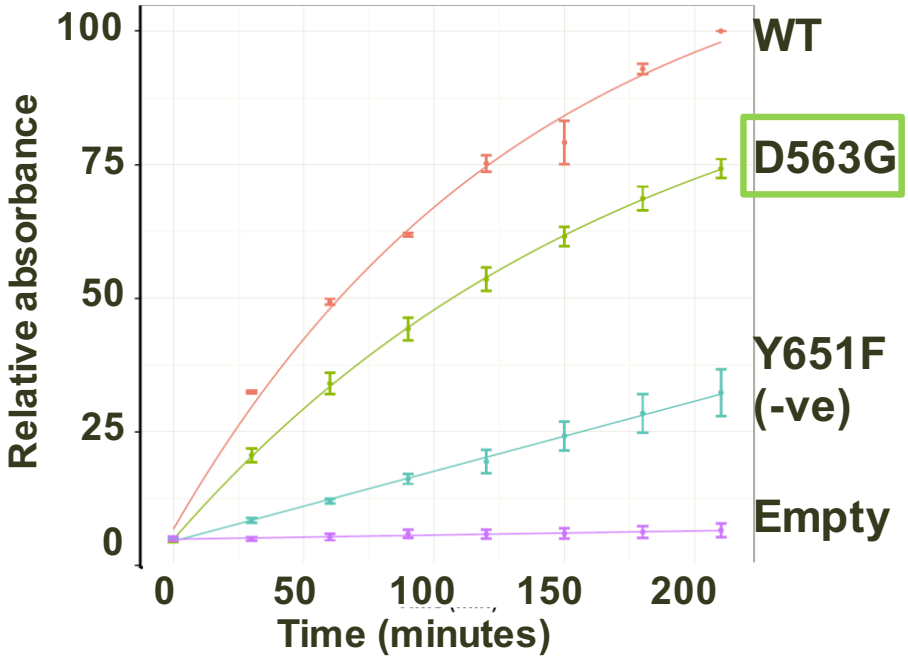


**Figure 1.4: Amidating activity of wild type PAM compared to that produced by carriers of T2D associated allele at rs35658696**. All results are normalised to wildtype PAM. Amidating activity of WT-PAM is displayed in orange, D563G-PAM (which associated T2D) is displayed in green and demonstrates a 25% reduction in amidating activity, Y651F-PAM which is catalytically null is displayed in blue, empty vector (EV) is displayed in purple (n=4). Error bars are mean ±SEM. S539W PAM was not included in this assay as no detectable protein was produced by cells transfected with this variant.

### PAM knockdown reduces the secretion of amidated peptides

Thomsen and co-authors, after examination of the islet secretome, suggested chromogranin A (CgA) and islet amyloid polypeptide (IAPP) as possible targets of PAM within the beta-cell due to the abundance and requirement of amidation [**54**, 59]. Knockdown of IAPP had no effect on insulin content or secretion. Knockdown of PAM resulted in altered Chromogranin A amidation and knockdown of CHGA resulted in a strikingly similar phenotype to PAM knockdown (reduced insulin content and reduced insulin secretion) [59]. This suggests that CgA is a substrate of PAM and that the phenotype observed may in part be mediated by a reduction in CgA amidation. It is of note that CgA is also highly expressed in L-cells and other neuroendocrine cell types [personal communications, Professor Fiona Gribble (Cambridge University),[45].

Importantly, PAM knockdown *in vitro* resulted in reduced total CgA being secreted into the supernatant [59]. This suggests that reduced PAM expression or function, as might be expected in D563G and S539W, may result in altered secretion and plasma concentration of amidated peptides *in vivo*.

These data raise the possibility that altered levels of amidated peptides may be contributing to the diabetes phenotype in carrier of S539W and D563G.

## 1.15 Physiological characterization of PTEN and its role in brown adipose function and tissue specific effects on insulin sensitivity

Phosphate and tensing homologue (PTEN) has been implicated in regulating insulin sensitivity, cancer risk and obesity [**3**, **320**, 61]. These effects are mediated by the negative regulatory effects of PTEN on the PI3K/AKT/MTORC pathway [**3**, **320**, 61].

Obesity and the associated increase in insulin resistance have been suggested to be driving the increased prevalence of T2D in our society [**175**, 2]. Understanding the counter intuitive association between increased BMI and insulin sensitivity seen in *PTEN* haploinsufficency may provide clinically relevant insight into mechanisms driving obesity and insulin sensitivity.

## PTEN and cancer biology

An association between cancer and diabetes was first reported in 1932[62]. Since then considerable epidemiological evidence has supported the link between diabetes and cancer. These studies have suggested increase risk of liver, pancreas, breast and endometrial cancer[63]. In support of this association genetic association studies have identified variation genes involved in cell cycle which increase the risk of cancer and diabetes [64]. More recently, penetrant familial cancer syndromes have been shown to have deranged glucose physiology (e.g. familial melanoma syndrome and CS) [**3**, 65].

*Phosphate and Tensing homolgue* (*PTEN*) is located at 10q23 and is made up of 9 exons which code for 403 amino acids and 4 functional protein domains[66]. Somatic mutation in *PTEN* are amongst the most common causes of cancer [67]. The functions of PTEN primarily relate to its action as a lipid phosphatase and its action on phosphatidylinositol (3,4,5)-trisphosphate (PIP3). This effect is mediated by the hydrolysis of PIP3 to Phosphatidylinositol 4,5-bisphosphate (PIP2) (opposing the effect of PI3K) [66]. Through the downstream effects of PIP3/AKT/MTORC pathway PTEN also negatively regulates protein synthesis, cell growth, metabolism, cell migration and cell cycle arrest and progression [50]. These factors, amongst others, mediate the tumour suppressor effect of PTEN [67].

## Metabolic impacts of PTEN

Similar to the tumour suppressor effects, the metabolic effects of PTEN relate to the downregulation of PIP3 dependent processes[67]. Of relevance, PI3K activates AKT which mediates the translocation of GLUT4 into the membrane [50, 67]. Effectively this means that PTEN, through its hydrolysis of PIP3, inhibits GLUT4 translocation into the membrane, this causes reduced insulin sensitivity [50, 67].

## GWAS associations suggest PTEN regulates insulin sensitivity

Examination of the PTEN locus in DIAGRAM and MAGIC consortia data has revealed a common allele that approaches but does not reach genome wide significance for increasing insulin resistance and diabetes risk **(table 1.3)**. Grinder-Hansen and co-author, investigated these findings by recruiting heterozygous and homozygous carriers of the G

| | MAF | Effect | T2D risk | HOMA-IR | BMI |
|---|---|---|---|---|---|
| rs11202614 | 0.15 | Upstream gene variant | 1.06(p=1.1 x $10^{-7}$) | -0.02 (6.0x$10^{-7}$) | -0.1 (p=0.003) |

**Table 1.3:** *PTEN* T2D risk allele characteristics

allele at rs11202614 and non-carriers and demonstrated that this allele was associated with peripheral insulin resistance using hyperinsulinaemic euglycaemic clamp [68].

## Cowden Syndrome

Cowden syndrome (CS) is a rare autosomal dominant cancer syndrome resulting from *PTEN* haploinsufficiency. The syndrome results in a constellation of symptoms including; intestinal hamartomas, skin tags and an increased risk of malignancy [69]. The diagnosis of CS is through consenus guidleines that requires; three or more major criteria, (including macrocephaly, Lhermitte-Duclos disease, or gastrointestinal hamartomas) or two major and three minor criteria [70]. If a family member has been diagnosed with CS diagnosis can be made with two major, 1 major and 2 minor or 3 minor criteria [70]. Major criteria include: endometrial cancer, thyroid cancer (follicular), gastrointestinal hamartomas, Lhermitte-duclos disease, macrocephaly, multiple mucocutaneous lesions (trichilemmomas, acral keratosis), macular pigmentation of the glans penis, mucocutaneous neuromas, and oral papillomas [70]. Minor criteria include: autism spectrum disorder, colon cancer, oesophageal glycogenic acanthosis, lipomas, cognitive impairment (ie, IQ  75), renal cell carcinoma, testicular lipomatosis, thyroid cancer, thyroid structural lesions, and vascular anomalies [70].

## *PTEN* haploinsufficiency provides insight into role of PTEN in regulation of insulin sensitivity

*PTEN* haploinsufficiency results in a striking clinical phenotype [**165**, 69]. Identifying individuals with CS provides an excellent opportunity to interrogate the metabolic effects of PTEN in humans. Indeed this approach was utilised by Pal and co-authors to elegantly demonstrated that individuals with *PTEN* haploinsufficency have markedly increased insulin sensitivity and that this is mediated through loss of inhibition on the PI3/AKT

pathway [50]. In addition to being insulin sensitive, individual with CS had a BMI that was 6 units higher than population based controls [50]. Whilst the cause of insulin sensitivity in Cowden syndrome has been convincingly attributed to down regulation of the PI3K/AKT pathway, the mechanism underlying the obesity phenotype remains unclear. Recently, PTEN has been linked to regulation of brown adipose tissue, a tissue that has been shown to be important for energy balance and weight control [**105**, 71].

## Brown adipose tissue

In 2009, it was demonstrated that brown adipose tissue (BAT) plays an important role in temperature regulation in humans and can be a substantial source of energy expenditure (EE) [72]. Brown adipose tissue is a subtype of adipose tissue that utilises fatty acids and glucose to produce heat. It is well adapted for this function with a high number of mitochondria and the presence of uncoupling protein-1 (UCP1) [73]. Uncoupling protein-1 'uncouples' the respiratory chain by increasing permeability of the inner mitochondrial membrane to protons, allowing fast substrate oxidation, converting the energy generated by the mitochondria to heat [**105**, 74]. BAT is activated by cold exposure and has been demonstrated to increase EE by 11.8% [**102**, 75]. In response to cold exposure, the blood flow to BAT increases, the uptake of free fatty acids and glucose increases and heat is produced [76].

In humans, BAT is located around the heart, kidneys, spine and in a large superficial deposit in the supra-clavicular region [72].

## PTEN and BAT

Animal models (mice and monkeys) are suggestive of a positive correlation between PTEN and BAT activity. Over expression of Pten in transgenic mice is associated with increased basal metabolic rate, reduced fat mass, and increased uptake of radioactive glucose tracer in BAT [61]. Surgical and histological examination of BAT in these transgenic mice suggests that Pten increases BAT activity and plays a role in the formation of brown adipocytes [**107**, 61]. Pharmacological agents inhibiting PI3K have demonstrated increased BAT activity and weight loss [77]. PI3K inhibitors are available for clinical use but are currently only licensed for use in lymphoma and other haematological malignancy[78]. If PTEN

positively regulates BAT activity in humans, PI3K inhibitors may be a viable option for the treatment of obesity [77]. To date the role of PTEN in regulation of BAT has not been directly assessed in humans. I hypothesise that loss of function mutations in *PTEN* (like in CS) may result in underactive BAT and reduced BAT formation and this may cause reduced EE and a predisposition to obesity.

## 1.16 Thesis Aims:

This thesis aims to address a bottle neck in the translation of genetic association signals into physiological and translational insights. Specifically, I aim to identify and characterise clinically important phenotypes in two genes, where variation is robustly associated with alter diabetes risk and glycaemic traits.

### 1.16.1 Structure:

- Chapter 2 outlines the common methods and techniques used throughout this thesis.
- Chapter 3 investigates two T2D risk alleles in *PAM*; D563G and S539W in historical data and stored samples. In this Chapter I aim to characterize the impact these alleles have on PAM enzyme activity and the incretin axis.
- Chapter 4 investigates the *PAM* T2D risk allele; D563G and S539W in a prospective study and in pharmacogentic data. In this chapter, I aim to assess amidated peptide profiles and the effect this has on glycaemic response to treatment with GLP-1 receptor agonists in carriers of D563G and S539W.
- Chapter 5 explores the role of PTEN in BAT function. In this chapter I develop a protocol for assessing maximal BAT activity and use this method, to determine the impact of *PTEN* haploinsufficiency on BAT.
- Chapter 6 uses the case of a mosaic *PTEN* mutation carrier to assess the effect of tissue specific downregulation of the PTEN/PI3/AKT pathway on insulin sensitivity and the other metabolic features of CS.

- Chapter 7 provides a general discussion of this thesis. This chapter outlines the implications for the management of T2D, as well as the implications for future investigations of complex physiological traits in the human model.

# 2
# Methods and techniques

## 2.1 Regulatory Compliance and Ethical Practice

### Informed consent

All study participants gave written informed consent prior enrolment into the studies. All studies were carried out in accordance with the declaration of Helsinki.

### Human Tissue Authority

All samples were stored in accordance with the Human Tissue Act 2004.

## 2.2 Study populations

### 2.2.1 Healthy participants

Healthy, non-diabetic, study participants were recruited from the Oxford Biobank (OBB) [48]. The OBB is a study cohort of approximately 9000 individuals from the Oxfordshire area maintained by the NIHR Oxford Bioresource [48]. The participants in the OBB have an age range of 30-65 years and do not have metabolic disease upon entry into the biobank. On recruitment into the OBB, participants undergo detailed measurement of metabolic and anthropomorphic parameters. These included measurement of; waist and hip circumference, weight, height, skin-fold thickness, fat biopsies (subset only) and dual energy x-ray absorbance (DEXA)(subset only). Additionally, DNA extracted from

blood samples is stored and is genotyped using genomewide arrays (Illumina Infinium Human Exome Beadchip 12v1 array platform and Affymetrix UK Biobank Axiom Array chip) [79]. Participants are consented to be re-contacted for physiological studies based on their genotype at time of initial enrolment.

### 2.2.2 Recruitment of healthy volunteers

To identify carriers of variants of interest genotype array data was interrogated. If the SNP of interest was not present and could not be confidently imputed then direct allelic discrimination assays were performed (see below for detail). Once identified, I posted a letter to the participant with a reply slip, prepaid envelope and patient information sheet (PIS) (more detail provided in relevant chapters). I posted a letter to 3-5 controls for every variant carrier identified.

### 2.2.3 Cowden syndrome cohort

Individuals with Cowden syndrome(CS) were identified through collaboration with Dr Lisa Walker (Clinical Geneticist, Oxford University Hospital Trust), Dr Katherine Lachlan (Clinical Geneticist, Southampton University Hospital Trust), and recruitment at the PTEN United Kingdom and Ireland Patient Symposium (https://ptenuki.org/). I presented the details of the study described in Chapter 5 and upon request provided participant information sheets. Participants recruited into the CS arm of the clinical study had the clinical diagnosis of CS, which was confirmed by clinical genetic testing and corroborated by Sanger sequencing on blood samples collected during the study. Diagnostic criteria for CS are provided in Chapter 1.

After the individual with CS expressed interest in the study they were provided a PIS and if still interested a study visit was organised and the volunteer enrolled in the study.

## 2.3 Clinical techniques

### 2.3.1 Blinding and randomisation

Where possible the genotype of volunteers was withheld from clinical staff until the completion of the study. In Chapters 3 and 4, a study intermediary was used to co-

ordinate recruitment of matched volunteers without unblinding of clinical staff. Dr Matt Neville (Scientific Co-ordinator, Oxford Biobank Bioresource) held all genotypic information and provided the name of the volunteers to be recruited without specifying genotype. In Chapter 5 it was not possible to blind participants or clinical staff due to the striking clinical features of CS.

### 2.3.2 Matching

Individuals who carried variants of interest were pairwise matched to non-carriers. Matching was based on the age, sex and body mass index (BMI). To facilitate blinding and avoid investigator bias, Dr Matt Neville (Scientific Co-ordinator, Oxford Biobank Bioresource), performed all matching based on criteria I provided him. The matching was performed to remove the effects of confounders on the outcome of interest.

### 2.3.3 Oral glucose tolerance test (OGTT)

The OGTT is a dynamic measure of glucose absorbance and elimination. It allows assessment of various homeostatic mechanisms that contribute to elimination of glucose from the blood. These include but are not limited to the assessment of glucose, insulin, and various other postprandial hormones. Additionally, various indexes of beta-cell function and insulin sensitivity can be derived from the OGTT. These indexes are well validated against the gold standard clamp studies [**227**, **226**, 32]. As discussed in Chapter 1, the OGTT is used clinically to diagnose T2D [7].

In Chapters 4 and 6 the OGTT was used to assess postprandial homeostatic mechanisms. In these chapters, a 75g pre-packaged WHO approved glucose load was given to study volunteers over 5 minute [7]. This was administered following a 12 hour fast. The use of a 5-minute administration was chosen as it is suggested (Dr Filip Knop, University of Copenhagen, personal communication) that this may prevent reactive hypoglycaemia in extended OGTTs which occurred in our pilot studies. The blood sampling protocol was different between Chapter 4 and 6, therefore this will be discussed within these chapters.

### 2.3.4 Matched isoglycaemic clamp

The matched isoglycaemic clamp is the gold standard measurement of the incretin effect [**229**, 16]. The incretin effect is the augmentation of insulin secretion by peptides released from the gut [16]. The isoglycaemic clamp is a two-day study. Study day 1 comprises a frequently sampled (every 5 minutes) OGTT which quantifies the total insulin response (stimulation by blood glucose elevation and stimulation by gastrointestinal released peptides). The sampling frame used in Chapter 4 was 4 hours to ensure the entire effect was captured. Day 2 comprises a variable intravenous infusion of 20 percent glucose to re-produce the same glucose profile as on study day 1 **(figure 2.1)**. This quantifies the stimulation of insulin secretion by blood glucose elevation alone. Subtraction of the insulin response during intravenous glucose infusion from insulin response during the OGTT allows the quantification of the incretin effect. This is usually expressed as a percentage and contributes 50-60 percent of the total insulin response[16]. On both study days a 15ml sample was drawn at -15, 0,15, 30, 45, 60, 90, 120, 180, 240 minutes following glucose administration. These samples were split into a serum tube, lithium heparin tube and EDTA plasma tube with DPP-IV inhibitor (details provided later in this chapter)[80].

The two study days were separated by no less than 7 days to ensure the first study did not impact on the second study. During study day 2, two cannulas were inserted. An antegrade cannula was inserted in the antecubital fossa for glucose delivery and a retrograde cannula was inserted into the dorsum of the contralateral hand for blood sampling. Blood was sampled and the glucose concentration measured every 5 minutes during the OGTT and the matched isoglycaemic clamp to allow precise matching. The HemoCue Glucose 201+ System (HemoCue, Ängelholm, Sweden), which measures blood glucose via the glucose dehydrogenase method, was used to perform the real-time blood glucose concentration on a single drop of whole blood.

### 2.3.5 Euglycaemic hyperinsulinaemic clamp (EUH clamp)

This is considered the gold standard measure of insulin sensitivity [82]. This study was performed with the assistance of two nurses, Sarah White (Research Nurse, University of Oxford) and Rachel-Craven Todd (Research Nurse, University of Oxford). A one-step

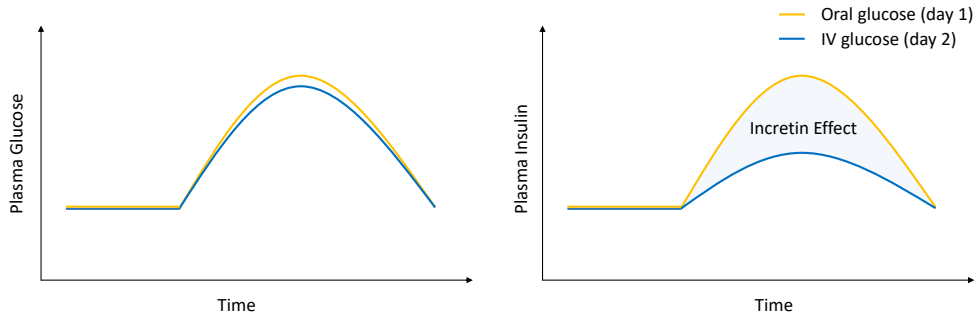


**Figure 2.1: Isoglycaemic Clamp** This figure demonstrates the measurement of the incretin effect. In the left panel the isolgylcaemic glucose profile of the OGTT and matched clamp are demonstrated and on the right the corresponding plasma insulin concentration that results from IV vs oral glucose loads. The difference between the two insulin responses despite the same glucose concentration is termed the incretin effect [81].

EUH Clamp was performed. The protocol was based on that described by DeFronzo et al [**3**, 82]. The participant attended the CRU following a 12 hour fast. An antegrade cannula was inserted in the right cubital fossa for delivery of 20 percent glucose and insulin delivery. A retrograde cannula was inserted into the dorsum of the contralateral hand for sampling of arterialised blood (as described above). The protocol included an initial 10 minute priming phase before steady state infusion was established based on estimated body surface area (derived from height and weight). This aimed to raise the serum insulin concentration by approximately 100uU/ml. The steady state insulin infusion was determined using the formula [Insulin Infusion rate (mU/minute) = 40mU/body surface area (m2)]. A concurrent variable glucose infusion was administered from 4 minutes until after completion of the study at 120 minutes to enable the blood glucose concentration to be clamped at 5mmol/L.

From the glucose infusion rate and the plasma insulin concentration the insulin mediated glucose uptake was calculated.

### 2.3.6 Biopsies

I biopsied adipose tissue from the gluteal and the abdominal regions of an individual with a mosaic *PTEN* mutation (discussed in Chapter 6). Biopsies were performed after a 12 hour fast and again 2 hours after the 75g oral glucose load [50]. The second biopsy was performed on the contralateral side to the initial biopsy. All biopsies were performed

under local anaesthetic. Ms Jane Cheeseman (Research Nurse, University of Oxford) supervised all biopsies. A 14 gauge Sterican needle attached to a 50ml syringe was inserted into the relevant adipose tissue deposit and suction applied as the needle was drawn through the fat deposit to remove a small volume of adipose tissue[50]. Samples were cleaned (via irrigation with sterile water over filter paper), wrapped in aluminium foil, labelled, and snap frozen in liquid nitrogen before being stored at -80 °C[50].

Muscle biopsy was performed by Professor Fredrik Karpe (University of Oxford). I assisted with tissue collection and sample preparation. I separated the muscle tissue from surrounding tissue. The sample was then weighed wrapped it aluminium foil, labelled, and snap frozen in liquid nitrogen before being stored at -80°C.

### 2.3.7 Brown adipose tissue activation

Participants attended the CRU fasted for 12 hours, where they changed into a hospital gown. A large bore cannula inserted in the antecubital fossa to allow blood sampling during the study. Surface anatomy was marked with metallic dots, to facilitate image interpretation. A water jacket was then applied at 36.5 degrees to maintain a thermal neutral temperature in study participants. The participants then reclined at approximately a 45 degree angle for 45 minutes. The jacket temperature was then set to 25°C. The jacket temperature was then reduced by 1 °C / minutes until 4°C was reached. This was maintained for 71 minutes (total cold exposure time of 90min). If the volunteers began to shiver it was deemed that maximal BAT activity had occurred and the temperature was increased by 3 degrees to abort shivering. This temperature was maintained for the remainder of the study unless participants again began to shiver. If the participant began shivering again the temperature was increased by a further 3 degrees. This process was continued until 90 min.

### 2.3.8 Indirect calorimetry

Indirect calorimetry was performed using the Europa Gas Exchange Monitor (GEM Nutrition Ltd, Cheshire, UK)[83]. The GEM is an open circuit gas exchange machine, where a pump draws in expired air from a ventilated hood. The measurement of oxygen and carbon dioxide concentration and flow rate allows determination of the oxygen

consumption and carbon dioxide production[83]. Using the modified Weir equation, EE(kcal) = 1.44(3.9VO2 +1.1VCO2), energy expenditure and respiratory quotient were derived [84]. From these values, fatty acid oxidation and carbohydrate oxidation were calculated [84]. The following equations were used;

- RQ= VCO2/VO2
- Protein Oxidatation (g/day) = 0.15 x REE) / 16.74
- Carbohydrate Oxidation (g/day) = [(4.55 x VO2 -3.21 x VO2) x1.44/Protein oxidation]
- Fat Oxidation (g/day) = [(1.67x VO2- 1.67 x VCO2) x 1.44] – 0.307 x Protein oxidation]

### 2.3.9 Infra-red thermography

Infra-red thermography was performed using the FLIR T450sc (FLIR Systems, Wilsonvile, USA). The FLIR T450sc was used to detect the temperature profile of the neck and upper thorax of study participant. The skin temperature in anatomical areas known to overlie BAT deposits was measured by FLIR T450sc using an uncooled microbolometer. Temperature measurement is achieved as the electrical resistance of the microbolometer is altered by infra-red light allowing calculation of the heat of the object at a given distance and emissivity. The distance of 1 metre was used for all investigations and the emissivity (the amount of infra-red light emitted at a given temperature) was set to standard value for skin (0.98$\varepsilon$). Images obtained were analysed using the FLIR Research IR Program (FLIR Systems, Wilsonvile, USA). Regions of interest were drawn based on anatomical landmarks and the compared to a reference region (sternum) **(figure 2.2)**. For detail of the FLIR T450sc use see Chapter 5. To ensure consistent head position I constructed a head rest using sponge (Tesco PLC, Welwyn Garden City, United Kingdom) and duct tape (Tesco PLC, Welwyn Garden City, United Kingdom). When in the head rest, volunteers' necks were extended and rotation minimised by the supporting sponge. For studies the head rest was covered with a pillow for hygiene reasons.

Aluminium foil was cut into 0.5cm$^2$ sections and placed over easily identifiable surface anatomy to allow images to be reproducibly analysed. Aluminium was fixed to skin using double sided adhesive tape. The right panel is an example of the raw image produced

by the thermal camera. Each pixel has a temperature. The aluminium foil can be clearly seen on the image. Aluminium foil was used as a marker due the large difference in emissivity of metal compared to skin, creating contrast on the thermographic image.

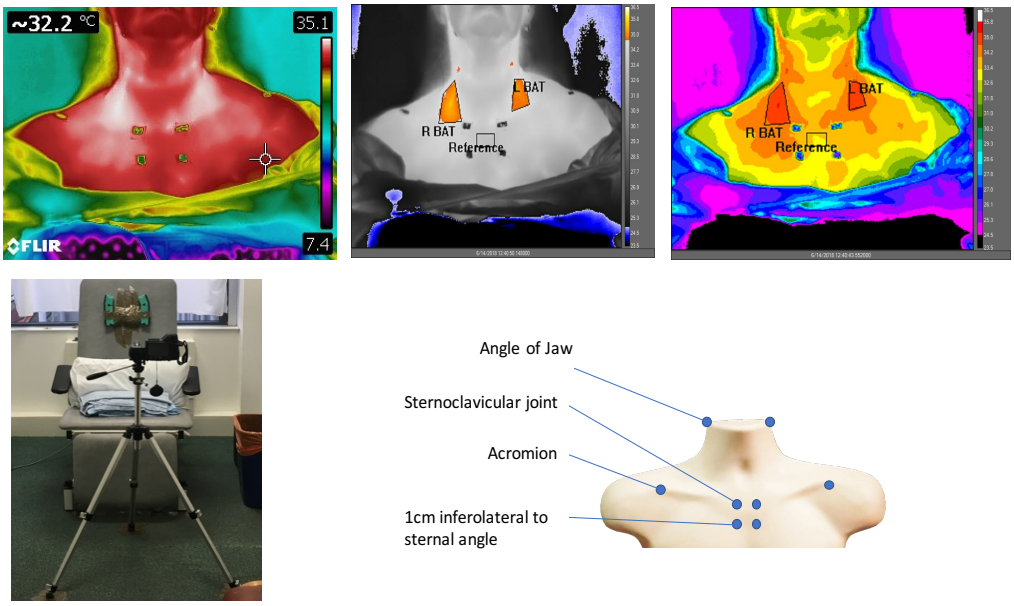


**Figure 2.2: Surface Anatomy Markers and Sample Infra-red Thermography Image.** This figure demonstrates the setup and analysis techniques used to thermographically assess BAT. The top left panel demonstrates an example of a the raw image and the visulaisation of markers on the thermal image. The middle panel demonstrates the "fire and ice" function of FLIR IR software, which highlights the hottest 5% of pixels. The top right panel demonstrates a 20 tone heat map. The physical set up is demonstrated in the bottom left panel, note the floor was marked to ensure the same distance (1m) was used for all studies. The bottom right panel demonstrates the location of surface anatomy markers.

## 2.4 Sample collection, storage and analysis

### 2.4.1 Blood sampling

Two techniques for blood sampling were employed for work contained in this thesis. Blood was drawn from either an anterograde cannula inserted into the antecubital fossa or from a retrograde cannula inserted into the dorsum of the hand. Retrograde cannulation was combined with the heated hotbox technique to arterialise venous blood [85]. This technique was employed when precise blood glucose concentration was required or when there was the possibility of substantial removal of glucose between the arterial and venous systems (e.g. hyperinsulinaemic-euglycaemic clamp).

Prior to blood sampling, 5 ml of blood was drawn to prevent dilution from previous flushes. The sample was then drawn and placed into either a serum, lithium heparin or plasma EDTA tube. In instances where GLP-1 measurement was undertaken 0.01 ml of 1 mM val-pyr (DPP-4 inhibitor) solution per ml of blood was added to the EDTA tubes. Tubes were stored frozen until blood collection [86].

In the case of plasma, samples were taken in chilled tubes and transferred on ice to be spun immediately. Serum was stored at room temperature in collection tubes for 30 minutes to allow blood to clot and was then centrifuged. Samples were centrifuged for 15 minutes at 3000 RPM and 4°C. Plasma and serum was then aliquoted and stored at -80°C.

Samples were logged into the Sapphire and the OWL sample storage systems and stored in accordance with the Human Tissue Act.

### 2.4.2 Glucose measurement

Glucose was measured through two methods, point of care measurement from whole blood using the Hemacue (described above) and on the Ilab 650 Analyser (Instrumentation Laboratory Ltd, Warrington, UK).

### 2.4.3 Insulin measurement

Serum insulin concentrations were determined using the Human Specific Insulin RIA Kit (EMD Milipore, Billerica, USA). Samples were analysed in duplicate. When samples were discordant (difference >20%), a third measurement was performed. Results were determined using a standard dilution curve of a known concentration of human insulin. A set of quality control sample of known concentration (low, medium and high) insulin were included at the start and end of each run. Each run held approximately 200 samples. I performed approximately 50% of the insulin assays with Ms Marjorie Gilbert (Research Technician, University of Oxford), Ms Amy Barrett (Research Technician, University of Oxford) and Ms Catriona Charlton (Research Technician, University of Oxford) analysing the other 50%. As per the protocol provided by Millipore, 100uL of serum was combined with 100uL of assay buffer, 100uL of I125 radiolabelled human insulin tracer, and 100uL of Human insulin tracer. This was vortexed, covered with cling film and left to incubate for 24 hours. 1.0 mL of precipitating agent was then added before the mix was again

vortexed and left to incubate for 20 minutes at 4°C. The mix was then centrifuged at 2000G at 4°C. The mix was then decanted into the radiation sink before the tubes with pellets at the bottom were counted on the gamma counter. Automatic calculation of the insulin concentration based on the I125 counts and a standard curve was performed by the Wizzard2 Gamma Counter (Perkin Elmer, Waltham, USA).

### 2.4.4 PAM serum activity assay

A radioisotope based kinetic assay was adapted from Mizuno et al [87]. Details on the choice of design and validation of the protocol are presented in Chapter 3. A brief overview is presented here.

A mastermix with all co-factors at optimum concentration was made. This included 0.5 mM Ascorbate and 4.0 µM CuSO4 (two required co-factors for PAM), 0.5 µM Ac-Tyr-Val-Gly (unlabelled precursor), 20,000 DPM I125- Ac-Tyr-Val-Gly (labelled precursor), 150 mM Na MES (pH5.5) (the optimum pH for PAM activity), and 0.1 mg/ml Catalase (to scavenge reactive oxygen species). Details on solution preparation are presented below. 50µL of mastermix was combined with 4µL of serum. This was then incubated at 37°C for 1 hour. The reaction was then stopped by transferring the samples into an ice bath and adding 5µL of 0.5 mM EDTA pH 8.0. The total amount of I125 was then determined by counting each sample for 5 minutes on the Wizzard2 Gamma Counter (Perkin Elmer, Waltham, USA) using the raw counts program. I then extracted the amidated fraction by adding 700 µL of fresh water-saturated ethyl-acetate and vortexing for 5 seconds. This dissolved the amidated product of PAM but not the unamidated product. As ethyl acetate containing the amidated product separated into a different phase from the mastermix (the upper phase), 350µl of the top phase was place this into a new RIA tube. The decay/minutes in the tube were then measured in the gamma counter. The amidation activity was then determined using the equation below **(figure 2.3)**.

$$\text{PAM Activity} = \frac{(2\times\text{amidated dpm}) - (2\times\text{blank dpm})}{20{,}000\ \text{(or average total counts)}} \times \frac{5000(\text{substrate in pmol})}{1\ \text{(time in hrs)}} \times \frac{1}{4\ \text{(vol serum uL)}}$$

**Figure 2.3: PAM Activity Equation.** Note: Enzyme activity is calculated in picomoles per microliter per hour using the equation.

### 2.4.5 Extraction of DNA

Two techniques for DNA extraction were used to generate the data presented in this thesis. For adipose and muscle tissue the GenElute Mammalian Genomic DNA Miniprep Kit (Sigma-Aldrich, Gillingham, UK) was used (see below for detail). For whole blood and buffy coats the Maxwell 16 (Promega Corporation, Madison, USA) was used (see below for detail).

### 2.4.6 Extraction of DNA from blood

After centrifugation (described above) the leukocyte enriched layer of "buffy coat" was separated from the plasma and red cells. The entire buffy coat ( 500 uL) was then inserted into the Maxwell 16(Promega Corporation, Madison, USA). The Maxwell is an automated DNA extraction system that uses preprepared cartridges to lyse, wash and elute DNA. Key to this process is the presence of paramagnetic beads which enhance DNA capture. The Maxwell was set to DNA, Buffy Coat and volume of 500µL. Two cycles using 600µL of the elution buffer (Promega Corporation, Madison, USA). Once extracted the DNA was stored at 4°C until sequencing or genotyping could be performed. The samples were stored in barcoded and trackable tubes and DNA quality and quantity checked using a spectrophometer.

### 2.4.7 Extraction of DNA from adipose and muscle tissue

I used the GenElute Mammalian Genomic DNA Miniprep Kit for DNA extraction from adipose and muscle samples (Sigma-Aldrich, Gillingham, UK). The protocol was provided by Dr Feng Chih Kuo (DPhil Candidate, University of Oxford). Samples of snap frozen adipose and muscle tissue were thawed on ice before being homogenised to assist in lysis. Tissue was then placed in a 1.5ml microfuge tube and combined with 180µL of lysis solution T (Sigma-Aldrich, Gillingham, UK), and 20µL of Proteinkinase K (Sigma-Aldrich, Gillingham, UK). The sample was then vortexed and placed in a water bath at 55 °C for 3 hours. Samples were vortexed intermittently to assist with lysis. If the sample was not homogenous at 3 hours, the sample was left to incubate for a further hour. Following

incubation 200µL of lysis solution C (Sigma-Aldrich, Gillingham, UK) was added to the lysate and vortexed. This was incubated at 70 °C for 10 minutes.

The column was then prepared by adding 500µL of column preparation solution to the GenElute Miniprep Binding Column (Sigma-Aldrich, Gillingham, UK). 200µL of 100% ethanol was added to the lysate and vortexed. The lysate was then applied to the column, then centrifuged at 6500G for 1 minute. The column was then washed twice with Wash Solution (Sigma-Aldrich, Gillingham, UK), this was achieved by adding 500µL of Wash Solution and centrifuging at first 6500G and then 12,000G. 200µL of Elution Solution (Sigma-Aldrich, Gillingham, UK) was then added to the column, incubated for 5 minutes at room temp and then centrifuged at 6500G. This was performed twice to maximise DNA elution.

### 2.4.8 Quantification of DNA

I used the ThermoScientific NanodropTM 8000 spectrophometer (Labtech International Ltd, East Sussex, UK) to determine DNA quantity and quality **(figure 2.4)**. The Nanodrop was blanked with nuclease free water prior to sample measurement. Each sample was measured using the standard protocol. The concentration (ng/µL), 260/230 ratio, and 260/280 ratio were exported.

## 2.5 Allelic discrimination assay design

Allelic discrimination assays were performed to identify carriers of genetic variants at rs35658696 and rs78408340. The genomic sequence surrounding these two location was submitted to LGC Genomics (LGC Limited, Middlesex, UK) and a bespoke oligonucleotides were synthesised with a flurophore attached to 5' end and a quencher attached to the 3' end.

Allelic discrimination genotyping is based on the principle that when a probe (oligonucleotide with quencher and flurophore) is the complement of the template DNA, it will bind. As Taq polymerase extends the primer, the quencher and flurophore will be cleaved. The loss of proximity of the quencher and flurophore results in emission of a certain wavelength which is then associated with the presence of that allele. Analysis

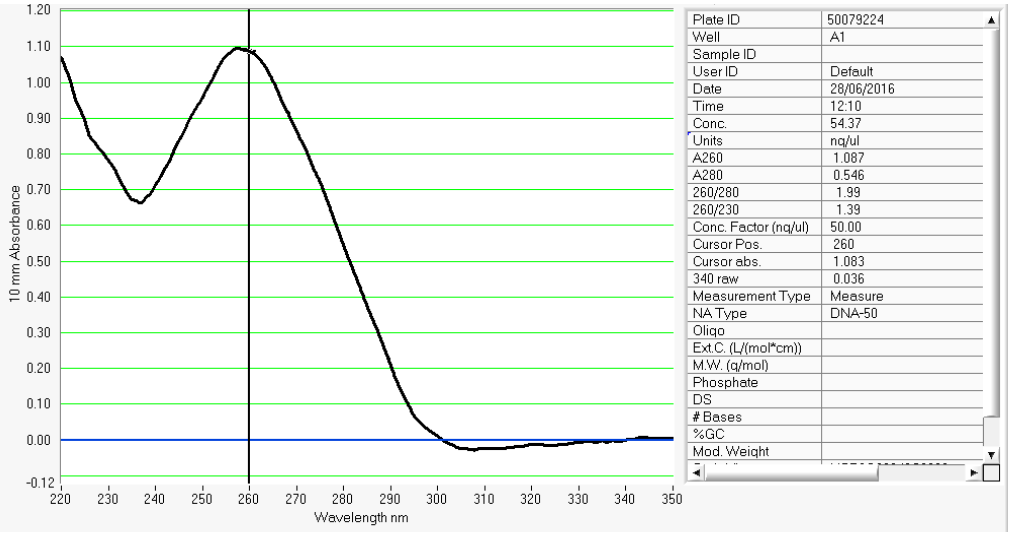


**Figure 2.4: Quantifying DNA concentration and quality using a spectrophotometer**This is a typical graph generated by the Nanodrop spectrophotometer. It is a graph of absobance across different wavelengths. This graph was generated whilst quantifying the amount of DNA present following extraction from a buffy coat. It demonstrates a peak at a wavelength of 260nm suggesting minimal RNA contamination and good quality DNA.

was performed using Sequence Detection Systems version 2.3.2 (Applied Biosystems, Foster City, United States). When using this technique (and if the minor allele is at high enough frequency) three clusters will form, common homozygotes, heterozygotes and rare homozygotes **(figure 2.5)**.

### 2.5.1 Medium throughput genotyping

DNA for medium throughput genotyping was provided by the Oxford biobank, GoDARTS and DIRECT Consortia in a 384 well format. DNA was stored by these cohorts in the form of a stockplate. DNA for a single-plex PCR reaction was transferred to 384 well PCR plate. This involved transferring 2µL of DNA from the stock plate to a PCR compatible plate and then drying down the DNA on a thermocycler. A reaction volume of 4µL per well with a 1.95uL of sterile water, 0.05µL of bespoke assay (LGC Limited, Middlesex, UK), and 2µL of HighROX mastermix (LGC Limited, Middlesex, UK) was used. To facilitate medium throughput genotyping I used epiMotion® 5075 TMX Liquid handling system (Eppenorf Limited, Strevenage, UK) to automate pipetting. Once the mastermix was combined with dried DNA, I sealed the plate and performed a PCR using a Tetrad PTC225

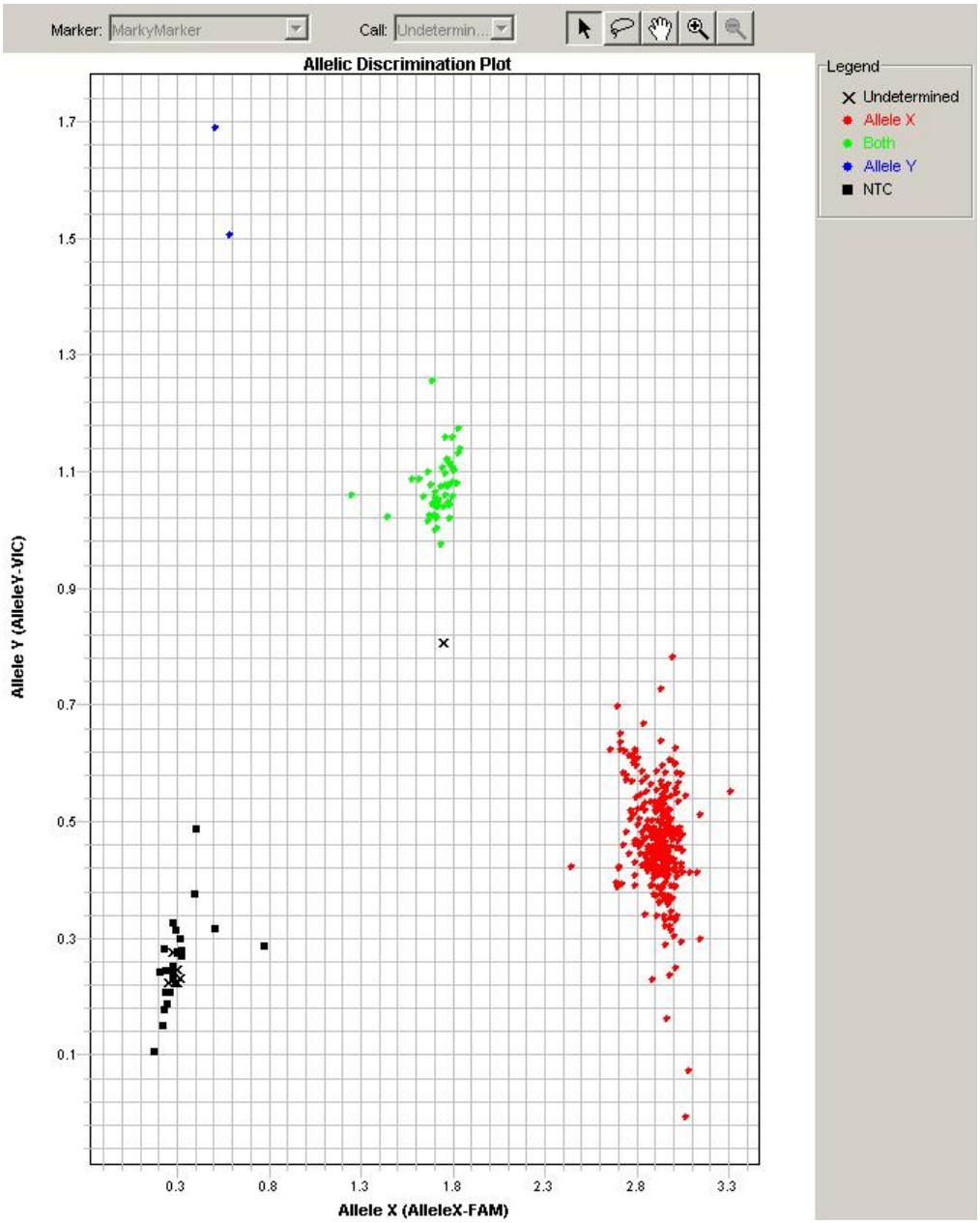


**Figure 2.5: Allelic Discrimination Cluster Plot].** This is a typical screen shot of the clustering observed when the intensity of light at the wavelength associated with VIC and FAM are graphed. In this example, blue circles indicate rare homozygous carriers of the risk allele at rs35658696, green circles indicate heterozygotes, and red circles indicate homozygous carriers of the protective allele. Black squares represent non-template controls and black crosses indicate samples that were a genotype call could not be made.

thermocycler (MJ Research, Waltham, United States). I used the Taqman program KAS 6155X setting (details below).

**KAS 6155X Program details;**

1. 94°C for 15 min
2. 94°C for 20 sec,
3. 61°C for 45 sec,
4. repeat step 2-3 nine times, reduces temperature by 0.6°C/cycle,
5. 94°C for 10 sec,
6. 55°C for 45 sec,
7. repeat steps 5-6 34 times.

## 2.6 Sanger sequencing

### 2.6.1 Primer design

Primers were designed to facilitate amplicon based bi-directional Sanger sequencing. In the case of SNPs in *PAM* (Chapter 3 4), this was used to confirm genotyping results by sequencing only the gene region containing the nucleotide of interest. In the case of *PTEN*, I sequenced all 9 exons of *PTEN* to excluded additional coding mutations as well as confirm reported mutations and exclude *PTEN* mutations in controls.

Primers for *PAM* were designed using Primer 3 under the supervision of Dr Amanda Bennett (Postdoctoral Research Scientist, University of Oxford). The sequence with the nucleotide of interest was entered into Primer 3 and a series of possible primer pairs were suggested by the program. A pair was chosen based on similar melting temperatures and GC content. An M13 tail was included to allow the use of universal sequencing primers. The nucleotide sequence of the amplicon generating primers and the sequencing primers is listed in the relevant chapters. Optimisation of conditions is presented in Chapter 3.

Published primers for *PTEN* were used for sequencing of all *PTEN* exons [50]. Prior to ordering the oligonucleotides, an *in silico* PCR was conducted for al primer pairs using the UCSC genome browser. All primer pairs generated PCR product in silico except for exon 9. A single nucleotide error was noted in the published oligonucleotide sequence.

However, given the success documented in the literature the primer was used despite the error. The *in silico* analysis also allowed the size of PCR product to be determined.

PCR protocols varied between chapters and are therefore discussed within the relevant chapters.

To allow visualisation of PCR products, two percent agarose gels were prepared by combining 3g of DNA grade Agarose (VWR International Ltd, Lutterworth, United Kingdom) and a solution of Electrophoretic Sequencing Grade TBE (0.445mM Tris Borate pH 8.3 + 10mMNaEDTA pH) (Geneflow Limited, Staffordshire, United Kingdom). 5µL of Ethidium Bromide (Sigma-Aldrich, Gillingham, UK) was added to the agarose gel to allow visualisation. Once set, the gel was loaded into a bath of TBE with and additional 10µL of Ethidium Bromide. 5uL of amplicon was combine with 5µL of Orange G loading dye. An electric current (400mA, 150V) passed through the TBE solution using the BioRad Power PAC 300 (Bio-Rad Laboratories, Hercules, United Stated) for 45min.

Agarose Gels were imaged using the ChemiDocTM MP (Bio-Rad Laboratories, Hercules, United Stated). Images were analysed using Image Lab Version 5.0, build 18 (Bio-Rad Laboratories, Hercules, United Stated).

The PCR product was incubated with 0.5µL of exonuclease I (New England Biolabs, Beverly, United States) and 0.5µL of shrimp alkaline phosphatase (Promega Corporation, Madison, United States), to remove any residual nucleotides. Sequencing primers were combined with cleaned PCR product and sent for commercial sequencing through Eurofins (Eurofins Bioanalytical Services UK, Milton, UK). Results were analysed in Mutation Surveyor (Soft-genetics, State College, USA).

## 2.7 Statistical Analysis

### 2.7.1 Decision to use paired statistical analysis

The decision to use a paired or unpaired T-test was based on the matching strategy employed. For data where individuals of interest were 1:1 pair matched to controls a paired analysis was used. The 1:1 matching of age, gender, BMI allowed the comparison of individuals of similar demographics which likley removed a portion of variation between individuals. As paired T-test measures the mean difference between individual pairs

rather than the difference between the mean of two groups, a paired statistical test better suited to the paired matching design I employed.

# 3
# *PAM* LEGACY DATA

## 3.1 Chapter synopsis

This Chapter describes the physiological characterization of carriers of two alleles (D563G and S539W) in *PAM* that are associated with increased risk of T2D. These alleles were chosen for characterisation as there is robust evidence of association with T2D and there was compelling *in vitro* evidence that these alleles impact beta-cell function. In this Chapter, I use allelic discrimination assays and Sanger sequencing to link these two alleles with existing phenotypic information and stored bio-samples to draw mechanistic insight. First, I will describe the development and validation of an assay to measure serum PAM activity in human serum, and then explore the impact of these alleles on PAM enzyme activity and GLP-1 (an amidated peptide and substrate of PAM important for glucose homeostasis) concentration in stored bio-samples.

## 3.2 Background and rationale

Genome wide association studies have identified over 400 regions of the genome where variation is associated with altered T2D risk [**246**, **8**, **1**, 38]. Translation of this progress into improvements in clinical care has been slow [**196**, 34]. A significant bottleneck in the translation of these signals is understanding the impact on intermediate pathways

that drive beta-cell dysfunction and T2D risk. Characterising these pathways may provide targets for prevention and treatment of disease as well as markers of disease progress.

As discussed in detail in Chapter 1, two independent coding alleles in peptidylglycine alpha-amidating mono-oxygenase (*PAM*) (p.S539W, rs78408340, minor allele frequency (MAF) 1%, OR: 1.47 and p.D563G, rs35658696, MAF 5%, OR: 1.23) alter T2D risk and beta-cell function [**10**, 37]. The *PAM* gene encodes the PAM protein, which is a required enzyme for the amidation of glycine extended peptides [**15**, 52]. The conversion of C-terminal glycine residue to an amide group (amidation) is required for complete biological activity of many hormones, including some that are known to regulate blood glucose concentration (e.g. gastrin, cholecystokinin, and glucagon like peptide 1) [**184**, **236**, **233**, **84**, 60]. Recently *in vitro* studies have shown that PAM deficiency in pancreatic beta-cells results in reduced insulin content and altered dynamics of insulin secretion [59]. This study also noted that carriers of D563G and S539W have reduced expression of plasma PAM protein [59]. This raises the possibility that a reduction in plasma levels of amidated hormones many be contributing to the T2D phenotype.

Glucagon like peptide 1 (GLP-1), a second line treatment for T2D, is itself amidated and interacts with a number of other amidated peptides [**188**, **100**, **84**, 88]. Glucagon like peptide 1 is one of the most important hormones for postprandial glucose control (described in detail in Chapter 1), a parameter that was shown to be abnormal in carriers of D563G and S539W [**10**, 37]. Amidation has been suggested to prolong GLP-1 half-life, which may effect GLP-1 plasma concentration and postprandial glucose control [89]. I hypothesise that individuals carrying T2D-risk alleles in *PAM* have reduced serum amidation activity and altered postprandial GLP-1 concentration, which could explain some of the increased risk of T2D risk.

In this Chapter, I will begin my physiological characterisation of the impact of *PAM* LoF alleles by interrogating existing cohorts, identifying stored samples of carriers of LoF alleles in *PAM* and performing informative assays. Specifically, I will measure serum amidation activity, fasting amidation profile and postprandial GLP-1 concentration.

### 3.2.1 Measurement of PAM activity in human serum

Five methods of measuring PAM activity have been described [**117**, **240**, **232**, 60]. All are based on the principle of measuring the consumption of required substrates or production of amidated peptide or glyoxylate (produced in 1:1 molar ratio with amidated peptide) **(figure 3.1)** [**117**, **240**, **232**, 60]. In the Gloyn Lab, we have previously used colourmetric detection of glyoxylate to measure PAM activity *in vitro* [45]. However, glyoxylate is produced by mammals and is present in serum in the range of 10µmol/L, making it problematic to use this method in human studies[**231**, 90].

Alternative methods, which are more amenable to use in humans, exist and have been utilised successfully [**117**, **240**, **232**, 60]. Measuring the consumption of oxygen, precursor protein, and the production of amidated peptide in serum have been used to measure PAM activity. Methods for the detection of these molecules included high pressure liquid chromatography, oxygen sensors, colourmetric readout, radioimmunoassay and radiotracer analysis. The most widely used in animal studies is radiotracer analysis[56]. This is the most flexible method as it is not substrate specific and requires minimal infrastructure (only gamma counter, fume hood, and water bath). With the exception of radioimmunoassay (which requires development of specific antisera), the radiotracer method is also the most specific. The relative specificity of the different techniques for measuring PAM activity is presented in **(table 3.1)**.

| Method | Specificity (pmol) | Substrate specific | Facilities required |
|---|---|---|---|
| Radiotracer | 0.15 | No | Gamma Counter |
| HPLC | 400 | No | HPLC + UV Detector |
| RIA | 0.005 | Yes | Gamma counter |
| Colourmetric | 600 | No | Spectrophotometer |
| Oxygen consumption | 2500 | No | Oxygen Electrode |

**Table 3.1:** Techniques for measuring amidation activity. Adapted from Kolhekar and colleagues [56], specificity is defined as three times the minimum limit of detection.

### 3.2.2 Principles of the radiotracer method of PAM activity measurement

The radiotracer method was first described by Mizuno and co-authors in 1986 [87]. A small glycine extended peptide is used as a substrate for PAM and combined with required co-factors (ascorbate, copper, and oxygen). A tracer peptide identical to the small glycine extended substrate (except for the addition of an I125 label (or similar) at the N terminus) is added in trace amounts. The biological substance being tested is added to the reaction mix to provide the enzyme. As with all kinetic assays, the enzyme should be the rate limiting factor and all other reagents should be added in excess. The reaction is allowed to proceed at 37°C for a given period of time (dependent on the activity of the sample tissue) before being stopped by reducing temperature, altering pH, or chelating a required co-factor. The radioactive decay products from the radiotracer (which will be in both c-terminally amidated and glycine extend form) are measured. The amidated product is extracted using ethyl acetate. Ethyl acetate will dissolve the uncharged amidated product but not the negatively charged glycine extended precursor. The ethyl acetate separates into an upper phase which can be extracted and counted independently giving a measure of the generation of amidated product. This method was optimised for use in stored human serum and then used to compare serum PAM enzyme activity in heterozygous and homozygous carriers of D563G, and matched non-carriers.

### 3.2.3 Amidation Increases GLP-1 plasma Stability Making it a Potential Mediator of Increased T2D Risk in Allele Carriers

Glucagon-like peptide-1 is an incretin hormone released from L cells in the gut [16]. It is released in response to oral nutrient ingestion and is a potent stimulator of insulin secretion[16]. Of note, GLP-1 increases the insulinogenic index (defined in chapter 1), and a reduction in GLP-1 concentration or action would likely produce a similar glycaemic pattern to that observed in carriers of S539W and D563G [**10**, 16]. In the postprandial setting both amidated and glycine extended GLP-1 are detectable in human plasma [**84**, 86]. However, the amidated proportion predominates [**84**, 86]. It has been report that GLP-1 (7-36) amide and GLP-1 (7-37) Gly are equipotent in binding the GLP-1 receptor

and stimulating insulin secretion [89]. However, examination of the degradation of both forms of GLP-1 in human plasma (ex-vivo) demonstrated that amidation increases the half-life of GLP-1 by approximately one third [89]. This raises the possibility that the plasma concentration of active GLP-1 may be reduced in carriers of *PAM* loss of function alleles. Additionally, *in vitro* PAM knockdown reduces the amount of amidated peptide (chromogranin A) secreted compared to wildtype this suggests that the possibility of reduced secretion of amidated GLP-1 (discussed in Chapter 1)[59]. The focus of this chapter will be on testing the hypothesis that loss of function alleles in PAM alter GLP-1 plasma levels via reduced amidation activity.

### 3.2.4 Opportunities for Examining GLP-1 Concentration in Existing Cohorts

Large cohorts of diabetic and non-diabetic individual exist around the world [**218**, ***69***, **219**, **134**, 91]. Some of these contain information that could provide information important to understanding the mechanisms that underpin increased T2D risk in carriers of S539W and D563G. To utilise this data, phenotypic information needs to be linked to genotypic information. Where array or sequencing data does not cover the SNP of interest, bespoke allelic discrimination assays provide a well validated means of identifying carriers of genotypes of interest[92]. Additionally, this method can be scaled to allow medium-throughput genotyping. This approach was used in combination with existing exome chip data to genotype the Oxford Biobank (OBB), the Family Study and the AdditionPRO (the three cohorts that have been used in this Chapter).

## 3.3 Methods

### 3.3.1 Allelic Discrimination Assay

Allelic discrimination assays were performed to identify carriers of genetic variants at rs35658696 (D563G) and rs78408340 (S539W). The genomic sequence surrounding these two locations was submitted to LGC Genomics (LGC Limited, Middlesex, UK) and bespoke oligonucleotides were synthesised with a flurophore attached to 5' end and a quencher attached to the 3' end.

DNA from the OBB was stamped out into 384 well assay plates. This involved the transfer of 2µL of DNA at approximately 20ng/µL. The DNA was then dried down onto the assay plates using thermocyclers, which were set to 80°C for 10min.

In each well containing DNA, 2µL High Rox Master mix (LGC Limited, Middlesex, UK) was combined with 2µL DNA free water and 0.05µL of oligonucleotide probe (LGC Limited, Middlesex, UK). A PCR reaction was then carried out using the KAS6155X program (detail provided in Chapter 2). The plates were then read on the ABI PRISM 7900HT Sequence Detection System (Applied Biosystems, Foster City, United States) using Sequence Detection System version 2.3.2 (Sequence Detection System). Individuals clustered into carriers of 0,1, or 2 copies of the risk alleles. Clusters were automatically called using SDS 2.3.2 software and confirmed with manual clustering (described in detail in chapter 2). Genotypic information was then linked to the study ID, well number and phenotype. This enabled genotypic information to be linked to existing phenotypic information and the samples of carriers identified for analysis.

### 3.3.2 Sequencing to Confirm Accurate Allelic Discrimination

To confirm that the allelic discrimination assay was correctly identifying carriers of T2D risk alleles in *PAM*, Sanger sequencing was performed on the DNA of 48 individuals who were identified as herterozygous for S539W.

I designed forward and reverse primers under the supervision of Dr Amanda Bennett (research scientist, University of Oxford) **(table 3.2)**.

| Primer | Sequence | Melting Point | FGC Content (%) |
|---|---|---|---|
| *PAM* forward | TGTAAAACGACGGCCAGTGAAT GGTCTGC ATTTCTCAATTTCATT | 71.3°C | 40% |
| *PAM* Reverse | CAGGAAACAGCTATGACCGAGT ACTGCA GCATTATTTGGATCTAT | 72.2°C | 42.2% |

**Table 3.2:** *PAM* primer sequence and characteristics

### 3.3.3 Generation of Amplicon

Deoxyribonucleic acid samples from 48 individuals identified by allelic discrimination as carrying one copy of the T2D risk allele at rs784043840 were picked from the OBB. In each well, 2.5 µL of DNA was combined with 8.45µL of DNA free water, 1.25µL of 10x Buffer, 1.0µL of MgCl2, 0.5µL of primer mix (5pmol/µL of forward and 5pmol/µL reverse primer),1.25µL of 2.5mM dNTPs, and 0.05µL of TAC gold. The plate was then run on the thermocycler on the TAQMAN40 program (10min at 95°C, and then 40 cycles of 15 seconds at 92°C and 60 seconds at 60°C).

The presence of appropriate sized products was confirmed by making a 2% agrose gel and loading PCR product and running at 150V at 400mA for 25min. The products were compared to a ladder of known product size **(figure 3.1)**.

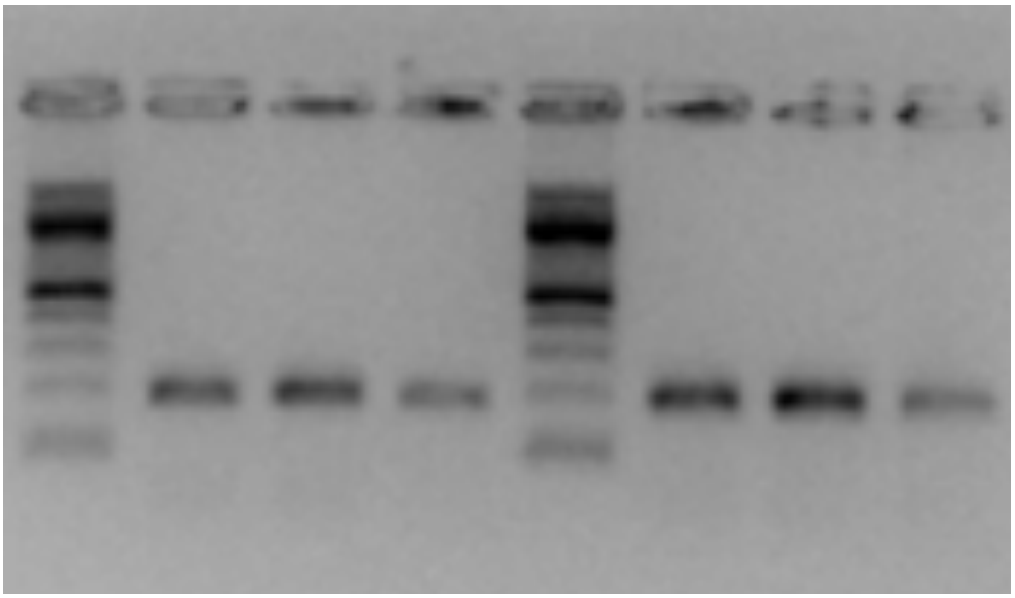

**Figure 3.1: Visualisation of PCR Product**This figure demonstrates bands of PCR product next to a 100 base pair ladder. The bands sit just below the 200 base pairs marker, corresponding to the predicted PCR product weight of 184 base pairs.

The PCR product was then cleaned using 0.5µL of exonuclease I (New England Biolabs, Beverly, United States) and 0.5µL of shrimp alkaline phosphatase (Promega Corporation, Madison, United States). 0.5µL of exonuclease and 0.5µL of shrimp alkaline phosphatase were added to the PCR product and run on the thermocycler using the EXOSAP program (37°C for 30min, and then 80°C for 15min). The cleaned product was then sent to Eurofins

for sequencing. The data from Eurofins was analysed in Mutation Surveyor (Soft-genetics, State College, USA). Forward and reverse sequences were analysed together and a mutation was called if both mutation was identified in both sequences.

### 3.3.4 PAM Serum Activity Assay

A radioisotope based kinetic assay was adapted from Mizuno et al [87]. Whilst the optimal concentration of co-factors for PAM activity are well documented in the literature, the adaption of the assay for use in human serum is not described. Trial of various serum concentrations and lengths of incubation were conducted. The optimum protocol is presented below and the validation of this is presented in the results section.

All required co-factors at optimum concentration were combined. This included 0.5 mM Ascorbate and 4.0 µM CuSO4 (two required co-factors for PAM), and Oxygen was provided by leaving the reaction mix open to air.

Unlabelled and labelled precursor glycine extended peptide was added to the master-mix to provide substrate and the ability to track enzyme activity. To minimise radiation use, unlabelled precursor peptide in addition trace amounts of labelled precursor peptide was added to the mastermix. Previously, a concentration of 0.5 µM Ac-Tyr-Val-Gly was used in pulverised tissue PAM assays and this concentration had provided sufficient substrate to ensure it was not the rate limiting factor [56]. I125- Ac-Tyr-Val-Gly at a concentration of 5,000 DPM per µL was added to the mastermix.

To bring the mastermix to optimum pH, 150 mM Na MES (pH5.5) was added. In contrast to other protocols, a second buffer was not used, since optimum pH can be achieved with a single buffer. Further to this, *in vitro* assays have been performed in the Gloyn lab using only a single buffer with good effect [59].

To scavenge reactive oxygen species 0.1 mg/ml Catalase was added. Mastermix of 50 µL volume was combined with was combined with 4µL of serum. This was then incubated at 37 °C for 1 hour.

The reaction was then stopped by transferring the samples into an ice bath and adding 5 µL of 0.5 mM EDTA pH 8.0. The total amount of I125 in each tube was then determined by counting each sample for 5 minutes on the Wizzard2 Gamma Counter

(Perkin Elmer, Waltham, USA) using the Raw Counts Program. The amidated fraction was then extracted by adding 700 µL of fresh water-saturated ethyl-acetate and vortexing for 5 seconds. This dissolved the amidated product of PAM but not the unamidated product. As ethyl acetate containing the amidated product separated into a different phase from the mastermix (the upper phase), 350 µl of the upper phase was transferred into a new RIA tube. The decay/minutes in the tube were then measured in the gamma counter. The amidation activity was then determined using the equation below **(figure 3.2)**.

$$\text{PAM Activity} = \frac{(2\times\text{amidated dpm}) - (2\times\text{blank dpm})}{20{,}000\ \text{(or average total counts)}} \times \frac{5000(\text{substrate in pmol})}{1\ \text{(time in hrs)}} \times \frac{1}{4\ \text{(vol serum uL)}}$$

**Figure 3.2: PAM Activity Equation**Note: Enzyme activity is calculated in picomoles per microliter per hour using the equation.

This assay was used on the stored serum of heterozygous and homozygous carriers of D536G in the OBB (details of the OBB found in Chapter 2) and matched controls. All matched pairs were included in the same assay batch to minimise batch effects. All samples were measured in triplicate. A curve of 0%, 25%, 50%, 75% and 100% recombinant PAM was included in all assays and provided assurance that the assay has a dose response effect. When comparing between genotypes, samples were normalised to wildtype.

### 3.3.5 Analysis of Fasting GLP-1 Amidation Profiles

The OBB has stored fasting plasma samples available for most of the approximately 9000 participants. Having identified carriers of the T2D risk allele S539W using as allelic discrimination assay, stored plasma samples from these individuals and age, gender and BMI matched controls had GLP-1 7-36 amide and GLP-1 7-37 Gly measured. I chose to measure GLP-1 profiles in carriers of S539W rather than D563G as it has the greater impact on insulinogenic index and T2D risk, it was therefore thought that the impact on GLP-1, if present, would be greatest in carriers of this allele. Currently the only validated method of measuring amidation specific GLP-1 is using an in-house antibody held by the Jens Holst lab. Samples were therefore sent to the Holst lab for analysis. It should be noted that these are fasting samples and are not optimal for assessing GLP-1 action, as GLP-1 main effect is in the post prandial period [93].

### 3.3.6 Analysis of Intact GLP-1, Glucose and Insulin Profiles following OGTT

Intact GLP-1 (active GLP-1 (7-36) amide and inactive GLP-1 9-36 amide), was measured in the Family study at ten time points over four hours and in the AdditionPro study at three time points over two hours (details of cohorts is provided in Chapter 2). In the AdditionPro Study, glucose and insulin data was also available at the three time points [**69**, 94]. Data was provided by the primary investigator, Professor Torben Hansen, University of Copenhagen.

The genotyping assay validated above was shared with our collaborators and the DNA was genotyped for carriers of the rs78408340 (S539W) allele. Data on rs35658696 (D563G) was available as both the AdditionPRO and Family Study had been genotyoed on an exome array that captured this allele [**69**, 94].

In both studies, each PAM T2D risk allele carrier was pairwise matched (age, gender and BMI) to two non-carriers. I decided excluded Individuals with T2D from the study due to concerns that the reduced incretin effect observed in T2D would bias the study [95].

## 3.4 Results:

### 3.4.1 Identification of S539W Carriers

Genotyping was performed to identify carriers of the S539W allele not captured on exome array **(figure 3.3)**. The genotyping failure rate was low, with an average failure rate of less than 1%. For quality control, Hardy Weinberg equilibrium (HWE) and minor allele frequency were also measured. The MAF was in the expected range (MAF = 0.9%) and did not significantly differ from HWE(p=0.52).

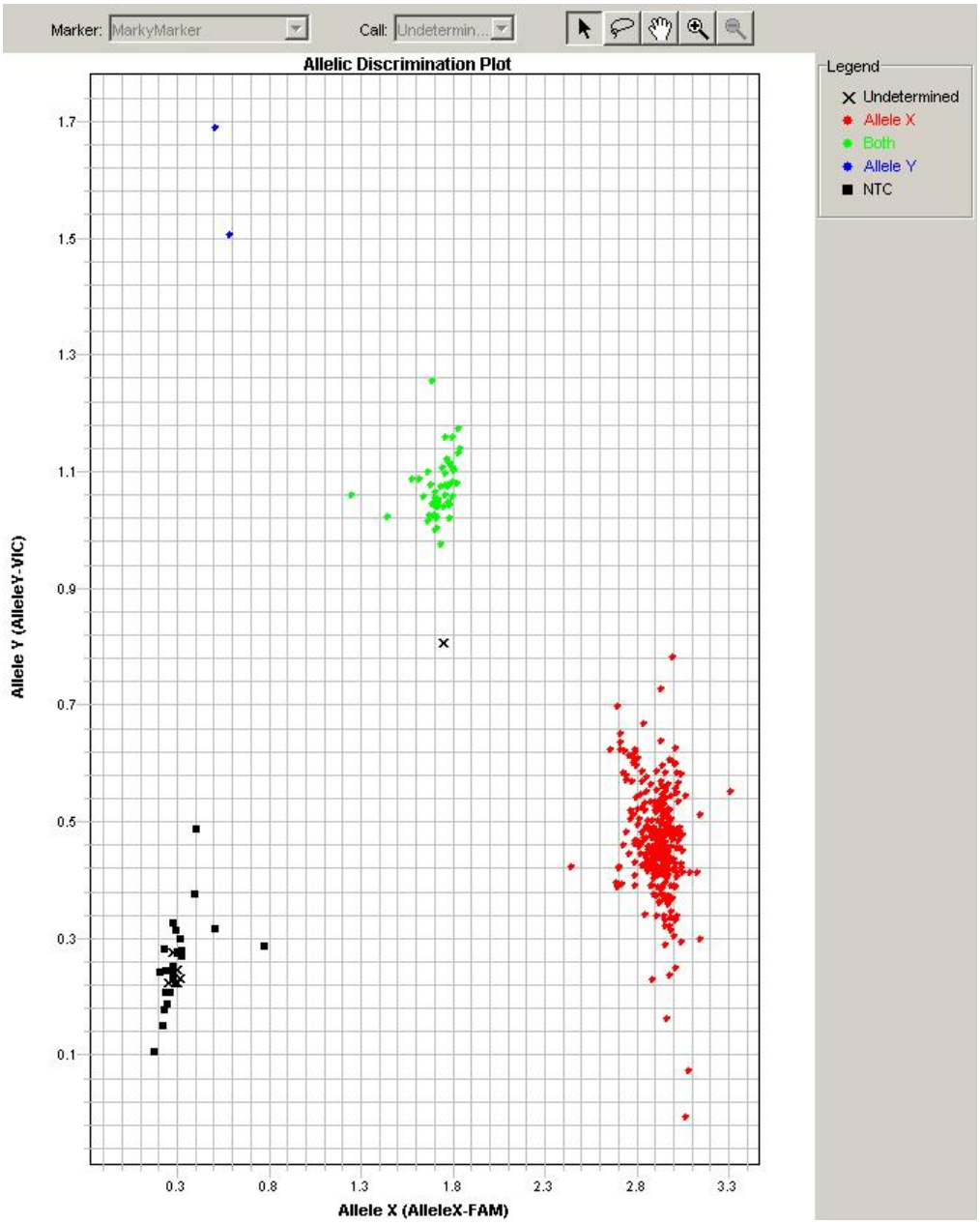


**Figure 3.3: Allelic Discrimination Cluster Plot].** This is a typical screen shot of the clustering observed when the intensity of light at the wavelength associated with VIC and FAM are graphed. In this example, blue circles indicate rare homozygous carriers of the risk allele at rs35658696, green circles indicate heterozygotes, and red circles indicate homozygous carriers of the protective allele. Black squares represent non-template controls and black crosses indicate samples that were a genotype call could not be made.

### 3.4.2 Concordance between sequencing and genotyping

To ensure the allelic discrimination assay was accurately identifying carriers of S539W, a subset of DNA samples identified as heterozygotes of S539W were sequenced. There was a 96% concordance between sequencing and allelic discrimination in the 45 sample selected for sequencing. An example of a typical the electropherogram confirming the genotyping is displayed below **(figure 3.4)**.

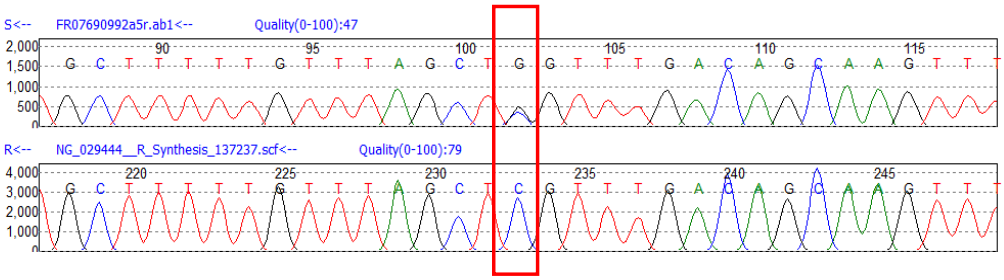


**Figure 3.4: Typical Electropherogram Corroborating Allelic Discrimination.** This is a typical electropherogram generated by Sanger sequencing of 48 samples picked to confirm Taqman allelic discrimination genotyping. The top panel is the sample sequence and the bottom panel is the reference sequence. The red box outlines where a heterozygous mutation has occurred, confirming the genotyping result.

### 3.4.3 Validation of PAM Assay

The radiotracer method for PAM activity was adapted from that proposed by Mizuno and co-authors[87]. Validation that PAM activity was being detected in a dose dependent manner was required. This was assessed by measuring the PAM activity in various dilutions of concentrated wildtype recombinant PAM, generated in-house by Ms S Sengupta (DPhil Student, University of Oxford). Six concentrations were compared: undiluted (100%) recombinant PAM, 75% concentration of recombinant PAM (diluted with water), 50% dilution, 25% dilution, 10% dilution and water (0%).

The assay detected increasing PAM activity with increasing concentration of recombinant PAM **(figure 3.5)**, suggesting the assay was sensitive to changes in PAM activity.

To use the assay confidently on human serum, the ability to detect PAM activity in human serum was also required, ideally within the linear range of the assay. Furthermore, it was important to demonstrate the assay was reproducible, to allow samples to be compared across multiple runs.

Four samples of serum were collected from staff (with consent and ethics approval) and the assay was performed in conjunction with the standard curve. This was repeated on two consecutive days and demonstrated that serum activity was within the linear range of the assay, and that the assay produced consistent results. The intra assay CV was 10.6%. There was some variation from day 1 to day 2, with inter assay CV of 12.4 %. This suggested that a sample of standard concentration or internal controls would be required for the assay to allow normalisation across assay runs.

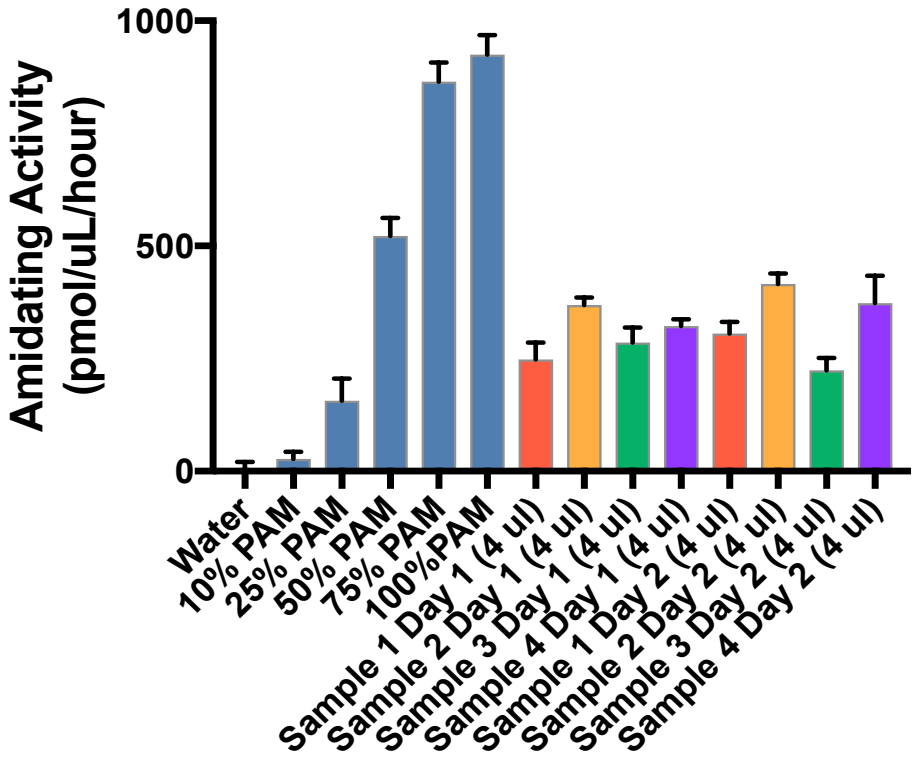


**Figure 3.5: Validation of in-house PAM Serum Activity Assay]**. Figure 3.7 shows the amidating activity of various samples in pmolµl/hr. The samples were measured in triplicate and the mean amidating activity is presented +/- the SEM. The samples in dark blue are a standard curve and demonstrate the assay's ability to detect PAM activity in a dose dependent manner. The remaining samples demonstrate that PAM activity can be detected with the addition of 4µL of human serum, and this result was reproducible the following day. The background radiation has been subtracted from all samples as determined by blank tubes included in the assay run.

### 3.4.4 Serum Amidation activity in carriers of the D563G allele of PAM

Having demonstrated that the assay for PAM serum activity was able to detect variation in re-combinant PAM concentration (and presumably the overall PAM activity of a sample)

and detect activity in human serum, samples of interest were assayed. The stored serum samples of heterozygous and homozygous carriers of D563G were assayed and compared to age, gender and BMI matched non-carriers. All controls were included in the same assay run as their matched pair. Assays were performed in triplicate and the average of the three measurements was taken. The assay was performed blind to the genotypes of samples. Dr Matt Neville (Oxford Biobank) acted as an intermediary supplying the sample IDs of the samples that were to be run, and once the assay had been performed, he supplied the genotypes. A two-tailed paired T-test was used to determine if the difference was significant.

Twenty-seven heterozygous carriers of D563G and 27 matched non-carriers had serum amidation measured in triplicate. The mean amidation activity was significantly lower in the heterozygotes compared to matched non-carriers (300 +/- 11 vs 374 +/- 14, p=0.0008). This represents a 20% reduction in serum amidation activity.

Twenty-one homozygous carriers of D563G and 21 matched non-carriers had serum amidation measured in triplicate. The mean amidation activity was significantly lower in the heterozygotes compared to matched non-carriers (272 +/- 10 vs 472 +/- 17, p= p=$1.4 \times 10^{-9}$). This represents a 38% reduction in serum amidation activity.

The assays demonstrated a substantial and significant reduction in PAM serum activity in heterozygous and homozygous carriers of D563G compared to matched non-carriers. A gene dose effect was observed, consistent with an additive model. Heterozygous carriers of D563G had a 20% reduction in serum amidating activity under the ideal conditions of the assay (p=$8.0 \times 10^{-4}$), whilst homozygous carriers had approximately double that reduction with a 38% reduction (p=$1.4 \times 10^{-9}$) **(figure 3.6)**.

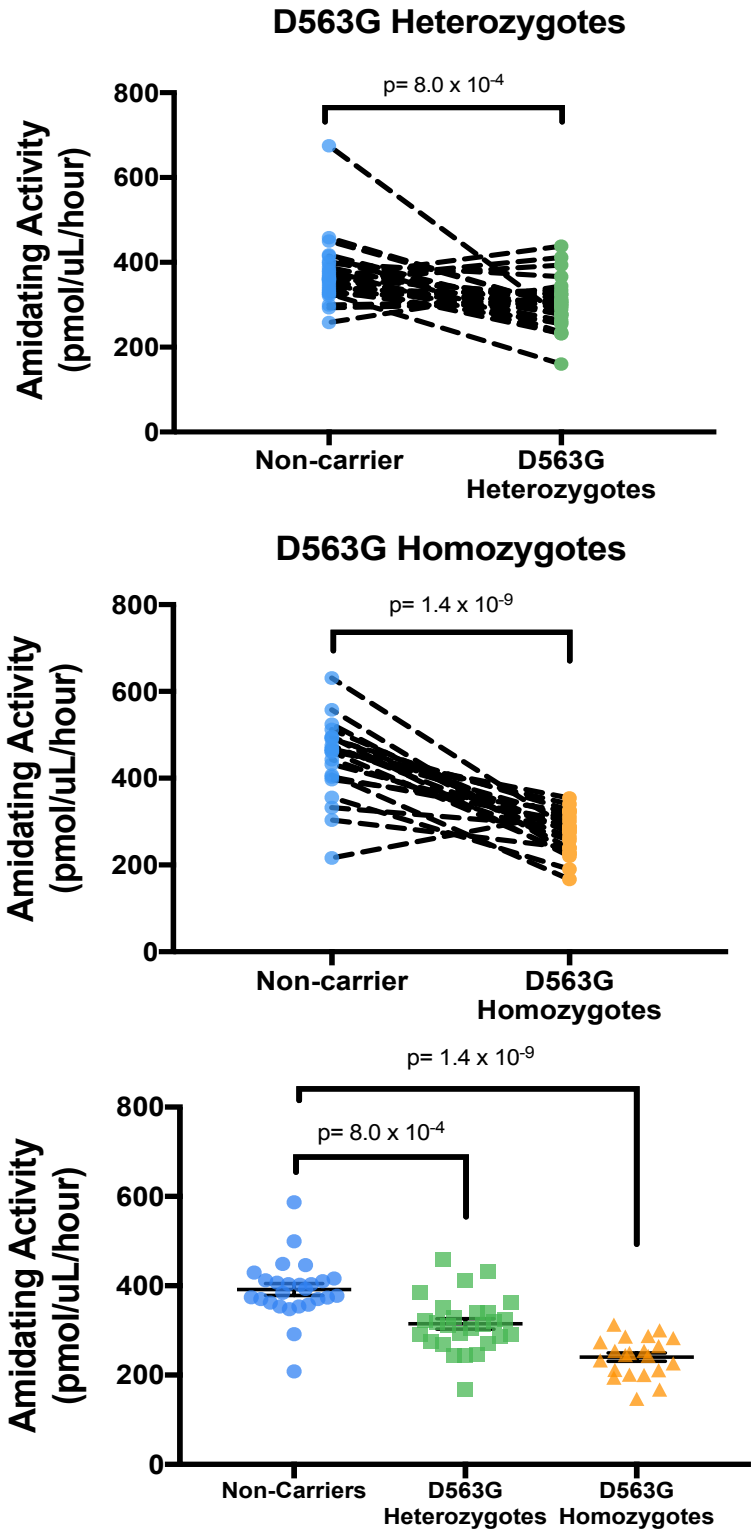


**Figure 3.6: Fasting GLP-1 Amidation Profiles of D536G Carriers and Matched Controls**. This figure demonstrates the reduction in serum enzyme activity in carriers of heterozygous and homozygous carriers of D563G compared to non-carriers (20%, $p=8.0x10^{-4}$), (38%, $p=1.4x10^{-9}$) respectively. Each sample was assayed in triplicate and the mean value has been displayed on the graph. The top two panels demonstrate the raw values and link carriers of D563G to their matched non-carrier. In the bottom figure the data has been normalised to wildtype. Statistical analysis was performed on raw data and utilised a two-tailed paired t-test.

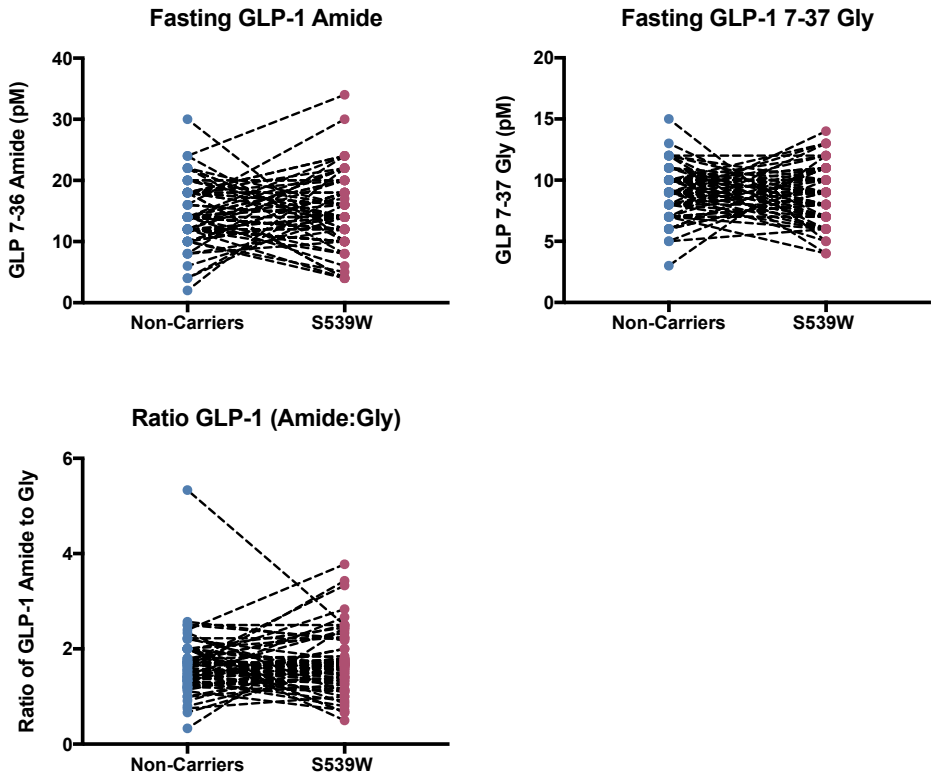


**Figure 3.7: Fasting GLP-1 Amidation Profiles of S539W Carriers and Matched Controls]**. This figure demonstrates the effect of carrying a single copy of the loss of function allele S539W on GLP-1 (7-36) amide, GLP-1 (7-37) Gly and the ratio of GLP-1 7-36: 7-37. Non-carriers are represented by blue circles, S539W carriers are represented by red circles and matched pairs are linked by a dotted line. A two-tailed paired T-test was used to determine significance.

### 3.4.5 Fasting GLP-1 amidation profile of S539W

To determine if the reduction in amidating activity observed had an impact on the amidation profile of peptides known to influence blood glucose, plasma GLP-1 (7-36) amide and GLP-1 (7-37) Gly were measured. I decided to measure GLP-1 (7-36) amide and GLP-1 (7-37) Gly plasma concentrations of carriers of S539W rather than D563G given the greater impact this allele has on T2D risk and the more severe impact on protein expression of the S539W allele [**262**, 51]. This decision was made as the assay is expensive and S539W was presumed to be more damaging and would increase the effect size and power of the study (comparison of OR and IGI provided in Chapter 1) [51]. As mentioned above, the OBB stored DNA was systematically genotyped to identify carriers of the rs78408340 risk allele (S539W). One hundred and six individuals in the OBB who carried the S539W allele were identified. Of these individuals, 76 had stored fasting plasma. Glucagon-like pepetide-1 (7-36) amide and GLP-1 (7-37) Gly were measured in the fasting plasma samples of 70 carriers of the S539W allele and 70 pairwise matched (age, sex, and BMI) controls **(table 3.3)**.

| | **Non-carriers** | **Carriers** | **P Value** |
|---|---|---|---|
| **Oxford Biobank: S539W** | | | |
| Number | 70 | 70 | N/A |
| Female / male | 27/43 | 27/43 | 1.0 |
| Age, mean (years) | 41.5 +/- 6.1 | 41.5 +/- 6.1 | 1.0 |
| BMI (kg/m$^2$) | 25.9 +/- 5.0 | 25.8 +/- 5.1 | 0.90 |

**Table 3.3:** OBB S539W Carriers and non-carriers: demographics and matching quality

There was no significant difference in glucagon-like peptide-1 (7-36) amide concentration between carriers and controls **(figure 3.7)**. Additionally, there was no significant difference in glucagon-like peptide-1 (7-37) Gly concentration between carriers and controls **(figure 3.7)**. The ratio of GLP-1 (7-36) amide to GLP-1 (7-37) Gly was then calculated. There was no significant difference in the ratio of GLP-1 (7-36) amide to GLP-1 (7-37) Gly between carriers and controls **(figure 3.7)**. It should be noted that in the fasting state both GLP-1 (7-37) Gly and GLP-1 (7-36) amide are close to the minimum detectable limit of measurement.

### 3.4.6 Intact GLP-1 profile in Family Study and the AdditionPro Study

Having demonstrated that heterozygous carriers of S539W have no difference in GLP-1 (7-36) amide, GLP-1 (7-37) Gly or the ratio between GLP-1 (7-36) amide and GLP-1 (7-37) in the fasted state (amidation ratio), the logical progression is to examine the GLP-1 response in the postprandial setting. Measurement in the postprandial setting is of more physiological interest as the majority of GLP-1 action occurs at this time [16].

In existing data, the intact GLP-1 profiles of S539W and D563G carriers were compared to matched non-carriers following stimulation with an 75g oral glucose load. This comparison was performed in two cohorts (Family Study and AdditionPro). The demographics of the two studies are provided below **(table 3.4 and 3.5)**.

| | Non-carriers | Carriers | P Value |
|---|---|---|---|
| **Family Study: D563G** | | | |
| Number | 48 | 24 | N/A |
| Female / male | 28/20 | 14/10 | 1.0 |
| Age, mean (years) | 38.5 | 37.07 | 0.58 |
| BMI (kg/m$^2$) | 26.4 | 26.5 | 0.92 |
| **Family Study: S539W** | | | |
| Number | 6 | 3 | N/A |
| Female / male | 0/6 | 0/3 | 1.0 |
| Age, mean (years) | 37.4 | 38.2 | 0.83 |
| BMI (kg/m$^2$) | 22.9 | 22.9 | 0.99 |

**Table 3.4:** Family study demographics and matching quality

The intact plasma GLP-1 (7-36 amide and 9-36 amide) concentration was compared in 24 carriers of the D563G and 48 matched controls. At baseline, in support of the observation made from the fasting data generated earlier in the Chapter, there was no significant difference between intact GLP-1 concentration between the groups. Following the oral glucose load, both groups increased their plasma GLP-1 as expected, and reached peak concentration 40min after the glucose load. The peak concentration was significantly higher in the D563G group (19.8 +/- 2.46 vs 13.7 +/- 1.02 pmol/L, p=0.0084) **(figure 3.8)**. This is the opposite direction of effect than was hypothesised, *in vitro* studies suggested a reduction in amidated peptide. Following the peak, both groups plasma GLP-1 concentration reduced to below baseline at 240min. The increment area under the curve (incAUC) was 1.5-fold higher in the D563G group compared to matched non-carriers (1229.9 +/- 126.5 vs 796.8 +/- 88.3pmol.L-1.min, p=0.006) **(figure 3.8)**. In this study, I was powered to detect a difference of 75 pmol.L-1.min.

The intact plasma GLP-1 (7-36 amide and 9-36amide) concentration was compared in 3 carriers of the S539W and 6 matched controls. Again, at baseline, there was no significant difference between GLP-1 concentration between the groups. Following the oral glucose load, both groups increased their plasma GLP-1 concentration as expected, however the S539W group peaked later and at a higher concentration than the control group. Only at one time point (180min) were the two curves significantly different (11.3 +/- 0.67 vs 5.33 +/- 1.61 pg/L, p=0.04). Whilst the incAUC was not significantly different the effects were directionally consistent with those observed in carriers of D563G. Carriers of S539W had a 1.3-fold higher incAUC compared to non-carriers (1,195.8 +/- 83.78 vs 950.4+/- 130.52 pmol.L-1.min, p=0.26) **(figure 3.8)**. This experiment was underpowered to detect an effect with only 3 individuals with the S539W allele being identified. This study was only powered to detect a minimum difference in GLP-1 incAUC of 424 pmol.L-1.min, These observations were utilised to facilitate power calculation for the prospectively designed study presented in Chapter 4.

| | Non-carriers | Carriers | P Value |
|---|---|---|---|
| **AdditionPro Study: D563G** | | | |
| Number | 290 | 145 | N/A |
| Female / male | 142/148 | 71/74 | 1.0 |
| Age, mean (years) | 66.6 | 66.5 | 0.91 |
| BMI (kg/m$^2$) | 27.6 | 27.6 | 1.0 |
| **AdditionPro Study: S539W** | | | |
| Number | 14 | 7 | N/A |
| Female / male | 8/6 | 4/3 | 1.0 |
| Age, mean (years) | 62.7 | 62.8 | 0.95 |
| BMI (kg/m$^2$) | 24.3 | 24.3 | 0.96 |

**Table 3.5:** AdditionPro Study: demographics and matching quality

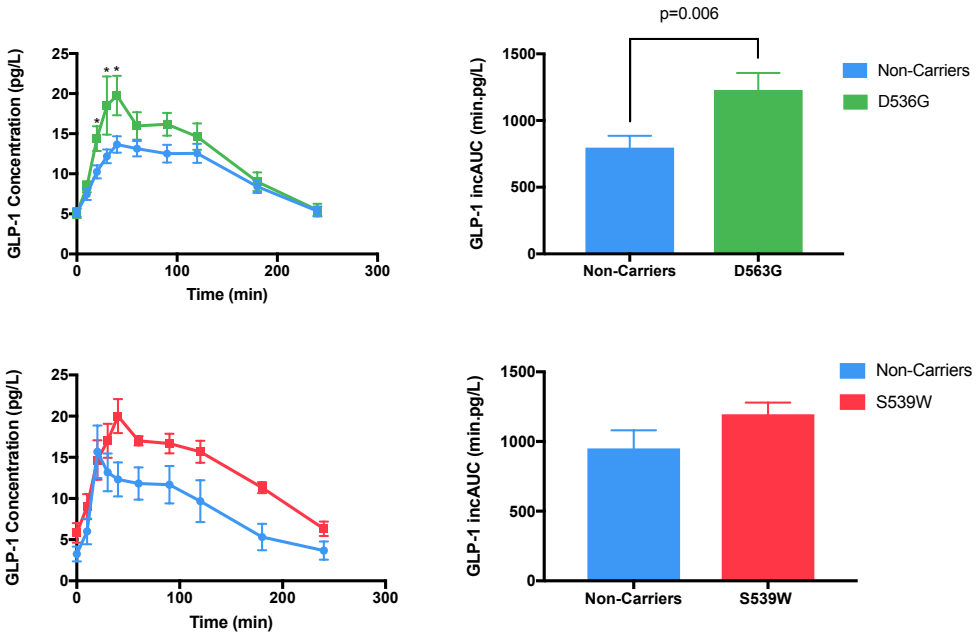


**Figure 3.8: Active GLP-1 Profile Over Time in Carriers of D563G and S539W Compared to Controls in the Family Study**. This figure depicts the intact GLP-1 plasma concentration following a 75g oral glucose load in carriers of the D563G (top) and the S539W (bottom) alleles and matched controls. The data presented are the mean +/- SEM, *p<0.05.

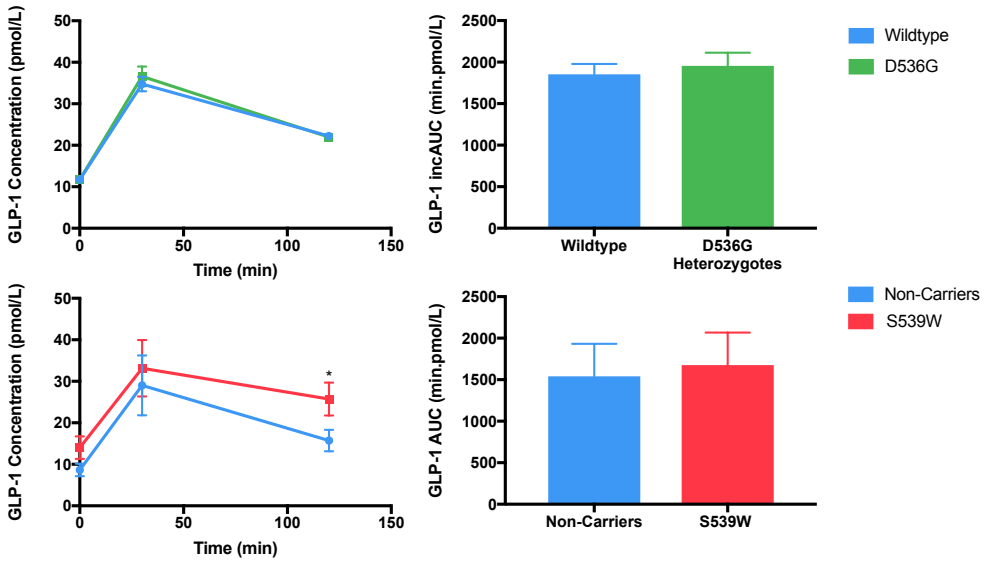


**Figure 3.9: Active GLP-1 Profile Over Time in Carriers of D563G and S539W Compared to Controls in the AdditionPro Study**. This figure depicts the intact GLP-1 plasma concentration following a 75g oral glucose load in carriers of the D563G (top) and the S539W (bottom) alleles and matched controls. The right hand panels demonstrate the incAUC calculated using the trapezoid method. Data are the mean +/- SEM *p<0.05, values not corrected for multiple testing.

In the AdditionPro Study, the intact plasma GLP-1 (7-36 amide and 9-36amide) concentration was compared in 145 carriers of the D563G and 290 matched controls. At baseline, there was no significant difference between GLP-1 levels between the groups. Following the oral glucose load, both groups increased their plasma GLP-1 levels as expected and reached peak concentration at 30min after the glucose load. Following this peak, both groups plasma GLP-1 concentration reduced to near baseline. At no point were the GLP-1 concentrations significantly different and there was no difference in GLP-1 incAUC (1954.76 +/- 158.95 vs 1853.02 +/- 125.81 pmol.L-1.min, p=0.63) **(figure 3.9)**.

The intact plasma GLP-1 (7-36 amide and 9-36 amide) concentration was compared in 7 carriers of the S539W and 14 matched controls. At baseline, there was no significant difference between GLP-1 concentration between the groups. Following the oral glucose load, both groups increased their plasma GLP-1 as expected and reached peak concentration at 30min after the glucose load. Following the peak both groups plasma GLP-1 concentration reduced to near baseline. At 120min the GLP-1 concentrations were significantly increased in the S539W group (25.7 +/-4.0 vs 15.7 +/- 2.6 pmol/L, p=0.04) and there was no difference in GLP-1 incAUC (1657.7 +/- 393.0 vs 1539.64 +/- 502.0 pmol.L-1.min, p=0.86) **(figure 3.9)**.

## 3.5 Discussion

Recently exome association studies and *in vitro* investigation has highlighted PAM as an important gene for glucose homeostasis[**194**, **11**, **246**, **253**, **10**, 91]. The study of the two LoF alleles in PAM (S539W and D563G) *in vitro* has demonstrated that increased risk of diabetes is in part mediated by beta-cell dysfunction [59]. Specifically, these alleles reduced beta-cell function by impairing the catalytic and non-catalytic functions of PAM. It has been demonstrated that PAM knockdown in cellular models causes reduced amidation of peptides. This observation, combined with wide expression of PAM (including in cell types which produce hormones that modulate insulin secretion) raises the possibility of altered plasma concentration of insulinogenic amidated peptides. This may contribute to the reduced beta-cell function and increased risk of T2D observed

in carriers of S539W and D536G. Studying carriers of LoF alleles in PAM presents an opportunity to investigate the role of PAM in glucose homeostasis *in vivo*.

To determine the impact of LoF alleles S539W and D563G, allelic discrimination assays were used to identify carriers. In carriers of D563G, serum PAM activity was measured and compared to non-carriers. There was a clear gene-dose reduction in amidating activity associated with carrying D563G, consistent with an additive reduction in PAM activity. The magnitude of this reduction is consistent with the previous observations from *in vitro* studies. Reproducing these observations in the human model was an important step in understanding the impact of these alleles. Often the reduction in protein function seen in cellular models can be minimised or negated by compensatory changes in the physiological setting (e.g. upregulation of an enzyme concentration to compensate for reduced activity). It is also important to note that these results do not suggest that, in a physiological setting, carriers of D563G have reduced serum amidation capacity. At physiological pH of serum, PAM is not active[**232**, 57]. Instead, the assay result demonstrates that, in the serum under optimal conditions, PAM has reduced amidating activity. This may be due to either reduction in total PAM volume or reduction in catalytic function, or both. These results suggest a reduction in the activity of PAM in the secretory vesicle. Peptidyl-glycine alpha-amidating monooxygenase co-locates with potential substrates along the secretory pathway, before both PAM and the amidated peptide are released systemically[45]. With the observation of reduction of PAM activity in the secretory vesicle, there may also be reduction in other intra-cellular functions of PAM (e.g. intracellular trafficking).

It is clear from the amidation assay that carriers of D563G have reduced PAM activity. However, the assay does not differentiate between reduction in total amount of PAM and reduction in activity. In this allele, the reduced PAM activity likely represents a combination of reduced catalytic activity in PAM (which was observed *in vitro*), and reduced plasma expression (which was identified with association with the plasma proteome)[**262**, 96] .

With the demonstration of profound reduction in PAM activity in carriers of D563G, there was a strong rationale to measure the functional impact on the plasma concen-

tration of amidated peptides implicated in glucose control. Glucagon-like peptide-1 concentration was therefore compared in carriers and non-carriers of PAM LoF alleles in the fasting state and in response to oral glucose.

No difference in the GLP-1 amidation profile was seen in the fasted state. This is likely the result of very low GLP-1 concentrations in the fasted state. Furthermore, a difference may not be expected given that no difference in plasma glucose or insulin concentration between S539W carriers and non-carrier was observed whilst fasting [51].

Unfortunately, samples following nutrient ingestion were not available for GLP-1 (7-36) amide and GLP-1 (7-37) Gly measurement. This necessitated examination of GLP-1 in existing cohorts or prospective collection of samples (which is performed in Chapter 4).

The examination of the Family Study (an existing cohort) demonstrated that there was a significant increase in the plasma concentration of intact GLP-1 in carriers of the D563G allele following administration of a 75g oral glucose load. A directionally consistent (non-significant) effect was also observed in carriers of S539W, although too few carriers of S539W were identified to produce an adequately power study (with effect size and SD observed in this study 9 vs 9 study would be required to achieve a power of 0.8 and an alpha of 0.05). These findings were not consistent with *in vitro* models, which demonstrated that secreted amidated peptides are reduced in PAM knockdown[59]. Additionally, this observation is not consistent with GWAS data, as elevated GLP-1 concentrations should improve beta-cell function and be protective of diabetes, yet this is not observed in carriers of PAM LoF alleles.

The exact mechanism driving this observation remains unclear and highlights the importance of performing studies in humans to corroborate *in vitro* investigation. Potential explanations include, a compensatory increase in GLP-1 secretion to offset a primary beta-cell defect or a compensatory increase in GLP-1 secretion to overcome increased competitive inhibition of GLP-1 by metabolites.

GLP-1 secretion is stimulated by nutrient entry into the small bowel [16]. This is determined by the rate gastric contents is presented to the 1st part of the duodenum [**119**, **264**, 16]. Glucagon like peptide 1 is a potent inhibitor of gastric emptying, creating a negative feed-back loop for control of GLP-1 secretion. Carriers of D563G and S539W

may have increased secretion of unamidated GLP-1 (which has a shorter half-life than its amidated counterpart) due to reduced amidation activity in the secretory vesicle [89]. This may result in higher concentrations of GLP-1 metabolites (particularly GLP-1 9-37amide) which have been demonstrated to be weak antagonists to active GLP-1 [97].

Evidence of negative feedback loops in GLP-1 concentration is provided by observations of GLP-1 plasma concentration following administration of DPP-IV inhibitors, where it has been shown that following DPP-IV inhibitor administration (which inhibits the breakdown of GLP-1) GLP-1 secretion reduces over time [98]. Arguing against the hypothesis of competitive inhibition, infusion of exendin 9-39 (a potent GLP-1 antagonist), has been shown not to increase GLP-1 secretion, although this study only examined a four hour period and more time may be required to develop feedback [14].

Interestingly, if reduction in PAM activity causes GLP-1 resistance, this has important implications for the use of incretin-based drugs, which are a second line treatment of T2D [8].

The results from the Family study were unexpected. Consideration should be given to the possibility that intact GLP-1 could be erroneously elevated due to collider stratification bias introduced by the selection of volunteers. I excluded individuals diagnosed with T2D from the analysis as the incretin effect is known to be reduced in T2D, and given that S539W and D563G alter T2D risk, I would expect an over-representation of individuals with T2D[95]. If these individuals were not excluded, regardless of the mechanism of increased risk of T2D, I would expect a reduction in the incretin effect. The Family Study, as the name suggests, had many related individuals. Given that the incretin effect is highly heritable, our observation may be driven by a genetic factor outside the PAM locus. Given the unexpected result, corroboration was sought in a second cohort.

Examination of the AdditionPro study, a larger and unrelated cohort that was more superficially phenotyped (three vs ten GLP-1 time points) did not reproduce the effects observed in the Family Study. Post-hoc analysis of carriers of the S539W allele revealed a nominally significant increase at 120 min following OGTT (p=0.04). Glucagon-like peptide-1 was only measured at 3 time points in the AdditionPro Study, it may be that the

effect observed in the Family Study was missed by the more superficially characterised AdditionPro Cohort.

Taken together, some uncertainty still exists as to whether D563G and S539W alter intact GLP-1 concentrations. However, given the directionally consistent effect of two independent alleles and multiple nominally significant difference at specific time points, on balance the data presented is suggestive that in humans reduced PAM function increases GLP-1 concentration in the postprandial setting. However, a prospective study is required to definitively show an effect. Future studies should ensure more detailed characterisation than occurred in the AdditionPro study to avoid the argument of under sampling leading to a negative result.

Given the importance of GLP-1 for glycaemic regulation and the potential effect of S539W and D356G alleles on GLP-1 response, there is a strong rationale to perform a prospective study (this will be a focus of Chapter 4).

Future studies should seek to confirm the observation of increased GLP-1 concentration in carriers of PAM LoF alleles and address the hypothesis of a compensatory increase in GLP-1 concentration due to GLP-1 resistance. Establishing GLP-1 resistance would require either; simultaneous measurement of GLP-1 plasma concentration and GLP-1 action, or exposure to GLP-1 at supraphysiological concentrations (as in the pharmacological treatment) and measurement of response. Additionally, future studies should include assessment of glycine extended GLP-1 and examine the concentration of other amidated peptides to determine if they are also affected by reduction in PAM activity.

## 3.6 Conclusion

Through identification of carriers of D563G and S539W and analysis of their stored plasma and serum samples, it was possible to characterise important phenotypes for understanding the mechanism of increased T2D risk. Carriers of D563G were shown to have reduced serum PAM amidating activity compared to non-carriers. In the postprandial setting, elevated GLP-1 concentrations were observed in carriers of D356G compared to non-carriers. Exactly how this influences beta-cell dysfunction and diabetes

risk remains unclear. Further studies to assess the impact of PAM risk alleles on GLP-1 and the concentration of other amidated peptides are required.

# 4

# *PAM* RBG AND PHARMACOGENETIC STUDIES

## 4.1 Chapter Synopsis

In this Chapter, I recruited carriers of the allele of greater effect (S539W) into a prospectively designed recruit-by-genotype study to confirm and extend the observations from retrospective data. I demonstrate that in comparison to age, gender and BMI matched controls, carriers of S539W have increased GLP-1 (7-37) Gly and total GLP-1 levels but a non-significant reduction in the incretin effect, suggesting GLP-1 resistance. This observation prompted assessment of the impact of D536G and S539W on treatment response to GLP-1 receptor agonists (GLP-1RA). Carriers of both alleles showed a clinically meaningful reduction in response to GLP-1RA as measured by HbA1c change after 6 months of therapy.

## 4.2 Background and Rationale

Treatment of T2D focuses on lowering glycemic exposure with lifestyle and pharmacological interventions [8]. Despite the availability of multiple medications to lower HbA1c, only 53% of individuals with T2D reach the glycemic target (HbA1c <7%) [**260**, 99]. Inter-individual response to pharmacological interventions is high and delay to treatment with the optimal medication contributes to a greater overall glycemic exposure and development of complications [**241**, 99]. Currently, T2D treatment algorithms suggest

clinical equipoise between the six second line agents [8]. Choice of second line agent tends to be driven by clinician preference, side effect profile and co-morbid conditions. There is potential to improve medication selection through "precision medicine" where genetic markers are used to indicate whether a patient is more or less likely to respond to a medication.

Recent advances in our understanding of the genetic architecture of complex diseases such as T2D offers opportunities for precision medicine. Monogenic diabetes provides a robust example that targeting the underlying genetically driven molecular pathology can improve HbA1c and reduce diabetic complications [100]. However, opportunities for extending this approach to complex forms of diabetes have lagged behind. The majority of alleles associated with T2D are common and have a small physiological impact, making meaningful derangement of a single pathway unlikely [101]. However, with the increasing sample sizes, low frequency variants with larger effect sizes have been identified [**172**, **173**, 101]. Characterizing the impact of these alleles on specific molecular pathways known to influence glucose homeostasis may facilitate precision medicine efforts for T2D.

Two independent coding alleles in peptidylglycine alpha-amidating mono-oxygenase (*PAM*) (p.S539W, rs78408340, minor allele frequency (MAF) 1%, OR: 1.47 and p.D563G, rs35658696, MAF 5%, OR: 1.23) alter T2D risk and beta-cell function [**1**, 37]. The *PAM* gene encodes the PAM protein, which is a required enzyme for amidation [**15**, 52]. The conversion of C-terminal glycine residue to an amide group (amidation) is required for full biological activity of many hormones, including some that are known to regulate blood glucose concentration (e.g. gastrin and cholecsystokinin) [**184**, **236**, **233**, 60]. Recently studies have shown *in vitro* that PAM deficiency in pancreatic beta-cells results in reduced insulin content and altered dynamics of insulin secretion [59]. Glucagon like peptide 1 (GLP-1), a second line treatment for T2D, is itself amidated and interacts with a number of other amidated peptides [8].

I hypothesised that individuals carrying T2D-risk alleles in PAM would have reduced serum amidation activity and altered GLP-1 concentration which could influence glucose homeostasis. Altered GLP-1 plasma levels or GLP-1 response in carriers of *PAM* T2D-risk alleles would have implications for the efficacy of two commonly prescribed medications

for type 2 diabetes, GLP-1 Receptor Agonists (GLP-1RA) and dipeptidyl-peptidase 4 inhibitors (DPP-IVi). As 10% of individuals carry a T2D-risk variant in the *PAM* gene this could impact medication choice for many individuals with T2D.

In Chapter 3, I investigated the effect of the T2D risk alleles in *PAM* on amidation activity in stored samples of carriers of D536G and of intact GLP-1 concentration (D563G and S539W). Carriers of D536G had 1.5 -fold higher intact GLP-1 plasma concentration in the postprandial setting (Family Study) and directionally consistent effect was observed in carriers of S539W. These observations were not reproduced in a second cohort that was more superficially characterised. It should be noted that there was a directionally consistent effect seen in carriers of S539W in the second cohort. In Chapter 3, I proposed that carriers of *PAM* LoF allele have GLP-1 resistance and compensatory increase in plasma concentration. Unfortunately, data to test this hypothesis was not available. This Chapter details the prospective collection of data to test this hypothesis and the hypothesis that these alleles will impact treatment response to incretin based medication.

### 4.2.1 Study design

## Choice of allele for characterisation

Two alleles have been identified in *PAM* that alter the risk of T2D **(table 4.1)** (additional details on both alleles are provided in Chapter 1). Variants were selected for investigation based on their frequency and effective size. Four recruitment strategies were possible. The Recruitment of;

(1) Heterozygous carriers of S539W,

(2) Heterozygous carriers of D563G,

(3) Homozygous carriers of D563G, or

(4) A combination of these three groups.

I chose to investigate heterozygous carriers of S539W as the effect size was larger in carriers of S539W than D563G (see below for power calculations). Additionally, I identified over 100 carriers of this allele in the Oxford Biobank (OBB) making recruitment of a

| Variant | Amino acid change | MAF | Insulinogenic Index | OR Diabetes |
|---|---|---|---|---|
| **rs35658696** | D563G | 5.30% | -1.96 | 1.23 |
| **rs78408340** | S539W | 0.65% | -8.42 | 1.47 |

**Table 4.1:** Identification of T2D risk alleles in *PAM*. Data are taken from the study by Steinthorsdottir and co-authors [51].

sufficient number of carriers possible. Whilst recruitment of homozygous carriers would be preferable, only 12 homozygous carriers of D563G were enrolled in the OBB and no homozygous carriers of S539W. This was too few volunteers to conduct a study, as historically the OBB has an approximately 30% response to recruitment rate [personal communication Prof F.Karpe (University of Oxford)].

The decision was made to recruit heterozygous carriers of S539W and age, gender and BMI matched controls.

### 4.2.2 Study Endpoints

#### PAM Serum Activity

The formation of biologically active mature peptide is important for many body functions. The final step in the maturation process for approximately 50% of hormones is the addition of an amide group (described in detail in Chapter 1). The only enzyme capable of mediating this reaction in mammals is PAM [56]. It therefore stands to reason that if amidation is the rate limiting step in producing mature peptide (which it is proposed to be for many peptides e.g. gastrin, thyroid releasing hormone, oxytocin, etc.) then reduction in the catalytic function of PAM would alter amidated peptide concentration [52].

As detailed in Chapter 1, study of the supernatant from HEK 293 cells transfected with D536G showed a reduced amidating activity, whilst in S539W no PAM was secreted onto supernatant[59]. Experiments in C57Bl6/J mouse knockout models have demonstrated profound effect on PAM activity in tissue extract (head and trunk) with a 50% reduction observed in heterozygous knockout mice [60]. As PAM co-localises in the secretory granule with amidated hormones and is then exocytosed, there is a strong rationale to expect that individuals who carry loss of function allele in PAM may have reduced amidating activity in their serum. Indeed, in Chapter 3 a gene-dose effect is observed

in heterozygous and homozygous carriers of D563G. Observations from GWAS and quantitative trait analyses, suggest the S539W allele has a greater impact on T2D risk and beta-cell function than D563G, whilst cellular studies suggest that the S539W allele may result in no secretion of active peptide [**245**, **10**, **262**, 38]. Measurement of PAM activity in carriers of S539W *in vivo* has not been performed to-date and will add to the understanding of the impact of S539W on amidated peptides.

## Amidated peptides

To identify amidated peptides that may be altered by a reduction in PAM activity the Uniprot database (a publically available protein database with functional information) was queried [102]. The search was refined by peptides identified in homo sapiens and those with the key words: amide or amidation, and blood. This result returned 133 peptides. It was not practical to measure all 133 peptides, and therefore the peptides most likely to be mediating the diabetes phenotype were selected for measurement. The 133 peptides were manually cross-referenced to identify amidated peptides that had been described in the literature to alter glucose homeostasis, that were secreted in response to nutrient ingestion, and had documented effect on the beta-cell. These peptides were then considered as potential candidates to be mediating the effect of *PAM* LoF alleles on T2D risk and were considered for serum/plasma measurement. Peptides were prioritised if a specific assay was available to measure the glycine extended peptide and the mature amidated peptide. The top 10 candidates are listed below **(table 4.2)**. Only the top 5 candidates were measured due sample volume and biological plausibility and assay availability.

As demonstrated in Chapter 3, in the case of GLP-1 it is often not possible to detect a difference in peptide levels in the fasting state, despite an effect existing in the stimulated state. This is a well-recognised phenomenon in endocrinology, with many tests developed to stress physiological systems to detect impairment in homeostasis (e.g. IVGTT and OGTT). For example, to diagnose adrenal insufficiency adrenocorticotropic hormone (ACTH) is administered to stimulate the adrenal glands to produced cortisol in a so called “short synacthen test (SST)”. When compared to SST (which stress the adrenal axis) basal

unstimulated random cortisol measurement has been described as an “unhelpful distriminators” [103]. A well-known example of this is individuals who have a normal fasting blood glucose, but impaired glucose tolerance [**192**, 2]. Therefore, peptides of interest were measured at two time points, the baseline and peak postprandial concentration.

## Gastrin

Gastrin is released from G cells in the stomach and duodenum in response to nutrient ingestion. The glycine extended gastrin precursor is completely biologically inactive [**234**, 52]. In the amidated form, gastrin augments glucose stimulated insulin secretion [104]. This occurs within the physiological range of plasma gastrin [104]. Importantly, gastrin is one of the few peptides where amidation is believed to be the rate limiting factor in production of active peptide [**234**, 52]. This is supported by the observation of a relatively large percentage of circulating gastrin in the glycine extended form[**234**, 52]. In the absence of glucose, supra-physiological doses are required to produce increased insulin secretion. In the physiological setting two mechanisms of action have been proposed for the effect of gastrin on beta-cells [104]. Firstly, there is a direct effect on the beta-cell, with gastrin hypothesised to increase the pool of immediately releasable insulin[104]. Secondly, gastrin increases gastric acid secretion which in turn stimulates other gut released peptides (Cholecystokinin and GLP-1) known to influence insulin secretion [104].These two hypotheses have developed as a result of the observation that if gastric acid is aspirated from the stomach concurrently with gastrin administration, there is a smaller magnitude of effect on insulin secretion than if gastrin is administered without aspiration[104].

Importantly, gastrin release is predominantly stimulated by protein and fat ingestion. There is only minimal release of gastrin with glucose ingestion alone. Following glucose ingestion, maximal plasma gastrin concentration occurs after 30 min [**233**, 104].

## Cholecystokinin

Cholecystokinin (CCK) is released from enteroendocrine I cells in the duodenum[105]. Cholecystokinin is released in response to nutrient ingestion and gastric acid [105]. The primary function of CCK is to mediate gallbladder contraction to facilitate the delivery

of bile acids to the duodenum for the breakdown of fat [105]. In addition to this, CCK has been implicated in satiety and intravenous infusion of CCK has been shown to reduce meal size by 30-50% [105].

Although infusion of CCK improves post-prandial glycaemia, it is likely that this effect is mediated by gastric emptying, rather than insulin secretion. Indeed, when nutrient was delivered directly into the duodenum at rates mimicking normal gastric emptying there was no difference in glycaemic or insulin response between CCK infusion and placebo [105]. Cholecystokinin reaches peak concentration 60 min following an oral glucose load [**233**, 106].

Despite this, CCK is still a peptide of interest as antibodies have been raised that are able to differentiate the amidated and glycine extended forms [106]. Measurement of the amidation profile of CCK may provide insight into the impact of reduced PAM activity on amidated peptide production.

## The incretin effect

The incretin effect is determined by both the secretion of GLP-1 and the beta-cell response to GLP-1. In Chapter 3, it was proposed that reduced beta-cell response to GLP-1 was driving a compensatory increase in GLP-1 concentration. To confirm this, concurrent measurement of both the secretory and response arms of the incretin axis is required.

The incretin effect refers to the difference in insulin response observed between oral and intravenous glucose loads [107]. This phenomenon is well studied and has been attributed to the release of two hormones (GLP-1 and GIP) in response to ingestion of nutrients (discussed in detail in Chapter 1) [16]. The gold standard method for measuring the incretin effect is to perform an OGTT and then reproduce an identical glucose profile using a variable intravenous glucose infusion **(figure 4.1)** [**101**, 16]. This allows the dissection of the amount of insulin secretion (or glucose disposal) due to direct stimulation by glucose on the pancreatic beta-cell, and the amount of insulin secretion due to the action of the gut released peptides on the beta-cell [46].

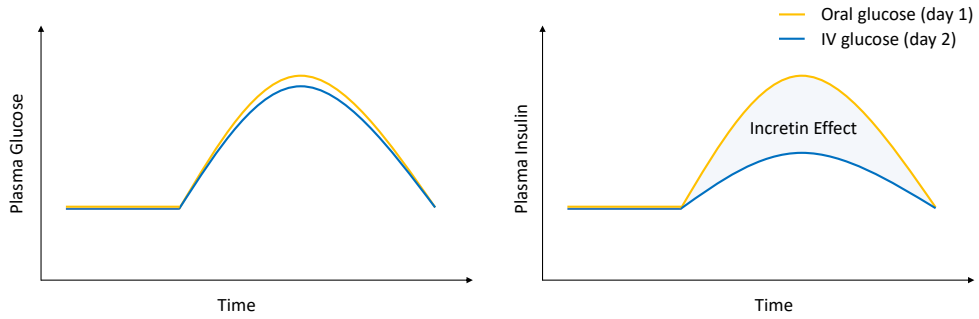


**Figure 4.1: The incretin effect**This figure demonstrates the incretin effect. In the left panel the isolgylcaemic glucose profile of the OGTT and matched clamp are demonstrated and on the right the corresponding plasma insulin concentration that results from IV vs oral glucose loads. The difference between the two insulin responses despite the same glucose concentration is termed the incretin effect [81]

## Thyroid Stimulating Hormone

Thyroid stimulating hormone (TSH) is a non-amidated hormone released from thyrotrope cells in the anterior pituitary [108]. It's secretion is under the control of thyroid releasing hormone (TRH) which is an amidated hormone [**184**, 108]. Thyroid releasing hormone is inactive in its glycine extended form and amidation is believed to be the rate limiting step for the development of mature peptide [52]. Heterozygous Pam knockout in mice results in an inability to maintain core temperature on exposure to cold [109]. Interestingly, this phenotype was reversed with exogenous supplementation of copper, a required substrate for PAM function [109]. Cold sensitivity is a defining feature of hypothyroidism and may suggest a defect in TRH action leading to reduced TSH production and circulating free triiodothyronine (T3) and free tetraiodothyronine (T4)[110].

Thyroid releasing hormone is not easily measured and is not routinely perform in NHS clinical laboratories (personal communication, Dr Tim James (head biomedical scientist, Department of Clinical Biochemistry, Oxford University Hospitals Trust). Thyroid stimulating hormone, which should broadly reflect TRH levels, is easily and cheaply measured. In this chapter, TSH has been used as a surrogate marker of TRH. It is noted that there are some limitations to this approach (e.g. TSH is controlled by several feedback loops).

| Amidated Peptide | Augments Insulin Secretion | Prandial role | Amidation Alters Function | Amidation Specific Assay | Localises to Beta-cells |
|---|---|---|---|---|---|
| GLP-1 | Yes | Yes | Yes | Yes | Yes |
| TRH | Yes | Yes | Yes | No | Yes |
| Gastrin | Yes | Yes | Yes | Yes | Ductal pancreatic cells |
| CCK | No | Yes | Unclear | Yes | No |
| IAPP | Unclear | No | Unclear | Yes | Yes |
| Neurokinin A + B | Yes | Yes | Yes | No | Islets |
| Substance P | Unclear | Yes | Yes | No | Islets |
| Secretin | Yes | Yes | Yes | No | Unclear |
| VIP | Yes | Yes | Yes | No | Sensory neurons in the pancreas |
| Oxytocin | Yes | No | Yes | No | Unclear |

**Table 4.2:** Candidate amidated peptides that may be mediating T2D phenotype in *PAM* LoF alleles]. The peptides in the upper section were measure at various points during an OGTT. These include GLP-1, TRH, Gastrin and CCK .

## 4.3 Chapter Aims:

To design and conduct a genotype–based recall study to determine the effect of *PAM* T2D risk alleles on:

1. Serum PAM enzyme activity
2. GLP-1 concentration, and the ratio of NH2 to glycine extended GLP-1
3. Additional amidated peptides (gastrin, cholecystokinin, TSH (surrogate for TRH))
4. Glycaemic traits
5. The incretin effect
6. Response to GLP-1 RA

## 4.4 Methods:

### 4.4.1 Ethics Approval and Clinical Trials Registry

This study was reviewed and approved by the NRES Oxford B Research Ethics Committee (15/SC/0072). All participants were over 18 years of age and provided written informed consent before recruitment into the study.

The study presented in this chapter was registered prospectively on the clinicaltrials.gov trial registry (NCT02723110).

### 4.4.2 Study Design and Recruitment

Twenty heterozygous carriers of the S539W allele and 20 age, gender and BMI matched non-carriers were recruited into a double-blind, observational, recruit-by-genotype study. Volunteers were recruited from the OBB.

### 4.4.3 Volunteer Identification and Recruitment

Carriers of S539W allele were identified in the OBB in Chapter 3 using an allelic discrimination assay (described in detail in Chapter 2). Non-carriers were also recruited from the OBB. Three to five matched non-carriers were invited to the study concurrently with each carrier to expedite recruitment. All participants were screened for the other T2D risk

| Inclusion Criteria | Exclusion Criteria |
|---|---|
| Age: 30-65 years | Previous resection or banding of the stomach, small bowel or large bowel |
| Non-diabetic (fasting BGL<5.5mmol/L) | On medication effecting insulin secretion, or glucose homeostasis |
| Enrolled in the OBB | Carrier of the D563G *PAM* variant |
| S539W heterozygote or matched control | Anaemia |
| Able to provide informed consent | Recent blood donation |

**Table 4.3:** Inclusion and exclusion criteria

allele in *PAM* (D536G). If a volunteer carried the D536G allele, they were excluded from the study **(table 4.3)**.

### 4.4.4 Study Protocol

Carriers and matched non-carriers of S539W underwent an oral glucose tolerance test (OGTT) and isoglycaemic clamp **(figure 4.2)** on separate days. The two study days were separated by no less than 7 days.

On Study Day 1, participants attended the CRU following a 12 hour fast. A retrograde cannula was inserted into the dorsum of the hand for blood sampling. The hand was placed in a "hotbox" to arterialise venous blood [85] **(figure 4.3)**. A 75g oral glucose load was administered over 5 minutes. Blood was sampled every 5 minutes for 240 minutes to determine blood glucose concentration.

On Study Day 2, participants attended the CRU following a 12 hour fast. A retrograde cannula was inserted into the dorsum of the hand for blood sampling. The hand was again placed in a "hotbox" to arterialise the venous blood. An anterograde cannula was placed in the antecubital fossa of the contralateral arm to allow intravenous glucose delivery. A variable intravenous infusion of 20% glucose was administered over 240 minutes to reproduce the glucose profile of the OGTT.

At 10 time points on both study days samples were drawn (15ml) and stored in 3 different tube types: potassium EDTA tubes with dipeptidyl peptidase IV (DPP-IV) inhibitor, lithium-heparin tubes and serum tubes. Potassium EDTA and lithium-heparin tubes were placed on ice and immediately centrifuged, then aliquoted on ice, and stored at -80°C.

The serum tubes were left at room temperature for approximately 30 min to facilitate clotting before centrifugation and storage at -80°C.

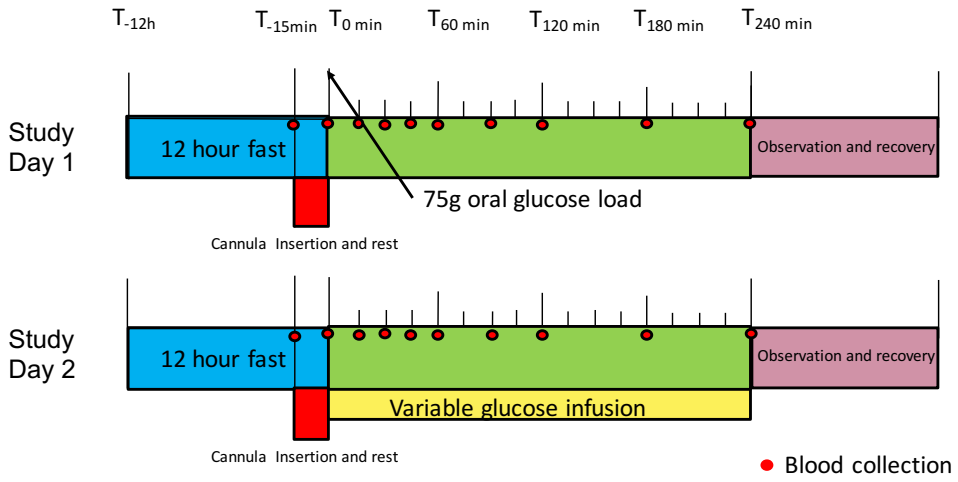


**Figure 4.2: Study Protocol: Frequently sampled OGTT and isoglycaemic clamp**

**Figure 4.3: Photo of volunteer during an OGTT** This image had been reproduced with participants consent. It demonstrates the use of the heated retrograde cannula insertion technique (yellow hotbox).

### 4.4.5 Confirmation of genotype

To ensure that volunteers of the correct genotype were included, the leucocyte rich layer or “buffy coat” was stored and DNA extracted following the completion of recruitment. Genotypes of samples collected from the participants were cross-referenced with those generated from DNA stored in the OBB.

### 4.4.6 Sample size calculation

Given the novel nature of this study, establishing the expected effect size was difficult. Due to uncertainty regarding the effect size in the primary outcome (incretin effect), an interim analysis at 20 v 20 volunteers was performed. An adaptive design approach was adopted with stringent criteria for stopping for futility or clear effect **(table 4.4)**. It was decided prospectively that if a trend towards a significant outcome was detected, a further 10 matched pairs would be included. The decision to continue to recruit further volunteers was based on the beta observed in the first 20 pairs **(table 4.4)**. This approach was used to allow an interim analysis and minimise the adjustment for multiple testing [protocol developed through collaboration with Dr Christopher Jennison (Biostatistician, University of Bath)]. Power calculations for secondary outcomes, based on the predicted effect sizes (where known) and standard deviations, are listed below **(table 4.5)**. To ensure transparency, the adaptive design with cut offs for proceeding to include an additional 10 pairs, was included prospectively on the clinical trials registry (clinicaltrials.gov).

| | Stop and reject null hypothesis | Effect size for rejecting null hypothesis | Stop and accept null hypothesis | Effect size for rejecting |
|---|---|---|---|---|
| Stage 1: (20v20) | Z > 2.18 | >15.2% | Z > 1.69 | -2.2% |
| Stage 2: (10v10) | Z < -0.32 | >11.8% | Z > 1.69 | <11.8% |

**Table 4.4: Adaptive study design** Criteria for accepting or rejecting the null hypothesis at both stages of clinical study

The criteria for stopping due to futility or rejection of the null hypothesis are based on a group sequential test and use the standard deviation of the incretin effect (7%).

The Z boundary has been calculated in statistical program 'R' using a group sequential test model and converted in to an effect size. Type I error rate for group sequential t-test = 0.05.

| Endpoint | Effect size | Standard deviation | Sample size required |
|---|---|---|---|
| PAM Activity | 50% | 20% [57] | 4 vs 4 |
| Intact GLP-1 incAUC | 245 (pmol.L-1.min) | 130 (pmol.L-1.min) | 9 vs 9 |
| IGI | 8.42 (µU.ml-1/mmol.L-1) | 13.41 (µU.ml-1/mmol.L-1) | 40 v 40 |
| Glucose incAUC | Unknown | 127 (mmolL-1.min) | Unknown |
| Insulin incAUC | Unknown | 8784(µU/ml) | Unknown |
| Incretin Effect | Unknown | 10% | Unknown |

**Table 4.5:** Power calculations. Estimates of effect size and standard deviation in PAM activity were taken from *in vitro* work by Thompson and co-authors [59]. Estimates of effect size and standard deviation in GLP-1 incAUC were taken from the result of Chapter 3 in the Family study. Estimates of effect size and standard deviation in IGI were taken from GWAS by Steinthorsdottir and co-authors [51].

### 4.4.7 DNA extraction

Following centrifugation of the EDTA tubes, the leuckocyte rich "buffy coat" was removed and stored at -80C. On completion of the study, genotypes were determined by extracting DNA using the Maxwell 16 (Promega Corporation, Madison, USA) (details provided Chapter 2). This DNA was then genotyped using allelic discrimination genotyping and compared to genotypes generated from the stored OBB DNA samples (details provided in Chapter 2).

### 4.4.8 Biochemical Analysis

Blood samples were collected at 10 time points during the OGTT. Prior to blood sampling, 5 ml of blood was drawn from the intravenous cannula to prevent dilution from previous flushes. To minimise total blood loss, this 5 ml of blood was returned to the patient following collection of the sample. The sample was drawn and placed into either a

serum, lithium heparin or plasma EDTA tube. Plasma tubes were stored frozen at -20°C until blood collection.

In the case of plasma, samples were collected in chilled tubes and transferred on ice to be spun immediately. Serum was stored at room temperature in collection tubes for 30 minutes to allow blood to clot and was then centrifuged. Samples were centrifuged for 15 minutes at 3000 RPM and 4°C. Plasma and serum was then aliquoted and stored at -80°C.

## Amidation activity

The amidation activity was measured at 4 time points in all carriers to determine if there was any alteration in serum amidation activity in the postprandial setting. The assay developed and validated in Chapter 3 was used. Fifty percent recombinant PAM was used as an internal control to allow comparison between the results in Chapter 3 and across multiple time points sampled during the OGTT.

## Insulin

Insulin concentration was measured using a commercial radioimmunoassay kit. The Human Specific Insulin RIA Kit (EMD Milipore, Billerica, USA) was used. Details of use are provided in the Chapter 2.

## Glucose

Glucose was measured on the day of the study. Glucose was measured using Ilab 650 Analyser (Instrumentation Laboratory Ltd, Warrington, UK). This was performed by Marjorie Gilbert (Research Technician, University of Oxford) and Amy Barrett (Research Technician, University of Oxford). I performed the realtime point of care glucose measurement on each blood draw to facilitate adjustment of the variable glucose infusion using The HemoCue Glucose 201+ System (HemoCue, Ängelholm, Sweden).

## GLP-1 (7-36)Amide and GLP-1 (7-37)Gly measurement

Plasma samples were sent to the Holst lab in Denmark for measurement of GLP-1 with in-house assays, which are specific for the amidation state. Samples were sent for all 10 time points of the OGTT [89].

### Gastrin and CCK Measurement

Gastrin and CCK were sent to the Rehfeld lab in Denmark who possess a specific assay for detection of the amidated and glycine extended forms of both peptides. Due to the limits of sample availability and the likelihoods that if a difference was present between carriers and non-carriers CCK and gastrin were only measure at baseline and peak postprandial concentration. The reported peak concentration for gastin and CCK are 30 and 60 min respectively [**236**, **233**, 106].

### TSH

Fasting serum samples were sent to the clinical biochemistry laboratory at the John Radcliffe Hospital. Analysis was performed by Dr Tim James using an ELISA based platform.

### Incretin Effect

The incretin effect was calculated using the two methods routinely used in the literature. Firstly, the incretin effect was measured using gastrointestinal mediated glucose disposal. This method calculates the incretin effect by measuring the difference in the amount of intravenous glucose and oral glucose required to produce the same glucose profile. The rational underpinning of this method is that additional glucose disposed of during an oral glucose load is due to incretin hormones. Measurement of insulin to determine the difference in the insulin AUC between OGTT and matched isoglycaemic infusion was also performed.

The incretin effect was calculated using the following formulae; 1. 100 x (oral glucose consumed - IV glucose administered) / oral glucose consumed 2. 100 x (insulin AUC OGTT - insulin AUC matched isoglycaemic clamp) / insulin AUC OGTT

## 4.4.9 Measurment of Response to GLP-1RA

Treatment response to GLP-1 receptor agonists (GLP-1RA) in carriers of *PAM* LoF alleles was assessed in three cohorts; Genetics of Diabetes Audit and Research in Tayside Scotland Study (GoDARTS)[**218**, 111], Innovative Medicines Initiative: DIabetes REsearCh on patient stratification (IMI-DIRECT)[112], and The Predicting Response to Incretin Based Agents (PRIBA) study. The three cohorts (PRIBA, DIRECT and GODARTs) (details of each cohort

| Variable | Beta | Standard Error | P Value |
|---|---|---|---|
| Baseline HbA1C | 0.65 | 0.06 | $2.0 \times 10^{-16}$ |
| Age at Diagnosis | 0.02 | 0.01 | 0.02 |
| Duration of Diabetes | 0.01 | 0.02 | 0.61 |
| Drug Group | -0.14 | 0.15 | 0.34 |

**Table 4.6:** Variables included in clinical modelling of treatment response. The variables above were identified through backward elimination in pharmacogenetics cohorts.

described in detail in Chapter 2) held treatment response data based on electronic patient records or prospective GLP-1 receptor agonists (GLP-1RA) response trials. I genotyped stored DNA for these studies for the two *PAM* LoF alleles (S539W and D563G). This data was used to determine if there was an altered response to GLP-1RA between carriers of *PAM* LoF alleles and non-carriers. Treatment response was defined as the reduction in HbA1c following 6 months of GLP-1RA therapy (baseline HbA1c – 6 month treatment HbA1c). If a 6-month HbA1c value was not recorded for a patient, a 3-month value was used instead. Any individual without a baseline HbA1c measurement or either a 3- or a 6-month measurement, was excluded from the analysis.

## Clinical modelling

The clinical model for assessing treatment response was developed using linear regression and backward elimination through the stepAIC function in the MASS package in R. A linear regression was performed adjusting for clinical covariates: baseline HbA1c, age at diagnosis, duration of diabetes and drug group (number of oral hypoglycaemic agents(OHAs) at initiation of GLP-1RA)( +/- insulin dose, and change on OHA)**(table 4.6)**.

## Combining data sets for Meta-analysis

The data was analysed in each cohort with the goal of producing the most comparable data across cohorts to allow for an effective meta-analysis. This involved using similar models but allowing them to be adjusted to account for differences in cohort demographics and structure. The regression models differed only because individuals on insulin,

| | Non-carrier | S539W | P Value |
|---|---|---|---|
| Age (years) | 50.9 +/- 5.8 | 50.6 +/- 5.9 | 0.23 |
| Gender (M/F) | 13/6 | 13/6 | 1.0 |
| BMI (kg/m$^2$) | 24.9 +/- 3.3 | 24.4 +/- 3.1 | 0.18 |
| Waist : hip ratio | 0.86 +/- 0.1 | 0.87 +/- 0.09 | 0.83 |

**Table 4.7:** Recruit-by-genotype study demographics and quality of matching

or who had a change in OHA, were excluded in GODARTs and DIRECT, but not PRIBA. Thus, there is an adjustment for insulin dose and OHA change that is only present in the regression model used to analyse PRIBA. The regression model for PRIBA included: baseline HbA1c, age at diagnosis, duration of diabetes, drug group (number of OHAs at the start of GLP-1RA), insulin dose change, and OHA change.

### Assessing the impact of *PAM* T2D risk alleles on response to metformin, sulphonylureas and DPP-IV inhibitors

The same model described above was also used to assess response to metformin, sulphonylureas (SU), and DPP-IV inhibitors (DPP-IVi). However, treatment response data was only assessed in GODARTs and Direct for DPP-IVi, and only GoDARTs for SU and metformin. This was done as data on SU, Metformin and DPP-IVi were not available in all cohorts.

## 4.5 Results:

### 4.5.1 Demographics

Twenty carriers of S539W and twenty matched non-carriers were recruited into the observational double blind recruit-by-genotype study. The demographics of the individuals recruited are displayed above **(table 4.7)**. One volunteer and their matched pair were excluded as repeat genotype testing revealed that the existing genotype was incorrect in the OBB record. Analysis of OBB records by Dr Matt Neville (Scientific Co-ordinator) suggested the sample on the OBB plate had been linked to the wrong volunteer.

### Quality of pairwise matching

Heterozygous carriers of the rs78408340 were identified by direct genotyping from stored samples and then re-genotyped to confirm status on study day. A subset of individuals was also sequenced to confirm correct identification of heterozygous carriers. Carriers of S539W were 1-to-1 matched to controls for age, gender and BMI **(figure 4.4)**. Based on the re-genotyping, one individual was identified as being mis-genotyped and they were excluded from the analysis, along with their matched pair.

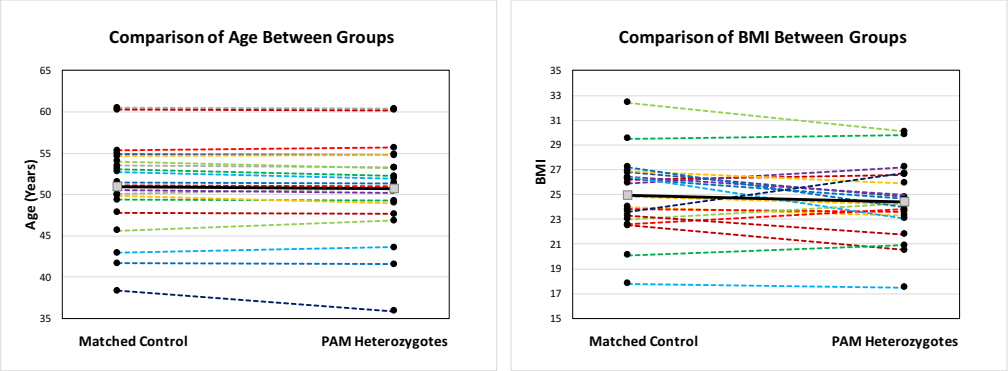


**Figure 4.4: Matching for Age and BMI Between Groups**This figure demonstrates the quality of matching. Pairwise matching was performed based on BMI, age, and sex. This figure demonstrates allele carriers were closely matched for age and BMI. Variant carriers and controls were perfectly matched for gender.

### 4.5.2 Glucose and Insulin

### Glucose

As expected, glucose concentration increased in both groups following oral glucose load. There was no significant difference between carriers and non-carriers in glucose profiles following an OGTT as measured by AUC **(figure 4.5)**.

### Insulin

As expected, insulin concentration increased in both groups following oral glucose load. There was no statistically significant difference between carriers and non-carriers in insulin profile following an OGTT, as measured by AUC **(figure 4.6)**. Although there does appear to be a trend towards carriers of S539W having a higher postprandial insulin level. The spread of i3nsulin AUC was greater in the carriers compared to non-carriers of S539W.

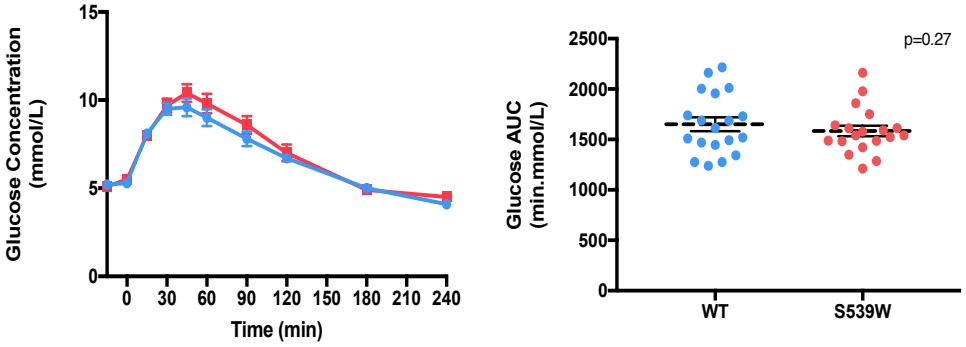


**Figure 4.5: Comparison of Glucose Profiles and AUC during OGTT**This figure demonstrates the glucose concentration over time following 75g oral glucose load in (left panel) and the glucose AUC during the OGTT (right panel) in carriers and non-carriers of S539W.

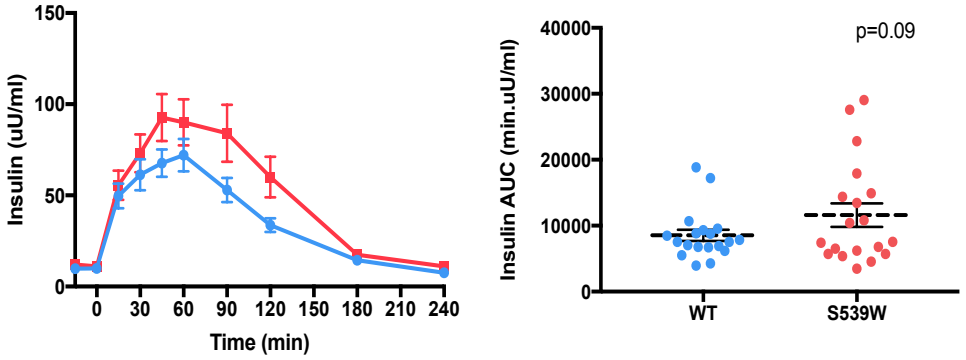


**Figure 4.6: Comparison of Insulin Profiles and AUC during OGTT**This figure demonstrates the insulin concentration over time following 75g oral glucose load in (left panel) and the glucose AUC during the OGTT (right panel) in carriers and non-carriers of S539W.

### 4.5.3 Quality control of match isoglycaemic clamp

Insulin plasma concentration was compared during the OGTT and isoglycaemic clamp to ensure that the expected increase with oral administration compared to intravenous administration could be observed. I observed a significant increase in insulin response to oral glucose compared to intravenous administration (10,074 +/- 1,009 vs 4,823 +/- 450 min.uU/ml, p<0.0001) **(figure 4.7)**. The clamp quality was also assessed by calculating the root mean square error (RMSE), which was 0.53 mmol/L **(table 4.8)**. This value is approximately equal to published computational models where RMSE was 0.55 mmol/L [113].

| Quality Control Measure | Value |
|---|---|
| Average Absolute Difference AUC | 48 min.mmol/L (3.7% of OGTT AUC) |
| Average Absolute Difference in Peak Glucose between OGTT and Isoglycaemic Clamp | 0.3 mmol/L |
| Average Absolute Difference in Time to Peak Glucose OGTT and Isoglycaemic Clamp | 6.5 min |
| Root Mean Square Error | 0.53 mmol/L |

**Table 4.8:** Assessment of matching quality with variable glucose infusion during isoglycaemic clamp

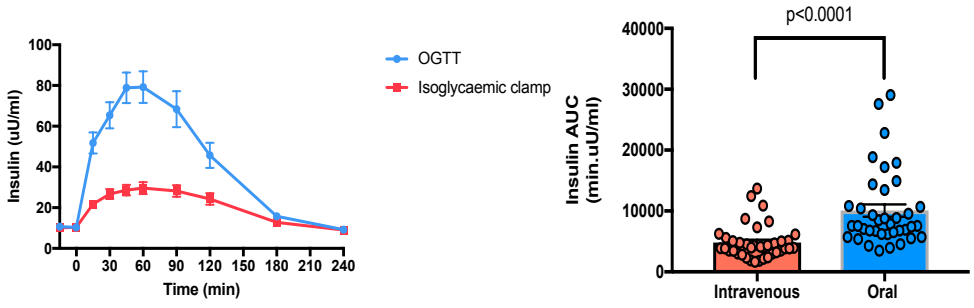


**Figure 4.7: The Incretin Effect in the Entire Cohort.** This figure confirms that I was able to reproduce the expected increase in insulin production with oral compared to intravenous glucose administration. The left panel demonstrates the insulin concentration over time following OGTT and matched isoglycaemic clamp. The right panel show the comparison of AUC for the OGTT and matched isoglycaemic clamp.

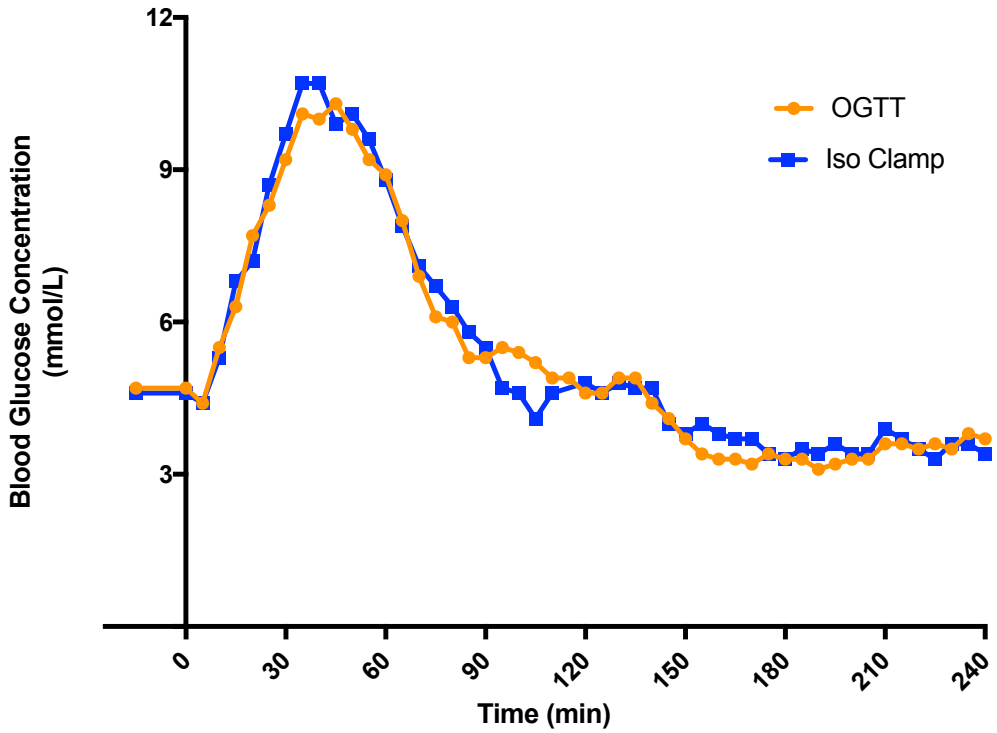


**Figure 4.8: Example of matched Isoglycaemic Clamp** This figure demonstrates a typical typical OGTT profile and matched isoglycaemic clamp. This curve is taken from the first participant to be enrolled in the study. The BGL from the OGTT are depicted in orange and the matched isoglycaemic clamp are depicted in blue.

### 4.5.4 Serum amidation activity

To determine if carriers of S539W have reduced amidating activity, I measured serum PAM activity in carriers of the S539W allele and matched non-carriers. I observed a 52% reduction in amidation activity in the serum of heterozygous carriers of the S539W allele **(figure 4.8)**.

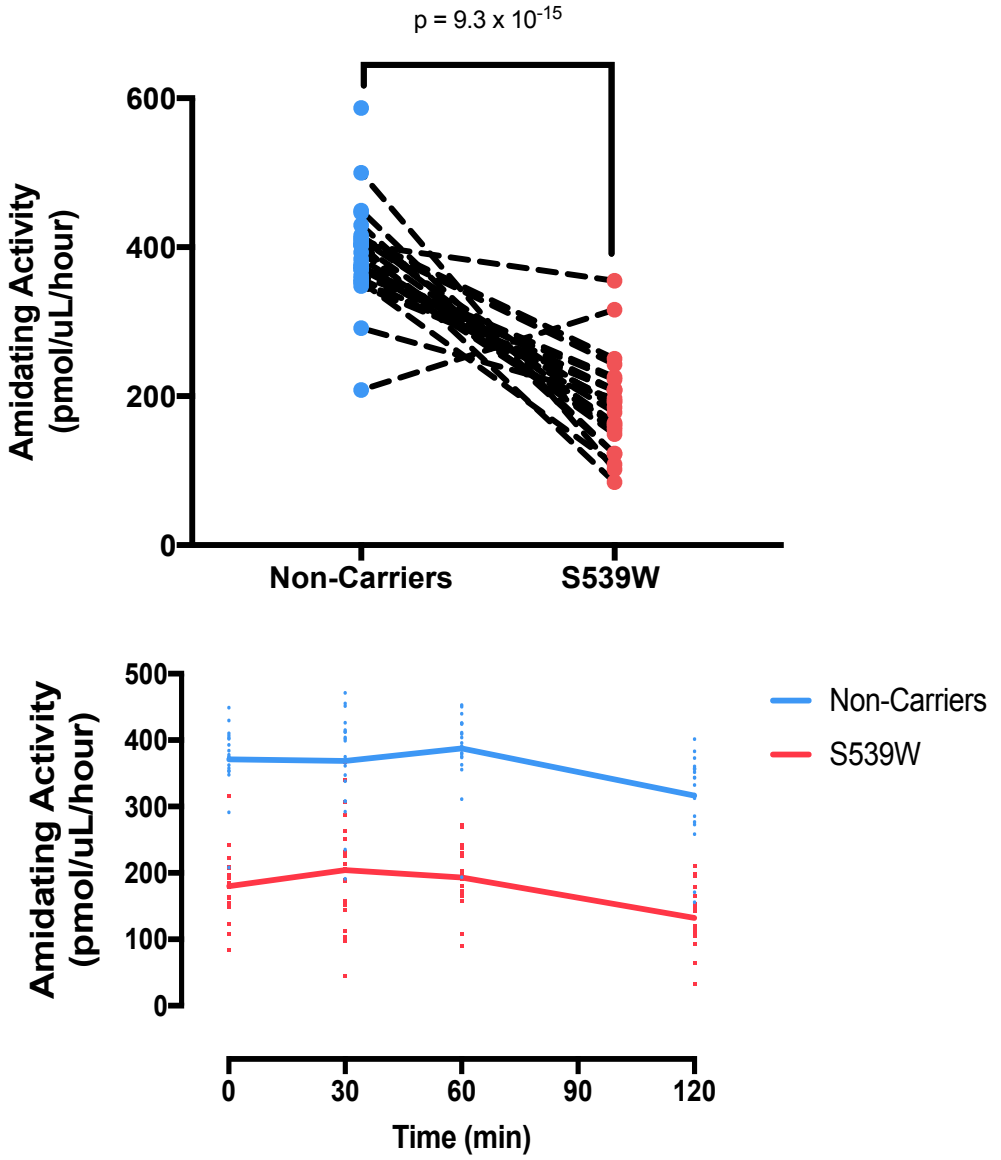


**Figure 4.9: Serum Amidation Activity**The figure demonstrates the reduction in serum enzyme activity in S539W carriers (52%, $p=9.3x10^{-15}$) compared to age, sex and BMI matched non-carriers (top panel). Individuals who did not have matched pairs were included in the analysis and a two-tailed unpaired T-test was used to compare the means of each group. The bottom panel demonstrates the change in amidation activity following an OGTT.

I also measured amidation activity of the serum of volunteers over time to establish if the effect observed in the fasting state was altered following an OGTT. This is the first example of a study where PAM activity was measured during an OGTT. Figure 4.12 demonstrates that there was no change in amidation activity over the course of an OGTT and the reduction in activity was maintained in S539W carriers compared to controls.

### 4.5.5 Plasma GLP-1 Concentration

The total GLP-1, unamidated GLP-1 (7-37 Gly and 9-37Gly), and amidated GLP-1 (7-36 amide and 9-36 amide) concentrations were compared in 19 carriers of the S539W and 19 matched controls. At baseline, in support of the observation made from the fasting data generated in Chapter 3, there was no significant difference between all forms of GLP-1 concentration between the groups whilst fasting. Following the oral glucose load, all forms of plasma GLP-1 increased in both groups. The amidated GLP-1 peaked at 30 min and was not significantly different between groups. The unamidated GLP-1 and total GLP-1 reached peak concentration approximately 45 min after the glucose load and was significantly higher in the S539W group compared to the controls (unamidated: 35.9 +/- 1.7 vs 31.4 +/- 1.43pmol.L-1, p= 0.016) (total: 65.0 vs 56.23 pmol.L-1, p=0.006)**(figure 4.9)**. The unamidated GLP-1 profile and total profiles were significantly higher in the S539W group (p=0.046 and p=0.037 respectively). There was no difference in the amidated profile between groups.

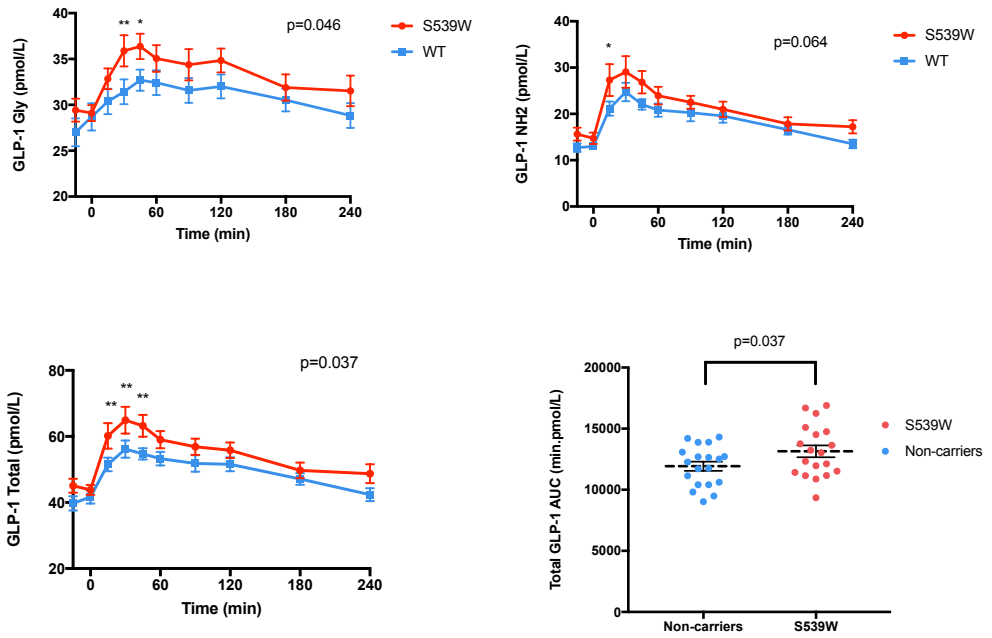


**Figure 4.10: GLP-1 Profile in Carriers of S539W and Controls**This figure demonstrates the unamidated GLP-1 profile (top left), amidated GLP-1 profile (top right), total GLP-1 bottom left and AUC total GLP-1 (bottom right). The data are presented as the mean +/- SEM. Data was analysed using 2-way repeated measures ANOVA or students T-test. Bonferonni correction was carried out to allow for multiple testing. *p<0.05, **p<0.01.

### 4.5.6 Plasma Gastrin concentration

#### Glycine Extended Gastrin

To determine the effect of carrying the S539W allele on gastrin Gly concentration, gastrin Gly levels were measured in 18 carriers and non-carriers of S539W. Two pairs were excluded prior to analysis, one for incorrect genotyping and another due to technical failure of the assay. I measured amidated and unamidated gastrin plasma concentration at baseline and 30 min, following 75g oral glucose load. There was no difference between carriers and controls at T0 or T30 (p=1.0 and p=0.6 respectively) **(figure 4.10)**.

#### Gastrin Amide

To determine the effect of carrying the S539W allele on gastrin amide concentration, gastrin amide levels were measured in 19 carriers and non-carriers of S539W. Amidated gastrin increased significantly in both the non-carriers and carriers from baseline to T30 ($p=6.3 \times 10^{-5}$ and $2.2 \times 10^{-4}$ ,respectively). There was no significant difference between groups at baseline (p=0.19) or T30 (p=0.41) **(figure 4.11)**. The fold increase in gastrin amide was significantly less in the S539W group compared to the control group (mean fold change. 1.63 vs 1.47, p=0.044).

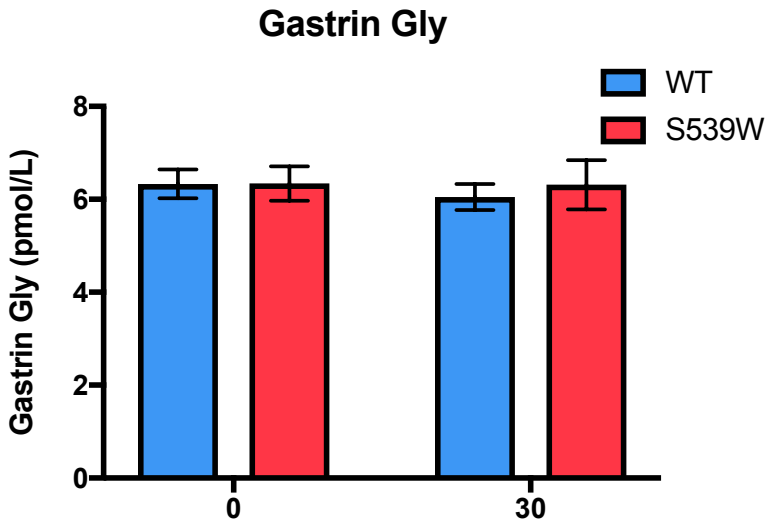


**Figure 4.11: Gastrin Gly Plasma Concentration at Baseline and Maximal Stimulation**Data are presented as mean +/- SEM. Gastrin gly was not significantly different at baseline (p=1.0) and was not significantly different at T30 (p=0.6). Given no hypothesis as to the direction of effect, a two-tailed t-test was performed.

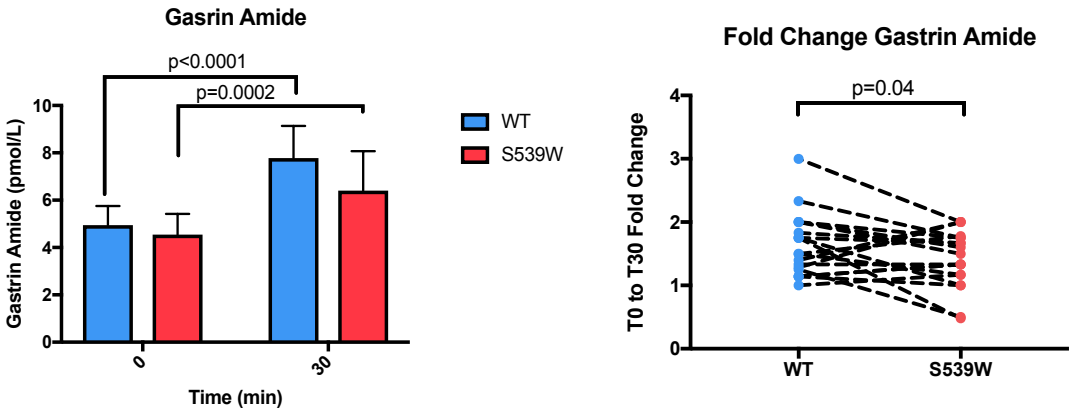


**Figure 4.12: Gastrin Amide Analysis** The analysis of carriers and non-carriers of S539W is based on 19 matched pairs. Data are presented as mean +/- SEM (left panel) or individual ratio values (right panel).

### Gastrin Amidation Ratio

The analysis of carriers and non-carriers of S539W is based on 18 matched pairs. Two pairs were excluded prior to analysis, one pair for incorrect genotyping and another due to technical failure of the assay at baseline gastrin Gly measurement. Data are presented as mean +/- SEM. The gastrin NH2:Gly ratio was not significantly different at baseline (p=0.18) or T30 (p=0.34). Given the hypothesis that this ratio would be reduced in S539W carriers at T30, a one-tailed t-test was performed. There was a significant increase in the amidation ratio from T0 to T30 in both the control group (p=0.0005) and the S539W group (p=0.02). There was no significant difference in amidation ratio increase between groups (p=0.23) **(figure 4.12)**.

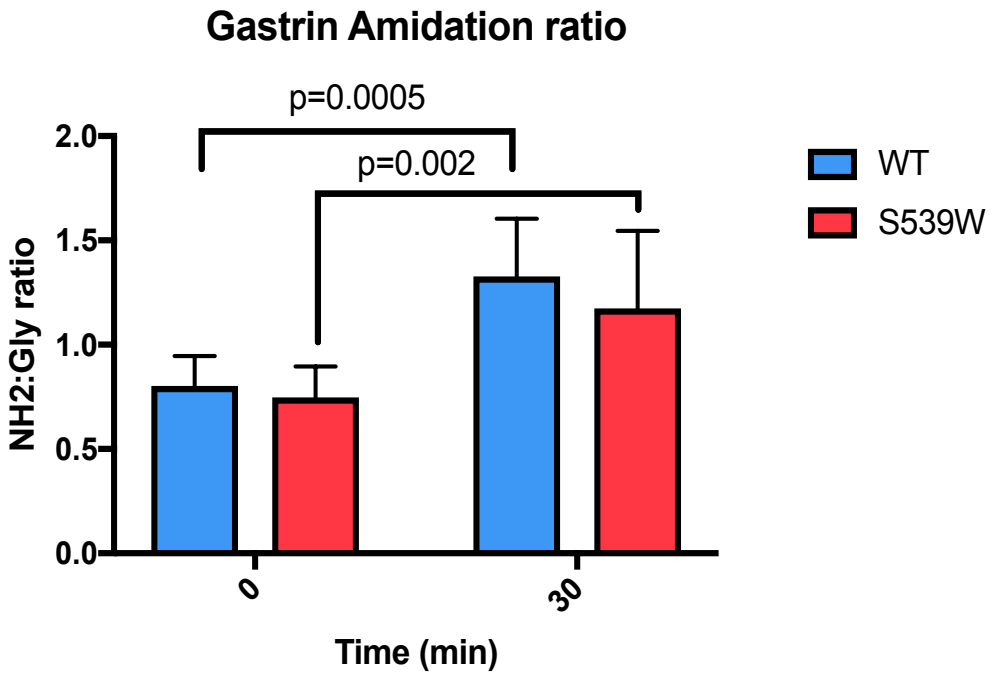


**Figure 4.13: Amidation Ratio at Baseline and on Maximal Stimulation**The analysis of carriers and non-carriers of S539W is based on 18 matched pairs. Data are presented as mean +/- SEM (left panel) or individual fold change (right panel).

### 4.5.7 Cholecystokinin Amide Analysis

To determine the effect of carrying the S539W allele on the amidation profile of cholecystokinin (CCK), CCK amide and CCK Gly concentration, I sent serum samples for measurement of CCK amide and CCK Gly concentration. Unfortunately, CCK Gly assays did not pass

quality control at the Rehfeld laboratory so these results have not been analysed. Cholecystokinin amide was measured in 19 carriers and non-carriers of S539W **(figure 4.13)**.

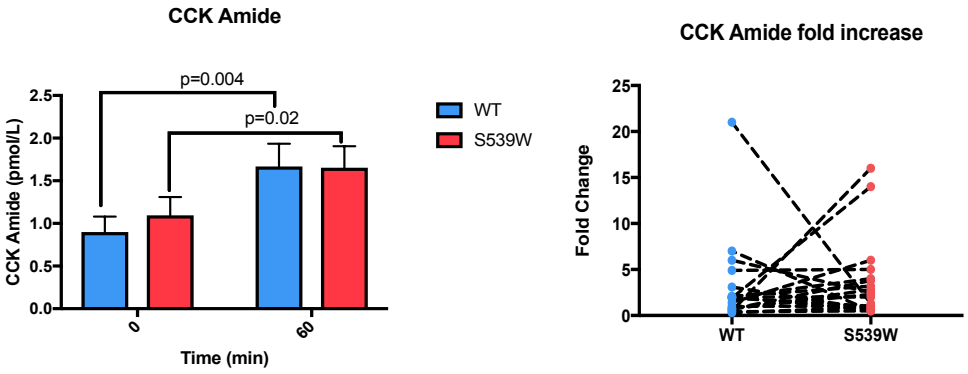


**Figure 4.14: CCK Amide Analysis**The analysis of carriers and non-carriers of S539W is based on 19 matched pairs. One pair was excluded prior to analysis for incorrect genotyping. Data are presented as mean +/- SEM. In both groups, there was a significant increase on CCK amide from T0 to T60 (WT, p=0.004  S539W, p=0.02). There was no significant difference in CCK amide fold increase between carriers and non-carriers of S539W (p=0.78).

### 4.5.8 TSH

To determine the effect of carrying the S539W allele on TSH concentration, samples were sent for measurement of TSH levels at the John Radcliffe Hospital Biochemistry Laboratory. Fasting serum samples for 19 carriers of S539W and 19 matched controls were measured for TSH concentration. There was no significant difference between carriers and controls (p=0.50) **(figure 4.14)**.

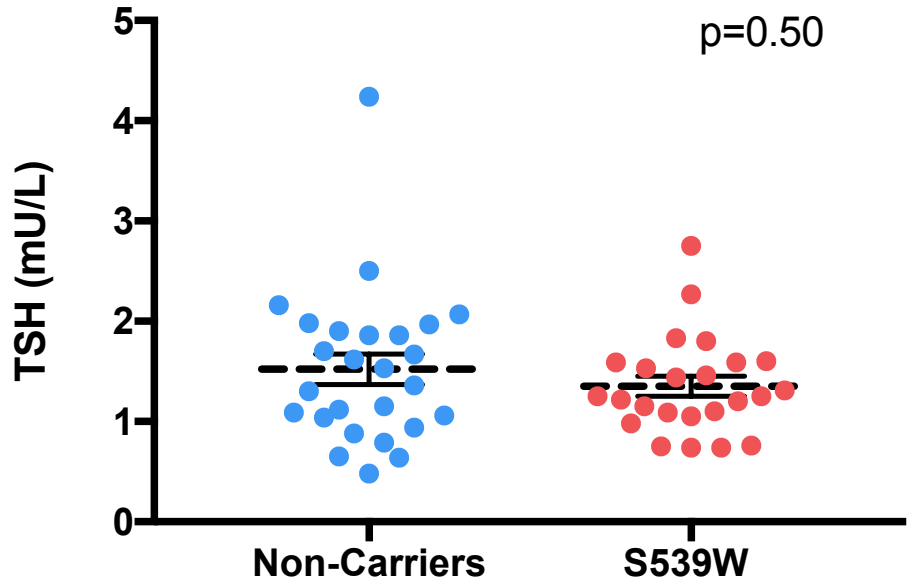


**Figure 4.15: TSH Concentration**The analysis of carriers and non-carriers of S539W is based on 19 matched pairs. One pair was excluded prior to analysis for incorrect genotyping.

### 4.5.9 The Incretin Effect

The isoglycemic clamp is the gold standard measure of beta-cell response to incretin hormones (GLP-1 and GIP). Given the increased GLP-1 concentrations following oral glucose challenge, a proportionate increase in the incretin effect would be expected if response to GLP-1 were intact. However, there was no difference in the incretin effect in carriers compared to non-carriers (-3.1%, p=0.50) **(figure 4.16)**. To quantify GLP-1 action, I compared the ratio of GLP-1 AUC to the incretin effect. Whilst not significant, there was a 1.3-fold increase in the ratio between GLP-1 AUC and the incretin effect in carriers of S539W than non-carriers (320+/-39 vs 247 +/-14 p=0.12).

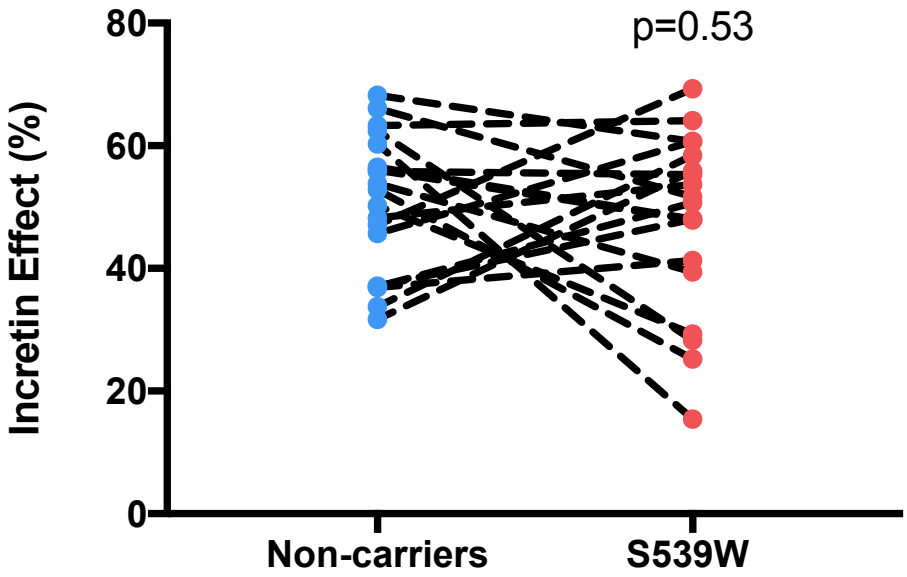


**Figure 4.16: The Incretin Effect**Comparison of the incretin effect between carriers of S539W and controls as measured by the percentage of glucose metabolised by the incretin effect. This is determined by the difference between glucose required to produce an isoglycaemic clamp and the 75g glucose load expressed as a percentage.

### 4.5.10 Treatment response

I assessed the effect of carrying a *PAM* LoF allele on response to GLP-1 therapy. To facilitate this, I genotyped three cohorts with treatment response data and generated a meta-analysis of these results.

#### Quality Control

All data under went quality to control to remove individuals from analysis where data was incomplete or unable to be linked to genotype **(figure 16)**. The initial data cleaning had already been performed prior to my analysis but I excluded additional volunteers based on genotyping failures.

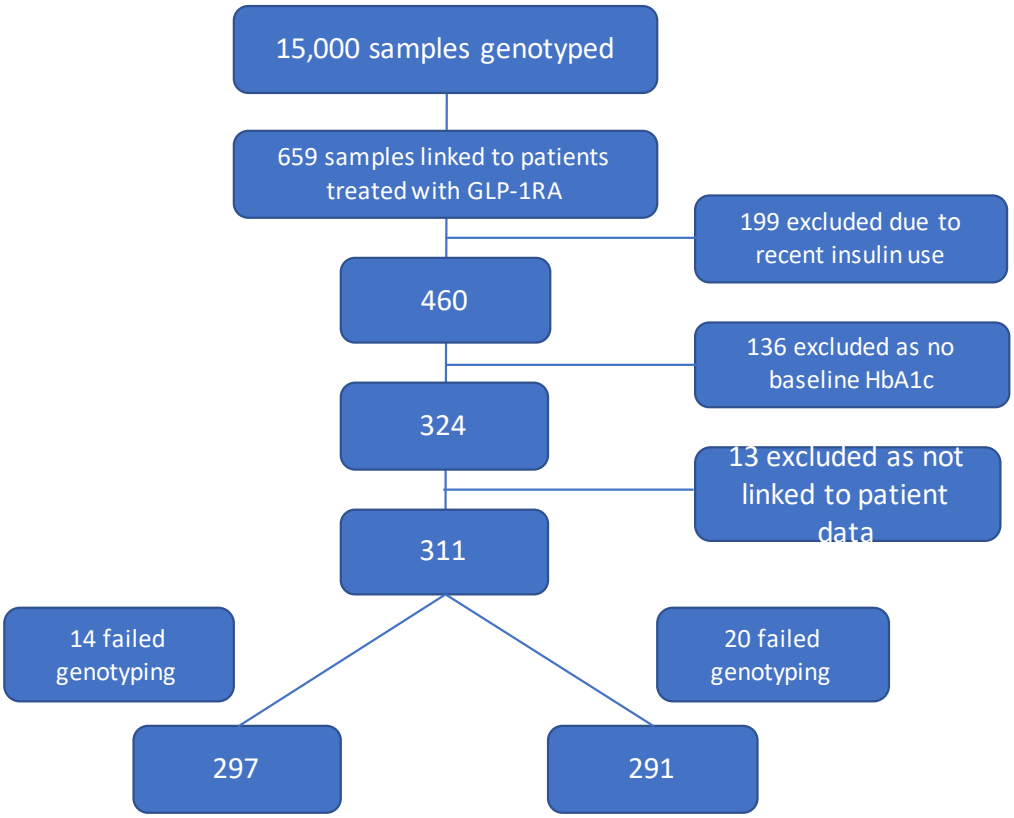


**Figure 4.17: Example of quality control and patient selection for inclusion in meta-analysis**This figure is an example of the quality control performed before data was included in the meta-analysis. In this example only the quality control process for data from GODARTs dataset for GLP-1RA response is shown. A total of 15,000 samples were genotyped for 2 independent alleles. Six hundred and fifty-nine individuals received the drug of interest, after removing individuals who were prescribed insulin within the previous 3 months, had no recorded HbA1c at baseline or both 3 months and 6 months, or did not have genotypic data, only 297 (D536G) and 291(S539W) individuals remained. Of the 15,000 individuals genotyped, only 297 and 291 individuals were included in the linear regression, the same model was used for both alleles.

## Genotyping success rates

The genotyping failure rate was low, with an average failure rate of less than 5%. All cohorts passed quality control with the alleles occurring at approximately the expected minor allele frequencies and were in Hardy Weinberg equilibrium (HWE) (except the DIRECT S539W cohort). In the DIRECT S539W cohort a single homozygous carrier was identified in a sample of 435 individuals, resulting in a divergence from HWE. The DNA quality in GODARTs was poor and this is reflected in the higher failure rate **(table 4.9)**.

| Cohort | Allele | MAF | HWE P Value | Failure rate |
|---|---|---|---|---|
| OBB | S539W | 1.1% | 0.52 | 0.9% |
| DIRECT | S539W | 1.8% | 0.02 | 0% |
| | D563G | 5.6% | 0.22 | 0.9% |
| GODARTs | S539W | 1.2% | 0.42 | 4.6% |
| | D563G | 6.2% | 0.37 | 7.2% |

**Table 4.9:** Genotyping failure rates, MAF and HWE across cohorts.

### 4.5.11 The response to GLP-1RA in carriers of the S539W and D536G

The effect of carrying a D536G or S539W allele on GLP-1RA treatment response was assessed by comparing the reduction in HbA1c following GLP-1RA administration at 3 or 6 months post treatment. This was assessed in three cohorts. The number of individuals in each cohort, the minor allele frequency and the effect size are provided in the tables 3.10 and 3.11.

Carriers of D536G had a reduced response to GLP-1RA in all three cohorts, however individually these studies were underpowered to detect an effect. When combined, there was a non-significant reduction of -0.25% HbA1c (p=0.050) per allele in carriers of D563G allele. Carriers of S539W had a reduced response to GLP-1RA in two of the three cohorts. The effect in the DIRECT cohort was large, and independently significant -0.67% (p=0.034). In the smallest cohort (GoDARTS), only four S539W carriers were identified, in these individuals a non-significant increased response to GLP-1RA was observed. When these studies were combined in a meta-analysis there was a significant and large reduction in treatment response in carriers of S539W to GLP-1RA (-0.55%. p=0.025). This represents a loss of 18% and 40% of the Hba1c lowering associated with GLP-1RA therapy in carriers of D5636G and S539W respectively. In our cohorts, none of the p.S539W carriers and only 10% of p.D563G carriers in whom GLP-1RA treatment was initiated, achieved the recommended HbA1c target of <7% compared to 30% of non-carriers. For both alleles, the variants were combined into independent meta-analyses **(figure 4.17)**.

| Cohort | Number in analysis | MAF | Beta | SE |
|---|---|---|---|---|
| DIRECT S539W | 354 | 1.7% | -0.67 | 0.32 |
| GoDARTS S539W | 297 | 0.67% | 0.41 | 0.75 |
| PRIBA S539W | 468 | 1.1% | -0.67 | 0.45 |
| DIRECT D536G | 354 | 5.7% | -0.32 | 0.20 |
| GoDARTS D536G | 291 | 7.7% | -0.11 | 0.24 |
| PRIBA D536G | 466 | 4.8% | -0.27 | 0.22 |

**Table 4.10:** The effect of S539W and D563G allele on GLP-1RA treatment response by cohort

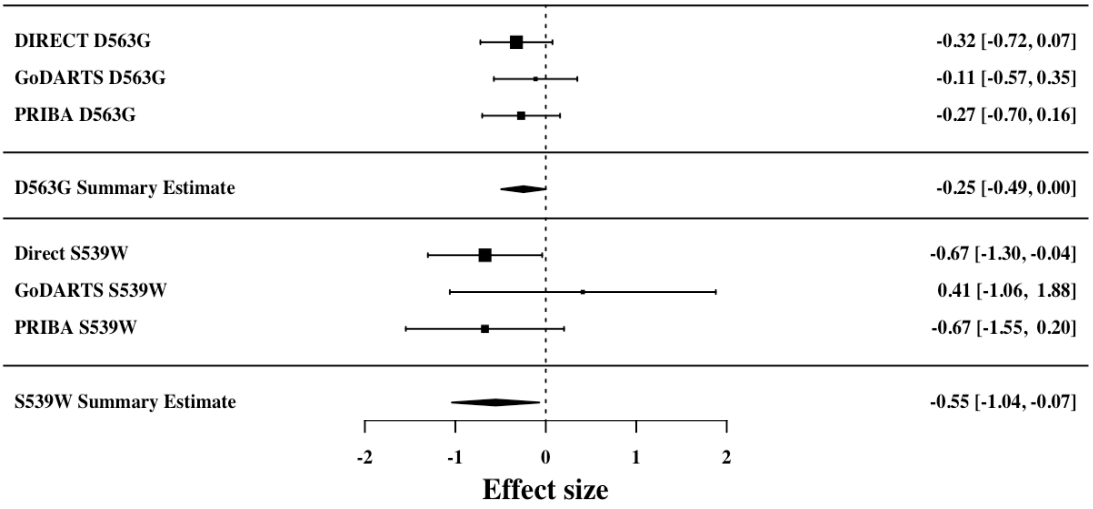


**Figure 4.18: Meta-analysis of the Effect of Carrying D536G and S539W on Response to GLP-1RA Therapy**This figure demonstrates the effect of carrying D536G and S539W on treatment response to GLP-1RA. Each cohort is displayed separately and the effect size is indicated by the location of a solid box with the 95% CI displayed either side. The line of no effect is indicated by a vertical dotted line. The summary estimate of the effect of each allele is displayed below the individual cohort summaries and is indicated by a solid black diamond with the centre of the diamond indicating the summary estimate and the lateral points the 95% CI.

### 4.5.12 The response to DPP-IVi in carriers of the S539W and D536G

Similarly, the effect of D536G and S539W on DPP-IVi treatment response was assessed by comparing the reduction in HbA1c following DPP-IVi administration at 3 or 6 months. This was assessed in two cohorts. When combined, there was no significant difference between allele carriers and non-carriers **(figure 4.18)**.

Finally, the effect of D536G and S539W on metformin and SU treatment response was assessed by comparing the reduction in HbA1c following metformin and SU administration at 3 or 6 months. This was assessed in the GODARTs cohort. There was no significant difference in treatment response to metformin or SU in carriers of *PAM* T2D risk alleles.

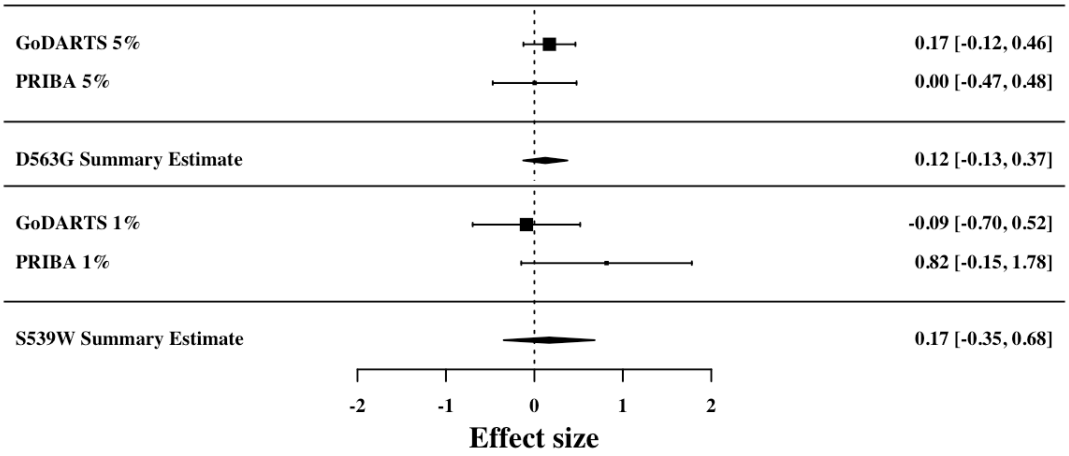


**Figure 4.19: Meta-analysis of the Effect of Carrying D536G and S539W on Response to DPP-IVi Therapy**This figure demonstrates the effect of carrying D536G and S539W on treatment response to DPP-IVi. Each cohort is displayed separately and the effect size is indicated by the location of a solid box with the 95% CI displayed either side. The value for no effect is indicated by a vertical dotted line. The summary estimate of the effect of each allele is displayed below the individual cohort summaries and is indicated by a solid black diamond with the centre of the diamond indicating the summary estimate and the lateral points the 95%CI.

| SNP | MAF | Beta(SE) | P Value |
|---|---|---|---|
| **Metformin** | | | |
| D563G | 6.7% | -0.035 (0.056) | 0.52 |
| S539W | 1.5% | 0.16 (0.11) | 0.15 |
| **Sulphonylurea** | | | |
| D563G | 6.7% | 0.049 (0.058) | 0.40 |
| S539W | 1.3% | 0.0033 (0.13) | 0.98 |

**Table 4.11:** The effect of S539W and D563G alleles on metformin and sulphonylurea treatment response

### 4.5.13 The response to DPP-IVi in carriers of the S539W and D536G to Sulphonylurea (SU) and Metformin

The impact of S539W and D563G on treatment response metformin to and SU was assessed in 2,463 individuals for the analysis of response to metformin and 2,282 individuals respectively. The treatment response was assessed using the same model as described for GLP-1RA and DPP-IVi. There were no significant differences in treatment response between carriers and controls to either metformin or SU **(table 4.11)**.

## 4.6 Discussion:

Large-scale genetic studies have identified *PAM* as an important gene for glucose homeostasis [**220**, **10**, 37]. We have recently shown that the diabetes associated alleles result in a loss of function and that loss of PAM in beta-cells influences the dynamics of insulin secretion [45]. Given the wide tissue expression of PAM and its key role in amidating GLP-1, I hypothesised that altered GLP-1 amidation could also influence insulin secretion and T2D-risk.

Studying carriers of LoF alleles in *PAM* provided an opportunity to investigate the role of PAM in glucose homeostasis and identify overlap with existing treatments. I show that carriers of the T2D-risk alleles p.S539W and p.D563G have a profound reduction in amidation activity and an increase in GLP-1 levels postprandially. Despite an elevated plasma total GLP-1 concentration, the incretin effect was non-significantly reduced in carriers of p.S539W. This suggested that carriers of p.S539W and p.D563G have GLP-1 resistance. I postulate that this resistance (which would likely be lifelong) has driven a compensatory increase in GLP-1 concentrations in carriers of *PAM* LoF alleles.

To assess GLP-1RA response, I conducted a meta-analysis of three cohorts where genotype data were available and demonstrate that carriers of p.S539W and p.D563G lost 40% and 18% of the expected HbA1c reduction at 6 months compared to non-carriers respectively. Of note, no carriers of p.S539W and only 10% of p.D563G carriers started on a GLP-1RA achieved their target of an HbA1c of <7% after 6 months of therapy, compared to 30% of non-carriers. Given that delay to adequate treatment has been shown to increase diabetic complications[114], this raises concerns about the use of GLP-1RA in this population. Whilst the GLP-1RAs are not directly harming carriers of p.S539W and p.D563G, since they do still reduce HbA1c, it does represent a lost opportunity to optimise HbA1c levels. Importantly, I also demonstrate that there was no reduction in response to metformin, sulphonylurea, or DPP-IVi. The latter two medications are considered equipotent, alternate second line medication choices. Based on this observation, it would appear that sulphonylureas and DPP-IVi may be superior choices in carriers of

*PAM* LoF for reducing HbA1c. It should be noted that other patient related factors may still make GLP-1RA an appealing choice (e.g. obesity).

Interpreting this treatment response data provides important physiological insight. The exogenous stimulation of the GLP-1 receptor with pharmacological agents (which vastly overwhelms physiological stimulation), allows assessment of the beta-cell response to GLP-1 receptor stimulation without having to consider compensatory effects. The observation that there is reduced response to GLP-1RA is in keeping with the observation that carriers of p.S539W and p.D536G have increased risk of T2D and reduced beta-cell function despite increased postprandial GLP-1 levels. It also supports the interpretation of the elevated GLP-1 levels as a consequence of GLP-1 resistance in carriers of *PAM* LoF alleles.

Even more intriguing is the observation that neither variant has an impact on treatment response to metformin, or SUs. This suggest that *PAM* T2D risk alleles interact specifically with GLP-1 action. The logical extension of this is that PAM interacts with a pathway stimulated by GLP-1, which is not shared with either SU or metformin. *In vitro* studies have demonstrated that *PAM* gene knockdown alters insulin content and reduces early exocytosis[59]. Electrophysiology studies estimate that 70% of the insulin secretory effect attributed to GLP-1 is due to cAMP mediated mobilisation of granules to facilitate early exocytosis[115]. It is possible that the reduction in insulin content and altered kinetics of exocytosis may specifically reduce response to GLP-1, but not other pharmacological agents. Equally GLP-1 has many non-beta-cell related effects which are not shared with metformin or SU. These include slowing of gastric emptying, reduction in appetite, and glucagon suppression[**265**, **264**, 16]. Additionally, some amidated peptides have been proposed to augment the incretin effect (most notably gastrin, where I demonstrate a reduced fold increase in carriers). It is not possible to exclude that reduced GLP-1 action is a result of loss of synergy with other amidated peptides.

The lack of effect observed on DPP-IVi (which works by increasing GLP-1 levels) can be attributed to the already elevated GLP-1 levels observed in carriers of *PAM* T2D risk alleles which would mask the effect of inhibiting the breakdown of the peptide. Future studies should focus on identifying the exact mechanism of GLP-1 resistance, as being

able to reverse GLP-1 resistance or indeed sensitise individuals to GLP-1, would be a useful clinical tool.

In the current clinical genetics landscape, it is not possible to use this information to stratify treatment. However, with the continued reduction in sequencing costs and possibilities for incorporating array-based genotyping into clinical care, it is foreseeable that genotype data will soon be routinely available to guide medication choice. In this setting, medication choice based, in part, on a response score of multiple alleles known to affect response to a class of drug, is a likely development. In the case of carriers of *PAM* risk alleles, these results suggest that a carrier would not respond as well as the general population to GLP-1RA and this knowledge may alter the clinical choice to prescribe GLP-1RA. Instead, one of the other second line medications may be favoured.

## 4.7 Conclusion

In conclusion, mechanistic examination of the *PAM* locus revealed that carriers of LoF alleles have reduced enzyme activity and GLP-1 resistance. The GLP-1 resistance in these carriers resulted in a specific and clinically meaningful reduction in response to GLP-1RA. This suggests that these agents should be avoided in carriers where possible. The observation of such a large impact on treatment response provides rationale for systematic investigation of GWAS variants for effects on medication response.

# 5

# *PTEN* AND BROWN ADIPOSE TISSUE

## 5.1 Chapter Synopsis

In this chapter I investigate the role of phosphatase and tensin homolog (PTEN) in the regulation of brown adipose tissue (BAT) development and activity. To this end, I recruited carriers and non-carriers of *PTEN* loss of function (LoF) mutations and compared their cold induced BAT activity. I developed and validated a protocol to measure maximal BAT activity (heat production and associated energy expenditure) *in vivo*. In this Chapter, I show that the protocol developed (utilising a personalised cooling protocol, infra-red thermography and indirect calorimetry) was able to detect known associations with BAT activity (cold exposure, and a negative correlation with obesity and age). I then demonstrate that individuals with a *PTEN* LoF mutation have reduced energy expenditure, BAT associated heat production and cold tolerance compared to matched controls. Based on these results I conclude that PTEN positively regulates BAT in humans.

## 5.2 Rationale for investigating the role PTEN in BAT regulation

### 5.2.1 Cowden Syndrome/ PTEN Harmatoma syndrome (PHTS)

Cowden syndrome (CS) is an autosomal dominant condition which results in a constellation of symptoms including; intestinal hamartomas, skin tags and an increased risk

of malignancy[116]. The phenotypic spectrum associated with mutations in *PTEN* is high, and it is not currently possible to predict the severity of the phenotype [**122**, 117]. Cowden's syndrome is the most common of three diagnostic classifications that fall under the umbrella of PTEN harmatoma tumour syndrome (PHTS) [117]. As with all PHTS sub-classifications, the symptoms of CS result from a loss of function mutation in *PTEN* [**374**, 117]. The role of PTEN as a tumour suppressor gene has been well studied, with mutations in *PTEN* resulting in an increased risk of cancer and benign overgrowth conditions [**374**, **165**, **160**, 118]. The diagnosis of CS is via the consensus guidelines (discussed in Chapter 1) [70]. The striking clinical phenotype of CS makes it possible to identify and recruit individuals with *PTEN* haploinsufficiency from the general population.

### 5.2.2 PTEN in metabolic regulation

In addition to the well-recognised effects on cancer predisposition, it has been demonstrated that PTEN also regulates metabolic processes [**3**, 68]. Specifically, PTEN inhibits PI3K/AKT pathway, by hydrolysis PIP3 to PIP2 (see Chapter 1 for detail). This action reduces GLUT 4 (insulin sensitive glucose transporters) translocation into the cell membrane [**3**, 61]. Individuals with CS are profoundly sensitive to insulin and protected from T2D [50].

The is also evidence that PTEN through its regulation of PI3K/AKT pathway may regulate beta-cell mass. In transgenic mice, over expression of AKT resulted in increased beta-cell mass [**369**, 119]. Complementing, this observation decreased PI3K activity is associated with a beta cell defect[120].

Somewhat paradoxically, people with CS are also obese [50]. This is unusual, as obesity usually predisposes to insulin resistance and T2D. The cause of obesity remains unclear in CS.

### 5.2.3 Brown adipose tissue physiology

Brown adipose tissue is a metabolically active tissue, the defining characteristic of which is the ability to utilise fatty acids and glucose to produce heat. Brown adipose tissue is located in the supraclavicular region (SCV), around the heart, and along the spine [72]. Functional isotope scans demonstrate cold induced uptake of radiolabelled glucose in the SCV region, around the heart and along the spine that is not present when volunteers

are thermoneutral [72]. Brown adipose tissue contains a high number of mitochondria to generate ATP, and the presence of uncoupling protein-1 (UCP1) allows ATP to be converted to heat [**283**, 121]. Uncoupling protein-1 "uncouples" the respiratory chain by increasing permeability of the inner mitochondrial membrane to protons, allowing fast substrate oxidation, converting the energy generated by the mitochondria to heat [**375**, 61]. Brown adipose tissue is activated by cold exposure and adrenergic stimulation (particularly beta-3 stimulation) [**279**, **102**, 122]. When active, BAT contributes up to 12-20% of the resting metabolic rate [**102**, 75]. These features support the prevailing hypothesis that the presence of BAT is an evolutionary adaptation to maintain core temperature in response to cold [**278**, **282**, 121].

It has been recognized for some time that BAT is present in small mammals and human infants, however it was not until relatively recently that its role in adult humans was appreciated [**102**, 71]. In 2009, it was demonstrated that BAT plays an important role in temperature regulation and can be a substantial source of energy expenditure in adults (EE) [**102**, 71]. As a result, there is growing interest in factors that regulate BAT, as these may represent therapeutic targets for obesity management. Equally, loss of BAT function may predispose to obesity, hitherto there are no reported monogenic causes of obesity that result from under active BAT [123].

### 5.2.4 Preclinical studies suggest Pten may regulate BAT in small mammals

Preclinical studies in mice, which have both over expressed and knocked down Pten suggest, Pten may regulate BAT [**107**, 61]. Over expression of Pten in transgenic mice is associated with increased basal metabolic rate, reduced fat mass, and increased BAT activity (tracer uptake on positron emission topography scans) [61]. Examination of the BAT of these mice demonstrated up regulation of *Pgc1A* and *Ucp1* (two genes essential for BAT function) and down regulation of Akt (a known target of Pten) **(figure 5.1)** [61]. Additionally, over expression of Pten *in vitro* resulted in increased differentiation of fibroblasts in to brown adipocytes [61]. During differentiation of mouse embryonic fibroblasts into brown adipocytes, up-regulation in Pten mRNA levels was also observed [61]. Administration of PI3K inhibitors (which act similarly to PTEN by inhibiting PI3K)

to small mammals (mice and rhesus monkey) resulted increase BAT activity and weight loss [77]. Taken together, these observations suggest that Pten positively regulates BAT activity and plays a role in the formation of brown adipocytes in mice and rhesus monkeys [**107**, 61]. Small mammals are more reliant on BAT for maintenance of body temperature than adult humans (as they have greater surface area to volume ratios and live in thermo-negative temperatures) [121]. Given the physiological difference between animals and man, there is a need to extend these study to humans.

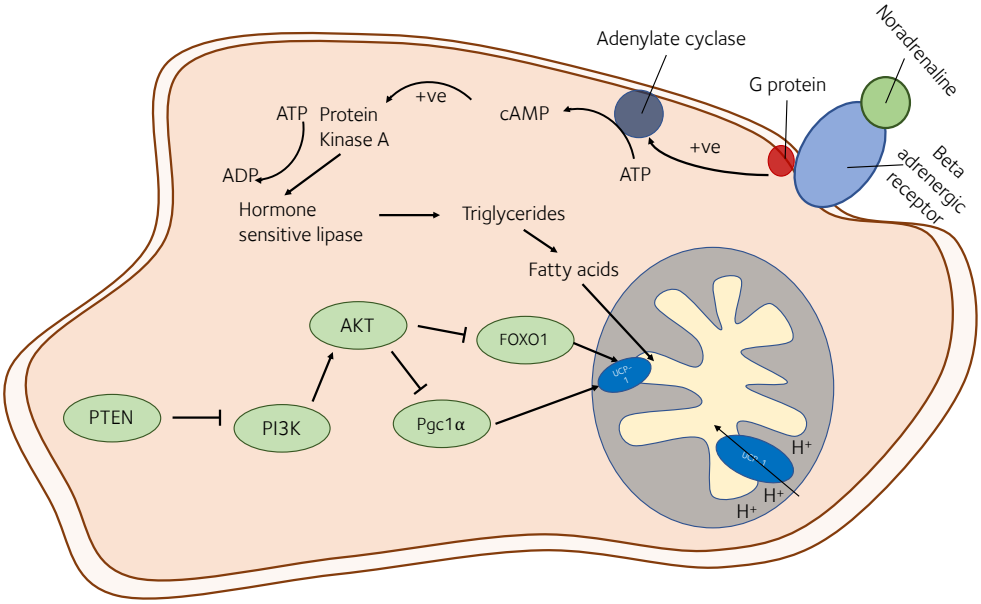


**Figure 5.1: Role of PTEN in BAT.** This figure demonstrates a brown adipocyte and the molecular pathways that control stimulation and the regulation of UCP-1. The PTEN/PI3K/AKT pathway is depicted in green and demonstrates how regulates the presence of UCP-1 in the mitochondrial membrane. The transport of H+ ions back down the proton gradient is used to produce heat [**105**, 122].

### 5.2.5 PTEN as a therapeutic target for obesity

Independent of the increased risk of diabetes, obesity carries significant health and economic burden. Public Health England estimated that in 2014-2015 6.1 billion pounds was spent in the NHS on obesity related complications [**257**, 124]. Obesity is characterised by the development of increased adipose tissue mass [125]. The metabolic consequence of increased adiposity, increased cancer predisposition, and the mechanical force associated increased body weight explain most complications [125]. Social stigma linked

with obesity can also lead to significant mental health issues and morbidity [126]. As such, there is a need to develop new therapeutic options to assist with the treatment of obesity. The incretin class of medication are currently among the most effective with dual GLP-1 and GIP agonist recently being shown to reduce weight by 11.3kg over 26 months [127]. If PTEN increases BAT activity, this would be a promising therapeutic target as medication already exists to alter the PTEN/PI3K pathway [77].

### 5.2.6 Hypothesis

It is my hypothesis that PTEN positively regulates BAT and that a loss of function mutation in *PTEN* (like those that lead to CS) result in underactive BAT due to reduced volume (developmental effects) and reduced activity (suppression of UCP-1 production). I hypothesise that the underactive BAT in patients with CS causes in a reduction EE and a predisposition to obesity.

### 5.2.7 Measurement of brown adipose tissue function

The measurement of BAT has proven difficult in both animal and human models [128]. In humans, measurement has been centred on imaging with computer tomography (CT) scans with functional tracers [129]. The main challenge lies in radiologically differentiating BAT from white adipose tissue (WAT) [129]. However, BAT and WAT display a different response to cold [129]. Brown adipose tissue can be identified using radiolabelled fluorodeoxyglucose (FDG) and positron emission tomography (PET)-CT scanning (18F-FDG PET/CT) during cold exposure [129]. This is currently the gold standard technique and is based on the premise that activated BAT takes up glucose from the circulation at a greater rate than WAT during cold exposure [130]. However, there are a number of limitations to this method. Firstly, this technique exposes subjects to a significant amount of radiation (upwards of 20 mSv) [129]. This substantial exposure to ionising radiation limits the use of 18F-FDG PET/CT in large studies of healthy volunteers, studies with repeated imaging, volunteers predisposed to malignancy (like in carriers of *PTEN* mutations) and studies with a younger population (e.g. children) [131]. Secondly, 18F-FDG PET/CT only measures glucose uptake into the tissue not fatty acids, which are the primary substrate for BAT [**298**, **299**, 132]. This may result in 18F-FDG PET/CT underestimating

BAT activation [133]. This method is also somewhat problematic in my proposed study population who have already been demonstrated to be extremely insulin sensitive, which independent of BAT activity, may alter tracer uptake [50]. Finally, 18F-FDG PET/CT are expensive and logistically difficult to co-ordinate with controlled cold exposure making them hard to perform in large numbers.

A number of radiation free functional imaging techniques have been proposed that utilize the properties of BAT to differentiate it from WAT [**268**, **292**, **109**, **115**, 133]. The leading radiation free modalities include, infra-red thermography (IRT), glucose chemical exchange saturation transfer MRI (CEST-MRI) and hyperpolarized pyruvate MRI [**268**, **292**, **109**, **115**, 133]. The properties that differentiate BAT from WAT can be elicited by cold exposure and include; heat production, increased blood flow and glucose/fatty acid concentration change in tissue following activation[**289**, **291**, **315**, **102**, 134].

### 5.2.8 Infra-red thermography

Infra-red thermography is a simple method of identifying BAT. Infra-red thermography measures the temperature of the skin overlying various thermogenic structures, providing a heat map superimposed on surface anatomy [135]. Thermal cameras measure temperature by calculating the temperature over an object by the amount of infra-red light emitted/reflected. Specifically, temperature measurement is achieved as the electrical resistance of an uncooled microbolometer is altered by the impact of infra-red light, allowing calculation of the heat of the object at a given distance and emissivity. The largest and most superficial BAT deposit is located in the supraclavicular fossa or lateral cervical region of the neck [**102**, 71]. The use of temperature measurement of the skin overlying the SCV deposit was initially prompted by the observation that this region maintained stable temperature despite cold exposure and so called thermal “hotspots” noted in this region were closely related to anatomical positions of BAT on 18F-FDG PET/CT and biopsy studies [**301**, 135]. The use of IRT has been validated in mice by comparing IRT to 18F-FDG PET/CT, and recently similar studies have been reproduced in humans [**303**, **304**, **315**, 136]. Studies comparing the gold standard 18F-FDG PET/CT imaging to IRT showed no correlation with single time point comparison

but were able to demonstrate a correlation with change SCV temperature with cold activation [**304**, 137]. Two independent studies have demonstrated a significant increase SCV BAT temperature detected by IRT in individual with positive 18F-FDG PET/CT imaging [**315**, 138]. Law and co-authors demonstrated that SCV hotspots correlated spatially to SCV BAT deposits identified on PET scan [139].

There is ongoing debate in the field about the analysis of IRT images. This is reflected in the large variation in analysis techniques **(table 5.1)** [**312**, **303**, **304**, **306**, **315**, **301**, **313**, **310**, **309**, **305**, **308**, **314**, **290**, 134]. Studies have used anatomically defined regions of interest (ROIs), fixed shape ROIs placed at author discretion and temperature based ROIs [**312**, **303**, **304**, **306**, **315**, **301**, **313**, **310**, **309**, **305**, **308**, **314**, **290**, 134]. Whilst the anatomical approach (drawing ROIs based solely on surface anatomy) incorporated skin not overlying BAT deposits and lead to loss of specificity, it was objective, unlike author placed ROIs. Some studies have manually drawn ROI based on heat patterns and anatomy in an attempt to include only BAT [135]. Other studies have employed specific temperature thresholds to assist in drawing ROIs [135]. These include identifying the hottest 10-25% of pixels in the ROI or the hottest 5% pixel in the image [135].

Similarly, there is no consensus on optimal BAT activation protocol. Protocols generally consist of an acclimatisation period (although length varies from 5 min to 2 hours) and a cooling phase (fixed or personalised and of varying time period, 2min to 2 hours) **(table 5.1)**. There is general agreement that most cooling protocols produce a BAT response within 10 min but that personalised extended cooling protocols tend to be superior in identifying maximal BAT activity [135]. Additionally, whilst difficult to prove, it has been proposed that personalised protocols also help minimise insulator effects in obese subjects (i.e. inadequate cooling due to insulation by adipose tissue) [135].

| Study | Acclimatisation Length | Cooling Method | Duration | Number of Volunteers | Analysis Technique |
|---|---|---|---|---|---|
| Lee (2011) | Not stated | Air, 17°C | 30min | 1 | Fixed size ROI placed at investigator discretion |
| Symonds (2012) | 1 hour | Both feet or 1 hand in 19-20°C water for 5min | 5 min | 7 | 10% hottest pixels |
| Robinson (2014) | 5 min | Single hand in 20°C water | 5 min | 55 | 25% hottest pixels |
| Kim (2014) | Nil | N/A: Hypothyroid | N/A | 1 | Fixed size ROI placed at investigator discretion |
| Jang (2014) | Not stated | Air, 19°C | 2 hours | 17 | Anatomical ROI with hottest 10% pixels |
| Salem (2016) | 30 min | Cooling vest at 8°C for | 100min | 11 | Fixed size ROI placed at investigator discretion |
| Robinson (2016) | 30 min | N/A: mental stress | N/A | 5 | Anatomical ROI with hottest 5% pixels |
| Gatidis (2016) | 15 min | No cold activation | N/A | 102 | Anatomical ROI |
| Ramage (2016) | 2 hours | Hands in 15°C water then air temp dropped to 16°C | 10 min | 9 | Fixed size ROI placed at investigator discretion |
| Ang (2017) | 45 min | Both hands & feet in 18°C | 15 min | 24 | Video/ No ROI |
| El Hadi (2016) | 1 hour | Both hands in 5°C water for | 20min | 30 | Fixed shape but not size ROI drawn at author discretion |
| Peterson (2017) | 30 min | Both feet in ice water for | 2 min | 14 | Fixed size ROI placed at investigator discretion |
| Scotney (2017) | 30 min | N/A: pre/post meal | N/A | 8 | Anatomical ROI with hottest 25% pixels |
| Law (2017) | 30 min | Cooling vest at 8°C | 100 min | 8 | Anatomical ROI with hottest 10% pixels |

**Table 5.1:** Techniques used to activate and measure BAT using IRT

### 5.2.9 Hyperpolarised pyruvate MRI

Activated BAT is characterized by increased oxidative phosphorylation, which contributes to supply of ATP which is then converted to heat through the mitochondrial uncoupling protein 1 [128]. During this process, pyruvate utilisation in the Kreb cycle increases. Hyperpolarised pyruvate scans seek to utilise the increase turnover of pyruvate and production of (lactate and bicarbonate) to measure BAT activity [128]. This is achieved by injecting pre- polarized [1-13C] pyruvate and imaging with MRI to monitor the production of downstream products such as 13°C bicarbonate and [1-13C] lactate. This technique has been used in rats to identify BAT deposits and which were later confirmed with histological examination for UCP-1[128]. Whilst a small number of studies using this technique have been performed in Oxford, the scans are logistically difficult to perform and expensive [personal communications A/Prof Oliver Rider (University of Oxford)].

### 5.2.10 Glucose chemical exchange saturation transfer MRI

Glucose chemical exchange saturation transfer MRI (CEST-MRI), has been reported to detect the metabolic difference between cancerous and normal tissue [140]. CEST-MRI allows the identification of metabolically active tissue by enhancing tissues with high metabolite concentrations by a factor of 106[140]. During BAT activation, there are higher concentrations of glucose and fatty acids when compared to WAT due to the increased metabolic activity and blood flow. CEST-MRI has yet to be validated in detecting human BAT, but its success in other metabolically active tissues, and the absence of radiation, makes it an attractive imaging modality. Currently, this technology is being investigated by The Department of Bioengineering at the University of Oxford but is not available for use in human studies [personal communication A/Prof Michael Chappell (University of Oxford)].

## 5.3 Chapter Aims:

I aimed to determine whether individual with *PTEN* haploinsufficiency have reduced BAT activity compared to match controls. Specifically, I aimed to:

1. Develop and validate a radiation free and reproducible method to measure activated BAT function and the impact on energy expenditure.

2. To measure the effect of a loss-of-function *PTEN* mutations (if any) on cold induced energy expenditure, SCV BAT temperature, and cold tolerance.

## 5.4 Methods

Given the range of protocols utilised to date and the varied or inconsistent results in regard to the ability to detect BAT activity, validation of the protocol was required prior to undertaking the primary study. Two pilot validation studies were performed prior to the main study to validate the IRT protocol, BAT activation protocol and my ability to concurrently measure energy expenditure during BAT activation. The two studies used different cooling protocols. The first pilot study focused on testing my ability to capture BAT activity with IRT. For this reason, a brief fixed cooling protocol was used (details provided below), this allowed more volunteers to be recruited and was more suited to the young, lean population recruited. The pilot second study focused on the logistical ability to combined a personalised cooling protocol, measurement of energy expenditure and IRT. This protocol was more time consuming (90min cooling vs 30min) but was more suited to the CS population (higher BMIs and greater adiposity).

### 5.4.1 Ethics Approval and clinical trials registry

This study was reviewed and approved by the NRES Oxford B Research Ethics Committee (15/SC/0510) and CuREC (R51600/RE001). All participants were over 18 years of age and provided written informed consent before recruitment into the study.

### 5.4.2 Pilots study one – validation of IRT

The first pilot study was designed to determine if IR thermography could detect a temperature change in the supraclavicular (SCV) BAT. This study activated BAT using a brief air temperature based cold exposure to determine if, using this method, known associations with BAT function could be reproduced. Additionally, I wanted to demonstrate the intra-individual reproducibility of the technique.

Twenty three volunteers were recruited into a 1 day study and 9 of the volunteers returned to repeat the protocol to determine reproducibility. All subjects attend the Clinical Research Unit (CRU) fasted and changed into a standard hospital gown. Volunteers were rested at room temperature for 30 minutes to minimize the effects of travel through cold and allow acclimatisation. A visual analogue scale from 1 to 10 was used to assess temperature perception in the subjects. Blankets were offered to maintain feeling of thermoneutrality during the acclimatisation phase. At the end of the 30-minute period, a baseline image was taken. Volunteers were then exposure to cold (3 periods of 10 minutes in the cold room at 5°C). Images were taken after each exposure in the acclimatization room. At the end of the 3rd and final cold exposure, subjects were returned to the acclimatization room for imaging. Three further images were taken, at 40, 50 and 60 minutes to capture BAT activity during the re-warming process **(figure 5.2)**. All images were independently analysed by myself and a second reviewer (Ms Maia Patrick-Smith, Medical Student, University of Oxford) using FLIR Research IR Max software (FLIR Systems, Wilsonvile, USA). The mean value of the two reviewers is presented. The BAT temperature was calculated as difference between the mean BAT temperature (left and right) and the reference region over the sternum).

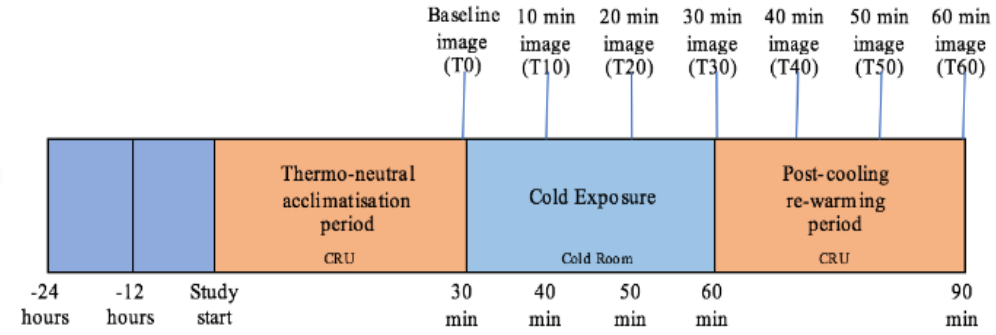


**Figure 5.2: Pilot Protocol Schematic**This figure demonstrates the protocol used in pilot study 1. Participants attended Clinical Research Unit (CRU), OCDEM, Churchill Hospital, had baseline measurement, were exposed to cold and had their SCV BAT deposits imaged at six time points.

### 5.4.3 Pilot study two – combined IRT and indirect calorimetry

The second pilot study used the identical protocol to the main study and attempted to test the feasibility of a personalized cool exposure and concurrent use of indirect calorimetry.

Cowden syndrome has previously been shown to be associated with obesity, a factor that can result in inadequate cooling [50]. Inadequate cooling has the potential to result in incomplete BAT activation, which may lead to false negative results. Whilst this can be overcome by severe cold exposure to ensure all individual maximally activate BAT, this would result in shivering and inability to measure EE due to BAT activation. Therefore, I chose a personalised cooling protocol. To date, a personalised cooling protocol has not been paired with IRT [135].

Eleven healthy volunteers completed the 2-hour personalised cooling protocol with concurrent IRT and indirect calorimetry. Participants attended the CRU fasted for 12 hours, where they changed into a hospital gown. Height, weight, waist, hip and head circumference were measured. Surface anatomy was marked with aluminium foil (detail provided in chapter 2), assisting with thermal image analysis. A water jacket was then applied at 36.5°C to keep volunteer's thermal neutral.**(figure 5.3)** The jacket temperature was then set to 25°C. The jacket temperature was then reduced by 1°C per minute until 4°C was reached. This was maintained for 71 minutes (total cold exposure time of 90min). If the volunteers began to shiver it was deemed that maximal BAT activity had occurred and the temperature was increased by 3°C to abort shivering. This temperature was maintained for the remainder of the study unless participants again began to shiver. If the participant began shivering again the temperature was increased by a further 3°C. This process was continued until 90 min **(figure 5.4)**.

### 5.4.4 Indirect calorimetry

Indirect calorimetry was performed using the Europa Gas Exchange Monitor (GEM) (GEM Nutrition Ltd, Cheshire, UK). The GEM is an open circuit gas exchange machine, where a pump draws in expired air from a ventilated hood. The measurement of oxygen, carbon dioxide concentration and flow rate allows determination of the oxygen consumption and carbon dioxide production. Using the modified Weir equation, EE(kcal) = 1.44(3.9VO2 +1.1VCO2), energy expenditure and respiratory quotient were derived. From these values, fatty acid oxidation and carbohydrate oxidation were calculated [84].

**Figure 5.3: Photograph of a Pilot Study**This figure is a still image taken during the pilot study and has been reproduced with the consent of the volunteer. It demonstrates the indirect calorimetry hood, and infra-red camera. Note: The camera was not used in this position. Imaging of the neck occurred sitting at 90 degrees with camera approximately at the level of the volunteer's cricoid cartilage.

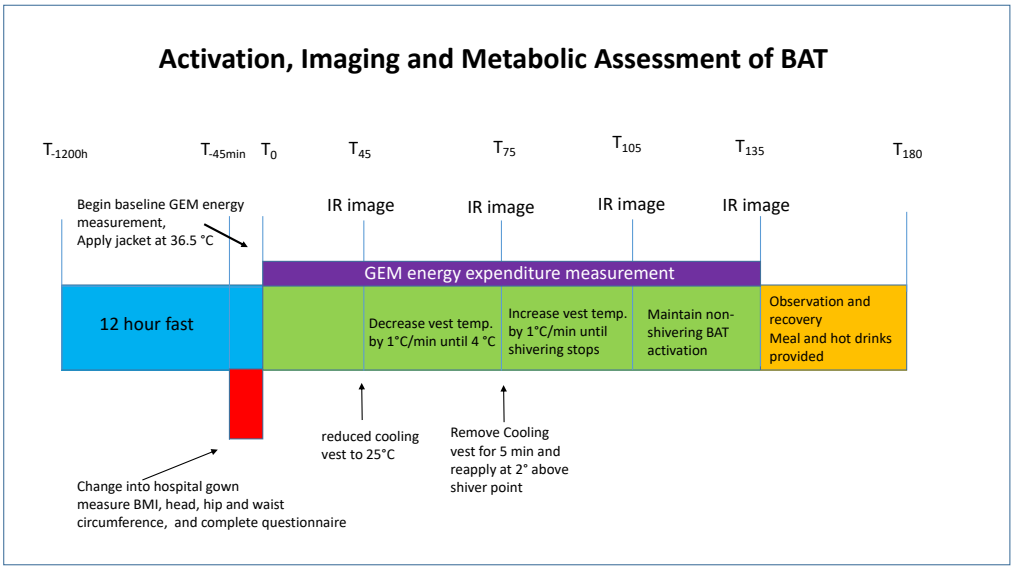


**Figure 5.4: Study Protocol: BAT Activation Protocol with Concurrent EE Measurement and IRT Imaging.**

### 5.4.5 Infra-red thermography

Infra-red thermography was performed using the FLIR T450sc (FLIR Systems, Wilsonvile, USA). The FLIR T450sc was used to detect the temperature profile of the neck and upper thorax of the study participant. The skin temperature in anatomical areas known to overlie BAT deposits (supraclavicular region) was measured by FLIR T450sc. The distance of 1 metre was used for all investigations and the emissivity (the amount of infra-red light emitted at a given temperature) was set to standard value for skin (0.98$\varepsilon$). Images obtained were analysed using the FLIR Research IR Program (FLIR Systems, Wilsonvile, USA). Regions of interest were drawn based on anatomical landmarks and the heat pattern following cold exposure. The heat pattern was drawn using the "fire and ice" function of FLIR, which highlights the hottest and coldest 5% of pixels. Regions of interest were drawn around the hottest 5% of pixels. These were then compared to a reference region (sternum) **(figure 5.5)**. To ensure consistent head position I constructed a head rest using sponge (Tesco PLC, Welwyn Garden City, United Kingdom) and duct tape (Tesco PLC, Welwyn Garden City, United Kingdom). When in the head rest, volunteers' necks were extended and rotation minimised by the supporting sponge.

Aluminium foil was cut into 0.5cm2 sections and placed over easily identifiable surface anatomy to allow images to be reproducibly analysed. Aluminium was fixed to skin using double sided adhesive tape. The middle panel of figure 5.5 is an example of the raw image produced by the thermal camera. The aluminium foil can be clearly seen on the image. Aluminium foil was used as a marker due the large difference in emissivity of metal compared to skin (emissivity of 0.04 vs 0.98$\varepsilon$), creating contrast on the thermographic image.

### 5.4.6 PTEN Study Design

Eight individuals diagnosed with CS and with confirmed mutations in the *PTEN* gene and eight age, gender and BMI matched non-carriers were recruited into an observational, recruit-by-phenotype study. The inclusion and exclusion criteria are presented below **(table 5.2)**.

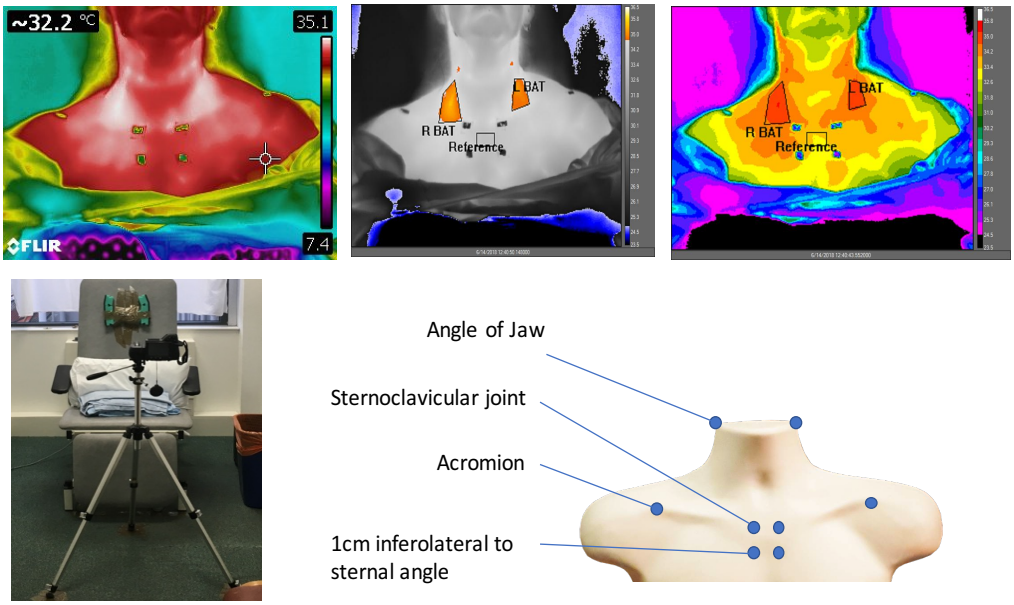


**Figure 5.5: Study Protocol: BAT Activation Protocol with Concurrent EE Measurement and IRT Imaging.**This figure shows the surface anatomy used to assist image analysis and thermographic image demonstrating how marking with aluminium foil provides identification relevant surface anatomy. Image has been reproduced with volunteer's consent and de-identified. The top 3 panels demonstrates how the BAT deposit can be identified by using the FLIR research IR software to identify the hottest part of the image to allow regions of interest to be drawn.

| Inclusion Criteria | Exclusion Criteria |
|---|---|
| CS + proven *PTEN* mutation | Malignancy within the last 2 years |
| Non-diabetic | Medication affecting insulin, glucose, or EE |
| Matched non-carriers | |

**Table 5.2:** Inclusion and exclusion criteria

### 5.4.7 Volunteer identification and recruitment

Individuals with Cowden syndrome were identified through collaboration with Dr Lisa Walker (Clinical Geneticist, Oxford University Hospital Trust), Dr Katherine Lachlan (Clinical Geneticist, Southampton University Hospital Trust), and recruitment at the PTEN United Kingdom and Ireland Patient Symposium. I presented the details of the study described above and upon request provided participant information sheets. Participants recruited into the Cowden's arm of the clinical study had the clinical diagnosis of Cowden syndrome, which was confirmed by clinical genetic testing and corroborated by Sanger sequencing off blood samples collected during the study. Non-carriers were recruited from the OBB.

### 5.4.8 Study Protocol

The study protocol was identical to that used in pilot study (described above) with the exception of the additional measurement of head circumference, measurement of body composition with bio-impedance and completion of a Cowden's syndrome screening questionnaire.

### 5.4.9 Confirmation of mutation status

To ensure that all CS patients had a LoF mutation in *PTEN* and all healthy controls did not, the leucocyte rich layer or "buffy coat" was collected and DNA extracted. All 9 exons were sequenced in forward and reverse using Sanger sequencing. Results for CS patients were cross-referenced with the mutation recorded by clinical labs.

### 5.4.10 Sample Size Calculation

Over expression of Pten in transgenic mice, (two-fold increase in Pten expression) resulted in a two-fold increase in FDG uptake compared to wildtype mice, with a standard deviation of 20% [61]. If a 50% reduction in PTEN expression, as might occur in a heterozygous carrier of a *PTEN* mutation, results in a 50% reduction with a similar standard deviation, then four matched pairs will need to be recruited (alpha=0.05, power=0.8). Given CS is extremely rare (1:200,000) in the general population, I attempted to recruit as many individuals in a 1 year period from November 2017 to November 2018 as possible.

### 5.4.11 DNA extraction

Following centrifugation of the EDTA tubes, the leukocyte rich "buffy coat" was removed and stored at -80°C. DNA was extracted using the Maxwell 16 (Promega Corporation, Madison, USA) (details provided Chapter 2). This DNA was then Sanger sequenced to confirm a *PTEN* mutation in CS patients or exclude one in volunteers. All nine exons were sequenced for all volunteers and patients.

## 5.5 Results

### 5.5.1 Pilot Study 1

#### Demographics

Twenty-three volunteers completed day one of the Pilot Study 1 protocol and nine volunteers completed day two **(table 5.3)**.

| | mean | DS | Range | n |
|---|---|---|---|---|
| Gender (M/F) | | | | 13F/10M |
| Age (years) | 35.5 | 13 | 20-56 | 23 |
| BMI (kg/m$^2$) | 22.5 | 3.4 | 16.9-29.2 | 23 |
| Waist : hip ratio | 0.8 | 0.1 | 0.7- 1.0 | 23 |

**Table 5.3:** Study demographics of pilot study 1

#### Quality Control

To assess for inter-reviewer bias or error in image interpretation, images were reviewed independently by two reviewers. The mean temperature differential between of both the left and right deposit and the reference region on the sternum was calculated, as was the max temperature differential between the left and right deposit and the reference region. I compared the value generated by each reviewer for each individual to assess the correlation between reviewers and highlight outliers. There was a strong correlation between reviewers for maximum temperature difference between left and right BAT depots and the reference region (r2=0.74 p<0.0001) and mean temperature difference between left and right BAT depots and reference region (r2=0.81 p<0.0001)**(figure 5.6)**. Images taken at the end of the cooling period were analysed as this was the time when BAT was most active**(figure 5.7)**.

#### Supraclavicular BAT temperature following cold exposure

Following cold exposure, the temperature differential between the reference region and the skin overlying the SCV BAT deposit increased, until maximal increase was reached at T30 (0.84 vs 1.47°C p<0.0001). After 20 minutes of rewarming the temperature

differential between BAT and the reference region was no different to baseline (0.84 vs 1.1 p= 0.40)**(figure 5.7)**.

## Reproducibility of infra-red thermography

To assess the intra-individual reproducibility of IRT to detect BAT activity. All volunteers were asked to return for a second visit. Nine volunteers completed a second visit. Visits were separated by no greater than 3 weeks. There was a moderate correlation between the first and second visit (r2=0.68, p=0.006) **(figure 5.8)**.

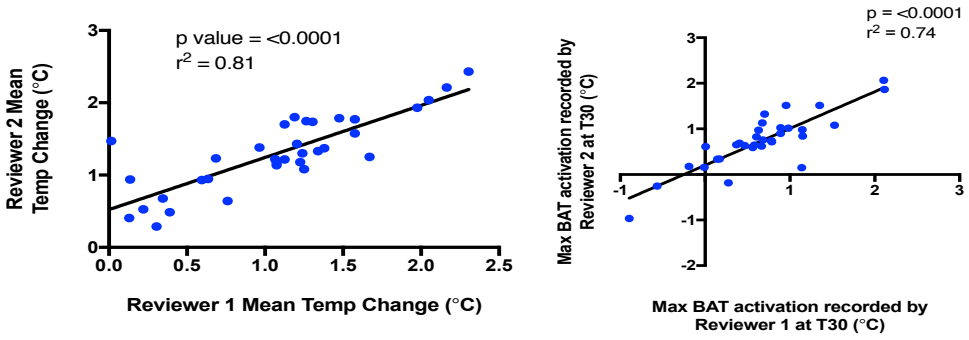


**Figure 5.6: Correlation Between Reviewers** This figure demonstrates the correlation between reviewer 1 and 2. Reviewers worked independently. All images were analysed by each reviewer in a single sitting. The left panel show the average temperature difference of the left and right deposit and the reference region, whilst the right panel shows the max difference between the left and right BAT deposit and the reference region.

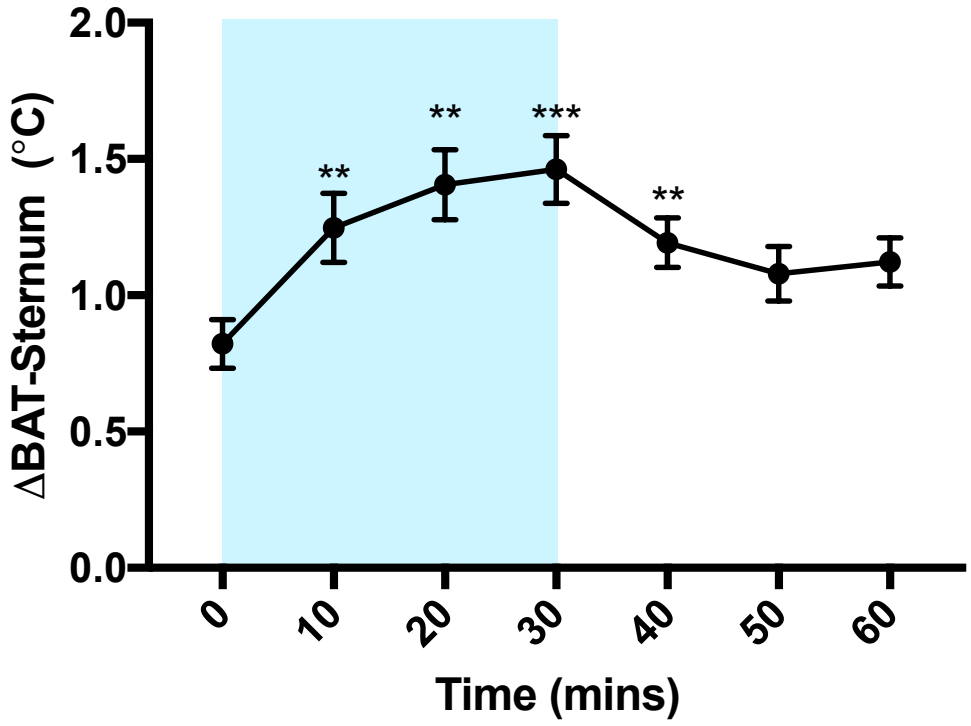


**Figure 5.7: Relative Supraclavicular Temperature Following Cold Exposure** This figure demonstrates the mean skin temp differential between the BAT deposit and the reference region following cold exposure. The light blue region demonstrates the time when the volunteers were exposed to cold. There was a significant increase in relative temperature in at 10, 20, 30, and 40 min compared to baseline. P values were adjusted with a Bonferroni correction. ** $p<0.01$, *** $p<0.001$.

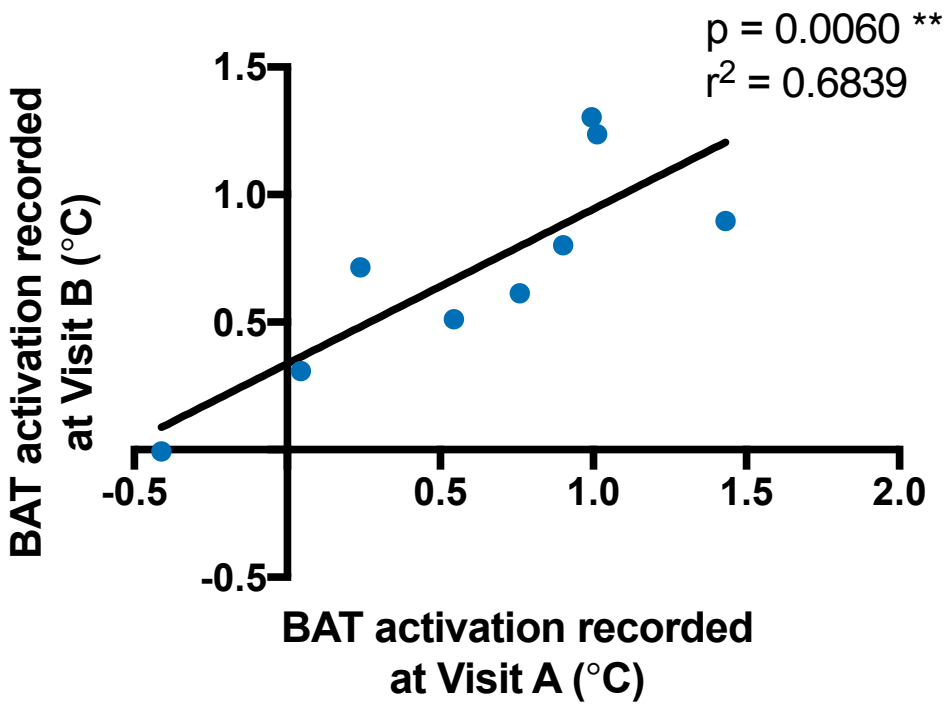


**Figure 5.8: Intra-subject Correlation of Repeated IRT** This figure demonstrates that IRT is reproducible in volunteers imaged repeatedly in a less than 3-week time frame.

## Correlations with previously established determinants of BAT activity

To assess IRT as a technique to detect BAT activity, I correlated the temperature change from of the BAT deposits relative to the reference region from T0 to T30 with previously demonstrated determinants of BAT activity (age, BMI, season). I observed a statistically significant negative correlation between age and BAT activity, but did not reproduce the association with BMI or season **(table 5.4)**. I assigned volunteers a 1 or 0 if their study was performed in summer of autumn. In regards to the effect of BAT on season there was a directionally consistent effect with the literature (albeit non-significant) with individuals tending to have lower BAT activity in summer. The detection of an association with BMI may have been limited by the individuals who participated in the study. The majority of individual had low-normal BMIs (average 22.5 kg/m2) and low to normal WHR (average 0.8).

| Variablee | Beta Coefficent | SE | P Value |
|---|---|---|---|
| BMI (kg/m$^2$) | 0.047 | 0.025 | 0.07 |
| Age (years) | -0.02 | 0.006 | 0.018 |
| Season | 0.18 | 0.16 | 0.29 |

**Table 5.4:** Associations with previously demonstrated determinants of BAT activity with IRT in pilot study 1

### 5.5.2 Pilot Study 2

#### Justification for second pilot study

Having demonstrated that IRT can identify changes in skin temperature overlying the largest superficial BAT deposits following cold exposure and that these correlate with age. I wanted to optimise the protocol to suit the investigation of CS and improve the protocol to allow concurrent measurement of EE due to non-shivering thermogenesis and substrate utilisation. Concurrent measurement of EE was not possible with the protocol used in Pilot study 1 as the cold exposure was achieved by entering a fixed temperature controlled room and this induced shivering in all volunteers. Shivering masks changes in EE and substrate utilisation due to BAT activity.

#### Recruitment and Demographics

Eleven volunteers completed the 2-hour protocol utilising a personalised cooling protocol via a temperature controlled water jacket, concurrent indirect calorimetry and IRT **(table 5.5)**.

#### Correlations with previously established determinants of BAT activity

I again observed that following cold exposure BAT temperature increased by 0.3°C (p=0.048). With the modification to the protocol, I was also able to demonstrate an increase in EE following cold exposure by 330kcal/day (p=1.6x10$^{-5}$)**(figure 5.9)**.

I attempted to re-produce already established associations with BAT activity. I examined BMI and age. Both correlations were directionally consistent with previously reported associations **(table 5.6)**. There was a statistically significant negative correlation between IRT and BMI (r= -0.58, p=0.048) but not age (r=-0.45, p=0.14).

| | mean | Range | n |
|---|---|---|---|
| Sex (M/F) | | | 7F/4M |
| Age (years) | 35 | 20-51 | 11 |
| BMI (kg/m$^2$) | 28 | 22-42 | 11 |

**Table 5.5:** The demographics of pilot study 2

There was a no statistically significant association between EE and either BMI or age. It is likely that I was underpowered to detect an association with only 11 volunteers.

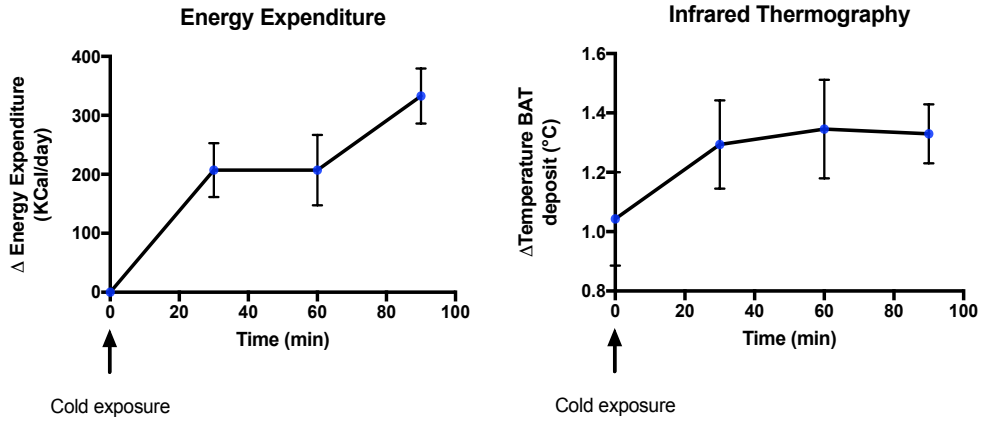


**Figure 5.9: EE and IRT Response Following Cold Exposure**This figure demonstrates the energy expenditure (left panel) and relative temperature increase following cold exposure. There was a significant increase from base line to the completion of the personalised cooling protocol in both EE ($p=1.6x10^{-5}$) and BAT deposit temperature ($p=0.048$).

| | BMI | Age) |
|---|---|---|
| Energy Expenditure (IC) | r= -0.223, p= 0.487 | r=-0.29, p=0.36 |
| Temperature Change (IR) | r=-0.58, p=0.048 | r= -0.45, p=0.14 |

**Table 5.6:** Reproducing associations with known determinants of BAT activity using a personalised cooling technique

| | Cowden (mean) | Control (mean) | P value |
|---|---|---|---|
| Sex (F/M) | (5/3) | (5/3) | N/A |
| BMI (kg/m$^2$) | 31.8 | 32.3 | 0.9 |
| Weight (Kg) | 99.3 | 96 | 0.7 |
| Percentage body fat | 31.9 | 36.2 | 0.6 |
| W:H Ratio | 0.9 | 0.9 | 0.8 |

**Table 5.7:** The demographics for the main study examining the effect of *PTEN* haploinsuficency on BAT Activity

### 5.5.3 PTEN and BAT

Between November 2017 and November 2018, 8 individuals with CS and 8 matched controls were recruited into an observational recruit-by-phenotype trial **(table 5.7)**. All 16 volunteers completed the 1 day protocol. One volunteer had to be replaced due failure of the GEM machine and loss of data mid-study. One volunteer's EE data was excluded due to persistent shivering despite increasing the temperature jacket.

### 5.5.4 *PTEN* Sequencing

All individuals with CS had *PTEN* mutations identified. Seven of eight of the mutations were protein coding. These mutations resulted in truncation, frameshift mutations, or missense mutations that were predicted by polyphen2 to be damaging **(table 5.8)**.

| Nucleotide Effect | Protein Effect | Exon | Protein Domain | Function Consequence |
|---|---|---|---|---|
| c.640C>T | p.214Q>X | 7 | C2 | Truncation |
| c.302T>C | p.101I>T | 2 | Phosphatase | Probably Damaging |
| g.70273het-dupG | intronic intron 5-6 | N/A | Frameshift | |
| c.513A>G | p.171Q>R | 6 | Phosphatase | Probably Damaging |
| c.97-99 het-delATT | p.33 (ILE>del) | 2 | Phosphatase | Phosphatase null |
| c.176C>CG | p.S59S>X | 6 | Phosphatase Truncation | |
| c.987-990het-delTAAA | p.329fsX | 8 | C2 Tensing | Frameshift |
| c.640-641het-delCA | p.213fsX | 7 | C2 Tensing | Frameshift |

**Table 5.8:** Mutations identified in CS carriers enrolled in the study. No mutation were identified in non-carriers. None of the mutations identified were recorded in GnomAD database.

### 5.5.5 Infrared thermography

To determine the activity of BAT the temperature of skin overlying the most superficial deposit was measured in individual with CS and matched controls. Whilst in both groups there was minimal response to cold there was a non-significant increase in controls and a non-significant decrease in the CS group. There was a significant difference in the temperature of the skin overlying the SCV BAT relative to reference region, the CS group had a 31% lower mean temperature than the control group (0.91 vs 1.31 °C, p=0.02) **(figure 5.10)**.

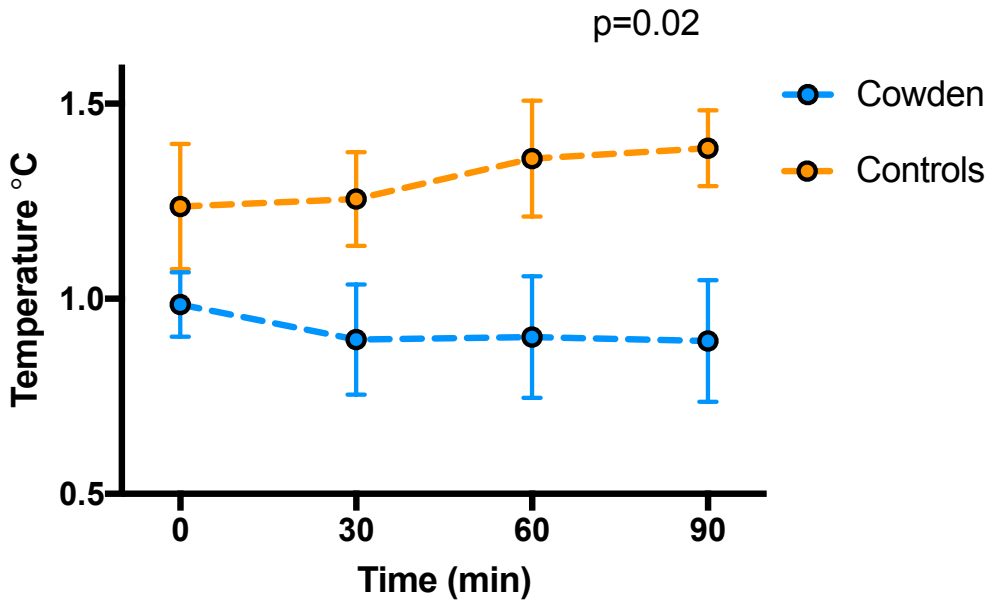


**Figure 5.10: Heat Produced by SCV BAT in Cowden Syndrome and Controls**This figure demonstrates the relative temperature of SCV BAT to sternal skin temperature in CS and controls. T0 represents baseline relative BAT temperature. Each individual's temperature is the mean of the left and right SCV BAT deposit. Data are the mean +/- SEM. P-vaule derived using RM-anova.

### 5.5.6 Indirect calorimetry

To determine the impact of reduced heat production by BAT, energy expenditure was measured using indirect calorimetry in individual with CS and matched controls. Interestingly, the CS group had a non-significant but substantially higher baseline EE **(figure 5.11)**. Following cold exposure, the control group had significantly increased EE at all time points with the maximum increase of 19% occurring at T90 (1523 +/- 86 vs 1813 +/- 93

Kcal/day, p=0.0006). However, in the CS group only at T90 was EE significantly increased from baseline at 10% (1981 +/-216 vs 2209 +/- 173, p=0.015). Whilst the increase over 90 minutes of cold exposure tended to be smaller in the CS group this was not significantly different **(figure 5.12)**. The maximum increase in EE was significantly reduced in the CS group (13.5 +/- 3.3% vs 23.9 +/- 2.3% p=0.02) **(figure 5.13)**.

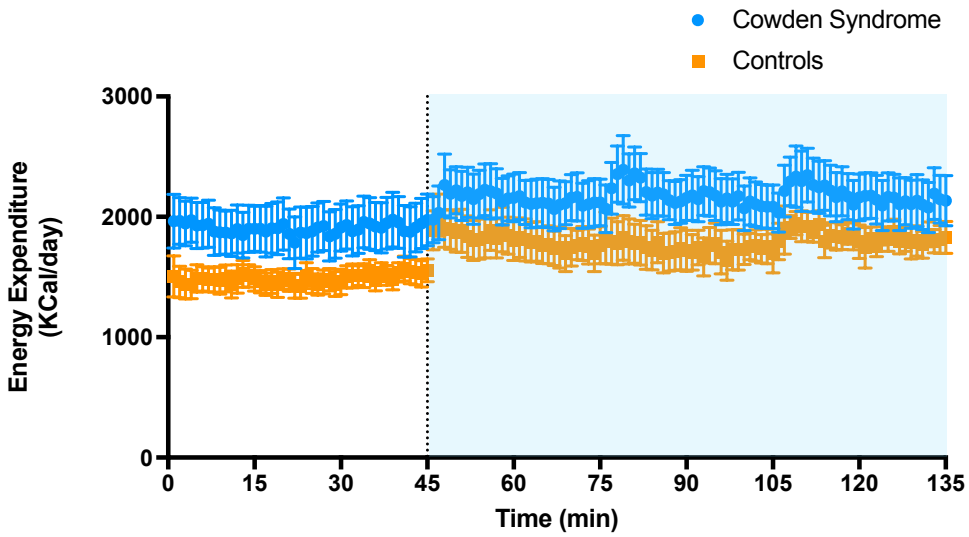


**Figure 5.11: Heat Produced by SCV BAT in Cowden Syndrome and Controls.** This figure demonstrates the absolute energy expenditure derived from indirect calorimetry using the modified Weir equation. Each data point is the mean EE determined over a 1 min gas exchange bin. Data are the mean +/- SEM.

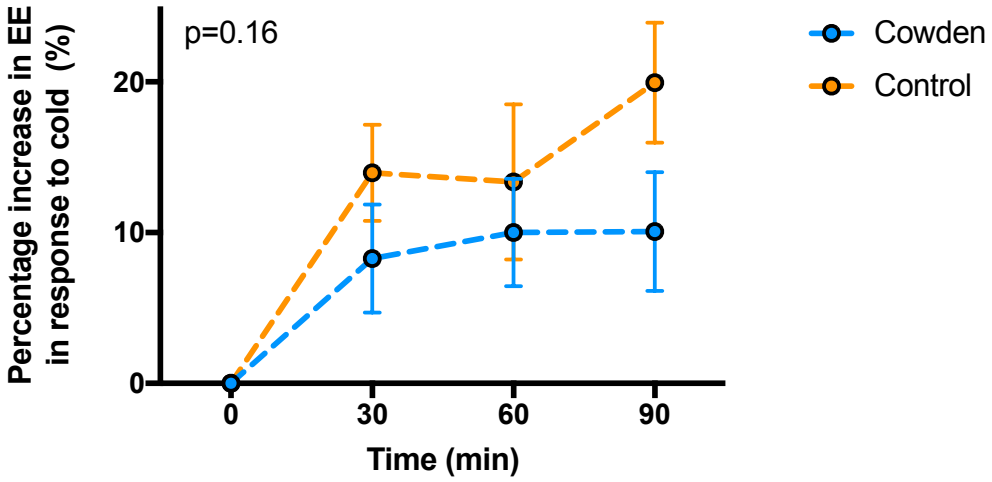


**Figure 5.12: Cold Induced Increase EE in Cowden Syndrome and Controls.** This figure demonstrates the absolute increase in EE following cold exposure. T0 is the baseline measurement. Energy expenditure was recorded as the mean energy expenditure over the preceeding 10 minutes. Data are mean +/- SEM. P vaule was calculated using RM ANOVA.

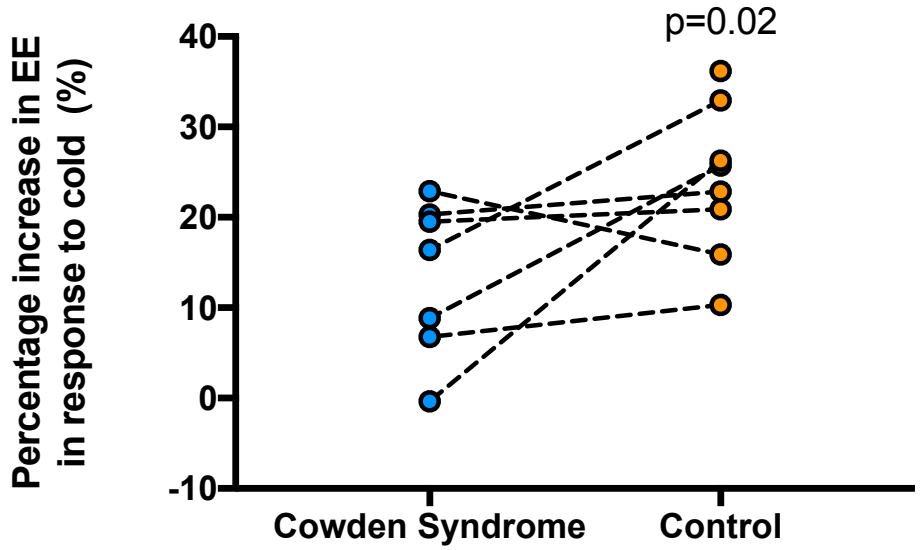


**Figure 5.13: Maximum EE Following Cold Exposure in CS and Controls.** This figure demonstrates the maximum increase in EE following cold exposure expressed as percentage increase from baseline. Each pair is linked with a dotted line to the matched individual. P value was calculated using an unpaired T-test as not all individuals had a pair.

### 5.5.7 Substrate Utilisation

As expected with cold exposure and BAT activation both the CS and control increased their fatty acid oxidation (FO), albeit non significantly (p=0.31 and p=0.15 respectively). There was no significant difference between FO profiles between groups (p=0.77) **(figure**

**5.14)**. The carbohydrate oxidation (CO) was not significant different after cold exposure in either group (p=0.99 and p=0.98 respectively). Again, there was no difference between the CO profiles between groups (p=0.59) **(figure 5.15)**.

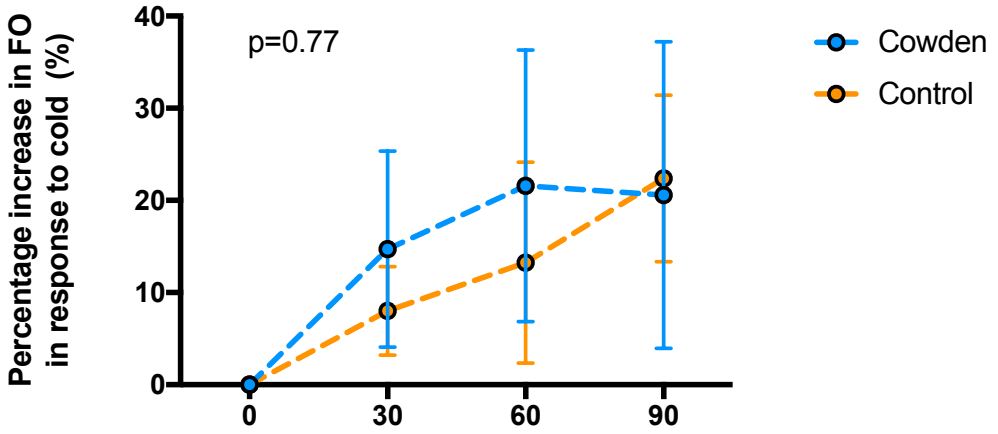


**Figure 5.14: Percentage Change in FO Following Cold Exposure in CS and Controls** This figure demonstrates the increase in FO following cold exposure expressed as percentage increase from baseline. Fatty acid oxidation was derived from respiratory quotient and EE derived from the modified Weir equation. Data are mean +/- SEM. P value was calculated using a RM Anova.

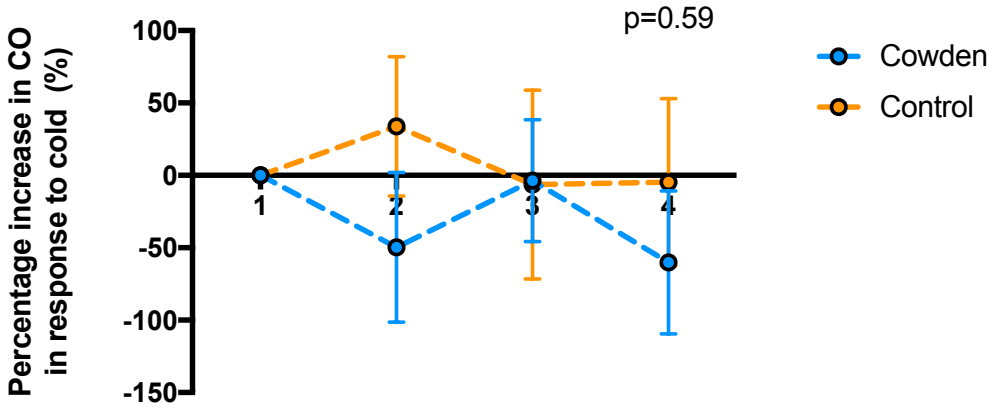


**Figure 5.15: Percentage Change in CO following Cold Exposure in CS and Controls** This figure demonstrates the increase in FO following cold exposure expressed as percentage increase from baseline. Carbohydrate oxidation was derived from respiratory quotient and EE derived from the modified Weir equation. Data are mean +/- SEM. P value was calculated using a RM Anova.

### 5.5.8 Cold tolerance

Cold tolerance was measured over two parameters. Temperature at onset of shivering and temperature of the jacket at completion of the study. Both outcomes are a measure of maximal non-shivering thermogenesis which is a function of BAT. If an individual did

not shiver throughout the study, i.e. tolerated the setting of 4°C, they were assigned a temperature of 2°. This assignment was performed as jacket temperature oscillates by 1°C around set temperature, imply the volunteer had tolerated 3 C. The mean temperature at onset of shiver was significantly higher in the CS group compared to control (5.9 +/- 1.7 vs 2.5 +/- 0.33°C, p=0.038). Similarly, the temperature of the jacket at the conclusion of the study was significantly higher in the CS group (15 +/- 2.8 vs 6.6 +/- 2.2°C, p=0.018) **(figure 5.16)**.

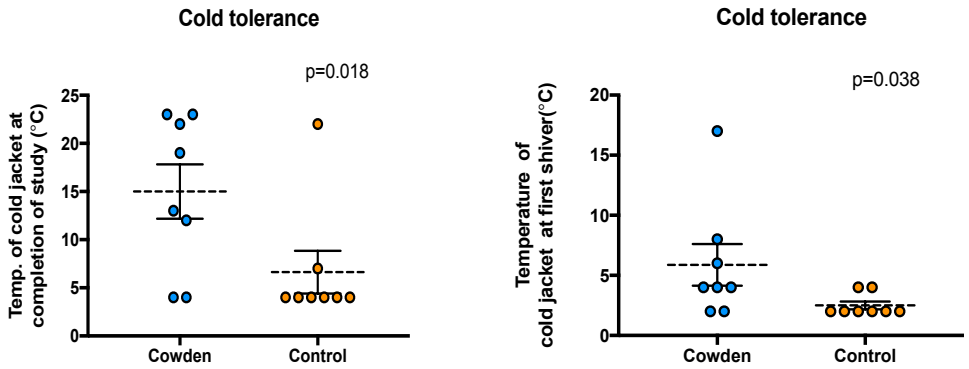


**Figure 5.16: Cold Tolerance in CS and Controls** TThe left panel demonstrate the temperature of the cold jacket at completion of the study. This is a measure of the maximum cold exposure that can be tolerated over 90min without shivering. The right panel demonstrates the temperature at which a first shiver occurred. If an individual did not shiver at the maximum cold exposure of 4°C of 90 min, this was conservatively assigned a value of 2°.

## 5.6 Discussion:

In this chapter I conducted two pilot studies to set up two protocols for measuring BAT activity with infrared thermography. In the first pilot study, I demonstrated that IRT was reproducible and could detect a change in BAT activity with a 30min uniform cold exposure and was able to reproduce the previously demonstrated relationship between age and BAT activity. In the second pilot study, I showed that using a controlled personalised cooling protocol delivered by cold jacket, IRT could be concurrently performed with indirect calorimetry to estimate both the heat production and the impact of BAT activation on EE. I then used this protocol to investigate the role of PTEN in the regulation of BAT.

With the appreciation that BAT contributes a significant portion of resting metabolic rate, interest has grown in augmenting BAT activity as a therapeutic tool for weight

loss [**107**, 135]. Research has focused on identifying pathways that regulate BAT in the hope of identifying means to augment BAT function. The PTEN/PI3k pathway has been proposed to regulate BAT [77]. Hitherto this relationship has only been examined in mouse, monkey, and cellular models [**107**, 61]. I sought to extend these studies to humans. Examining the BAT activity of patients with CS provided the opportunity to explore the effect of knockdown of PTEN on BAT function in the human setting and attempt to explain the obesity phenotype seen in CS.

Using the protocol developed in this Chapter, I demonstrated that carriers of *PTEN* loss of function mutations had significantly lower skin temperature overlying superficial BAT deposits. Presumably this was a result of decrease heat production by their SCV BAT deposits (the characteristic function of BAT). This corresponded to a 43% lower maximum increase in EE in response to cold exposure. In support of these findings, the CS group had a significantly reduced cold tolerance and began to shiver at higher temperatures, likely a result of reduced non-shivering thermogenesis and initiation of shivering thermogenesis to maintain body temperature. Based on these findings it is highly likely that under active BAT contributes to a positive energy balance and weight gain in CS.

The resting energy expenditure was non-significantly higher in the CS group, this is likely a result of the larger size of individual with CS. Whilst the groups were well matched for BMI, the CS group was on average taller (3cm) and heavier (3.3kg) and had a lower percentage body fat 31.9 vs 36.2%. This is in keeping with the previous finding of increased BMI but no significant difference in percentage adiposity or muscle mass (i.e. proportional increase in muscle and fat) [50]. The non-significantly increased age and greater adiposity (two factors negatively associated with BAT activity) observed in the control group adds weight to the conclusion that PTEN positively regulates BAT.

In this study, both the CS group and the control group had minimal BAT activity compared to the pilot studies. This is likely due to the demographics of the participants recruited. The pilot studies selected individual with the optimum demographics to have a large BAT response (younger, and leaner individuals) to assist in demonstrating the method could detect BAT activity. In contrast, the PTEN study demographics were based on matching individual with a predisposition to obesity.

The demonstration of positive regulation of BAT by the PTEN supports the use of PI3Ki in the treatment of obesity. The Gloyn group has previously demonstrated the CS patients have of reduced concentration of downstream products of PTEN/PI3K/AKT signalling pathway on adipose biopsy [50]. This, combined with the animal studies suggesting increased BAT activity and weight loss on administration of PI3Ki, as well as my data showing LoF mutation in PTEN reduces BAT function in humans, provides a compelling rationale that PI3Ki will increase BAT activity in humans and result in increased EE [**3**, 77]. The degree of EE increase would need to be determined by dosing studies. Based on the increase seen with over expression PTEN in animal models and the reduction seen with LoF *PTEN* mutations in humans it is tempting to hypothesise that the increase would be dose dependent [61].

In addition to promoting UCP-1 formation, PI3K also has increases AKT and which mediates translocation of GLUT4 into cell membranes. Therefore, use of PI3Ki to achieve weight loss will have to be counterbalanced with the expectation that it will make individuals more insulin resistant (at least until weight is lost) [77]. Indeed, this has been the case with the use of PI3Ki to treat malignancy in humans and has been demonstrated in mouse models [**317**, 141]. This effect is transient and in animal models insulin sensitivity returns to normal within cessation of PI3Ki [77]. Given the return of insulin sensitivity with cessation of PI3Ki, the relative ease of managing elevated blood glucose concentration (with medications that may further promote weight loss) and the expected improvement in insulin sensitivity, the case could be made that in some individual the benefits of weight loss may outweigh glycaemic complications.

In this Chapter, I propose and validate a method to concurrently image BAT activity and measure EE. The strengths of this were discussed in the chapter. However, there are a number of limitations to the use of this method. When analysing the images I viewed both the heat map and the anatomical markers before drawing the regions of interest around the BAT, this allows bias and subjectivity to be introduced into the analysis. I explored the option of using a purely anatomical definition of the ROI. This resulted in loss of sensitivity of the analysis with the temperature change of the BAT deposit being masked by including skin that was not heated by a subcutaneous BAT deposit.

Using the anatomical only method, I was unable to detect previously demonstrated associations of age and BMI that was possible with the inclusion of the heat map (data not presented). To minimise the bias, I used two heat maps to draw my ROIs, one with a 20-colour gradient to provide a full overview of the temperatures in the upper torso and neck and a second heat map identified on the hottest 5% of pixels which often (but not always) outlines only the BAT deposit. In addition, to provide rigor, the images were reviewed by two independent reviewers and the average was taken.

The field of BAT investigation has been assisted by the development of IRT as a cheap radiation free imaging modality. The field would be aided by consensus regarding cooling protocols and imaging analysis. Currently, it is hard to compare literature and draw conclusion as negative (or positive) studies may be due to inadequate cooling, or image analysis.

## 5.7 Conclusion

In this chapter, I describe the combination and validation of multiple modalities of BAT measurement into a single 2 hour protocol. I then use of this protocol to demonstrate that individual with CS have reduced BAT activity. This supports the conclusion that PTEN positively regulates BAT and the PTEN/PI3K pathway is a valid target for obesity in humans.

# 6

# PTEN MUTATION MOSAICISM

## 6.1 Chapter Synopsis

Phosphatase and tensing homologue (PTEN) has been shown to regulate insulin sensitivity and energy balance. Therapeutic manipulation of the PTEN/PI3K/AKT pathway is currently utilised for molecularly targeted cancer treatment (PI3K inhibitor therapy) and has been proposed for use in weight loss. However, the desired effects of increased energy expenditure and tumour suppressor action are accompanied by insulin resistance. Understanding the tissue specific metabolic effects of PTEN may facilitate improvements in PI3K inhibitor therapy. Cowden syndrome is a rare autosomal dominant cancer syndrome that results from *PTEN* haploinsufficency. To explore the tissue specific effects of PTEN/PI3K/AKT pathway in the human setting, I examined the clinical case of a rare mosaic carrier of a truncating mutation in exon 7 of *PTEN*. Using Sanger sequencing, I characterised the degree of PTEN mosaicism in accessible insulin sensitive tissues (muscle and adipose) and compared the insulin sensitivity in the mosaic CS patient (OGTT and EUH Clamp) to historical data for CS and controls. In keeping with the relatively high degree mosaicism observed in insulin sensitive tissue, the proband demonstrated similar insulin sensitivity to the CS patient group.

## 6.2 Background and Rationale

Cowden syndrome is a rare autosomal dominant cancer syndrome that results from mutations in the *PTEN* gene (described in detail in Chapter 1)[116]. Cowden syndrome is characterised by macrocephaly and increased risk of cancer, particularly of the thyroid, breast, endometrium and skin[**165**, 116].

To date, only 5 cases of mosaic *PTEN* mutations have been reported [**162**, **163**, **159**, **160**, 118]. In 3 of these (case 1,2  5), the proband presented with regional overgrowth, with multiple lipomas/neoplasms/lesions [**159**, **160**, 118]. On these occasions, the lipomas/neoplasms were sequenced, and a second mutation or nullzigosity was identified in multiple tumours in the region of overgrowth (the mutation was identical in all tumours). The conclusion in these papers was that a second hit mutation in a mosaic distribution had caused the presentation. In the 3rd case, the proband had a mild CS phenotype, with macrocephaly and thyroid disease [142]. He was identified after his daughter presented with CS. The fourth case was an individual who fulfilled the clinical criteria for CS (see Chapter 1) but did not have a *PTEN* mutation on Sanger sequencing of blood. Evaluation with next generation sequencing demonstrated low level mosaicism in blood (1.7%) and subsequent evaluation of other tissue demonstrated a greater percentage mosaicism (25-50%) [143]. These cases are summarised below **(table 6.1)**.

These reports have documented the effects of *PTEN* mosaicism on cancer risk and overgrowth. Pal and co-authors recently demonstrated that individuals with Cowden syndrome are constitutively insulin sensitive despite being obese [50]. Hither to, the effect of mosaicism on the metabolic features of Cowden syndrome has not been reported. Here, for the first time, I describe the effects of mosaicism on gold standard measures of insulin sensitivity, adipose tissue distribution and glycaemic traits.

| Case | Paper | Mutation | Presentation | Method of detection | Percentage Mosaicism |
|---|---|---|---|---|---|
| 1 | (Zhou, 2000)[144] | Germline: p.R335X Mosaic: p.R130X | Multiple neoplasms and regional overgrowth | Sanger | Not stated |
| 2 | (Caux, 2007)[118] | c.403A>G (p.I135V) with mosaic loss of heterozygosity | Multiple lipomas and regional overgrowth | Sanger | Not stated |
| 3 | (Lindhurst 2011)[145] | c.966A>G, 967delA. | CS in progeny, thyroiditis, macrocephaly | Sanger | 10% in blood |
| 4 | (Pritchard 2013)[143] | c.767-768delAG | Lhermitte-Duclos disease, macrocephaly, mucosal papillomas, acral keratoses, hamartomatous polyps, ganglioneuroma, lipomas, goiter | NGS<br><br><br><br>Sanger | 1.7% blood,<br><br><br><br>tumour:50%,<br>skin:50%,<br>colon:50%<br>cervix:25% |
| 5 | (Salo-Mullen 2014)[146] | c.403A>G; p.I135V | Early-onset breast cancer, macrocephaly, regional overgrowth, acral keratoses, uterine fibroids, hemangiomas, and neuroendocrine tumour | Sanger | “47% of cells” |

**Table 6.1:** Previously Reported Cases of *PTEN* mosaicism, methods of detection and phenotype of the proband

### 6.2.1 Metabolic effects of PTEN

Phosphate and tensing homologue is a dual specificity protein and lipid phosphatase. It primarily acts by inhibiting the phosphatidylinositol 3 kinase (PI3K) pathway [66]. This effect is mediated by hydrolysing the phosphatidylinositol (3,4,5)-trisphosphate (PIP3) to phosphatidylinositol (4,5)-bisphosphate (PIP2) (the opposite effect of PI3K)[147]. The metabolic effects of PTEN relate to the downregulation of PI3 dependent processes. Of relevance, PI3 activates AKT which mediates the translocation of GLUT4 into the membrane[148]. Effectively this means that PTEN, through its hydrolysis of PIP3, inhibits GLUT4 translocation into the membrane, this causes reduced insulin sensitivity. As outlined in Chapter 5, AKT also mediates the breakdown of PGC1$\alpha$ and FOXO which upregulate uncoupling protein 1 (UCP-1) synthesis [61]. The UCP-1 protein is the characteristic protein that allows brown adipose tissue to produce heat [73]. In Chapter 5, I demonstrate that PTEN positively regulates BAT activity, which may contribute to weight gain in CS. These two downstream processes may explain the main metabolic phenotype observed in *PTEN* haploinsufficency, obesity and insulin sensitivity [50]. Through the downstream effects of PIP3/AKT/MTORC pathway PTEN also negatively regulates cell survival, growth and proliferation [1]. These factors (amongst others) mediate the tumour suppressor effect of PTEN.

### 6.2.2 Mosaicism

Mosaicism refers to a post-zygotic mutation in cells derived from a single zygote that results in at least two genetically distinct populations of cells [**378**, 149]. Mosaicism can be divided into three subgroups; germline, somatic and gonosomal (combination of somatic and germline) [**378**, 149]. The pattern of mosaicism is largely determined by the timing and location of the *de novo* mutation. For example, very early mutations may result in a uniform percentage of mosaicism across the body, whilst those occurring after differentiation into endoderm, ectoderm or mesoderm will only effect tissue from this lineage (e.g. a mutation in endoderm may affect lung, pancreas, and thyroid etc.). For the investigation of the metabolic effects of PTEN, both uniform and tissue specific mosaicism may provide additional insight. Uniform mosaicism may provide insight into gene dose

effect (e.g. is there a level of PTEN suppression proportional to insulin sensitivity). Tissue specific mosaicism will allow assessment of physiological impact of PTEN in a subset of organs. It is important to note that there can be variation in percentage mosaicism even in uniform mosaicism. The percentage mosaicism can change over time, particularly if the mutation confers a growth advantage (which is likely in *PTEN* mutations). The variation in rate of cell turn over, or tissue specific survival benefit may cause variation in percentage mosaicism in different tissue.

## 6.3 Clinical Case

The proband is a 65 year-old man with a history of atrial fibrillation and asthma. At age 50 years, he developed an anal skin tag and was subsequently investigated with a colonoscopy. This revealed multiple (>40) hyperplastic polyps located throughout the caecum, colon and rectum **(figure 6.1)**. Repeat colonoscopy three years later identified extensive polyp regrowth. Given rapid recurrence of polyps, yearly screening with colonoscopies was initiated. Despite the frequent screening, numerous new polyps were identified with each subsequent colonoscopy. Following referral to a clinical geneticist, it was noted that he had macrocephaly, skin lesions on his face suggestive of trichilemmoma, and papules on his tongue. There was no obvious mosaic distribution of skin lesion (e.g. lines Blaschko). There was a high degree of clinical suspicion of CS. However, he denied a family history of CS or family history of thyroid, breast, or endometrial cancer (classical symptoms of CS). To identify a *de novo* mutation and confirm diagnosis, blood was collected for targeted sequencing of *PTEN* which revealed 18% mosaicism for a *PTEN* mutation. The mutation was located in exon 7 of *PTEN* (c.640C>T, p.Q214X) and resulted in a premature stop codon and truncation in the C2 phosphatase domain. The C2 phosphatase domain is important for membrane binding and is thought to play a role in position of the catalytic core (which is responsible for enzymatic activity of the protein) in the membrane [**379**, 66]. As the mutation is truncating it is likely to result in haploinsufficiency rather than a dominant negative pattern (which is often seen in missense *PTEN* mutations) [**5**, 150].

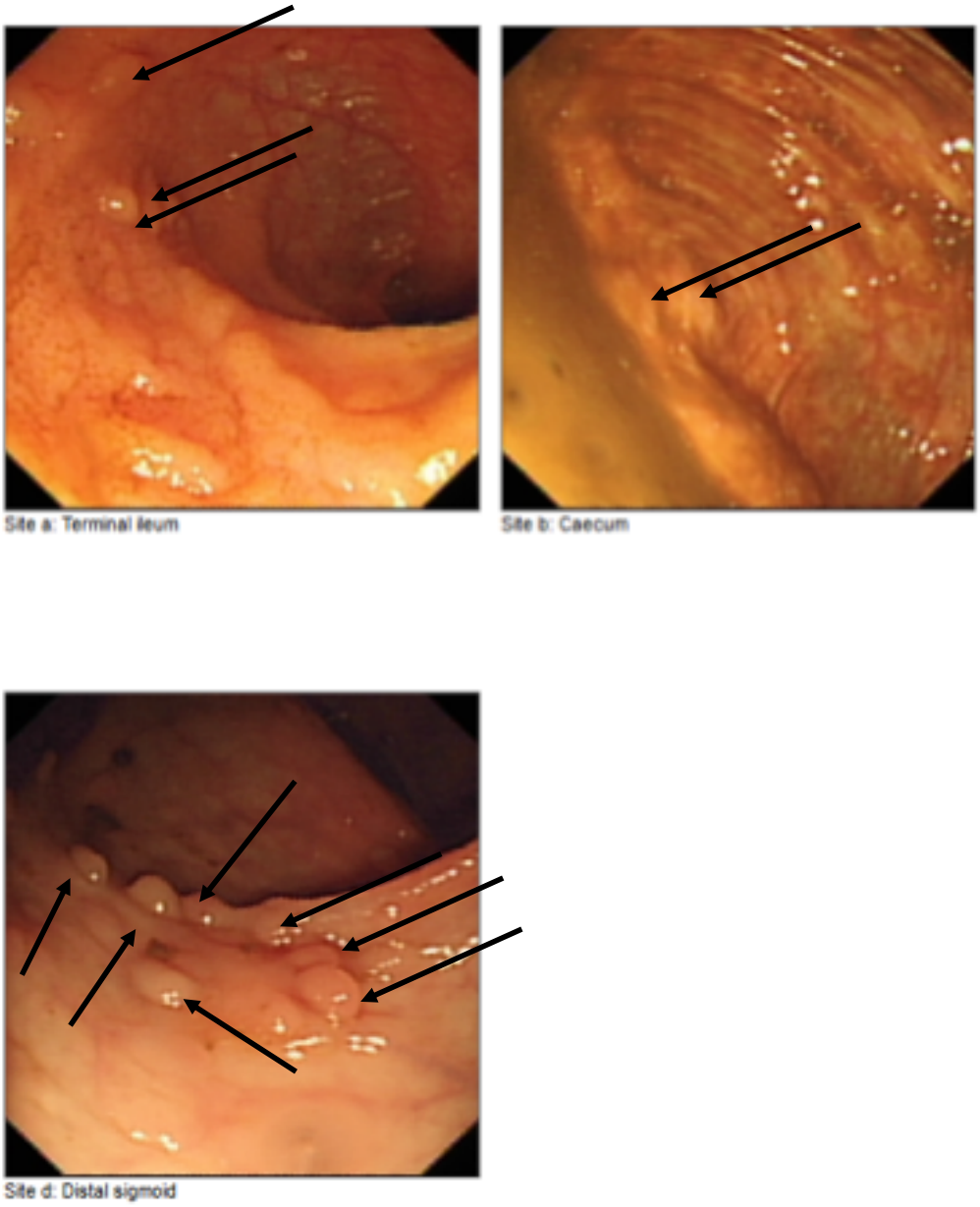


**Figure 6.1: Colonoscopy** This figure comprises 3 still images of the terminal ileum, caecum and distal sigmoid colon obtained during colonoscopy of the proband. The images demonstrate the abundance of small polyps. The majority are less than 5mm in diameter. Polyp location has been indicated by black arrows.

Following diagnosis, screening revealed thyroid carcinoma for which the proband underwent a total thyroidectomy. The proband's two daughters underwent genetic testing, one daughter was heterozygous for the same *PTEN* mutation, whilst the other daughter had two copies of the wildtype allele **(figure 6.2)**.

Based on the clinical feature of the proband's presentation and the transmissions

of the mutation to his daughter it is likely that the proband has widespread mosaicism affecting at least the gametes, oral mucosa, colon, thyroid, and skin. Given the wide spread manifestation of symptoms effecting tissue of different embryological origin (endoderm and ectoderm), it is tempting to hypothesize that a *PTEN* mutation may be uniform and also be present in metabolically relevant tissue (muscle, fat and liver).

The aim of this Chapter is to determine the percentage mosaicism in accessible insulin sensitive tissue and determine the effect this has on the metabolic phenotype of Cowden's syndrome.

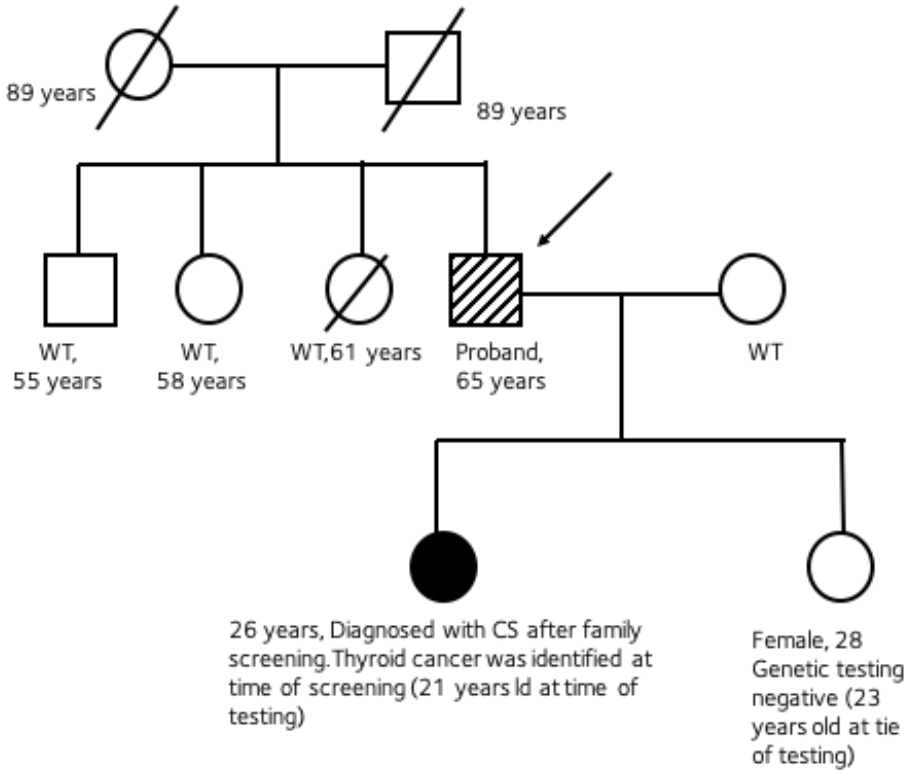


**Figure 6.2: Pedigree**This figure demonstrates the distribution of Cowden syndrome in three generations of the proband's family. The pedigree was drawn from history from the proband and confirmed by the treating geneticist. The proband's daughter who has the diagnosis of CS, was included in the study presented n Chapter 5, as a result I was able to confirm she carries the same mutation as the proband.

## 6.4 Methods

### 6.4.1 Characterization of Mosaicism

To enable characterisation of the mosaicism in insulin sensitive tissue, gluteal adipose tissue, abdominal adipose tissue, and muscle tissue were biopsied for DNA extraction.

Adipose tissue biopsies were performed after a 12 hour fast [50]. All biopsies were performed under local anaesthetic. Ms Jane Cheeseman (Research Nurse, University of Oxford) supervised all biopsies. A 14 gauge Sterican needle attached to a 50ml syringe was inserted into the relevant adipose tissue deposit. Suction was applied as the needle was drawn through the fat deposit to remove a small volume of adipose tissue [50]. Samples were cleaned (via irrigation with sterile water over filter paper), wrapped in aluminium foil, labelled, and snap frozen in liquid nitrogen before being stored at -80 °C [50].

The muscle biopsy was performed by Professor Fredrik Karpe (University of Oxford). The biopsy was performed under local anaesthetic. An incision was made over the vastus lateralis, tissue was separated until muscle was on view and a punch biopsy was performed. I assisted with tissue collection and sample preparation. I separated the muscle tissue from surrounding tissue. The sample was then weighed, wrapped in aluminium foil, labelled, and snap frozen in liquid nitrogen before being stored at -80°C.

The samples were thawed and DNA was extracted using a GenElute Mammalian Genomic DNA Miniprep Kit. Amplicon based Sanger sequencing was used to sequence all exons in *PTEN* in all tissues sampled (forward and reverse). This allowed direct screening for secondary mutations in *PTEN* and calculation of the percentage mosaicism by comparing the sequencing peak intensity on electropherogram. Mutation analysis was performed using Mutation Surveyor (Soft-genetics).

### 6.4.2 Characterization of metabolic phenotype

#### Control populations

To accurately characterize the proband's metabolic phenotype the proband's metabolic characteristics were compared to existing published data for patients with CS and healthy matched controls [50]. Data for 15 CS patients and 15 matched controls was available

for Oral Glucose Tolerance Test (OGTT), 5 CS patients and 5 matched controls were available for euglycaemic-hyperinsulinaemic clamp (EUH clamp) and 6 CS patients and 6 matched controls were available for DEXA imaging. Data on CS patients and controls were kindly provided by Pal and co-authors [50].

Given the multiple factors that affect insulin sensitivity matching is important to minimise confounding effects. Multiple strategies for matching were considered. Firstly, 1 to 1 matching of the nearest CS patient and control was considered. Unfortunately, the pool to match from was limited to 5 pairs who completed the EUH clamp, of these there was no appropriate match. Whilst the proband was only 3 years older than the oldest CS, the BMI of this individual was substantially higher at 30 compared to 24. Whilst one of parameter of age or BMI could be matched, both could not. Secondly, I considered matching to the proband to a carrier of the same mutation (his daughter) however the substantial differences in age, BMI and sex, would not allow the effect of mosaicism to be isolated. I chose to match the proband to the entire sample of individuals undergoing the OGTT/EUH clamp/DEXA in the hope that additional number may offset the effects of age and BMI. This is a substantial limitation of the study.

The metabolic phenotype of the proband was characterized by a frequently sampled 2 hour OGTT, EUH clamp and DEXA **(figure 6.3)**. The OGTT comprised a 75g glucose load. Insulin and glucose were measure at 0, 30, 60, 90 and 120 min. Glucose was measured on the Ilab 650 Analyser (Instrumentation Laboratory Ltd, Warrington, UK) and insulin concentration was determined using the Millipore Human Insulin RIA Kit (details in Chapter 2). The EUH clamp comprised a primed, continuous insulin infusion administer over 120 min. Glucose was clamped at 5mmol/L with a variable glucose infusion. Glucose and insulin were measured at 0, 30, 60, 80, 90, 100, 110, and 120 min **(figure 6.3)**. Insulin sensitivity was derived from the mean glucose infusion rate and ambient insulin during the EUH clamp [82].

Adiposity was assessed using the gold standard test for fat volume and distribution, the dual energy x-ray absorptiometry (DEXA) scan. This was performed using iDEXA machine (GE heathcare, Chicago, USA), and results were analysed in Encore Software

and compared to population data stored in the Encore software and data provided by Pal and co-authors.

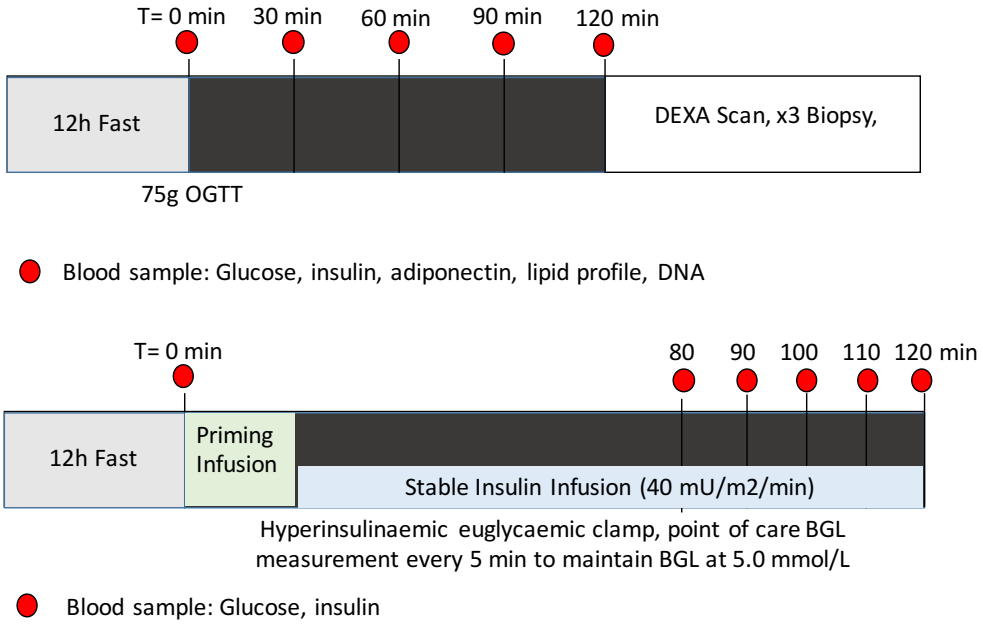


**Figure 6.3: Study Schematic**The study schematics depicts the 2 day study protocol. Day 1 comprised muscle and fat biopsy and OGTT. Day 2 comprised an EUH clamp. The schematic demonstrates the study protocol and the time points at which bloods are taken for analysis.

## 6.5 Results

### 6.5.1 Demographics

The demographics of the proband was compared to the demographics of the CS and controls provide by Pal and co-authors. The proband was older and leaner than the average CS patient and their matched controls for the OGTT, EUH Clamp and DEXA **(table 6.2)**. The proband also self-reported his exercise activity as high. Both the CS and control groups had a spread of low, medium and high self-reported activity.

### 6.5.2 Sanger Sequencing

To determine the percentage mosaicism and exclude a second mutation in *PTEN*, Sanger sequencing was performed. This confirmed the mutation detected during clinical screening (c.640C>T, p.Q214X) was the only mutation present in *PTEN* and established that the percentage mosaicism was substantially higher in insulin sensitive tissues than blood

| | Control | Cowden | Mosaic |
|---|---|---|---|
| **OGTT** | | | |
| Sex (M/F) | 7/8 | 7/8 | 1/0 |
| Mean Age (range) | 45 (34-67) | 44 (29-62) | 65 |
| Mean BMI (range) | 32 (23 – 40) | 32 (23 - 42) | 23.8 |
| **EUH Clamp** | | | |
| Sex (M/F) | 2/3 | 2/3 | 1/0 |
| Mean Age (range) | 42 (31-60) | 39 (29-62) | 65 |
| Mean BMI (range) | 31 (29 – 33) | 30 (28 - 33) | 23.8 |
| Self-reported Activity: | | | |
| Low | 2 | 2 | 0 |
| Medium | 2 | 2 | 0 |
| High | 1 | 1 | 1 |
| **DEXA** | | | |
| Mean Age (range) | 40 (31 -41) | 38 (24-62) | 65 |
| Mean BMI (range) | 32 (29 – 41) | 33 (30 – 43) | 23.8 |

**Table 6.2:** The demographics for pre-existing data for CS patient, matched control and the proband for OGTT, EUH Clamp and DEXA

**(figure 6.4)**. Percentage mosaicism was calculated for the forward and reverse sequence by comparing the amplitude of peaks on electropherogram using the mutation quanitifer function in Mutation Surveyor (Soft-Genetics), the mean of these is presented below.

### 6.5.3 Metabolic Characterisation

Having determined that the proband had a heterozygous loss of function in 30-36% percent of alleles in insuln sensitive tissues much higher than that observed in blood, I then assessed the impact on the metabolic phenotype with OGTT, EUH clamp and DEXA scan.

In all groups blood glucose increased following the oral glucose load and then decreased back toward baseline. It should be noted that there was no statistically significant difference in glucose profile in the data provided by Pal and co-authors between CS and control groups in the OGTT. The postprandial plasma insulin concentration increased following glucose load in all groups. The magnitude of the increase in the proband was substantially lower compared to the control group, and was in a similar range to the CS

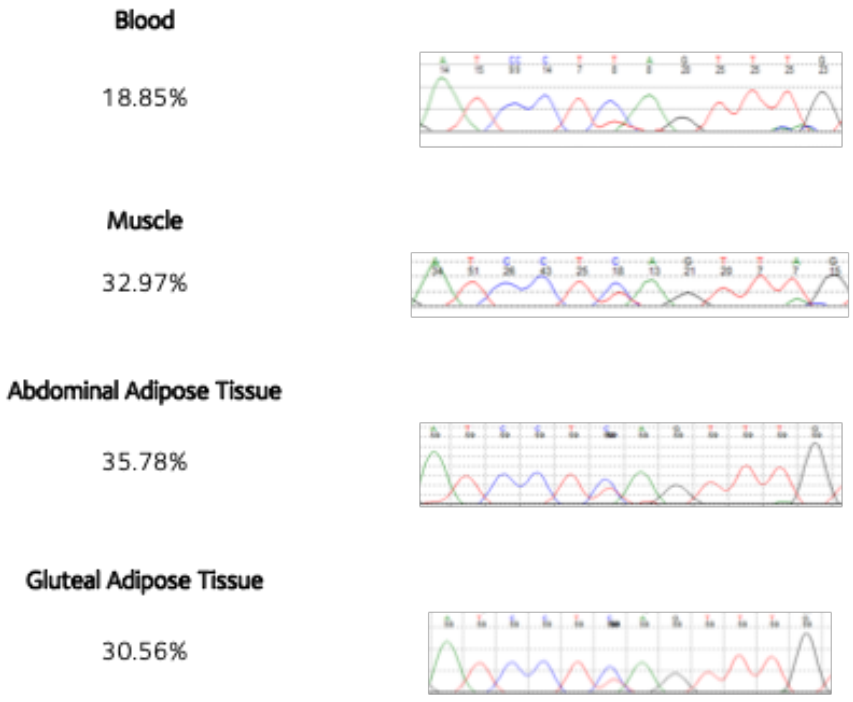


**Figure 6.4: Electropherogram and Mutation Percentage**This figure demonstrates the electropherogram for each tissue sequenced and the percentage mosaicism present in each tissue. Sequencing results were analysed using the advance two directional analysis function in Mutation Surveyor (Soft-Genetics). Mutation percentages were calculated using the mutation quantifier function.

patient group **(figure 6.5)**. Derived measure from the OGTT were suggestive of insulin sensitivity at a similar level to CS patients **(table 6.3)**.

To confirm the observation of increased insulin sensitivity, an EUH clamp was performed. The EUH clamp demonstrated the proband had a higher glucose infusion rate to plasma insulin concentration ratio (M:I ratio) than the average Cowden patient, which was substantially higher than the average of the control group **(figure 6.6)**.

| | Control | Cowden | Mosaic |
|---|---|---|---|
| **OGTT** | | | |
| Fasting insulin (pmol/L) | 74.3 (22.1–184.6) | 29.2 (8.7–99.3) | 44.4 |
| HOMA-IR | 1.3 (0.4–3.3) | 0.61 (0.4-1.9) | 0.82 |
| IGI30 | 199 (91–512) | 47 (8–510) | 129 |
| Matsuda Index | 8.9 (4.6–33.8) | 19.6 (6.3–54.1) | 17.9 |

**Table 6.3:** OGTT derived measures of1. insulin sensitivity and beta cell function. This table compares OGTT derived measures of insulin sensitivity and beta cell function in controls, CS patients and the mosaic proband. In HOMA-IR and fasting insulin, higher values indicate less insulin sensitivity whilst higher Matsuda index indicates greater insulin sensitivity. Higher IGI30 indicates increased beta cell function. Values presented are the geometric mean +/- range.

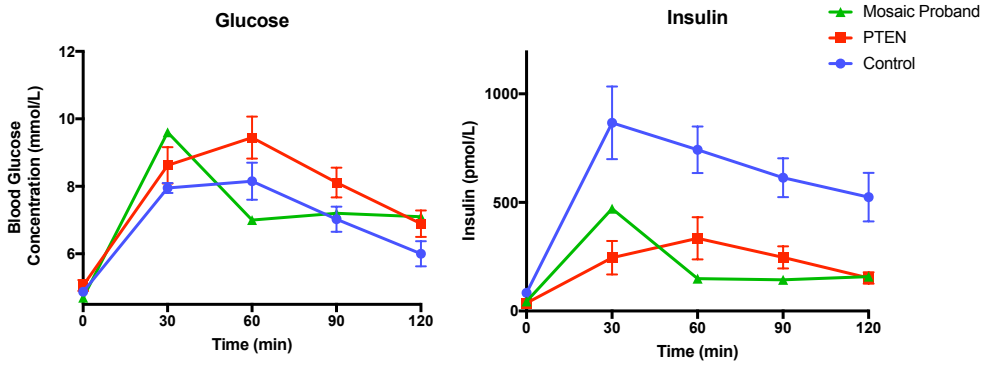


**Figure 6.5: Oral Glucose Tolerance Test.** This figure demonstrates the glucose (left panel) and insulin (right panel) response to a 75g glucose load. The Mosaic individual is compared to 15 Cowden Syndrome Patients and 15 controls. The mean values for Cowden syndrome patients and controls and been presented. Data for CS and controls are mean +/- SEM.

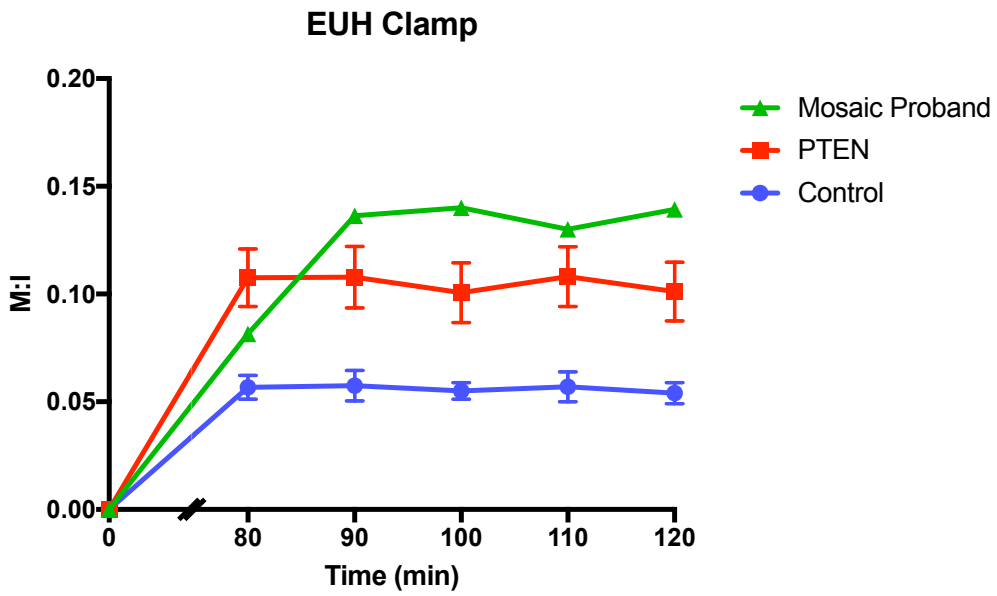


**Figure 6.6: Hyperinsulinaemic-Euglycaemic Clamp.** This figure demonstrates the insulin sensitivity of the proband compared to 5 Cowden's Syndrome patients and 5 controls as measured by the gold standard EUH clamp. The M:I ratio is the ratio of milligrams per kilogram of body weight per minute of glucose metabolised (M) and the miliunits per litre of insulin in the plasma (I). The mean values for Cowden's syndrome patients and controls have been presented. Data for CS and controls are mean +/- SEM.

The proband had a normal BMI (23.8). Whereas the CS patients had an average BMI of 32 (23 - 42) Kg/M2. The controls were matched to CS patients for BMI, this makes comparison of the proband to these groups somewhat problematic, as regardless of the effect of PTEN both are substantially more obese than the proband. To overcome this the iDEXA Encore software was also used to plot the adiposity on a centile chart of stored population data from the USA. The total percentage adiposity for the proband's age was 20.7% which was in the 18th centile for his age and sex **(figure 6.7)**. Whereas the mean total adipose tissue percentage for the CS group was 38.2%. The distribution of fat was similar across the control group, CS group and mosaic proband **(table 6.4)**.

| | Lean Body Mass (kg) | Total Fat (%) | Android Fat (%) | Gynoid Fat (%) | Android/ Gynoid ratio |
|---|---|---|---|---|---|
| Controls | 52.0 | 40.6 | 52.2 | 47.2 | 1.1 |
| Cowden | 54.6 | 38.2 | 48.2 | 43.9 | 1.1 |
| Mosaic | 55.4 | 20.7 | 22.1 | 22.4 | 1.0 |

**Table 6.4:** Adipose tissue distribution in CS, controls and the proband

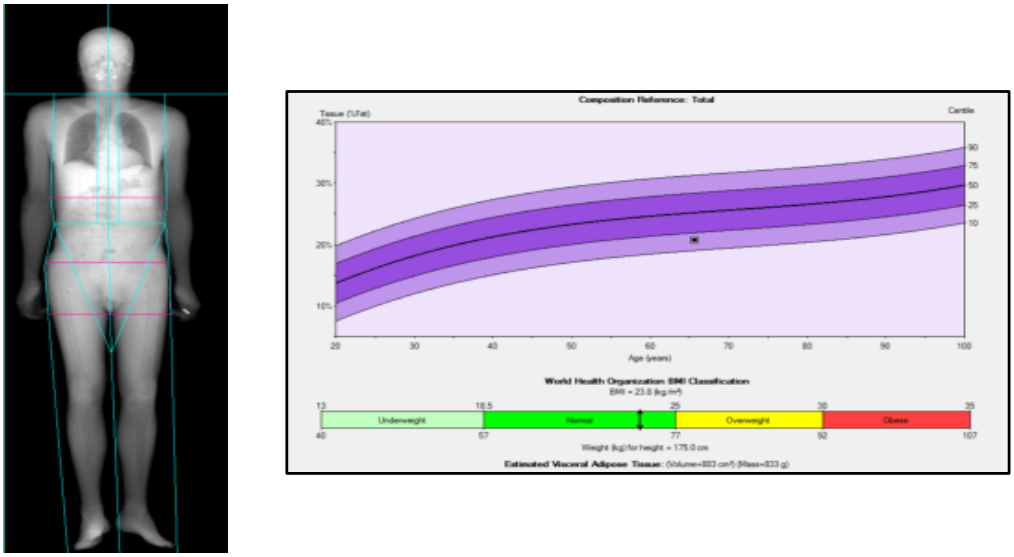


**Figure 6.7: Dual Energy X-ray Absorptiometry** This figure depicts the fat mass and distribution seen on DEXA, BMI and the fat mass as a percentage of total mass. Additionally, it provides detail of where the mosaic individual fat mass percentage lies on a population distribution.

## 6.6 Discussion

This is the 6th report of mosaicism in *PTEN*. Previous reports describe the impact of mosaicism on the cancer phenotype. Since these cases were published, it has been demonstrated that, in addition to a cancer phenotype, individuals with *PTEN* haploinsufficiency also have profound insulin sensitivity and increased adiposity [50]. In this case report, the proband had a truncating mutation in exon 7 of *PTEN*, resulting in a mild cancer phenotype, no increase in adiposity, and profound insulin sensitivity. I show, using the gold standard measure of insulin sensitivity, the EUH clamp and indices derived from an independent oral glucose tolerance test, that the proband is as insulin sensitive as individuals diagnosed with CS. The metabolic characterisation presented above is in keeping with the percentage mosaicism revealed in the sequencing of insulin sensitive tissues and a leaner phenotype. I show that the mutation percentage in DNA extracted from accessible insulin sensitive tissues (muscle and two adipose tissue depots) was double that in blood. Interestingly, the proband did not demonstrate increased adiposity, an expected feature of the metabolic phenotype of CS. In Chapter 5, I demonstrated that PTEN positively regulates for brown adipose tissue (a tissue that increases energy expenditure) function, a conclusion supported by animal studies [**107**, 61]. In this individual, I sampled both muscle and white adipose tissue (two tissues embryologically similar to brown adipose tissue) and found high levels of mosaicism but no obesity phenotype. It is important to note that the obesity phenotype is particularly sensitive to environmental and lifestyle factors and the proband's self-reported physical activity was categorised as high and may be attributable to environmental factors. The lower BMI observed in proband compared to CS patient group may have contributed to the marked insulin sensitivity observed. Ideally, a comparison with age, gender matched carriers and controls would have been performed. Unfortunately, none of the 5 individual who underwent EUH clamp were of a similar age or BMI. Additionally, the recruitment of healthy volunteers was limited as the OBB only has individuals up to 60 years of age [79].

In the clinical setting blood is often the only tissue that is sampled for the diagnosis of genetic disorders. When a mosaic mutation is identified, there is often uncertainty

for patients and clinicians as to how severe the phenotype will be. This is particularly important in cancer causing mutations such as loss of function variants in *PTEN*. Both this case of mosaicism and that reported by Gammon and co-authors demonstrated an intermediate cancer phenotype [142]. The case reported by Prichard and co-authors demonstrated a severe cancer phenotype with barely detectable level of mosaicism in blood [143]. Whilst the other cases of mosaicism consistently demonstrate that when detected, a second hit mutation in *PTEN* results in extremely severe phenotype with regional overgrowth. These cases are reminiscent of Proteus syndrome (a regional overgrowth syndrome due to an activating mutation in the AKT gene), with such a severe overgrowth phenotype that they are likely incompatible with life if present globally [145]. In support of this comparison, mice studies have demonstrated that global homozygous PTEN knockout is embryologically lethal [**320**, 151]. Proteus syndrome like CS, results from mutations in the PTEN/PI3K/AKT pathway and is also rare [145]. There is a degree of overlap in the clinical presentation of carriers of mutations that effect mediators of the PTEN/PI3K/AKT pathway. Eighty-five percent of people with CS have a *PTEN* mutation identified, in 10% of the individuals with CS but PTEN mutation negative, a mutation was identified in PI3KCA or AKT [152]. Whilst PTEN is relatively uniformly expressed in all cell types, other mediators of the PTEN/PI3K/AKT pathway are not and this may allow assessment of tissue specific effects of the pathway (discussed below).

The cancer phenotype is inherently different from a metabolic phenotype. Cancer risk is stochastic, with a random mutation in a single cell being able to give rise to cancer, whereas the metabolic phenotype is driven by the combined effect of all the insulin sensitive cells in the body. Whilst difficult to prove, this may suggest that metabolic phenotypes are more closely linked to the percentage mosaicism. Whilst it is not possible to draw a robust conclusion from a single case report, the insulin sensitivity is in keeping with the relatively high percentage mosaicism. Importantly, for both the cancer and metabolic phenotypes, my data and that of Pritchard and co-authors highlights that simply sampling a single tissue type, like blood, may not be representative of the percentage mosaicism in other (including metabolically active) tissues [143]. In instances where a clear tissue distribution of the mutation can be determined based on an embryological

pattern, it may be possible to tailor screening. However, in developmentally early mutations, like that seen in the proband, it is not possible to predict the percentage mutation in metabolically relevant tissue by sampling only blood.

A limitation of this study was that it was a case report. This was unavoidable as mosaic variants impacting PTEN/PI3K/AKT pathway are rare. Consequently, it is difficult to provide definitive insight into the importance of tissue specific impacts of alteration of the PI3/AKT pathway. Examining alleles that occur at a higher frequent and are less damaging alleles may provide an alternative route to robust insight. If these alleles have different expression patterns, contrasting the effects of the two alleles may provide insight into tissue specific effects of the PI3K/AKT pathway.

Recently, two variants, TBC1 Domain family, member 4 gene (TBC1D4) (p.R363X) and AKT2 gene (p.P50T), that impact the PTEN/PI3K/AKT pathway and alter insulin sensitivity and diabetes risk, were identified in founder populations [**173**, 153]. The effect of these variants on insulin sensitivity and diabetes risk contributes to the understanding of tissue specific insulin signalling [**173**, 153]. Both variants result in deleterious effects on important proteins in the PTEN/PI3K/AKT pathway. TBC1D4 is a mediator of the Rab induced GLUT4 membrane translocation [**173**, 154]. AKT2 is one of the most important members of the AKT family in insulin signalling [**382**, 66]. R363X only affects the isoform of TBC1D4 expressed in muscle and not in adipose or liver tissue [42]. This results in a profound insulin resistance and an odds ratio for diabetes of 10.3 [42]. This in contrast to the AKT2 mutation which is probably less damaging to protein function, but is expressed broadly across liver, fat, and muscle. P50T also causes insulin resistance but this only results in an odds ratio for T2D of 1.1 [153]. Taken together, this could suggest that the severity of the impact of genetic variants on the AKT pathway is more important than the breadth of insulin sensitive tissue affected in determining insulin sensitivity and diabetes risk. This also suggests that if the PI3K/AKT pathway could be upregulated in a tissue specific manor and altering muscle alone is enough to have profound effects on diabetes risk. Alternatively, if PI3K activity was downregulated to achieve targeted cancer treatment or weight loss, these studies would suggest that sparing muscle may reduce the associated insulin resistance.

Modulation of the PI3K/AKT pathway, has been suggested as a potential therapeutic treatment for obesity, cancer and diabetes [**105**, **107**, 141]. Indeed, trials of the PI3K inhibitor, CNIO-PI3Ki, in monkeys and mice have shown promising results [77]. Cowden syndrome and other genetic variants in the AKT pathway provide a unique opportunity to identify and utilise genetic variation to assess the potential impact of therapeutic manipulation in this metabolically important pathway in humans. Whilst the cancer phenotype in CS argues strongly against the potential long-term use of therapeutics which globally inhibit PTEN, the data provided in this report and the other studies discussed above makes it tempting to hypothesise that activation of the PI3/AKT pathway specifically in insulin sensitive tissues may be a future therapeutic target to treat diabetes and insulin resistance. Additionally, the studies discussed above suggest that variants impacting the AKT pathway distal to PI3K maintain the impact on insulin sensitivity throughout the signalling cascade [**173**, 153]. This may suggest that therapeutic activation of this pathway distal to PI3K may provide a more specific effect on insulin sensitivity whilst maintaining potency.

## 6.7 Conclusion

I have reported for the first time the impact of *PTEN* mosaicism on gold standard measures of insulin sensitivity and contrasted the effect seen in the proband to carriers of heterozygous germline *PTEN* mutations and controls. Further study of genetic variants in the PTEN/PI3K/AKT pathway may continue to provide insight and guidance in therapeutic manipulation of this metabolically important pathway.

# 7
# *DISCUSSION*

Type 2 diabetes is a complex genetic and metabolic disease. Over 400 regions of the genome have been identified where variation is associated with altered T2D risk [**186**, **8**, 34]. Translation of these signals into mechanistic insight and improvements in clinical care has been relatively slow. In this thesis, I attempt to address this bottleneck in translation by characterising the physiological impact of loss of function (LoF) alleles in two genes that regulate glucose physiology and diabetes risk (*PAM* and *PTEN*). The work in this thesis establishes the clinically relevant phenotypes of GLP-1 resistance (amongst others) in carriers of *PAM* LoF alleles and supports the PTEN/PI3K/AKT pathway as a regulator of brown adipose tissue in humans.

To determine the role of PAM on GLP-1 physiology and PTEN on brown adipose tissue function, I used naturally occurring genetic variation and recruited individuals with down regulated gene function. In these individuals, I used a battery of tests to probe the physiological pathway in question.

## 7.1 Recruit-by-genotype studies

The majority of alleles associated with T2D are common and have a small physiological impact [**246**, 38]. Identifying these subtle changes in human studies, where between subject variation is high, is a challenge. This is particularly difficult when the sample

size cannot be increased (e.g. when in investigating rare alleles, rare diseases like Cowden syndrome, or when using low throughput phenotyping). This was the case in Chapters 3, 4, and 5. To maximize statistical power and the likelihood of a definitive result, I employed 3 strategies. Firstly, I sought to increase the effect size between groups by sampling from the extremes of genetic risk (e.g. comparing non-carriers to carriers of S539W rather than D563G, as S539W has a greater impact on beta-cell function and T2D risk)[**262**, 51]. Secondly, I attempted to minimize the variation by pairwise matching carriers and non-carriers. Finally, I used gold standard physiological tests (e.g. the matched isoglycaemic clamp) in the hope that increased sensitivity and specificity compared to surrogate measures would enable detection or exclusion of an effect associated with the allele in question.

Recruit-by-genotype studies can provide complementary insights to cohort and *in vitro* data. Specifically, recruiting individuals by genotype allows detailed and specific characterization and hypothesis testing in the human model that is impractical at a cohort level. This recruit-by-genotype approach is increasingly accessible due to increases in size and number of genotyped biobanks [155].

## 7.2 Potential impacts on clinical care

In Chapters 3 and 4, I explore the impact of two LoF alleles in *PAM* (D563G and S539W) on serum amidation activity, GLP-1 profiles and response to blood glucose lowering medication. PAM enzyme activity was significantly and substantially reduced in heterozygous carriers of S539W (-52%, $p=9.3x10^{-15}$) and D563G (20%, $p=8.0x10^{-4}$) compared to matched non-carriers. Associated with this reduction in enzyme activity was a significantly higher total GLP-1 concentration (AUC) in the post-prandial period, S539W (10% p=0.037) and D563G (30%, p=0.02). This effect was reproduced across multiple cohorts. Despite this I observed no increase in the incretin effect, I propose that *PAM* LoF allel carriers have GLP-1 resistance. Finally, in keeping with my hypothesis of GLP-1 resistance, carriers of S539W and D563G alleles have reduced response to GLP-1 receptor agonists -40% (p=0.025) and -18% (p=0.050) respectively.

## 7.3 Personalised medicine

Delay to reaching glycaemic target is associated with a higher HbA1c level and increased rate of diabetic complications [**241**, 99]. In Chapter 4, I show that after 6 months of GLP-1RA therapy, carriers of *PAM* LoF were less likely to achieve an HbA1c of <7% (S539W 0%, D563G 10%, vs non-carriers 30%). The logical clinical impact of this observation is that clinical outcomes of carriers of LoF alleles can be improved by using agents that are not affected by GLP-1 resistance. I show that the reduction in treatment response is specific to GLP-1RA (admittedly the SGLT2 class of oral hypoglcaemic agents was not tested). Based on the normal glycaemic response to other second line agents in *PAM* LoF allele carriers (sulphonylureas and dipeptidyl peptidase IV inhibitors) there is a strong case to prescribe these agents over GLP-1RA. GLP-1RA have a number of beneficial non-glycaemic effects, most notably, weight loss and reduced rates of cardiovascular events [**328**, **327**, 156]. It remains unclear if carrying a LoF allele affects these outcomes of GLP-1RA therapy. Retrospective, examination for the impact of *PAM* LoF alleles on these outcomes in large cohorts collected to examine cardiovascular outcomes is currently underway [**328**, 156]. In addition, to providing information on the cardiovascular outcomes these studies provide the opportunity to reproduce my findings and assess for agonist specific effects.

The clinically available GLP-1RA are biologically very different [19]. They vary in structure, frequency of dosing, potential of immunogenicity, half-life and duration of drug exposure [157]. Of particular importance for *PAM* LoF allele carriers, there is variation in amidation status amounst GLP-1RA (e.g liraglutide, the most prescribed agonist is unamidated whilst exenatide is amidated) [**362**, 158]. It is difficult to comment on the effect that any of these changes may have on response to treatment in carrier of *PAM* LoF alleles as the mechanism of GLP-1 resistance remains unclear. It is reasonable to hypothesise that if an umamidated GLP-1RA is administered the rate of amidation of these agonists may vary between carriers and non-carriers and this may affect drug response. The biological differences between the agonists is highlighted by different outcomes in large trials examining cardiovascular events and weight loss [**329**, **328**, **327**, 19]. The sample size examined in this thesis did not allow for separate analysis of the

individual agonists. With the availability of large data sets from pharmaceutical safety and cardiovascular trials, examination of the effect of *PAM* alleles (and other T2D associated alleles) may reveal agonist specific effects [**328**, **327**, 156]. These studies may be able to assess the impact of *PAM* alleles on cardiovascular outcomes associated with GLP-1 RA.

## 7.4 Drugability of the PAM pathway

The impact of PAM on GLP-1 sensitivity, beta-cell function and diabetes risk raises the question of whether the pathway is drugable [**10**, **262**, 37]. Importantly the work presented on PAM did not provide evidence of a causal link between amidation activity and GLP-1 sensitivity, only an association. However, previous studies have shown a link between catalytic activity of the PAM enzyme and beta-cell function [59]. Specifically, when catalytic inhibitors were applied to beta-cells a defect in insulin content was observed [59]. This suggests rescuing PAM function in carriers of S539W and D563G or augmenting PAM function in non-carriers may provide improved glycaemic control, potentially this may also sensitise individuals to GLP-1.

Supplementation of factors that facilitate amidation (copper) have rescued phenotypes and reduced tissue amidation induced by heterozygous PAM knock out in mice [109]. In these mice, addition of dietary copper rescued the phenotype of cold intolerance due to impaired TRH function (observed only under cold stress) [109]. Interestingly, the authors observe reduced UCP-1 expression and BAT activity, which they attribute to reduced stimulation of the noradrenaline production. Whilst no difference between TSH levels was observed in carriers and controls in my sample, S539W and D563G are associated with increased height and BMI. Binding of 2 copper molecules to PAM is required for PAM function [**12**, 109]. In mice, copper is the only non-synthesised PAM co-factor [109]. This differs from humans as they rely on dietary intake of both copper and ascorbate [109]. Copper deficiency has been shown in humans to reduce amidated peptide levels [159]. Most notably in Menkes disease (a disease of copper transport deficiency due to mutations in ATP7A, resulting in cognitive impairment, seizures and hypothermia), where reduction in amidated peptides of the hypothalamic/pituitary/adrenal/thyroid axis has been noted [**359**, 160]. Daily copper intake of 2mg is required to

avoid copper deficiency and maintain normal copper stores [161]. Copper deficiency has been noted at 0.38mg/day [161]. It should be noted that there is no evidence to suggest that supplementation of copper replete individuals will improve PAM function. Further examination of the impact of dietary supplementation of copper (and ascorbate) of serum amidation in humans may strengthen the case for its use in augmenting PAM function.

## 7.5 Thereputic manipulation of PTEN/PI3K/AKT pathway

In chapter 5, I examined the *PTEN* locus, which has previous been shown to regulate insulin sensitivity through the PTEN/PI3K/AKT pathway. Previous reports have shown *PTEN* haploinsufficency results in obesity in humans [50]. Recent, animal studies have also implicated PTEN as a regulator of BAT, and pharmaceutical inhibitors of the PI3K have shown specific promising weight loss results in small mammals, but this hypothesis had yet to be tested in humans [**107**, 150]. I sought to validate PTEN as a regulator of BAT (and potential therapeutic target) and under active BAT as a cause of obesity in CS. To this end I recruited 8 patients with CS and 8 matched control and examined BAT function using a novel protocol. Using this protocol, I demonstrated that carriers of *PTEN* loss of function mutations had significantly lower skin temperature overlying superficial BAT deposits (-31%, p=0.02). Presumably this was a result of decrease heat production by their SCV BAT deposits. This corresponded to a 43% lower maximum increase in EE in response to cold exposure. In support of a reduced BAT function, the CS group had a significantly reduced cold tolerance and began to shiver at higher temperatures (5.9 1.7 vs 2.5 0.33 C, p=0.038), presumably an adaption to compensate for inadequate non-shivering thermogenesis. This provides a strong rationale that PTEN is a positive regulator of BAT in humans and a promising therapeutic target for obesity.

In Chapter 6, I examined a mosaic carrier of a *PTEN* mutation to understand the phenotypic impact of restricted tissue mutation. This study was limited as it was a case report and the age and BMI of the proband limited good quality matching. Additionally, whilst there were differences in percentage of mosaicism between tissues, all tissue tested did have some degree of *PTEN* mutation making conclusions difficult to draw regarding tissues specific effects. The proband who has relatively high percentage mosaicism in

insulin sensitive tissue displayed a mild cancer phenotype, and insulin sensitivity but not obesity. From the existing literature, and Chapters 4 and 5 it is clear there are adverse on target effects. Some of these are mediated or manifest in tissue specific disease (e.g. increased insulin sensitivity in white adipose tissue, increased heat production in BAT, increased malignancy in breast and thyroid)[**3**, 116]. This case study suggests it is possible to overcome some on target effects (in this case, the obesity phenotype and retain insulin sensitivity). Whilst it is not currently possible to target the PTEN/PI3K/AKT pathway in just one tissue (e.g. it is not possible to use a PI3Ki and target only BAT to produce weight loss but not insulin resistance). A more feasible option for utilising PI3Ki for weight loss or treatment of malignacy would be pairing PI3Ki with a GLP-1RA or SGLT2 inhibitors which are weight negative, and may be able to control the PI3Ki associated hyperglycaemia [**330**, 16].

Moving forward with therapeutic manipulation of the PTEN/PI3K/AKT pathway should include consideration of all known effects of the pathway. Cowden syndrome is poignant example of the multiple metabolic (and oncogenic) effects mediated by this pathway. Down regulation improves glycaemic control but is associated with increased cancer risk and obesity. Indeed, manipulation of the PTEN/PI3K/AKT pathway with PI3K inhibitors in malignancy has been shown to increase glycaemia [141]. Interestingly, increased plasma insulin concentration that results from this PI3K inhibitor induced glycaemia has been associated with reduced effectiveness [78]. The proposed mechanism is that reactive hyperinsulinemia drives reactivation of the PI3K-mTOR pathway [78]. The logical extension of this is the use of insulin sparing hypoglcaemic agents (e.g. SGLT2 inhibitors and GLP-1RA which control glycaemia but produce a net reduction in insulin secretion and exposure) [78].

## 7.6 Developing novel tests to characterize relevant phenotypes

One of the major challenges in characterizing the physiological impact of causal alleles is having a suitable, sensitive and specific test to assess the phenotype or trait of interest.

The extension of *in vitro* studies into the human model is often suboptimal as non-specific surrogate measures are used to reproduce the observation in humans. Beta-cell mass is one such example. It is currently possible to demonstrate that certain genes or pharmaceutical exposures affect beta-cell proliferation and apoptosis and by extension beta-cell mass *in vitro*. For example, CCND2 has been implicated as gene regulating beta-cell proliferation *in vitro* and in mouse models [**333**, 162]. However, demonstrating that genetic variation in this gene alters beta cell mass is problematic in humans. Whilst studies such as the mixed meal tests, OGTTs and arginine stress test have been proposed there is no definitive test, currently the closest approximation is the arginine stress test [163]. This is a challenge I had to overcome for the measurement of BAT and amidation activity.

In the case of BAT activity, there was a sensitive and specific test but it was not appropriate use an 18FDG CT-PET scan in my study population due to the pre-existing risk of malignancy [**299**, 151]. Additionally, no accepted protocol existed for activation and measurement of maximal BAT activity with concurrent imaging and indirect calorimetry [164]. This required development and validation of a novel protocol. Validating a test of an important clinical endpoint can be a substantial contribution to the field. The protocol for BAT activation and measurement presented in Chapter 5 has been utilised in 3 subsequent projects in OCDEM to examine the effect of genetic variation in KCNK3, MC4R and circadian rhythm on BAT activity.

## 7.7 Future direction

Extending observations from cellular studies and GWAS to prospective studies in humans is a logical progression. Examining a single molecular path in a human poses a challenge. The interplay and feedback between physiological pathways makes isolating and testing a specific pathway difficult. Recruit-by-genotype studies are an efficient way to examine physiological impacts of alleles in the human model [**166**, 47]. As the cost of genotyping and sequencing continues to decrease, it is likely that the size of biobanks and GWA studies will increase. The UK biobank (one of the largest biobanks) currently has approximately 500,000 individuals genetic information and associated phenotype [165]. This data has already been used to help with the identification more signals of

moderate effect size and the ability to investigate alleles that were previously too rare to find adequate numbers of volunteers [36]. Of relevance to this thesis, the largest exome sequencing effort to date (24,791 cases and 22,440 controls) demonstrated a gene level signal in *PAM* that remained normally significant even after removing the 35 strongest individually associated T2D variants [166]. This suggests that *PAM* harbours additional variants that cause disease, some of which may be rare and of moderate effect [166]. If physiological tests allow this may mean extension of our knowledge into the molecular pathways that contribute beta-cell failure and altered insulin sensitivity.

Of the existing loci identified that alter diabetes risk, there is significant overlap with pathways targeted for therapeutic use (e.g PPARG and thiazolidinediones)[**188**, **8**, **1**, 166]. It is logical that carriers of alleles that alter a pathway used to therapeutically lower glucose exposure may have altered response to these medications. In this thesis, I have examined a single locus and show an effect on treatment response. It is a logical extension to perform additional genome wide associations studies to identify predictors of treatment response. It is realistic to expect in the future that probability of drug response may be determined by a combination of genetic response score and demographic factors. Efforts to identify patient characteristic that predict good/poor treatment response are ongoing. For example the Mastermind consortium have provided a framework for improving sulphonylurea and thiazolidinediones prescribing based on sex and BMI [167].

## 7.8 Conclusion

In conclusion, in this thesis I have aided in addressing the challenge of translating genetic associations into physiological insight and clinical application. In Chapter 3 and 4, I demonstrate that carriers of LoF alleles in *PAM* have altered PAM function, GLP-1 physiology and that alter response to a commonly used hypoglycaemic agent. In Chapters 5 and 6, I use individuals with CS to demonstrate PTEN positively regulates BAT function and that percentage mosaicism in muscle and fat may predict insulin sensitivity. These investigations add support to the recruit-by-genotype method as a means derive

physiological insight. The combination of these results and the novel techniques developed may pave the way for improvement in the use of current therapeutic options and development of novel agents for the treatment of type 2 diabetes and obesity.

# References


[1] Guariguata, L. et al. “Global estimates of diabetes prevalence for 2013 and projections for 2035”. *Diabetes Res Clin Pract* 103.2 (2014), pp. 137–49.

[2] International-Diabetes-Federation. *IDF Diabetes Atlas Eight Edition*. Report. 2017. URL: http://www.diabetesatlas.org/.

[3] Voight, B. F. et al. “Twelve type 2 diabetes susceptibility loci identified through large-scale association analysis”. *Nat Genet* 42.7 (2010), pp. 579–89. URL: http://www.ncbi.nlm.nih.gov/pubmed/20581827.

[4] Roglic, G. and Unwin, N. “Mortality attributable to diabetes: estimates for the year 2010”. *Diabetes Res Clin Pract* 87.1 (2010), pp. 15–9.

[5] Gilhotra, R. A. et al. “Non-traumatic lower limb amputation in patients with end-stage renal failure on dialysis: an Australian perspective”. *Ren Fail* 38.7 (2016), pp. 1036–43.

[6] Kahn, S. E., Hull, R. L., and Utzschneider, K. M. “Mechanisms linking obesity to insulin resistance and type 2 diabetes”. *Nature* 444.7121 (2006), pp. 840–6.

[7] Government Document. 2011. URL: http://www.who.int/diabetes/publications/diagnosis_diabetes2011/en/.

[8] Inzucchi, S. E. et al. “Management of hyperglycemia in type 2 diabetes: a patient-centered approach: position statement of the American Diabetes Association (ADA) and the European Association for the Study of Diabetes (EASD)”. *Diabetes Care* 35.6 (2012), pp. 1364–79.

[9] Adler, A. I. et al. “Association of systolic blood pressure with macrovascular and microvascular complications of type 2 diabetes (UKPDS 36): prospective observational study”. *Bmj* 321.7258 (2000), pp. 412–9.

[10] Stratton, I. M. et al. “Association of glycaemia with macrovascular and microvascular complications of type 2 diabetes (UKPDS 35): prospective observational study”. *Bmj* 321.7258 (2000), pp. 405–12.

[11] Rorsman, P. and Renstrom, E. “Insulin granule dynamics in pancreatic beta cells”. *Diabetologia* 46.8 (2003), pp. 1029–45. URL: http://www.ncbi.nlm.nih.gov/pubmed/12879249.

[12] Kahn, C. R. “The molecular mechanism of insulin action”. *Annu Rev Med* 36 (1985), pp. 429–51.

[13] Cryer, P. E. “Minireview: Glucagon in the pathogenesis of hypoglycemia and hyperglycemia in diabetes”. *Endocrinology* 153.3 (2012), pp. 1039–48.

[14] Edwards, C. M. et al. “Glucagon-like peptide 1 has a physiological role in the control of postprandial glucose in humans: studies with the antagonist exendin 9-39”. *Diabetes* 48.1 (1999), pp. 86–93. URL: http://diabetes.diabetesjournals.org/content/diabetes/48/1/86.full.pdf.

[15] Marathe, C. S. et al. “Relationships Between Gastric Emptying, Postprandial Glycemia, and Incretin Hormones”. *Diabetes Care* 36.5 (2013), pp. 1396–1405. URL: http://www.ncbi.nlm.nih.gov/pmc/articles/PMC3631884/.

[16] Baggio, L. L. and Drucker, D. J. “Biology of Incretins: GLP-1 and GIP”. *Gastroenterology* 132.6 (2007), pp. 2131–2157. URL: http://www.sciencedirect.com/science/article/pii/S001650850700580X.

[17] Edholm, T. et al. “Differential incretin effects of GIP and GLP-1 on gastric emptying, appetite, and insulin-glucose homeostasis”. *Neurogastroenterol Motil* 22.11 (2010), 1191–200, e315.

[18] Zhou, J. et al. “Ubiquitination is involved in glucose-mediated downregulation of GIP receptors in islets”. *Am J Physiol Endocrinol Metab* 293.2 (2007), E538–47.

[19] Drucker, D. J. “Mechanisms of Action and Therapeutic Application of Glucagon-like Peptide-1”. *Cell Metab* 27.4 (2018), pp. 740–756.

[20] Cordiner, R. and Pearson, E. R. “Reflections on the Sulphonylurea Story. A Drug Class at Risk of Extinction? Or A Drug Class Worth Reviving?” *Diabetes Obes Metab* (2018).

[21] Bergman, R. N. et al. “Accurate Assessment of $\beta$-Cell Function”. *The Hyperbolic Correction* 51.suppl 1 (2002), S212–S220. URL: http://diabetes.diabetesjournals.org/content/diabetes/51/suppl_1/S212.full.pdf.

[22] Matthews, D. R. et al. “Homeostasis model assessment: insulin resistance and beta-cell function from fasting plasma glucose and insulin concentrations in man”. *Diabetologia* 28.7 (1985), pp. 412–9.

[23] Retnakaran, R. et al. “Hyperbolic relationship between insulin secretion and sensitivity on oral glucose tolerance test”. *Obesity (Silver Spring)* 16.8 (2008), pp. 1901–7.

[24] Levy, J. C., Matthews, D. R., and Hermans, M. P. “Correct homeostasis model assessment (HOMA) evaluation uses the computer program”. *Diabetes Care* 21.12 (1998), pp. 2191–2.

[25] Strawbridge, R. J. et al. “Genome-Wide Association Identifies Nine Common Variants Associated With Fasting Proinsulin Levels and Provides New Insights Into the Pathophysiology of Type 2 Diabetes”. *Diabetes* 60.10 (2011), pp. 2624–2634. URL: http://www.ncbi.nlm.nih.gov/pmc/articles/PMC3178302/.

[26] Dimas, A. S. et al. “Impact of type 2 diabetes susceptibility variants on quantitative glycemic traits reveals mechanistic heterogeneity”. *Diabetes* 63.6 (2014), pp. 2158–71. URL: http://www.ncbi.nlm.nih.gov/pubmed/24296717.

[27] Phillips, D. I. et al. “Understanding oral glucose tolerance: comparison of glucose or insulin measurements during the oral glucose tolerance test with specific measurements of insulin resistance and insulin secretion”. *Diabet Med* 11.3 (1994), pp. 286–92.

[28] Hansen, T. et al. “The BIGTT test: a novel test for simultaneous measurement of pancreatic beta-cell function, insulin sensitivity, and glucose tolerance”. *Diabetes Care* 30.2 (2007), pp. 257–62.

[29] Matsuda, M. and DeFronzo, R. A. “Insulin sensitivity indices obtained from oral glucose tolerance testing: comparison with the euglycemic insulin clamp”. *Diabetes Care* 22.9 (1999), pp. 1462–70.

[30] Belfiore, F., Iannello, S., and Volpicelli, G. “Insulin sensitivity indices calculated from basal and OGTT-induced insulin, glucose, and FFA levels”. *Mol Genet Metab* 63.2 (1998), pp. 134–41.

[31] Herzberg-Schafer, S. A. et al. “Evaluation of fasting state-/oral glucose tolerance test-derived measures of insulin release for the detection of genetically impaired beta-cell function”. *PLoS One* 5.12 (2010), e14194.

[32] Cersosimo, E. et al. “Assessment of pancreatic beta-cell function: review of methods and clinical applications”. *Curr Diabetes Rev* 10.1 (2014), pp. 2–42.

[33] Visscher, P. M. et al. “10 Years of GWAS Discovery: Biology, Function, and Translation”. *Am J Hum Genet* 101.1 (2017), pp. 5–22.

[34] Mahajan, A. et al. “Fine-mapping of an expanded set of type 2 diabetes loci to single-variant resolution using high-density imputation and islet-specific epigenome maps”. *bioRxiv* (2018). URL: `https://www.biorxiv.org/content/biorxiv/early/2018/01/09/245506.full.pdf`.

[35] Grotz, A. K., Gloyn, A. L., and Thomsen, S. K. “Prioritising Causal Genes at Type 2 Diabetes Risk Loci”. *Curr Diab Rep* 17.9 (2017), p. 76.

[36] Mahajan, A. et al. “Refining the accuracy of validated target identification through coding variant fine-mapping in type 2 diabetes”. *Nat Genet* 50.4 (2018), pp. 559–571.

[37] Huyghe, J. R. et al. “Exome array analysis identifies new loci and low-frequency variants influencing insulin processing and secretion”. *Nature genetics* 45.2 (2013), pp. 197–201. URL: `http://www.ncbi.nlm.nih.gov/pubmed/23263489`.

[38] Fuchsberger, C. et al. “The genetic architecture of type 2 diabetes”. *Nature* 536.7614 (2016), pp. 41–47.

[39] Partnership, A. M. *Type 2 Diabetes Knowledge Portal.GCKR. 2018/April/27*. Web Page. URL: `http://www.type2diabetesgenetics.org/variantInfo/variantInfo/GCKR`.

[40] Rees, M. G. et al. “Cellular characterisation of the GCKR P446L variant associated with type 2 diabetes risk”. *Diabetologia* 55.1 (2012), pp. 114–22.

[41] Freathy, R. M. et al. “Common variation in the FTO gene alters diabetes-related metabolic traits to the extent expected given its effect on BMI”. *Diabetes* 57.5 (2008), pp. 1419–26.

[42] Moltke, I. et al. “A common Greenlandic TBC1D4 variant confers muscle insulin resistance and type 2 diabetes”. *Nature* 512.7513 (2014), pp. 190–193. URL: `http://dx.doi.org/10.1038/nature13425`.

[43] Ng, H. J. and Gloyn, A. L. “Bridging the Gap Between Genetic Associations and Molecular Mechanisms for Type 2 Diabetes”. *Current Diabetes Reports* 13.6 (2013), pp. 778–785. URL: `http://dx.doi.org/10.1007/s11892-013-0429-1`.

[44] Bonnefond, A. and Froguel, P. “Disentangling the Role of Melatonin and its Receptor MTNR1B in Type 2 Diabetes: Still a Long Way to Go?” *Curr Diab Rep* 17.12 (2017), p. 122.

[45] Raimondo, A. et al. “Type 2 Diabetes Risk Alleles Reveal a Role for Peptidylglycine Alpha-amidating Monooxygenase in Beta Cell Function”. *bioRxiv* (2017).

[46] Perley, M. J. and Kipnis, D. M. “Plasma insulin responses to oral and intravenous glucose: studies in normal and diabetic sujbjects”. *J Clin Invest* 46.12 (1967), pp. 1954–62.

[47] Atabaki-Pasdar, N. et al. “Statistical power considerations in genotype-based recall randomized controlled trials”. *Scientific Reports* 6 (2016), p. 37307. URL: `http://www.ncbi.nlm.nih.gov/pmc/articles/PMC5122840/`.

[48] Tan, G. D. et al. “The in vivo effects of the Pro12Ala PPARgamma2 polymorphism on adipose tissue NEFA metabolism: the first use of the Oxford Biobank”. *Diabetologia* 49.1 (2006), pp. 158–68.

[49] Shah, M. et al. “TCF7L2 Genotype and alpha-Cell Function in Humans Without Diabetes”. *Diabetes* 65.2 (2016), pp. 371–80. URL: http://www.ncbi.nlm.nih.gov/pubmed/26525881.

[50] Pal, A. et al. “PTEN mutations as a cause of constitutive insulin sensitivity and obesity”. *N Engl J Med* 367.11 (2012), pp. 1002–11. URL: http://www.ncbi.nlm.nih.gov/pubmed/22970944.

[51] Steinthorsdottir, V. et al. “Identification of low-frequency and rare sequence variants associated with elevated or reduced risk of type 2 diabetes”. *Nature genetics* 46.3 (2014), pp. 294–8. URL: http://www.ncbi.nlm.nih.gov/pubmed/24464100.

[52] Eipper, B. A., Stoffers, D. A., and Mains, R. E. “The biosynthesis of neuropeptides: peptide alpha-amidation”. *Annu Rev Neurosci* 15 (1992), pp. 57–85.

[53] Merkler, D. J. “C-terminal amidated peptides: production by the in vitro enzymatic amidation of glycine-extended peptides and the importance of the amide to bioactivity”. *Enzyme and microbial technology* 16.6 (1994), pp. 450–6. URL: http://www.ncbi.nlm.nih.gov/pubmed/7764886.

[54] An, Z. et al. “A mass spectrometry-based method to screen for alpha-amidated peptides”. *Proteomics* 12.2 (2012), pp. 173–82.

[55] Eipper, B. A. et al. “Peptidylglycine alpha-amidating monooxygenase: a multifunctional protein with catalytic, processing, and routing domains”. *Protein science : a publication of the Protein Society* 2.4 (1993), pp. 489–97. URL: http://www.ncbi.nlm.nih.gov/pubmed/8518727.

[56] Kolhekar, A. S., Mains, R. E., and Eipper, B. A. “Peptidylglycine alpha-amidating monooxygenase: an ascorbate-requiring enzyme”. *Methods Enzymol* 279 (1997), pp. 35–43.

[57] Gaier, E. D. et al. “Genetic determinants of amidating enzyme activity and its relationship with metal cofactors in human serum”. *BMC Endocr Disord* 14 (2014), p. 58.

[58] Oyarce, A. M. and Eipper, B. A. “Neurosecretory vesicles contain soluble and membrane-associated monofunctional and bifunctional peptidylglycine alpha-amidating monooxygenase proteins”. *Journal of neurochemistry* 60.3 (1993), pp. 1105–14. URL: http://www.ncbi.nlm.nih.gov/pubmed/8436961.

[59] Thomsen, S. K. et al. “Type 2 diabetes risk alleles in PAM impact insulin release from human pancreatic beta-cells”. *Nat Genet* 50.8 (2018), pp. 1122–1131.

[60] Czyzyk, T. A. et al. “Deletion of peptide amidation enzymatic activity leads to edema and embryonic lethality in the mouse”. *Developmental Biology* 287.2 (2005), pp. 301–313. URL: //www.sciencedirect.com/science/article/pii/S0012160605005920.

[61] Ortega-Molina, A. et al. “Pten positively regulates brown adipose function, energy expenditure, and longevity”. *Cell Metab* 15.3 (2012), pp. 382–94.

[62] Smith, U. and Gale, E. A. “Cancer and diabetes: are we ready for prime time?” *Diabetologia* 53.8 (2010), pp. 1541–4.

[63] Giovannucci, E. et al. “Diabetes and cancer: a consensus report”. *Diabetes Care* 33.7 (2010), pp. 1674–85.

[64] Morris, A. P. et al. “Large-scale association analysis provides insights into the genetic architecture and pathophysiology of type 2 diabetes”. *Nat Genet* 44.9 (2012), pp. 981–90. URL: http://www.ncbi.nlm.nih.gov/pubmed/22885922.

[65] Pal, A. et al. “Loss-of-Function Mutations in the Cell-Cycle Control Gene CDKN2A Impact on Glucose Homeostasis in Humans”. *Diabetes* 65.2 (2016), pp. 527–33.

[66] Hopkins, B. D. et al. “PTEN function: the long and the short of it”. *Trends Biochem Sci* 39.4 (2014), pp. 183–90.

[67] Lee, Y. R., Chen, M., and Pandolfi, P. P. “The functions and regulation of the PTEN tumour suppressor: new modes and prospects”. *Nat Rev Mol Cell Biol* 19.9 (2018), pp. 547–562.

[68] Grinder-Hansen, L. et al. “A common variation of the PTEN gene is associated with peripheral insulin resistance”. *Diabetes Metab* 42.4 (2016), pp. 280–4.

[69] Farooq, A. et al. “Cowden syndrome”. *Cancer Treat Rev* 36.8 (2010), pp. 577–83. URL: http://www.ncbi.nlm.nih.gov/pubmed/20580873.

[70] Pilarski, R. et al. “Cowden syndrome and the PTEN hamartoma tumor syndrome: systematic review and revised diagnostic criteria”. *J Natl Cancer Inst* 105.21 (2013), pp. 1607–16.

[71] Cypess, A. M. et al. “Identification and importance of brown adipose tissue in adult humans”. *N Engl J Med* 360.15 (2009), pp. 1509–17.

[72] Marken Lichtenbelt, W. D. van et al. “Cold-activated brown adipose tissue in healthy men”. *N Engl J Med* 360.15 (2009), pp. 1500–8.

[73] Virtanen, K. A. et al. “Functional brown adipose tissue in healthy adults”. *N Engl J Med* 360.15 (2009), pp. 1518–25.

[74] Lee, P. et al. “Hot fat in a cool man: infrared thermography and brown adipose tissue”. *Diabetes Obes Metab* 13.1 (2011), pp. 92–3.

[75] Claessens-van Ooijen, A. M. et al. “Heat production and body temperature during cooling and rewarming in overweight and lean men”. *Obesity (Silver Spring)* 14.11 (2006), pp. 1914–20.

[76] Kooijman, S. et al. “Inhibition of the central melanocortin system decreases brown adipose tissue activity”. *J Lipid Res* 55.10 (2014), pp. 2022–32.

[77] Ortega-Molina, A. et al. “Pharmacological inhibition of PI3K reduces adiposity and metabolic syndrome in obese mice and rhesus monkeys”. *Cell Metab* 21.4 (2015), pp. 558–70.

[78] Hopkins, B. D. et al. “Suppression of insulin feedback enhances the efficacy of PI3K inhibitors”. *Nature* 560.7719 (2018), pp. 499–503.

[79] Karpe, F. et al. “Cohort Profile: The Oxford Biobank”. *Int J Epidemiol* 47.1 (2018), 21–21g.

[80] Orskov, C. et al. “Tissue and plasma concentrations of amidated and glycine-extended glucagon-like peptide I in humans”. *Diabetes* 43.4 (1994), pp. 535–9.

[81] Plummer, M. P. et al. “Incretins and the intensivist: what are they and what does an intensivist need to know about them?” *Critical Care* 18.1 (2014), p. 205. URL: https://doi.org/10.1186/cc13737.

[82] DeFronzo, R. A., Tobin, J. D., and Andres, R. “Glucose clamp technique: a method for quantifying insulin secretion and resistance”. *Am J Physiol* 237.3 (1979), E214–23.

[83] Kennedy, S. et al. “Comparison of the GEM and the ECAL indirect calorimeters against the Deltatrac for measures of RMR and diet-induced thermogenesis”. *J Nutr Sci* 3 (2014), e52.

[84] Acosta, F. M. et al. “Physiological responses to acute cold exposure in young lean men”. *PLoS One* 13.5 (2018), e0196543.

[85] Nauck, M. A. et al. “Critical evaluation of the ’heated-hand-technique’ for obtaining ’arterialized’ venous blood: incomplete arterialization and alterations in glucagon responses”. *Clin Physiol* 12.5 (1992), pp. 537–52.

[86] Ørskov, C. et al. “Tissue and plasma concentrations of amidated and glycine-extended glucagon-like peptide I in humans”. *Diabetes* 43.4 (1994), pp. 535–539. URL: `http://www.scopus.com/inward/record.url?eid=2-s2.0-0028281773&partnerID=40&md5=160d5c6c19b04f5d46065cd8104ac6aa`.

[87] Mizuno, K. et al. “Peptide C-terminal alpha-amidating enzyme purified to homogeneity from Xenopus laevis skin”. *Biochem Biophys Res Commun* 137.3 (1986), pp. 984–91.

[88] Holst, J. J. et al. “Glucagon-like peptide-1, glucose homeostasis and diabetes”. *Trends in molecular medicine* 14.4 (2008), pp. 161–8. URL: `http://www.ncbi.nlm.nih.gov/pubmed/18353723`.

[89] Wettergren, A. et al. “Amidated and non-amidated glucagon-like peptide-1 (GLP-1): non-pancreatic effects (cephalic phase acid secretion) and stability in plasma in humans”. *Regul Pept* 77.1-3 (1998), pp. 83–7. URL: `http://www.ncbi.nlm.nih.gov/pubmed/9809800`.

[90] Maeda-Nakai, E. and Ichiyama, A. “A spectrophotometric method for the determination of glycolate in urine and plasma with glycolate oxidase”. *Journal of biochemistry* 127.2 (2000), pp. 279–87. URL: `http://www.ncbi.nlm.nih.gov/pubmed/10731695`.

[91] Cederberg, H. et al. “Increased risk of diabetes with statin treatment is associated with impaired insulin sensitivity and insulin secretion: a 6 year follow-up study of the METSIM cohort”. *Diabetologia* 58.5 (2015), pp. 1109–17.

[92] Biosystems, A. *Allelic discrimination getting started guide*. Web Page. 2010. URL: `docs.appliedbiosystems.com/pebiodocs/04347822.pdf`.

[93] Umapathysivam, M. M. et al. “Comparative effects of prolonged and intermittent stimulation of the glucagon-like peptide 1 receptor on gastric emptying and glycemia”. *Diabetes* 63.2 (2014), pp. 785–90.

[94] Gjesing, A. P. et al. “Fasting and oral glucose-stimulated levels of glucose-dependent insulinotropic polypeptide (GIP) and glucagon-like peptide-1 (GLP-1) are highly familial traits”. *Diabetologia* 55.5 (2012), pp. 1338–45.

[95] Nauck, M. et al. “Reduced incretin effect in type 2 (non-insulin-dependent) diabetes”. *Diabetologia* 29.1 (1986), pp. 46–52.

[96] Sun, B. B. et al. “Genomic atlas of the human plasma proteome”. *Nature* 558.7708 (2018), pp. 73–79.

[97] Knudsen, L. B. and Pridal, L. “Glucagon-like peptide-1-(9-36) amide is a major metabolite of glucagon-like peptide-1-(7-36) amide after in vivo administration to dogs, and it acts as an antagonist on the pancreatic receptor”. *Eur J Pharmacol* 318.2-3 (1996), pp. 429–35.

[98] Holst, J. J. and Deacon, C. F. “Inhibition of the activity of dipeptidyl-peptidase IV as a treatment for type 2 diabetes”. *Diabetes* 47.11 (1998), pp. 1663–70.

[99] Dawed, A. Y., Zhou, K., and Pearson, E. R. “Pharmacogenetics in type 2 diabetes: influence on response to oral hypoglycemic agents”. *Pharmgenomics Pers Med* 9 (2016), pp. 17–29.

[100] Gloyn, A. L. et al. “Activating mutations in the gene encoding the ATP-sensitive potassium-channel subunit Kir6.2 and permanent neonatal diabetes”. *N Engl J Med* 350.18 (2004), pp. 1838–49.

[101] Mahajan, A. et al. “Refining the accuracy of validated target identification through coding variant fine-mapping in type 2 diabetes”. *Nat Genet* 50.4 (2018), pp. 559–571.

[102] Apweiler, R. et al. “UniProt: the Universal Protein knowledgebase”. *Nucleic Acids Res* 32.Database issue (2004), pp. D115–9.

[103] Sherlock, M. and Stewart, P. M. “The Short Synacthen Test and Its Utility in Assessing Recovery of Adrenal Function in Patients With Central Adrenal Insufficiency”. *J Clin Endocrinol Metab* 104.1 (2019), pp. 17–20.

[104] Rehfeld, J. F. and Stadil, F. “The effect of gastrin on basal- and glucose-stimulated insulin secretion in man”. *J Clin Invest* 52.6 (1973), pp. 1415–26.

[105] Steinert, R. E. et al. “Ghrelin, CCK, GLP-1, and PYY(3-36): Secretory Controls and Physiological Roles in Eating and Glycemia in Health, Obesity, and After RYGB”. *Physiol Rev* 97.1 (2017), pp. 411–463.

[106] Rehfeld, J. F. “Accurate measurement of cholecystokinin in plasma”. *Clin Chem* 44.5 (1998), pp. 991–1001.

[107] McIntyre, N., Holdsworth, C. D., and Turner, D. S. “NEW INTERPRETATION OF ORAL GLUCOSE TOLERANCE”. *Lancet* 2.7349 (1964), pp. 20–1.

[108] Brent, G. A. “Mechanisms of thyroid hormone action”. *J Clin Invest* 122.9 (2012), pp. 3035–43.

[109] Bousquet-Moore, D. et al. “Reversal of physiological deficits caused by diminished levels of peptidylglycine alpha-amidating monooxygenase by dietary copper”. *Endocrinology* 150.4 (2009), pp. 1739–47.

[110] Wiersinga, W. M. “Adult Hypothyroidism”. In: *Endotext*. Ed. by De Groot, L. J. et al. South Dartmouth (MA): MDText.com, Inc., 2000.

[111] GoDarts et al. “Common variants near ATM are associated with glycemic response to metformin in type 2 diabetes”. *Nat Genet* 43.2 (2011), pp. 117–20. URL: `http://www.ncbi.nlm.nih.gov/pubmed/21186350`.

[112] Koivula, R. W. et al. “Discovery of biomarkers for glycaemic deterioration before and after the onset of type 2 diabetes: rationale and design of the epidemiological studies within the IMI DIRECT Consortium”. *Diabetologia* 57.6 (2014), pp. 1132–42.

[113] Choi, K. et al. “A Computational Method to Determine Glucose Infusion Rates for Isoglycemic Intravenous Glucose Infusion Study”. *IEEE J Biomed Health Inform* 20.1 (2016), pp. 4–10.

[114] Holman, R. R. et al. “10-year follow-up of intensive glucose control in type 2 diabetes”. *N Engl J Med* 359.15 (2008), pp. 1577–89.

[115] Gromada, J., Holst, J. J., and Rorsman, P. “Cellular regulation of islet hormone secretion by the incretin hormone glucagon-like peptide 1”. *Pflugers Arch* 435.5 (1998), pp. 583–94.

[116] Liaw, D. et al. “Germline mutations of the PTEN gene in Cowden disease, an inherited breast and thyroid cancer syndrome”. *Nat Genet* 16.1 (1997), pp. 64–7.

[117] Blumenthal, G. M. and Dennis, P. A. “PTEN hamartoma tumor syndromes”. *Eur J Hum Genet* 16.11 (2008), pp. 1289–1300. URL: http://dx.doi.org/10.1038/ejhg.2008.162.

[118] Caux, F. et al. “Segmental overgrowth, lipomatosis, arteriovenous malformation and epidermal nevus (SOLAMEN) syndrome is related to mosaic PTEN nullizygosity”. *Eur J Hum Genet* 15.7 (2007), pp. 767–773. URL: http://dx.doi.org/10.1038/sj.ejhg.5201823.

[119] Bernal-Mizrachi, E. et al. “Islet beta cell expression of constitutively active Akt1/PKB alpha induces striking hypertrophy, hyperplasia, and hyperinsulinemia”. *J Clin Invest* 108.11 (2001), pp. 1631–8.

[120] Bernal-Mizrachi, E. et al. “Defective insulin secretion and increased susceptibility to experimental diabetes are induced by reduced Akt activity in pancreatic islet beta cells”. *J Clin Invest* 114.7 (2004), pp. 928–36.

[121] Cannon, B. and Nedergaard, J. “Brown adipose tissue: function and physiological significance”. *Physiol Rev* 84.1 (2004), pp. 277–359.

[122] Cypess, A. M. et al. “Activation of human brown adipose tissue by a beta3-adrenergic receptor agonist”. *Cell Metab* 21.1 (2015), pp. 33–8.

[123] Wang, Q. et al. “Brown adipose tissue activation is inversely related to central obesity and metabolic parameters in adult human”. *PLoS One* 10.4 (2015), e0123795.

[124] Public-Health-England. “Health matters: obesity and the food environment” (2017). URL: https://www.gov.uk/government/publications/health-matters-obesity-and-the-food-environment/health-matters-obesity-and-the-food-environment--2#resources.

[125] Arroyo-Johnson, C. and Mincey, K. D. “Obesity Epidemiology Worldwide”. *Gastroenterol Clin North Am* 45.4 (2016), pp. 571–579.

[126] Avila, C. et al. “An Overview of Links Between Obesity and Mental Health”. *Curr Obes Rep* 4.3 (2015), pp. 303–10.

[127] Frias, J. P. et al. “Efficacy and safety of LY3298176, a novel dual GIP and GLP-1 receptor agonist, in patients with type 2 diabetes: a randomised, placebo-controlled and active comparator-controlled phase 2 trial”. *Lancet* 392.10160 (2018), pp. 2180–2193.

[128] Lau, A. Z. et al. “Noninvasive identification and assessment of functional brown adipose tissue in rodents using hyperpolarized (1)(3)C imaging”. *Int J Obes (Lond)* 38.1 (2014), pp. 126–31.

[129] Lans, A. A. van der et al. “Cold-activated brown adipose tissue in human adults: methodological issues”. *Am J Physiol Regul Integr Comp Physiol* 307.2 (2014), R103–13.

[130] Hany, T. F. et al. “Brown adipose tissue: a factor to consider in symmetrical tracer uptake in the neck and upper chest region”. *Eur J Nucl Med Mol Imaging* 29.10 (2002), pp. 1393–8.

[131] Huang, B., Law, M. W., and Khong, P. L. “Whole-body PET/CT scanning: estimation of radiation dose and cancer risk”. *Radiology* 251.1 (2009), pp. 166–74.

[132] Bartelt, A. et al. “Effects of adipocyte lipoprotein lipase on de novo lipogenesis and white adipose tissue browning”. *Biochim Biophys Acta* 1831.5 (2013), pp. 934–42.

[133] Cypess, A. M. et al. “Brown fat in humans: consensus points and experimental guidelines”. *Cell Metab* 20.3 (2014), pp. 408–15.

[134] Ang, Q. Y. et al. “A new method of infrared thermography for quantification of brown adipose tissue activation in healthy adults (TACTICAL): a randomized trial”. *Journal of Physiological Sciences* 67.3 (2017), pp. 395–406. URL: https://www.ncbi.nlm.nih.gov/pmc/articles/PMC5477687/pdf/12576_2016_Article_472.pdf.

[135] Law, J. et al. “Infrared Thermography”. *Handb Exp Pharmacol* (2018).

[136] Carter, E. A. et al. “Association of heat production with 18F-FDG accumulation in murine brown adipose tissue after stress”. *J Nucl Med* 52.10 (2011), pp. 1616–20.

[137] Gatidis, S. et al. “Is It Possible to Detect Activated Brown Adipose Tissue in Humans Using Single-Time-Point Infrared Thermography under Thermoneutral Conditions? Impact of BMI and Subcutaneous Adipose Tissue Thickness”. *PLoS One* 11.3 (2016), e0151152.

[138] Jang, C. et al. “Infrared thermography in the detection of brown adipose tissue in humans”. *Physiol Rep* 2.11 (2014).

[139] Law, J. et al. “Thermal imaging is a non-invasive alternative to PET-CT for measurement of brown adipose tissue activity in humans”. *Journal of Nuclear Medicine* (2017).

[140] Rivlin, M. et al. “Molecular imaging of tumors and metastases using chemical exchange saturation transfer (CEST) MRI”. *Sci Rep* 3 (2013), p. 3045.

[141] Geuna, E. et al. “Complications of hyperglycaemia with PI3K-AKT-mTOR inhibitors in patients with advanced solid tumours on Phase I clinical trials”. *Br J Cancer* 113.11 (2015), pp. 1541–7.

[142] Gammon, A. et al. “PTEN mosaicism with features of Cowden syndrome”. *Clinical Genetics* 84.6 (2013), pp. 593–595. URL: http://dx.doi.org/10.1111/cge.12078.

[143] Pritchard, C. C. et al. “A mosaic PTEN mutation causing Cowden syndrome identified by deep sequencing”. *Genet Med* 15.12 (2013), pp. 1004–1007. URL: http://dx.doi.org/10.1038/gim.2013.51.

[144] Zhou, X. P. et al. “Germline and germline mosaic PTEN mutations associated with a Proteus-like syndrome of hemihypertrophy, lower limb asymmetry, arteriovenous malformations and lipomatosis”. *Hum Mol Genet* 9.5 (2000), pp. 765–8.

[145] Lindhurst, M. J. et al. “A mosaic activating mutation in AKT1 associated with the Proteus syndrome”. *N Engl J Med* 365.7 (2011), pp. 611–9.

[146] Salo-Mullen, E. E. et al. “Mosaic partial deletion of the PTEN gene in a patient with Cowden syndrome”. *Fam Cancer* 13.3 (2014), pp. 459–67.

[147] Maehama, T. and Dixon, J. E. “The tumor suppressor, PTEN/MMAC1, dephosphorylates the lipid second messenger, phosphatidylinositol 3,4,5-trisphosphate”. *J Biol Chem* 273.22 (1998), pp. 13375–8.

[148] Kohn, A. D. et al. “Expression of a constitutively active Akt Ser/Thr kinase in 3T3-L1 adipocytes stimulates glucose uptake and glucose transporter 4 translocation”. *J Biol Chem* 271.49 (1996), pp. 31372–8.

[149] Biesecker, L. G. and Spinner, N. B. “A genomic view of mosaicism and human disease”. *Nat Rev Genet* 14.5 (2013), pp. 307–20.

[150] Ortega-Molina, A. et al. “Pten positively regulates brown adipose function, energy expenditure, and longevity”. *Cell Metab* 15.3 (2012), pp. 382–94. URL: http://www.ncbi.nlm.nih.gov/pubmed/22405073.

[151] Di Cristofano, A. et al. “Pten is essential for embryonic development and tumour suppression”. *Nat Genet* 19.4 (1998), pp. 348–55.

[152] Orloff, M. S. et al. “Germline PIK3CA and AKT1 mutations in Cowden and Cowden-like syndromes”. *Am J Hum Genet* 92.1 (2013), pp. 76–80.

[153] Manning, A. et al. “A Low-Frequency Inactivating Akt2 Variant Enriched in the Finnish Population is Associated With Fasting Insulin Levels and Type 2 Diabetes Risk”. *Diabetes* (2017).

[154] Hatakeyama, H. et al. “Cooperative actions of Tbc1d1 and AS160/Tbc1d4 in GLUT4 trafficking activities”. *J Biol Chem* (2018).

[155] Corbin, L. J. et al. “Causal Analyses, Statistical Efficiency And Phenotypic Precision Through Recall-By-Genotype Study Design”. *bioRxiv* (2017).

[156] Hernandez, A. F. et al. “Albiglutide and cardiovascular outcomes in patients with type 2 diabetes and cardiovascular disease (Harmony Outcomes): a double-blind, randomised placebo-controlled trial”. *Lancet* 392.10157 (2018), pp. 1519–1529.

[157] Drucker, D. J. “The Ascending GLP-1 Road From Clinical Safety to Reduction of Cardiovascular Complications”. *Diabetes* 67.9 (2018), pp. 1710–1719.

[158] FDA. *Byetta*. Report. 2009. URL: https://www.accessdata.fda.gov/drugsatfda_docs/label/2009/021773s9s11s18s22s25lbl.pdf.

[159] Steveson, T. C. et al. “Menkes protein contributes to the function of peptidylglycine alpha-amidating monooxygenase”. *Endocrinology* 144.1 (2003), pp. 188–200.

[160] Jayawant, S., Halpin, S., and Wallace, S. “Menkes kinky hair disease: an unusual case”. *Eur J Paediatr Neurol* 4.3 (2000), pp. 131–4.

[161] Turnlund, J. R. “Human whole-body copper metabolism”. *Am J Clin Nutr* 67.5 Suppl (1998), 960s–964s.

[162] He, L. M. et al. “Cyclin D2 protein stability is regulated in pancreatic beta-cells”. *Mol Endocrinol* 23.11 (2009), pp. 1865–75.

[163] Sjostrand, M. et al. “Assessment of beta-cell function in young patients with type 2 diabetes: arginine-stimulated insulin secretion may reflect beta-cell reserve”. *J Intern Med* 275.1 (2014), pp. 39–48.

[164] Law, J. et al. “Infrared Thermography”. *Handb Exp Pharmacol* (2018).

[165] Rusk, N. “The UK Biobank”. *Nat Methods* 15.12 (2018), p. 1001.

[166] Flannick, J. A. et al. “Genetic discovery and translational decision support from exome sequencing of 20,791 type 2 diabetes cases and 24,440 controls from five ancestries”. *bioRxiv* (2018), p. 371450. URL: https://www.biorxiv.org/content/biorxiv/early/2018/07/31/371450.full.pdf.

[167] Dennis, J. M. et al. “Sex and BMI Alter the Benefits and Risks of Sulfonylureas and Thiazolidinediones in Type 2 Diabetes: A Framework for Evaluating Stratification Using Routine Clinical and Individual Trial Data”. *Diabetes Care* 41.9 (2018), pp. 1844–1853.

# Appendices

# A

# Amidated Peptides in Human Serum

## A.1 Amidated Serum Peptides indentified in the UniProt database

I interogatted the Unitprot database to identify possible peptides mediating T2D risk and beta-cell function phenotypes in carriers of *PAM* LoF alleles [102]. I specifically restricted my search to blood as this is an easily accesiblenand acceptable tissue to sample. The search terms for interrogating the database were: *homo sapiens* and blood/plasma/serum and amide/amidation. For ease of interpretation the results displayed in the table have been limited to the first amidated peptide (i.e. breakdown products that also remain amidated have not been included). The one exception to this is the proglucagon breakdown produuct, which have all been listed due to the importance for this thesis.

| Gene names | Protein names | Length |
|---|---|---|
| ACAD8 | Isobutyryl-CoA dehydrogenase | 415 |
| ACADSB | Short/branched chain specific acyl-CoA dehydrogenase | 432 |
| ACADVL VLCAD | Very long-chain specific acyl-CoA dehydrogenase, mitochondrial (VLCAD) (EC 1.3.8.9) | 655 |
| ACHE | Acetylcholinesterase | 614 |
| ADA ADA1 | Adenosine deaminase | 363 |
| ADA2 ADGF CECR1 IDGFL | Adenosine deaminase 2 | 511 |

| Gene names | Protein names | Length |
|---|---|---|
| ADCY10 SAC | Adenylate cyclase type 10 | 1610 |
| ADCYAP1 | Pituitary adenylate cyclase-activating polypeptide | 176 |
| ADM AM | Adrenomedullin ; Proadrenomedullin | 185 |
| ADM2 AM2 | Adrenomedullin-2 | 148 |
| AKT1 PKB RAC | Protein kinase B | 480 |
| AKT2 | Protein kinase Akt-2 | 481 |
| ANPEP APN CD13 PEPN | Aminopeptidase N | 967 |
| ART4 | NAD(P)(+)–arginine ADP-ribosyltransferase ( | 236 |
| ART4 DO DOK1 | Ecto-ADP-ribosyltransferase 4 | 314 |
| AURKA | Aurora kinase A | 403 |
| AVP ARVP VP | Vasopressin-neurophysin 2-copeptin | 164 |
| BLVRB FLR | Flavin reductase | 206 |
| BTD | Biotinidase | 543 |
| BTK AGMX1 ATK BPK | Tyrosine-protein kinase BTK | 659 |
| C4A CO4 CPAMD2 | Complement C4-A | 1744 |
| C4B CO4 CPAMD3; C4B_2 | Complement C4-B | 1744 |
| CALCA CALC1 | Calcitonin gene-related peptide 1 | 128 |
| CALCA CALC1 | Calcitonin | 141 |
| CAMK4 CAMK CAMK-GR CAMKIV | Calcium/calmodulin-dependent protein kinase type IV | 473 |
| CES1 CES2 SES1 | Liver carboxylesterase 1 | 567 |
| CHGA | Chromogranin-A (CgA) | 457 |
| CLCN2 | Chloride channel protein 2 (ClC-2) | 898 |
| CLCN3 | H(+)/Cl(-) exchange transporter 3 | 818 |
| CLCN5 CLCK2 | H(+)/Cl(-) exchange transporter 5 | 746 |
| CLCN6 KIAA0046 | Chloride transport protein 6 (Chloride channel protein 6) (ClC-6) | 869 |
| CNDP2 CN2 CPGL HEL-S-13 PEPA | Cytosolic non-specific dipeptidase | 475 |
| CNR2 CB2A CB2B | Cannabinoid receptor 2 | 360 |
| COMT | Catechol O-methyltransferase | 271 |
| CRH | Corticotropin-releasing factor | 196 |
| CRY1 PHLL1 | Cryptochrome-1 | 586 |
| CRY2 KIAA0658 | Cryptochrome-2 | 593 |
| CSF1R FMS | Macrophage colony-stimulating factor 1 receptor | 972 |
| CTSC CPPI | Dipeptidyl peptidase 1 | 463 |
| CTSK CTSO CTSO2 | Cathepsin K | 329 |
| CYLD CYLD1 KIAA0849 HSPC057 | Ubiquitin carboxyl-terminal hydrolase CYLD | 956 |
| DHCR7 D7SR | 7-dehydrocholesterol reductase | 475 |
| DHFR | Dihydrofolate reductase | 187 |
| DHPS DS | Deoxyhypusine synthase | 369 |

| Gene names | Protein names | Length |
|---|---|---|
| DNMT1 AIM CXXC9 DNMT | DNA (cytosine-5)-methyltransferase 1 | 1616 |
| DPH5 AD-018 CGI-30 HSPC143 NPD015 | Diphthine methyl ester synthase | 285 |
| DPYD | Dihydropyrimidine dehydrogenase [NADP(+)] | 1025 |
| EHMT2 BAT8 C6orf30 G9A KMT1C NG36 | Histone-lysine N-methyltransferase EHMT2 | 1210 |
| F11 | Coagulation factor XI | 625 |
| F7 | Coagulation factor VII | 466 |
| FGA | Fibrinogen alpha chain | 866 |
| FGB | Fibrinogen beta chain | 491 |
| FGG PRO2061 | Fibrinogen gamma chain | 453 |
| GAST GAS | Gastrin | 101 |
| GCDH | Glutaryl-CoA dehydrogenase, mitochondrial | 438 |
| GCG | Glucagon [Cleaved into: Glicentin; Glicentin-related polypeptide (GRPP); Oxyntomodulin (OXM) (OXY); Glucagon; Glucagon-like peptide 1 (GLP-1) (Incretin hormone); Glucagon-like peptide 1(7-37) (GLP-1(7-37)); Glucagon-like peptide 1(7-36) (GLP-1(7-36)); Glucagon-like peptide 2 (GLP-2)] | 180 |
| GHRL MTLRP UNQ524/PRO1066 | Ghrelin | 117 |
| GLRX2 GRX2 CGI-133 | Glutaredoxin-2, mitochondrial | 164 |
| GLRX5 C14orf87 | Glutaredoxin-related protein 5 | 157 |
| GNA11 GA11 | Guanine nucleotide-binding protein subunit alpha-11 | 359 |
| GNA12 | Guanine nucleotide-binding protein subunit alpha-12 | 381 |
| GNA13 | Guanine nucleotide-binding protein subunit alpha-13 | 377 |
| GNAI2 GNAI2B | Guanine nucleotide-binding protein G(i) subunit alpha-2 | 355 |
| GNAQ GAQ | Guanine nucleotide-binding protein G(q) subunit alpha | 359 |
| GNAZ | Guanine nucleotide-binding protein G(z) subunit alpha (G(x) alpha chain) | 355 |
| GOT1 | Aspartate aminotransferase, cytoplasmic | 413 |
| GPD1L KIAA0089 | Glycerol-3-phosphate dehydrogenase 1-like protein (GPD1-L) | 351 |
| GSTK1 HDCMD47P | Glutathione S-transferase kappa 1 (EC 2.5.1.18) (GST 13-13) (GST class-kappa) (GSTK1-1) (hGSTK1) (Glutathione S-transferase subunit 13) | 226 |
| GSTO1 GSTTLP28 | Glutathione S-transferase omega-1 | 241 |
| GSTZ1 MAAI | Maleylacetoacetate isomerase | 216 |
| HAVCR2 TIM3 TIMD3 | Hepatitis A virus cellular receptor 2 | 301 |
| HPSE HEP HPA HPA1 HPR1 HPSE1 HSE1 | Heparanase | 543 |

| Gene names | Protein names | Length |
|---|---|---|
| HSP90AA1 HSP90A HSPC1 HSPCA | Heat shock protein HSP 90-alpha | 732 |
| HSP90B1 GRP94 TRA1 | Endoplasmin | 803 |
| LTF GIG12 LF | Lactotransferrin | 710 |
| MAP2K1 MEK1 PRKMK1 | Dual specificity mitogen-activated protein kinase kinase 1 | 393 |
| MAPK1 ERK2 PRKM1 PRKM2 | Mitogen-activated protein kinase 1 | 360 |
| MAPK14 | Mitogen-activated protein kinase 14 | 360 |
| MICAL1 MICAL NICAL | [F-actin]-monooxygenase MICAL1 | 1067 |
| MIF GLIF MMIF | Macrophage migration inhibitory factor | 115 |
| MMACHC | Methylmalonic aciduria and homocystinuria type C protein | 282 |
| MUC5AC MUC5 | Mucin-5AC | 5654 |
| NAMPT PBEF PBEF1 | Nicotinamide phosphoribosyltransferase | 491 |
| NAT1 AAC1 | Arylamine N-acetyltransferase 1 | 290 |
| NMU | Neuromedin-U | 174 |
| NOS1 | Nitric oxide synthase, brain | 1434 |
| NOS3 | Nitric oxide synthase, endothelial | 1203 |
| NOTCH1 TAN1 | Neurogenic locus notch homolog protein 1 | 2555 |
| NPFF | Pro-FMRFamide-related neuropeptide FF | 113 |
| NPR1 ANPRA | Atrial natriuretic peptide receptor 1 | 1061 |
| NPR3 ANPRC C5orf23 NPRC | Atrial natriuretic peptide receptor 3 | 541 |
| NPY | Pro-neuropeptide Y [Cleaved into: Neuropeptide Y] | 97 |
| NUDT5 NUDIX5 HSPC115 | ADP-sugar pyrophosphatase | 219 |
| OSGEP GCPL1 | Probable tRNA N6-adenosine threonylcarbamoyltransferase | 335 |
| OTUB1 OTB1 OTU1 HSPC263 | Ubiquitin thioesterase OTUB1 | 271 |
| OTUD5 | OTU domain-containing protein 5 | 571 |
| OXT OT | Oxytocin-neurophysin 1 (OT-NPI) [Cleaved into: Oxytocin (Ocytocin); Neurophysin 1] | 125 |
| PADI4 PAD4 PADI5 PDI5 | Protein-arginine deiminase type-4 | 663 |
| PAPSS2 ATPSK2 | Bifunctional 3'-phosphoadenosine 5'-phosphosulfate synthase 2 | 614 |
| PARG | Poly(ADP-ribose) glycohydrolase (EC 3.2.1.143) | 976 |
| PBEF1 hCG_18025 | Nicotinamide phosphoribosyltransferase (NAmPRTase) (EC 2.4.2.12) | 491 |
| PFKFB4 | 6-phosphofructo-2-kinase/fructose-2,6-bisphosphatase 4 | 469 |
| PFN1 | Profilin-1 (Epididymis tissue protein Li 184a) (Profilin I) | 140 |
| PGD PGDH | 6-phosphogluconate dehydrogenase, decarboxylating (EC 1.1.1.44) | 483 |

| Gene names | Protein names | Length |
|---|---|---|
| PKLR PK1 PKL | Pyruvate kinase PKLR | 574 |
| PLA2G15 LYPLA3 UNQ341/PRO540 | Group XV phospholipase A2 | 412 |
| PLB1 PLB | Phospholipase B1, membrane-associated | 1458 |
| PMCH MCH | Pro-MCH | 165 |
| PNP NP | Purine nucleoside phosphorylase (PNP) | 289 |
| POMC | Pro-opiomelanocortin (POMC) | 267 |
| PPOX | Protoporphyrinogen oxidase | 477 |
| PRKACA PKACA | cAMP-dependent protein kinase catalytic subunit alpha | 351 |
| PRNP ALTPRP PRIP PRP | Major prion protein (PrP) | 253 |
| PSMA7 HSPC | Proteasome subunit alpha type-7 | 248 |
| PSMB5 LMPX MB1 X | Proteasome subunit beta type-5 | 263 |
| PTGIS CYP8 CYP8A1 | Prostacyclin synthase | 500 |
| PYGL | Glycogen phosphorylase, liver form | 847 |
| QRFP | Orexigenic neuropeptide QRFP (P518) | 136 |
| RAC1 TC25 MIG5 | Ras-related C3 botulinum toxin substrate 1 | 192 |
| RAN ARA24 OK/SW-cl.81 | GTP-binding nuclear protein Ran | 216 |
| RAP1A KREV1 | Ras-related protein Rap-1A | 184 |
| RSAD1 | Radical S-adenosyl methionine domain-containing protein 1, mitochondrial | 442 |
| RUNX1 AML1 CBFA2 | Runt-related transcription factor 1 | 453 |
| SAMHD1 MOP5 | Deoxynucleoside triphosphate triphosphohydrolase SAMHD1 | 626 |
| SEPT9 KIAA0991 MSF | Septin-9 | 586 |
| SETD2 HIF1 HYPB KIAA1732 KMT3A SET2 HSPC069 | Histone-lysine N-methyltransferase SETD2 | 2564 |
| SIRT1 SIR2L1 | NAD-dependent protein deacetylase sirtuin-1 | 747 |
| SIRT2 SIR2L SIR2L2 | NAD-dependent protein deacetylase sirtuin-2 | 389 |
| SIRT5 hCG_37419 | NAD-dependent protein deacylase sirtuin-5, mitochondrial | 310 |
| SIRT5 SIR2L5 | NAD-dependent protein deacylase sirtuin-5, mitochondrial | 310 |
| SIRT6 SIR2L6 | NAD-dependent protein deacetylase sirtuin-6 | 355 |
| SNX20 SLIC1 | Sorting nexin-20 | 316 |
| SPX C12orf39 | Spexin | 116 |
| ST3GAL2 hCG_32368 | ST3 beta-galactoside alpha-2,3-sialyltransferase 2 | 350 |
| ST3GAL2 SIAT4B | CMP-N-acetylneuraminate-beta-galactosamide-alpha-2,3-sialyltransferase 2 | 350 |
| STEAP3 TSAP6 | Metalloreductase STEAP3 | 488 |
| STK10 LOK | Serine/threonine-protein kinase 10 | 968 |
| TAC1 NKA NKNA TAC2 | Protachykinin-1 (PPT) | 129 |

| Gene names | Protein names | Length |
|---|---|---|
| TAC4 | Tachykinin-4 | 113 |
| TF PRO1400 | Serotransferrin | 698 |
| TKT | Transketolase | 623 |
| TM7SF2 ANG1 | Delta(14)-sterol reductase | 418 |
| TRPT1 | tRNA 2'-phosphotransferase 1 | 253 |
| UBA6 MOP4 UBE1L2 | Ubiquitin-like modifier-activating enzyme 6 | 1052 |
| UCN | Urocortin | 124 |
| USP10 KIAA0190 | Ubiquitin carboxyl-terminal hydrolase 10 | 798 |
| USP17L10 | Ubiquitin carboxyl-terminal hydrolase 17-like protein 10 | 530 |
| USP17L15 | Ubiquitin carboxyl-terminal hydrolase 17-like protein 15 | 530 |
| USP17L18 | Ubiquitin carboxyl-terminal hydrolase 17-like protein 18 | 530 |
| USP17L19 | Ubiquitin carboxyl-terminal hydrolase 17-like protein 19 | 530 |
| USP17L21 | Ubiquitin carboxyl-terminal hydrolase 17-like protein 21 | 530 |
| USP17L24 | Ubiquitin carboxyl-terminal hydrolase 17-like protein 24 | 530 |
| USP17L5 | Ubiquitin carboxyl-terminal hydrolase 17-like protein 5 | 530 |
| USP25 USP21 | Ubiquitin carboxyl-terminal hydrolase 25 | 1055 |
| USP3 | Ubiquitin carboxyl-terminal hydrolase 3 | 520 |
| USP3 | Ubiquitinyl hydrolase 1 | 503 |
| USP3 | Ubiquitinyl hydrolase 1 | 498 |
| VIP | VIP peptides | 170 |
| WNK1 | Serine/threonine-protein kinase WNK1 | 2382 |

**Table A.1:** Amidated peptides in human blood as listed in the UniProt database [102] . The search terms for interrogating the database were: *homo sapiens* and blood/plasma/serum and amide/amidation.